

GEOLOGICA ULTRAJECTINA

Mededelingen van de  
Faculteit Aardwetenschappen  
Universiteit Utrecht

No. 189

**Orbital forcing in late Neogene lacustrine  
basins from the Mediterranean**

*A magnetostratigraphic and cyclostratigraphic study*

Nicole van Vugt



# Orbital forcing in late Neogene lacustrine basins from the Mediterranean

*A magnetostratigraphic and cyclostratigraphic study*

## Astronomische forcering in laat Neogene lacustrine bekkens uit het Middellandse Zeegebied

*Een magnetostratigrafisch en cyclostratigrafisch onderzoek*

(met een samenvatting in het Nederlands)

PROEFSCHRIFT

ter verkrijging van de graad van Doctor aan de Universiteit Utrecht

op gezag van de Rector Magnificus, Prof. Dr. H.O. Voorma,

ingevolge het besluit van het College voor Promoties in het openbaar te verdedigen op

dinsdag 20 juni 2000 des ochtends te 10.30 uur

door

**Nicole van Vugt**

geboren op 20 december 1970, te Leende

Promotor:

Prof. dr. C.G. Langereis

The investigations were supported by the Netherlands Council for Earth and Life Sciences (ALW) with financial aid from the Netherlands Organisation for Scientific Research (NWO).

ISBN 90-5744-050-4

There is something magical about rhythm,  
it ever makes us believe we have taken possession of the divine.

*J.W. Goethe*

Members of the dissertation committee:

Prof. dr. D.V. Kent  
Faculty of Geology, Rutgers University  
Piscataway, USA

Prof. dr. C.S. Doukas  
Faculty of Earth Sciences, University of Athens  
Athens, Greece

Prof. dr. J. E. Meulenkamp  
Faculty of Earth Sciences, Utrecht University  
Utrecht, the Netherlands

Prof. dr. H. Visscher  
Faculty of Biology, Utrecht University  
Utrecht, the Netherlands

Prof. dr. P.L. de Boer  
Faculty of Earth Sciences, Utrecht University  
Utrecht, the Netherlands

The research for this thesis was carried out at:  
Palaeomagnetic Laboratory 'Fort Hoofddijk'  
Faculty of Earth Sciences, Utrecht University  
Budapestlaan 17, 3523 JR Utrecht, the Netherlands  
<http://www.geo.uu.nl/~forth>

# Contents

Bibliography	8
Samenvatting (summary in Dutch)	9
Prologue	15
Chapter 1: Magnetostratigraphy-based astronomical tuning of the early Pliocene lacustrine sediments of Ptolemais (NW Greece) and bed-to-bed correlation with the marine record	21
Chapter 2: Cyclostratigraphy and $^{40}\text{Ar}/^{39}\text{Ar}$ dating of lower Pliocene lacustrine sequences of the Ptolemais Basin, NW Greece	41
Chapter 3: Magneto- and cyclostratigraphy and mammal-fauna's of the Pleistocene lacustrine Megalopolis Basin, Peloponnesos, Greece	69
Chapter 4: Dominant expression of eccentricity versus precession in the lithology of Mediterranean continental (lacustrine) deposits	93
Chapter 5: Improved precision of the Messinian APTS from sedimentary cycle patterns in the lacustrine Lava section (Servia Basin, NW Greece)	107
Chapter 6: Magnetostratigraphic dating of a Pliocene fluvio-lacustrine succession on Rhodes (Greece) and the recognition of astronomically forced sedimentary cycles	127
Chapter 7: Rock-magnetic properties of lignite-bearing lacustrine sediments from the Megalopolis and Ptolemais Basins (Greece) as possible climate proxies	143
Epilogue	157
Synopsis (summary in Greek)	159
Acknowledgements	161
Curriculum Vitae	163

# Samenvatting

De bewegingen van de Aarde om haar as en om de Zon zijn niet constant. Periodieke variaties zorgen voor klimaatsveranderingen op Aarde, zoals de ijstijden. In de geologie, vooral in sedimenten die afgezet worden op de zeebodem, in een meer of in een moeras, zien we zulke klimaatsveranderingen terug. Door nu deze sedimenten te bestuderen, kunnen geologen informatie over het klimaat van miljoenen jaren geleden terugvinden. Met die informatie kunnen nauwkeuriger voorspellingen gedaan worden over klimaatsveranderingen in de toekomst. Bovendien biedt de specifieke periodiciteit van de klimaatsvariaties de mogelijkheid om heel precies te bepalen hoe oud gesteentenlagen zijn.

## Zwalkende Aarde

De bewegingen van de Aarde worden beïnvloed door de aantrekkingskracht van andere planeten en de maan. De Aarde ‘zwalkt’ in feite over haar baan rond de Zon. Voor dit onderzoek waren twee van die zwalkende bewegingen belangrijk (zie Figuur 1). Ten eerste was dat de excentriciteit van de Aardbaan. De Aarde draait namelijk om de Zon in een baan die regelmatig van vorm verandert. Deze vorm verandert – van cirkel naar maximale ellips en terug – met perioden van ongeveer 100.000 en 400.000 jaar, en dit heeft invloed op het klimaat op Aarde. Wanneer de baan een cirkel is, is de afstand van de Aarde tot de zon gedurende het hele jaar constant, dus de Aarde ontvangt elke dag van het jaar evenveel warmte van de zon. Wanneer de aardbaan ellipsvorming is, staat de zon in één van de brandpunten van de ellips. De Aarde staat dan gedurende een deel van het jaar dichterbij de zon en ontvangt meer dan gemiddelde zonnestraling, en de rest van het jaar er juist verder vanaf. Gedurende het hele jaar ontvangt de Aarde 1 à 1,5% minder zonnestraling dan wanneer de baan cirkelvorming is.

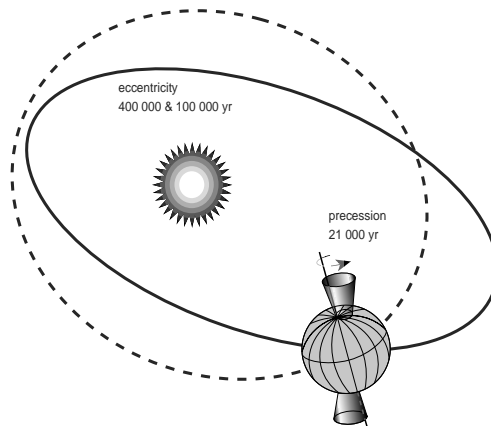


Figure 1. Eccentriciteit is de verandering in de baan van de Aarde om de Zon. Precessie is de tolbeweging van de rotaties van de Aarde.



Ten tweede kennen wij op Aarde seizoenen door de scheefstand van de rotatieas ten opzichte van het baanvlak van de Aarde om de Zon. Het is op het noordelijk halfrond zomer op 21 juni omdat de noordpool dan maximaal naar de zon toe gekeerd is, en op 21 december is de situatie omgekeerd. De rotatieas zelf beweegt ten opzichte van het baanvlak. Dit is vergelijkbaar met de beweging van een tol die bijna uitgedraaid is. Terwijl de tol zelf nog een behoorlijke draaisnelheid heeft, zie je de as een trage beweging maken, waarbij de top langs een cirkel beweegt, terwijl de punt op z'n plaats blijft. De rotatieas van de Aarde maakt deze beweging ook, waarbij het middelpunt van de Aarde stilstaat, en de twee polen in 21.000 jaar een cirkel beschrijven. Dus over 10.000 jaar staat de Aarde aan de andere kant van de Aardbaan wanneer de zomer begint.

Als de baan van de Aarde een perfecte cirkel zou zijn, zou dit verschuiven van de seizoenen verder geen invloed hebben op het klimaat. Maar omdat de aardbaan een ellips is, kan het dus gebeuren dat het op het noordelijk halfrond winter is als de Aarde het dichtst bij de zon staat, en dan zijn de winters zacht. Een half jaar later – als het zomer is – staat de Aarde het verst van de zon af. De zomers op het noordelijk halfrond zijn dan koel, en het ijs op de noordpool en in de bergen smelt dan bijna niet, zoals tijdens de ijstijden. In de omgekeerde situatie zijn de noordelijke winters streng, maar de zomers warm. Kortom, als de aardbaan een ellips is, veroorzaakt de precessie een cyclus van afwisselend veel en weinig contrast tussen de seizoenen. Als de aardbaan cirkelvormig is, heeft precessie weinig invloed, en is het contrast tussen de seizoenen steeds middelmatig.

## **Klimaatveranderingen vastgelegd in gesteenten**

Al deze astronomische bewegingen beïnvloeden het klimaat op Aarde. Ze veroorzaken bijvoorbeeld ijstijden, maar ook minder drastische klimaatveranderingen (van koel en droog naar warm en vochtig), die we allemaal terug kunnen vinden in gesteenten. In het Middellandse Zeegebied, bijvoorbeeld, zijn veel sedimenten uit de laatste vijf miljoen jaar te vinden. Een groot deel van die sedimenten zijn oorspronkelijk gevormd op de bodem van de Middellandse Zee, maar ze liggen nu op het land en zijn dus gemakkelijk te bestuderen. In die sedimenten is een regelmatig patroon van gekleurde lagen te zien. Dat patroon komt overeen met de periodieke variaties van beide astronomische bewegingen. We kunnen dus concluderen dat de samenstelling van het sediment beïnvloed is door het klimaat, dat cyclisch veranderde als gevolg van de astronomische bewegingen. De zee is dus eigenlijk een soort camera, met het sediment als film, die veranderingen in het klimaat opgenomen heeft. Door die film beeldje voor beeldje te bekijken – dus door het sediment laagje voor laagje te bestuderen – kunnen we de klimaatvariaties van vijf miljoen jaar geleden reconstrueren. Bovendien kunnen we de typische periode waarmee het klimaat verandert gebruiken om vast te stellen hoeveel tijd er nodig is geweest om een gesteentenlaag te vormen. Als we ergens een vast ijkpunt hebben – bijvoorbeeld de top van de zeebodem die overeenkomt met het heden – kunnen we zulke gesteentenlagen tellen en de ouderdom van een bepaalde laag nauwkeurig bepalen.

De variaties in het klimaat zijn op de bodem van de zee niet zo goed te merken als op het

land. De camera heeft als het ware een filter voor de lens zitten, die sommige zaken wel doorlaat, en andere niet. Om het totale plaatje te kunnen zien, moeten we ook naar films van andere camera's kijken. Die hebben een ander filter op hun lens, dat andere zaken tegenhoudt en doorlaat. Desondanks, door te combineren, wordt het beeld toch vollediger. In dit onderzoek hebben we sedimenten bestudeerd die niet op de bodem van de zee zijn gevormd, maar op het land, zodat het beeld van het klimaat completer kan worden. Ook kunnen we zo het effect van klimaatsveranderingen op verschillende soorten sedimentaire afzettingen gaan begrijpen, en kunnen de lagen van allerlei soorten gesteenten nauwkeurig gedateerd worden.

In dit proefschrift worden de resultaten beschreven van een onderzoek naar sedimenten die gevormd zijn in ondiepe meren en moerassen. De 'filters' van een meer of moeras zijn op twee punten minder handig dan die voor een diepe zee. Ten eerste is een meer of moeras veel ondieper, en kan makkelijk een periode droog vallen. Als het niet onder water staat, wordt er geen sediment bewaard – soms verdwijnt er zelfs sediment door erosie – en zit er in feite een 'haat' in de opname van het klimaat. Ten tweede is een meer of moeras vaak kleiner dan een zee, dus de rand is nooit ver weg. Lokale gebeurtenissen – die bij een zee alleen aan de rand invloed hebben – kunnen de opname van het klimaat in het meer- of moerasediment verstoren of zelfs verbergen. Een aardbeving kan bijvoorbeeld een aardverschuiving veroorzaken die de sedimentlagen in een meer door elkaar roert, zodat het oorspronkelijke patroon niet meer herkend kan worden. In dit onderzoek moesten we dus rekening houden met deze ongewenste verschijnselen. Dat hebben we gedaan door steeds verschillende verticale doorsneden (secties) te bekijken. De overeenkomsten tussen die secties zijn waarschijnlijk veroorzaakt door het klimaat, terwijl de verschillen een lokaal fenomeen suggereren. Ook kun je hiaten op deze manier vaak herkennen: omdat het moment van droogvallen en weer onderlopen vaak niet overal tegelijkertijd gebeurde, zie je dat de secties elkaar aanvullen.

Om te bewijzen dat de regelmatige lagen die we in de gesteentenlagen herkenden inderdaad veroorzaakt zijn door die astronomische klimaatsvariaties, moesten we aantonen dat iedere laag gemiddeld evenveel tijd vertegenwoordigt als zo'n typische astronomische periode. Die gemiddelde tijdsduur kun je uitrekenen als op een aantal niveaus in de sectie de precieze ouderdom bekend is. Die ouderdommen hebben we bepaald met magnetostratigrafie, de techniek die gebruik maakt van het patroon van de historische omkeringen van het aardmagneetveld. In het verleden is het aardmagneetveld herhaaldelijk en onregelmatig omgekeerd. Er is inmiddels precies bekend wanneer het naar het noorden en naar het zuiden wees. In gesteente zitten korreltjes die magnetisch zijn, en die zich dus gedragen als een kompasnaaldje. Zolang het gesteente zacht is, kunnen die korreltjes draaien, maar als het door hard geworden is, zitten ze vast. Door de magnetische richting van het sediment te meten, kun je dus bepalen welke lagen gevormd zijn in een noordgericht (normaal) magneetveld, en welke in een omgekeerd veld. De magnetische 'streepjescode' die zo ontstaat kan vergeleken worden met de bekende magnetische tijdschaal. De niveaus in het sediment waar de magnetische richting omkeert zijn dus tijdslijnen, waarvan we precies weten hoe oud ze zijn. Het aantal lagen tussen twee magnetische tijdslijnen gedeeld door de tijdsduur van het interval geeft de gemiddelde duur van een laag.

Doordat we nu precies wisten hoe oud het gesteente was, konden we het patroon van de sedimentlagen vergelijken met het patroon in de berekende, periodieke veranderingen in de astronomische bewegingen van de Aarde, en zo is van iedere laag precies bekend hoe oud die is. Ook konden we het sediment laag voor laag vergelijken met de even oude gekleurde lagen in de Middellandse Zee sedimenten.

## **Uitkomsten van dit onderzoek**

Voor dit proefschrift zijn drie fossiele meren op bovenstaande manier onderzocht en met elkaar vergeleken. Het sediment dat in deze meren is afgezet is nu goed te bestuderen doordat er dagbouw mijnen in gegraven zijn voor bruinkoolwinning.

Hoofdstuk 1 & 2: Bij Ptolemais in Noord Griekenland lag vier á vijf miljoen jaar geleden een ondiep meer, dat iedere twintigduizend jaar veranderde in een moeras. Dit werd veroorzaakt doordat bij een droger klimaat (veroorzaakt door astronomische bewegingen) het waterniveau van het meer zakte en riet de kans kreeg om het hele meer te overgroeien. In dit moeras was zoveel dood plantenmateriaal, dat er niet genoeg zuurstof was om het te verteren, zodat het in bruinkool kon veranderen. Na tienduizend jaar werd het klimaat weer vochtiger, en steeg het waterniveau in het moeras. Daardoor verdronk het riet en ontstond er weer een open meer waar kalk afgezet werd. We kunnen dit nu nog terug zien in een afwisseling tussen bruinkool en kalklagen (zie Figuur 2). Naast precessie kunnen we ook andere astronomische perioden herkennen in dit oude meer, maar veel minder duidelijk.

Hoofdstuk 3: Bij Megalopolis in Zuid Griekenland was een miljoen jaar geleden een ander soort meer, met een steile en een flauw hellende kant. Aan de steile kant spoelde zand en klei het meer in, aan de flauwe kant waren rietmoerassen. Als het klimaat warm en vochtig was, groeide het riet tot ver in het meer, en werd er in het hele meer veel organisch materiaal bewaard dat we nu terugvinden als bruinkool. Iedere honderdduizend jaar werden de zomers kouder en droger door de veranderende excentriciteit van de Aardbaan (er was dan een ijstijd in de Alpen en het noorden van Europa), waardoor het riet niet goed meer kon groeien. Sediment werd dan niet meer tegengehouden door planten en kon zo ver het meer in spoelen om klei- en zandbanken te vormen. Andere typische perioden kunnen we wel herkennen, maar het patroon wordt gedomineerd door de honderdduizend jaar afwisseling in excentriciteit.

Hoofdstuk 4: In het zuidwesten van Roemenië lag vier miljoen jaar geleden een meer dat heel erg veel leek op dat in Megalopolis. We vinden dezelfde afwisseling van bruinkool en klei, die ook hier gerelateerd is aan klimaatsveranderingen om de honderdduizend jaar, teweggebracht door excentriciteit. Vier miljoen jaar geleden waren er echter geen ijstijden, zoals o.a. in het even oude Ptolemais sediment is te zien, waar precessie (twintigduizend jaar) het patroon in het gesteente bepaalde.

Uit de verschillen en overeenkomsten tussen deze drie meren kunnen we opmaken dat niet het globale klimaatsregime (bijvoorbeeld wel of geen ijstijden) bepalend was voor de astronomische periode waarmee de gesteentelagen afwisselen, maar het soort meer.

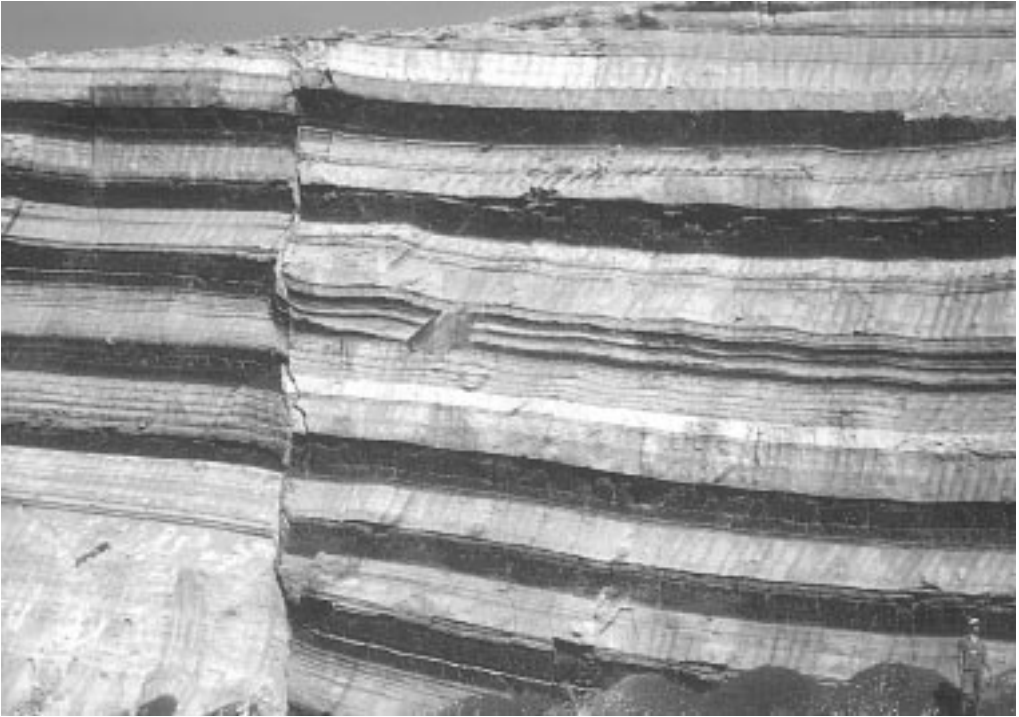


Figure 2. Regelmatige afwisseling van kool- en kalklagen in de mijnen van Ptolemais in Griekenland. De lagen zijn ongeveer 1 m dik.

Honderdduizend jaar is dominant in meren met veel klei- en zandaanvoer, waar de hoeveelheid begroeiing bepalend is, en twintigduizend jaar is dominant in kalkmeren, waar het meerniveau bepalend is.

Hoofdstuk 5: Onder het sediment in Ptolemais dat in hoofdstuk 1 & 2 beschreven is, ligt nog ouder meersediment, dat met name aan de randen van het bekken goed te zien is, bijvoorbeeld in de mijn bij het dorpje Lava. Dit meer onderging ook veranderingen veroorzaakt door periodieke klimaatsvariaties, maar veel minder extreem dan de eerder genoemde meren. Fysische eigenschappen van het sediment die we in heel veel lagen gemeten hebben laten daardoor ook een subtiel veranderende curve zien. Met zo'n curve konden we kwantitatief vaststellen dat er ook in dit meer periodieke veranderingen in het sediment zitten die veroorzaakt zijn door precessie.

Hoofdstuk 6: Ook in Rhodos, in een bekken van 3 à 4 miljoen jaar oud met heel grof sediment (veel zand en grind) was een regelmatige afwisseling te zien in de lagen. Deze is veroorzaakt door een regelmatige verandering in het bekken van een moerassig meer waar veel planten in groeiden via een ondiep open meer naar de delta van een rivier. Met behulp van paleomagnetisme konden we aannemelijk maken dat de 30 meter dikke afwisselingen dezelfde periode hebben als precessie. Het patroon was echter niet duidelijk genoeg om het precies te vergelijken met de astronomische bewegingen.

Hoofdstuk 7: Tenslotte hebben we gekeken of magnetische eigenschappen geschikt zijn om klimaatsveranderingen vast te leggen, zoals uit diverse onderzoeken is gebleken. Zowel in Ptolemais als in Megalopolis is gebleken dat er geen verband is tussen de sediment afwisselingen en de gemeten magnetische eigenschappen.

Met dit onderzoek is de basis gelegd voor een veelheid aan vervolgonderzoek in deze sedimenten. Doordat nu precies bekend is hoe oud iedere laag is en hoeveel tijd er in een laag vertegenwoordigd is, kunnen de in het sediment geregistreerde klimaatsveranderingen in verschillende secties vergeleken worden. Op termijn kunnen we op die manier gaan begrijpen hoe variaties in de baan van de aarde klimaatsveranderingen veroorzaken.

# Prologue

Geologists want to unravel the long and complicated history of the Earth. Thus, they need to understand the concept of time. Relative time control through superposition enables to discover the order of occurrence of geological processes. Absolute age data are needed to study the duration of geological processes, a requirement to understand the underlying mechanisms. The range of tools for obtaining age control has improved and expanded over the past centuries.

Already in the seventeenth century, Steno laid the foundation for stratigraphy by putting forward his principle of superposition. He stated that when a sedimentary layer is deposited, it must be deposited on top of the underlying layer, which must thus be older (Steno, 1669). Fossils found in the sediments could be used to correlate strata that contained the same fossils over large distances, thereby implicitly assuming that extinctions and first occurrences are synchronous events. Hence, biostratigraphy has grown into a very successful dating tool, especially for marine sediments which have abundant, often globally occurring microfossils. A major breakthrough in the perception of geological time came when the creationist Hutton shifted the paradigm of the limited biblical time scale to a virtually 'eternal' earth (Hutton, 1795–1899). Now every imaginable geological process, however slow, was feasible. A physical restriction to this eternity came shortly after the discovery of radioactive minerals by Becquerel. Since 1906, the radioactive decay of suitable isotopes is used to determine the time elapsed since the formation of a mineral, and provides us with a measure of the absolute age of rocks – and of the Earth itself. Of course, these minerals should have formed at the same time as the rocks they are part of. This is not always the case; sediments, for example, consist of minerals that are older than the time of deposition.

In 1954, magnetostratigraphy was added to the scope of geological dating methods (Hospers, 1954). Iron bearing minerals in rocks can record the direction of the ambient magnetic field, and preserve this 'palaeomagnetic' information over geological time. In the beginning of this century it was discovered already that certain rocks had palaeomagnetic directions parallel to the present-day field, while others, of a different age, were magnetised in the opposite direction (Brunhes, 1906; Matuyama, 1929). This was caused by frequent reversals of the Earth's magnetic field during the geological past. The global and simultaneous character of magnetic polarity reversals makes them very suitable as time markers. Integration of these magnetic data and radiometric dating led to the first geomagnetic polarity time scale (GPTS) (Cox et al., 1963), that has been revised and updated many times since (e.g. Cande and Kent, 1995).

The accuracy and detail of the geological time scale was recently greatly improved with a new technique: astronomical tuning. The hypothesis that regular variations in the Earth's orbital parameters cause climate cycles that are recorded in the geological archive was already put forward in the previous century, at first related only to the Pleistocene ice ages (Adhémar, 1842; Croll, 1864). This astronomical theory of the ice ages was put on a firm mathematical basis by the Serbian civil engineer Milutin Milankovitch (1941). He calculated the orbital motion of the Earth over time, based on the influence of the gravitational forces

of the Sun, the Moon and the planets. From that, he derived the amount of solar radiation (insolation) received over the Earth during the summer. This calculated insolation was dominated by the frequencies related to eccentricity, obliquity and precession. His theory initially seemed to be confirmed by a good correlation with Alpine river terraces that were attributed to glacial periods. However, these terraces later proved to be of tectonic origin and have much younger ages than initially inferred, one of them even containing a rusty bicycle frame. Moreover, (often incorrect) radiometric age determinations were inconsistent with Milankovitch's predicted glacial and interglacial periods, and the theory was strongly disputed. Improved radioactive dating, the combination of magneto- and biostratigraphy and the study of more complete records clarified the Pleistocene time scale by the late 1960's. This brought forward the major discovery that the oxygen isotope ratios of foraminifera – which is an indication of the amount of land ice at the time these fossils were living – from deep-sea cores were undoubtedly related to the astronomical periods of Milankovitch (Hays et al., 1976; Shackleton and Opdyke, 1973). More recently, the same periods were also recognised in older, pre-ice age times. (Herbert and Fisher, 1986; Olsen, 1986; Shackleton et al., 1990). These periods are expressed as regular fluctuations in climate-sensitive physical or chemical parameters or as cyclic sedimentary layers. A succession of astronomically forced sedimentary cycles can then be correlated in detail to a calculated insolation curve, as was suggested already in 1895 by Gilbert (1895). This has evolved into an astronomically tuned (polarity) time scale (APTS) for the last 10 million years (Shackleton et al., 1990; Hilgen, 1991; Shackleton et al., 1995; Hilgen et al., 1995; Lourens et al., 1996), that proved to be much more precise and accurate than previous time scales (Wilson, 1993; Renne et al., 1994). The APTS is mainly based on marine records, because they tend to be more continuous in both lateral and stratigraphic sense, and because they contain more or less uniform global fossil foraminiferal transitions. Especially Mediterranean sections proved to be suitable, because the sediments in this semi-enclosed marine basin are particularly susceptible to astronomically induced climate cycles.

Hence, cyclostratigraphy has improved the geological time scale, but more importantly, it has furthered our knowledge of climate changes. However, the mechanisms behind the forcing of climate cycles are not fully understood yet. The climatic response to the astronomical cycles is often not linear and affected by oceanic feedback processes. Moreover, marine sediments record a signal not only of local climate changes, but also of global oceanic variations. Valuable additional information for unravelling climatic forcing mechanisms must thus be found in continental environments. These environments are more perceptible to external controls such as climate. On the other hand, influences such as local basin architecture, tectonics and biological events are recorded much better as well, and might thus overprint or obscure the climatic signal. Furthermore, continental records are often thought to be discontinuous and highly variable in a lateral sense, a big handicap for studying series of lithological cycles. Still, incorporating continental records into the astronomically tuned time scales and palaeoclimate databases will be indispensable for a good understanding of (astronomically forced) climate changes.

## Summary of the present work

A multi-disciplinary research program at the Faculty of Earth Sciences in Utrecht aimed at a correlation of the continental and marine realm from the Mediterranean Neogene. The objective was to compare lithological patterns and forcing characteristics, and to unravel the process of astronomical forcing of climate. The expertise in magnetostratigraphy, cyclostratigraphy, sedimentology, palaeontology, palynology, isotope chemistry and organic chemistry is combined to characterise continental basins. This thesis reports on the first phase of the program: time control through providing an astronomically tuned cyclostratigraphic frame for the studied continental records.

The continental sedimentary basins for this study had to meet several criteria. First of all, they need to be time-equivalent to the (astronomically tuned) marine sections in the Mediterranean, and thus of Late Miocene, Pliocene or Pleistocene age. Secondly, they must display a regular sedimentary pattern likely to be proven as an expression of astronomically forced climate cycles. Finally, the sediments have to be exposed in sufficiently large outcrops to apprehend lateral variations in the cyclic pattern and discover possible unconformities. All these criteria were met in open pit coal mines in Greece and Romania – where rhythmic coal seams are perfectly exposed over large distances – and in regularly layered coastal badlands in southern Rhodes

The research strategy proceeded as follows. A first-order age estimate from regional geology and (small mammal) fossils was established, then detailed age calibration points were found by means of magnetostratigraphy and – if possible – radiometric dating. Following this second order time control, a cyclostratigraphic framework for the basin fill was constructed. We then demonstrated that astronomical periods were present in these sedimentary cycles and established the relation between the lithological and astronomical phases. Finally, the lithological cycle pattern was tuned to an astronomical target curve, resulting in a highly accurate time frame.

Our work started in the Lower Pliocene lignite mines of Ptolemais in northern Greece. Meter-scale lignite and carbonate beds alternate in a regular pattern. Three parallel sections provided ample data to compose the magnetostratigraphic (**Chapter 1**) and cyclostratigraphic frame (**Chapter 2**). This enabled us to prove that precession forced the sedimentary cycles. Initially, the phase relation was not clear, causing two opposing models. We found inconsistencies in the tuning of one model, and coherence in the other model. Therefore, we interpreted that lignite layers represent minima, and carbonate layers maxima in solar radiation. Additional palynological and organic petrological studies showed that the lignite was accumulated in a swamp, and the carbonate beds in a deeper lake. This implies an increase in precipitation during periods with warmer summers, and confirms earlier observations in the Mediterranean of increased humidity during insolation maxima. Each cyclic layer was correlated to a peak in the summer insolation curve, and thus to the marine reference section, except for a small interval in the middle of the Ptolemais succession.

To obtain an additional, independent age control, several of the intercalated volcanic ash layers in Ptolemais were radiometrically dated. These ages essentially confirm the precessional forcing, but the absolute ages are systematically 100–200 kyr younger than the magnetostrati-



graphic ages. An attempt at tuning the cycles with the radiometric ages as tie points failed because the patterns did not match. We discuss this discrepancy in more detail in **Chapter 2**. The second study area was the Pleistocene Megalopolis basin in southern Greece, also a lignite mine (**Chapter 3**). In contrast to Ptolemais, the sediment in Megalopolis is composed of detrital material (clay, silt, sand) alternating with lignite, and the layers are ~10 meters thick. Thinner lignite cycles occur in between the main lignite seams. Combined bio- and magnetostratigraphy resulted in only one time control point: the base of the present normal polarity Brunhes Chron. Palynological data suggest a climatic origin for the sedimentary cycles that can be related to glacial-interglacial alternations. It appears that the pattern of the main sedimentary cycles fits well with eccentricity, and the smaller cycles with insolation. Here, the lignite represents the warm phase (maximum in eccentricity or insolation). Despite the good fit with eccentricity, we found that some discrepancies exist in comparison with marine  $\delta^{18}\text{O}$  records (the so-called '400-kyr' or 'Stage 11' problem). We suggest that the sedimentary record of Megalopolis, and therefore the local climate, was influenced directly by eccentricity, and not by the global Pleistocene glacial climatic regime.

From a third lignite basin in Romania, we studied the early Pliocene Lupoia section (**Chapter 4**), which is time-equivalent to Ptolemais, but has a sedimentary environment similar to the middle Pleistocene Megalopolis section. Magnetostratigraphy yielded three age calibration points that connects the lignite seams with eccentricity maxima, as in Megalopolis. Based on these three studies on lignite basins, we conclude that the astronomical period that was dominantly recorded in the sediment is determined by the sedimentary environment, rather than by the global climatic regime (**Chapter 4**).

The link between astronomical forcing and sedimentation was further explored in the Messinian lacustrine deposits from the southern margin of the Ptolemais Basin (Chapter 5). A small mine with a massive lignite seam at the base provides access to a succession of lacustrine marls with regularly intercalated dark-coloured marl layers. Gamma ray and magnetic susceptibility records quantify these subtle lithological changes. The fine-grained marl yielded a good palaeomagnetic signal. Together with the small-mammal fauna, this provided accurate age control and allowed spectral analysis of the gamma ray and susceptibility records. This showed that the lithological cycles have the same period as precession, and that obliquity also influenced the record. Palynological data suggest that the dark-coloured layers represent periods of decreased humidity. Correlation of the cycles to the insolation curve results in precise ages for the recorded polarity reversals, that confirm and refine the astronomical polarity time scale for the Messinian.

The hypothesis that sedimentary cycles in continental successions can be astronomically forced was finally tested in the relatively high-energy environment of the middle Pliocene fluvio-lacustrine Apolakkia Formation on Rhodes (**Chapter 6**). The basic sedimentary cycle in this formation is recognised in two of the three studied sections. The base of a cycle is formed by a palustrine facies association with mainly organic-rich marl, that gradually changes into a shallow lacustrine facies. The top is formed by coarse grained sand and conglomerate beds of a delta-plain association. Based on the magnetostratigraphy, it is likely that the cycles were forced by precession. Since no typical modulation pattern was recognised in the cycles, no attempt was made at tuning them to the insolation curve.

Another aim of this research was to assess the potential of magnetic parameters to serve as climate proxies. Many magnetic parameters can be measured relatively quickly compared to conventional climate indicators, and several reports have been published that they can reliably record climate changes. The successions from Ptolemais and Megalopolis – well-understood in terms of palaeoclimatic cycles – were therefore ideal to test the potential of magnetic parameters as climate proxies (**Chapter 7**). We found that in Ptolemais the magnetic characteristics were not related with lithology. In Megalopolis, a strong secondary magnetic phase was discovered, carried by greigite. This greigite was found to be abundant in clay and absent in lignite or organic-rich lithologies. Despite this clear relation with absolute lithology, no relation was found with the phases of the sedimentary cycles.

- Adhémar, J.A., 1842. Révolutions de la mer. *privately published*.
- Brunhes, B., 1906. Recherches sur la direction d'aimantation des roches volcaniques. *J. Phys.* 5, 705-724.
- Cande, S.C. and Kent, D.V., 1995. Revised calibration of the geomagnetic polarity time scale for the Late Cretaceous and Cenozoic. *Journal of Geophysical Research* 100, 6093-6095.
- Cox, A.V., Doell, R.R. and Dalrymple, G.B., 1963. Geomagnetic polarity epochs and Pleistocene geochronometry. *Nature* 198, 1049-1051.
- Croll, 1864. On the physical cause of the change of climate during geological epochs. *Phil. Mag.* 28, 121-137.
- Gilbert, G.K., 1895. Sedimentary measurement of geological time. *J. Geol.* 3, 121-127.
- Hays, J.D., Imbrie, J. and Shackleton, N.J., 1976. Variations in the Earth's orbit: pacemaker of the Ice Ages. *Science* 194, 1121-1132.
- Herbert, T.D. and Fisher, A.G., 1986. Milankovitch climatic origin of mid-Cretaceous black shale rhythms, central Italy. *Nature* 321, 739-743.
- Hilgen, F.J., 1991. Astronomical calibration of Gauss to Matuyama sapropels in the Mediterranean and implication for the Geomagnetic Polarity Time Scale. *Earth and Planetary Science Letters* 104, 226-244.
- Hilgen, F.J. et al., 1995. Extending the astronomical (polarity) time scale into the Miocene. *Earth and Planetary Science Letters* 136, 495-510.
- Hospers, J., 1954. Magnetic correlation in volcanic districts. *Geological magazine* 91, 352-360.
- Hutton, J., 1795-1899. Theory of the Earth, with proofs and illustrations. *Cadell Junior and Davies, London* 1 & 2.
- Lourens, L.J. et al., 1996. Evaluation of the Plio-Pleistocene astronomical timescale. *paleoceanography* 11, 391-413.
- Matuyama, M., 1929. On the direction of magnetisation of basalt in Japan, Tyosen and Manchuria. *Japan. Acad. Proc.* 5, 203-205.
- Milankovitch, M., 1941. Kanon der Erdbeustrahlung und seine Anwendung auf das Eiszeitenproblem. *Royal Serbian Academy, Special Publication* 133, 1-633.
- Olsen, P.E., 1986. A 40-million-year lake record of Early Mesozoic orbital climatic forcing. *Science* 234, 842-848.
- Renne, P.R. et al., 1994. Intercalibration of astronomical and radioisotopic time. *Geology* 22, 783-786.
- Shackleton, N.J., Berger, A. and Peltier, W.R., 1990. An alternative astronomical calibration of the lower Pleistocene timescale based on ODP Site 677. *Transactions of the Royal Society of Edinburgh: Earth Sciences* 81, 251-261.
- Shackleton, N.J., Crowhurst, S., Hagelberg, T., Pisias, N.G. and Schneider, D.A., 1995. A new Late Neogene time scale: application to leg 138 sites. *Proceedings of the Ocean Drilling Program, Scientific Results* 138, 73-97.
- Shackleton, N.J. and Opdyke, N.D., 1973. Oxygen isotope and paleomagnetic stratigraphy of equatorial Pacific core V28-238: Oxygen isotope temperatures and ice volume on a 105 and 106 year scale. *Quat. Res.* 3, 39-55.

P r o l o g u e

Steno, N., 1669. De solido intra solidum natvraliter contento dissertationis prodromus ... *Florence: Ex Typographia Sub Signo Stellae.*

Wilson, D.S., 1993. Confirmation of the astronomical calibration of the magnetic polarity time scale from sea-floor spreading rates. *Nature* 364, 788-790.

# Magnetostratigraphy-based astronomical tuning of the early Pliocene lacustrine sediments of Ptolemais (NW Greece) and bed-to-bed correlation with the marine record

## Abstract

Continental deposits from the early Pliocene lacustrine Ptolemais basin in NW Greece display rhythmical alternations of lignite and marl beds. Three parallel sections from this area are studied using magnetostratigraphy and cyclostratigraphy. The presence of the greater part of the Gilbert Chron enables the recognition of astronomical periodicities in the succession. Especially the precessional influence is evident, as it determines the lithological cycles. The continental Ptolemais composite section is correlated to the most recent astronomical time scale - and thus to the marine reference section: the Rossello composite from Sicily (Langereis et al., 1991) - on a bed-to-bed scale. It is concluded that lignite corresponds to an insolation minimum (beige layer in the Rossello composite), and marl to an insolation maximum (grey layer in the Rossello composite). This implies a precipitation increase during insolation maxima in early Pliocene continental Greece.

*This chapter is published as: van Vugt, N., Steenbrink, J., Langereis, C.G., Hilgen, F.J. and Meulenkamp, J.E., 1998. Magnetostratigraphy-based astronomical tuning of the early Pliocene lacustrine sediments of Ptolemais (NW Greece) and bed-to-bed correlation with the marine record, Earth and Planetary Science Letters 164(3-4), 535-551.*

## Introduction

Palaeoclimate and -environment reconstructions are a key to understanding modern climate changes, and geological deposits are a natural archive for past climate. The Milankovitch climatic periodicity, for example, can be recognised as cyclic patterns in the lithology of sediments. Hilgen (1987) studied such patterns in Mediterranean Neogene marine records. Individual sapropels and carbonate cycles in the Trubi and Narbone Formations were correlated to precession cycles (Hilgen, 1991a; 1991b) and later to peaks in the summer insolation curve (Lourens et al., 1996) using the La90 solution (Laskar, 1990). Shackleton et al. (1995) obtained similar results in the Pacific Ocean by matching gamma-ray variations in deep sea cores to the Ber90 insolation time series (Berger and Loutre, 1991).

For a better understanding of the climatic response to astronomical parameters, the continental record should be studied as well. Lacustrine sediments in particular can give valuable information on the palaeoclimate and -environment, as demonstrated by Kent et al. (1995) and Olsen et al. (1996) in the Triassic Newark Basin. The sedimentary cycles they studied have frequencies similar to the present day values for astronomical variables. However, there is no reliable astronomical solution for the Triassic to establish a detailed correlation, nor is there a time-equivalent marine record to compare the climatic response with.

We have started an extensive programme to make bed-to-bed correlations between continental and marine sediments in the Mediterranean, in particular to the Rossello Composite (Langereis et al., 1991), which is the basis for the Pliocene astronomical polarity time scale (APTS) (Hilgen 1991a; 1991b; Lourens et al. 1996). One of the main goals of this programme is to reconstruct the palaeoclimate and -environment of the Neogene, both in the marine and continental realm. So far, we have focused on the lacustrine, rhythmically bedded lignite and marl alternations in Ptolemais, Northern Greece. The purpose of this article is to provide a magnetostratigraphic framework for the Ptolemais basin fill and, - with the cyclostratigraphic frame provided by Steenbrink et al. (1999) - correlate the lithological cycles with the marine record and a suitable astronomical time series. Together with the sedimentological study and the  $^{40}\text{Ar}/^{39}\text{Ar}$  ages (Steenbrink et al., 1999) this will be the basis for further palaeoclimate studies on the Ptolemais area.

## Geological setting

The elongated palaeolacustrine basin of Ptolemais is located between Florina and Kozani, approximately 100 km west of Thessaloniki (Figure 1). It is part of a 250-km long graben system that opened in the Late Miocene and was divided into sub-basins in the Pleistocene (Mercier et al., 1989; Pavlides et al. 1986). Displacement along normal lystric faults related to this Pleistocene tectonic phase caused a bedding tilt of up to  $15^\circ$  NNW. The basement consists of metamorphic schists in the west, and crystalline limestone in the east (Kaouras, 1989). Large-scale lignite quarries in the eastern half of the basin provide expansive unweathered outcrops. The three studied sections are named after the pits in which they were located: Vorio, Komanos and Tomea Eksi (Figure 1).

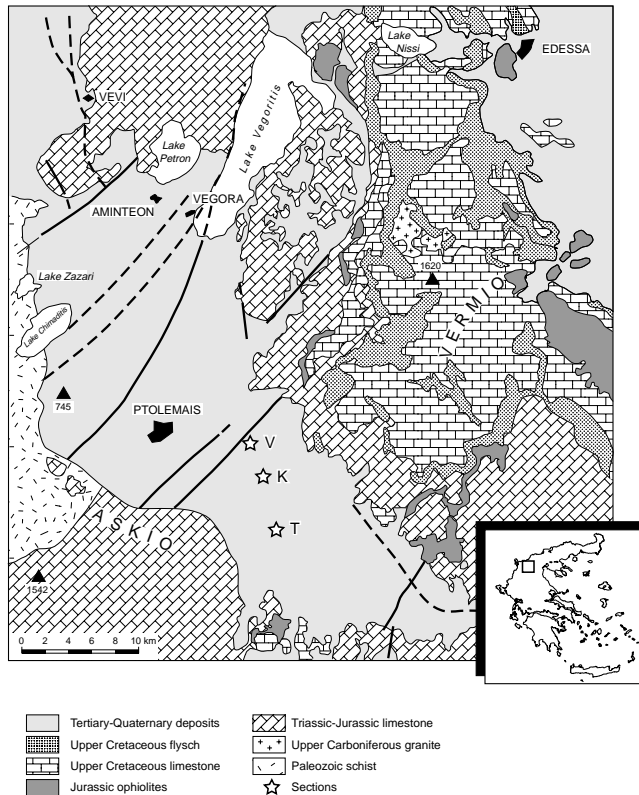


Figure 1. Geological sketch map of the Ptolemais basin. V (K, T) is location of Vorio (Komanos, Tomea Eksi) section (after Papakonstantinou, 1979).

The basin fill has been divided into three formations: the Lower Formation, the Ptolemais Formation and the Upper Formation (Ehlers, 1960). The Lower Formation overlies the crystalline basement, and is composed of lacustrine carbonate-rich marls. Only the top of this formation is exposed. The Upper Formation consists of fluvio-lacustrine marls with intercalated clay, sand and conglomerate beds.

Of main interest to this study is the Ptolemais Formation, that was dated as early Pliocene (Early Ruscinian, MN Zones 14 and 15) on the basis of palaeontologic data from small mammals (van de Weerd, 1978; de Bruin, pers. comm.) and gastropods (Gramann, 1960). The Ptolemais Formation is subdivided into three members: the Kyrio, Theodoxus and Notio member (from bottom to top). The lowermost (Kyrio) member typically shows a rhythmic alternation of lignite and organic-rich grey marl beds, forming 30 lithological couplets with an average thickness of 2 m. In few localities, however, massive lignites without marl represent the Kyrio member. In the middle (Theodoxus) member, white marls alternate with thin lignites or dark grey organic-rich marls. One thick lignite layer divides this member in two. Because of the large lateral changes in bed-thickness and lithological

expression, the rhythmic pattern is not as clear as in the other members. We estimate that there are six cycles with a typical thickness between 4 and 6 m each. The uppermost (Notio) member features nine of the same couplets as the Kyrio member, followed in one section by 11 couplets in which the lignite phase is represented by a dark brown clay bed, and in other sections by banded xylite. The couplets in the entire Ptolemais Formation can be recognised and correlated across most of the basin. Intercalated volcanic ash layers verify this correlation, and show that the rhythmic alternations are synchronous. They represent basin-wide lithological changes rather than lateral facies shifts (Steenbrink et al., 1999). We labelled the couplets in each member with a number, ascending towards the top (K1-30, T1-6 and N1-20).

The lithology of the Theodoxus and Notio members in the Komanos quarry differs from that in the two other sections. Starting gradually and laterally discontinuous from cycle K28 upwards, the lignites are replaced by thin brown horizons, and instead of grey marls we found beige marls lacking any organic material and with a loose, brittle texture. Samples from this part tend to break into little pieces shortly after retrieving them or during laboratory treatment. The likely cause for this alteration is oxidation of the organic material during deposition of overlying layers.

Above cycle K13 in Tomea Eksi, the regular alternation is disturbed by lens-shaped layers cutting into the underlying sediment, indicating unconformities. The first recognisable lithological cycle above this interval is K23. In Komanos, we find field evidence for a hiatus in approximately the same interval; a shallow scouring surface between cycles K18 and K19 is a sign for erosion, the thin palaeosol on top of this surface is interpreted as a period of non-deposition. For a more detailed (cyclo)stratigraphic description we refer the reader to (Steenbrink et al., 1999).

## Sampling and laboratory methods

The three parallel sections, Vorio, Tomea Eksi and Komanos, in the Lower and Ptolemais Formations were sampled for palaeomagnetic studies (see Figure 1 for locations). An electrical drill was used to take oriented rock samples with a diameter of 2.5 cm. In the laboratory, these cores were cut into specimens with a length of 2.2 cm. The average stratigraphic distance between the sampling sites was 40 cm. Intervals around polarity reversals were later re-sampled with sampling intervals as small as 2 cm. Non-lignite lithology was preferred, because we knew from test samples that pure lignite does not give meaningful palaeomagnetic results. The outcrops in the mines were less than a year old, so hardly any digging was necessary to reach the unweathered rock. The lithology and thickness of the layers and the position and orientation of the samples were minutely recorded in field journals.

Bulk susceptibility was measured on a KLY-2 Kappa bridge. The natural remanent magnetisation (NRM) was measured on a 2G SQUID cryogenic magnetometer. Specimens with a negative (diamagnetic) susceptibility and an NRM below  $10 \mu\text{Am}^{-1}$  were discarded because test samples did not give consistent magnetic directions in this situation. The lignitic samples were progressively demagnetised in an alternating field (AF) up to 125 mT. The other

samples were thermally demagnetised with temperature increments of 30 and 50°C, up to 570°C. The delicate samples from the top of the Komanos section were exposed to alternating field treatment to prevent them from falling apart during demagnetisation. Twenty samples were progressively magnetised in a DC pulse field to acquire an isothermal remanent magnetisation (IRM). After each step, the remanence of the samples was measured on a JR5 spinner magnetometer. After saturation, the IRM was thermally demagnetised, and susceptibility was measured after each temperature increment.

## Results

### *Magnetic properties*

Many low-intensity samples did not give any sensible result, and were therefore discarded. The description of the characteristics of the remaining samples is divided in thermal and alternating field treatment.

Thermal demagnetisation generally reveals two non-viscous NRM-components (a viscous component is removed at 150–200°C): a characteristic, normal or reversed component that decays towards the origin until ~390°C, and a low intensity component that does not decay, but forms a cluster near the origin above ~500°C (Figure 2a), often in the direction west/down. The susceptibility increases at ~390°C, and decreases again after ~520°C. A small number of samples, with high intensities, have only one component above 200°C, that reaches its maximum unblocking temperature at ~500°C (Figure 2b). Many samples show a large intensity decrease between 150 or 200°C and 230°C followed by no decay until 320°C. This is caused by an exothermal reaction of the organic material in the rocks during heating. This reaction caused the samples to reach temperatures as high as 320°C, although the furnace was set at 230°. Consequently, the intensity decreased according to the actual (higher) temperature, and no further decrease would occur in the next steps, until the previously reached temperature was exceeded. Around polarity reversals, some samples have a high temperature (HT) component (between 350–390 and 540°C) with a polarity opposite to the lower temperature component (Figure 2c). Although the unblocking temperature spectra generally overlap, the two polarities can be separated.

Alternating field demagnetisation shows two types of behaviour. In both types a viscous component is removed at 5–15 mT. The most common type I (Figure 2d) reveals a single characteristic magnetisation that is fully demagnetised at 60/80 mT. Near reversals, the magnetisation sometimes contains two components, a low coercivity (LC: 15–25/40 mT) and a high coercivity component (HC: 25–60/80 mT), with opposite polarities and overlapping coercivity spectra (Figure 2e). The other type (II) only occurs in the Komanos section, and mainly in the top part of this section. The magnetic remanence is fully demagnetised between 80 and 125 mT (Figure 2f). Generally, only one component can be recognised in these samples, but occasionally two directions with opposite polarities can be seen (Figure 2g). Type-I intensity-decay curves are concave, with a large intensity decrease at low coercivities and a small decrease at higher coercivities (Figure 2h). The intensity of type II samples decreases more linearly (Figure 2h).



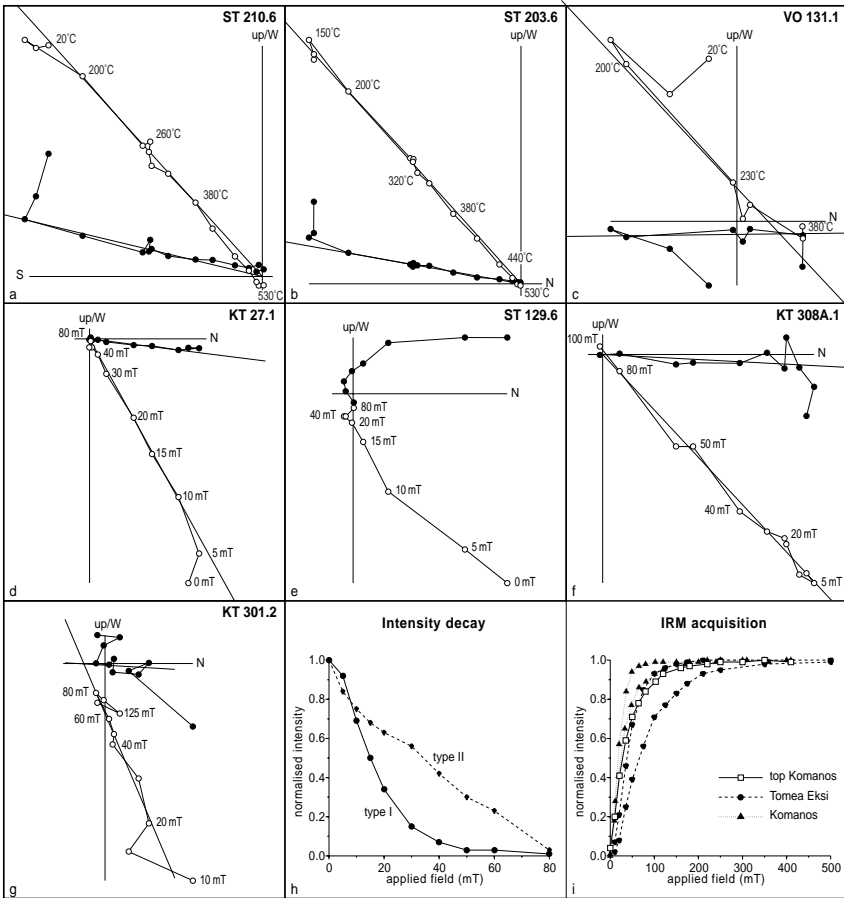


Figure 2. Demagnetisation diagrams. Closed (open) circles denote the projection on the horizontal (vertical) plane. For details see text. Figure 2h is an intensity decay curve during alternating field demagnetisation of a typical type I and type II sample (see text for discussion). Figure 2i shows IRM acquisition diagrams of some characteristic samples. Typically, saturation is reached at fields of 100-200 mT; only occasionally higher fields (up to ~400 mT) are needed. The top part of Komamos consistently shows higher than average saturation fields.

In summary, samples with HT/LT (HC/LC) components with opposite polarities occur near reversals. In the same intervals, consecutive samples may have different polarities, even when they have only one component. This can only mean that these directions were not acquired simultaneously. van Hoof and Langereis (1991) described similar features in the marine Rossello composite section from Sicily. They concluded that their LT component was of earlier origin, whereas their HT component was acquired later, during early diagenesis. This 'delayed acquisition' was caused by cyclically changing redox conditions in the buried sediment. In Ptolemais, however, the pattern is not as consistent as on Sicily. Instead of one component carrying the earlier direction (LT), and the other the delayed one (HT),

we find a seemingly random connection between the characteristics of a component (HT vs. LT or HC vs. LC) and its polarity. Nevertheless, the exact position of a reversal is determined by those intervals in which the HT and LT (HC and LC) consistently have the same polarity, meaning that a reversal is always positioned on top of an interval with mixed polarities.

Most samples reach IRM-saturation at fields between  $\sim 125$  and  $\sim 200$  mT, but saturating fields up to 500 mT are occasionally encountered (Figure 2i). Together with the maximum unblocking temperatures and coercive forces, this indicates that (titano) magnetite and/or iron sulphides could carry the NRM. The type-II samples from the top of Komanos consistently saturate at higher than average fields (Figure 2i), suggesting the NRM is carried by an oxidised magnetite.

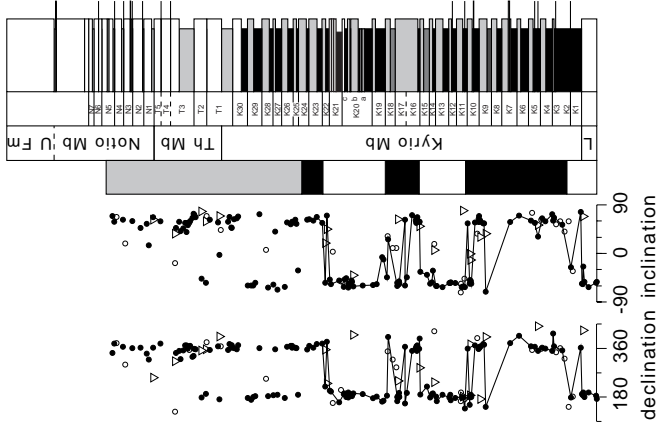
### *Magnetostratigraphy*

The magnetic directions derived from the demagnetisations are plotted versus stratigraphic level for each section, with respect to the cyclostratigraphic frame for the Ptolemais Formation (Figure 3). The Vorio section reveals two normal polarity intervals, one in the lower half of the Kyrio member - containing the distinctive ash layer in cycle K7 - and one in the Notio member. In the middle part of Vorio, where the lithology consists of lignite only, both normal and reversed samples occur more or less at random; we regard the polarity pattern for this interval as inconclusive. In the Tomea Eksi section, we recognise the same two normal intervals. In addition, we find another two normal intervals in the middle (above K14) and top (around K23-28) of the Kyrio member. At the transition between the Theodoxus and Notio members we found no reliable data. All samples in the top 50 m of the Lower Formation (not completely shown in Figure 3) recorded reversed polarity. In the Komanos section, we find a matching polarity pattern in the largest part of the Kyrio member, with the three normal intervals approximately around the same cycles (see also Table 1). In the top of the section, where the lithology and magnetic properties are different from those in the rest of the basin fill, the polarity pattern is not consistent with the two other sections. Based on field observations and analysis of the demagnetisation and IRM-acquisition diagrams, we suggest that the organic material has been oxidised after deposition and burial, thus changing the mineralogy. The newly formed or altered magnetic minerals in the sediment are then (re)magnetised and preserve a younger remanence, with possibly a different polarity. The palaeomagnetic results of the upper half of the Komanos section are therefore not used for the construction of a composite magnetostratigraphy.

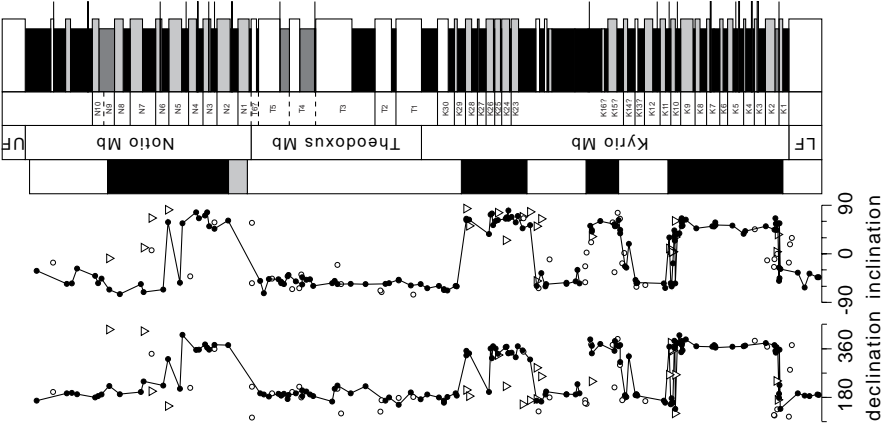
### *Ptolemais composite section*

Through careful comparison of outcrops throughout the mining area, local features are separated from consistent (i.e. laterally continuous) patterns. These consistent cycle patterns are used to construct a cyclostratigraphic composite section for the Ptolemais basin (Figure 5a), see (Steenbrink et al., 1999) for details. The palaeomagnetic results of the different sections are integrated into a polarity pattern for the composite section. Because we find clear indications for delayed acquisition, we consider the position of each polarity boundary in the composite section to be at the highest (youngest) level with consistent polarity (Table 1).

KOMANOS



TOMEA EKSI



VORIO

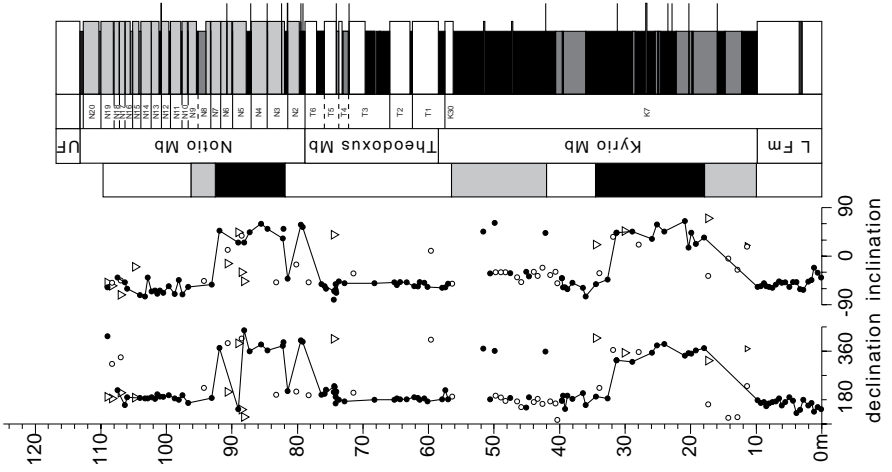


Figure 3. Palaeomagnetic results, polarity zones, stratigraphic names, cycle numbers and lithology of three Ptolemais sections. Closed (open) circles denote reliable (less reliable) characteristic components; triangles denote high-temperature or high-field components. In the polarity column, black (white) indicates normal (reversed) polarity, while shaded indicates undetermined polarity. In the lithological column, black (shaded) indented beds denote lignite (marly/clayey equivalent of lignite) beds, shaded (white) protruding beds denote grey (beige) marl beds; thin extra protruding layers denote volcanic ash layers and dark-shaded layers in the Kyrio Mb. in Vorio denote sand lenses.

The resulting composite Ptolemais magnetostratigraphy reveals four normal and five reversed intervals. Because the Ptolemais Formation was deposited during the early Pliocene (van de Weerd, 1978; de Bruin, pers. comm.), there is only one option for correlation to the APTS (Lourens et al. 1996). Hence, the four normal intervals represent the Thvera, Sidufjall, Nunivak and Cochiti Subchrons in the Gilbert Chron (Figures 4, 5a).

With the palaeomagnetic reversals as age-calibration points, we can determine the average duration of the lignite-marl couplets. In Figure 4a, the APTS is plotted versus the cumulative number of Ptolemais-cycles and their corresponding polarity. It appears that lines connecting consecutive reversals have similar slopes, with the exception of the Sidufjall and overlying reversed Subchron where the line is significantly less steep. The upper boundary of the Sidufjall, on top of cycle K18, coincides with the earlier mentioned unconformity. A scouring surface and palaeosol were interpreted as erosion and non-deposition respectively. If we assume a three-cycle gap at this point in the Ptolemais column, all the calibration points can be linearly correlated with a slope of  $21.6 \pm 0.5$  kyr per couplet (Figure 4b). Since this agrees very well with the average period of a precession cycle, we believe that the lithological cycles in Ptolemais are related to precession by its influence on the Mediterranean climate, as also found for the carbonate cycles in the marine Rossello record

Table 1: positions of the magnetic reversal horizons

Vorio	Komanos	Tomea Eksi	Composite	i-cycle Ptol	i-cycle RC	Age, Ma
U. Cochiti	mN7		IN9	IN9	403	403 4.188
L. Cochiti	mN3		IN1 - IN2	mN3	414	413 4.300
U. Nunivak			IK29	IK29	433	433 4.493
L. Nunivak		mK22	below K23	mK22	446	445 4.632
<i>U. Sidufjall</i>		<i>top K18</i>	<i>above K16</i>	<i>top K18</i>	<i>464</i>	<i>460 4.799</i>
L. Sidufjall		IK16	IK15?	IK16	469	469 4.896
U. Thvera	?	base mK11	IK11	base mK11	478	478 4.998
L. Thvera	?	mK2 / IK3?	IK2	IK2	497	500 5.236

Table 1. Position of polarity reversals in the Ptolemais sections, K, T and N refer to the member; numbers refer to the cycle in that member; *l* and *m* refer to the phase (lignite or marl). Composite means the Ptolemais composite section; i-cycle Ptol (RC) denotes the insolation cycle correlated to the lithological cycle in which the reversal was found in the Ptolemais (Rossello composite) section. Ages of reversals after [5]. Italics denote the position of the hiatus rather than of the true upper Sidufjall reversal.

(Hilgen, 1991; Lourens et al. 1996). Independently from our method, a similar average duration of the lithological cycles in Ptolemais of  $21.8 \pm 0.8$  was derived with  $^{39}\text{Ar}/^{40}\text{Ar}$  dates (Steenbrink et al., 1999).

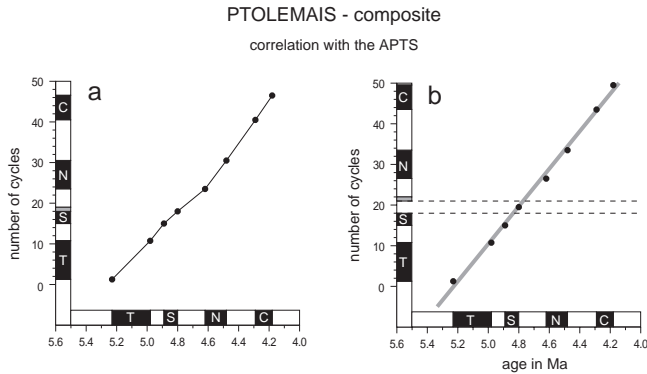


Figure 4. Cumulative number of cycles in the Ptolemais composite section and their polarity versus the APTS. Black (white) denotes normal (reversed) polarity. T, S, N and C indicate the Thvera, Sidufjall, Nunivak and Cochiti Subchrons respectively. (a). There are clearly two linear segments through Thvera and Sidufjall, and through Nunivak and Cochiti, respectively. (b). Incorporating a 3 cycle hiatus allows a single linear correlation through all Subchrons.

## Discussion

### *Correlation to an astronomical target curve*

The next step is to correlate the Ptolemais-cycles to a suitable astronomical curve, e.g. climatic precession from the astronomical solutions Bergo (Berger and Loutre, 1991) or La90 (Laskar, 1990). Precession curves include the modulating effect of eccentricity and have proved successful in astronomical calibration of sedimentary cycles (Hilgen, 1991a; 1991b). The precession index does not include the influence of obliquity, however, although obliquity is clearly reflected in marine lithological cycles. Early studies on Mediterranean sapropel sequences (Rossignol-Strick, 1983) used a monsoon index derived from a low-latitude insolation gradient. More recently, Lourens et al. (1996) suggested the use of  $65^\circ\text{N}$  summer (average of June and July) insolation as a target curve, because it better expresses the influence of obliquity. They concluded that a consistency in phase relationships through the Pliocene and Pleistocene is best maintained using La90 with present-day values for both the dynamical ellipticity of the Earth and tidal dissipation. The  $65^\circ\text{N}$  insolation is now generally used as a target curve for both mid and low latitudes (Lourens et al., 1996; Hilgen et al., 1995; Langereis et al., 1997; SHACKLETON AND Crowhurst, 1997). The i-cycle codification of insolation peaks, introduced in (Lourens et al., 1996), shall be used here for easy reference.

In Mediterranean sapropel sequences as well as in the carbonate cycles of the Rossello composite a maximum in summer insolation (warm summers and generally more precipitation) corresponds to a grey layer or a sapropel (both enriched in organic material), and a minimum in insolation (relatively cool summers and less precipitation) corresponds to a beige or homogeneous layer. This phase relation between Mediterranean marine lithology and insolation was determined by correlating the sapropels of the past 500 kyr with oxygen isotope stage boundaries as age calibration points (Rossignol-Strick, 1983; Vergnaud-Grazzini et al., 1977) and by  $^{14}\text{C}$  dating of the youngest sapropel in the Mediterranean (Hilgen et al., 1993 and references therein). The Ptolemais Formation is of Pliocene age, and studies on modern basins in the area (Loh, 1992; Bottema, 1974) did not (aim to) determine the modern continental or lacustrine equivalent of a sapropel. To derive an independent conclusion on a possible phase relation, we preferred not to make any a priori assumption. Therefore, we tried both option I: lignite corresponds to minimum insolation (beige or homogeneous layers in the marine record); and option II: lignite corresponds to maximum insolation (organic-rich layers in the marine record). Fortunately, option I was clearly more consistent and caused fewer discrepancies than option II, as is discussed below. This means that a lignite is correlated to a minimum in insolation (cool summers and generally arid) and marl to a maximum (warm summers and generally humid). This implies that the organic-rich layers in the Rossello composite are thus correlated with the relatively organic-poor layers (marl) in Ptolemais and vice versa.

A difficulty with Ptolemais is the lack of a straightforward cyclic representation of eccentricity, e.g. small and large scale clusters of precessionally forced cycles or a measurable quantity (e.g. carbonate content) that reveals the typical periodicities of eccentricity. Hilgen (1991a,b) used such observations to make a first (400 kyr eccentricity) and second (100 kyr eccentricity) order correlation to the astronomical target curve. In other cases (e.g. Shackleton et al., 1995), an age model for the geological record is constructed based on low-resolution features such as magnetostatigraphy and biostratigraphy. Such a model is then progressively refined and finally calibrated to an astronomical target curve. Our approach is based on the magnetostatigraphy of Ptolemais and the position of the corresponding reversal horizons in the astronomically calibrated Rossello composite. The time scale of Lourens et al. (1996) correlates the Rossello section with the summer insolation time series. This time scale thus provides the approximate position of the Ptolemais reversal horizons with respect to insolation. This is only an approximate correlation because of possibly different delayed acquisition of the magnetic remanence between the Rossello and Ptolemais sections. Thus, the fact that a reversal horizon in the Rossello is correlated to a specific insolation cycle does not necessarily imply that the corresponding reversal in Ptolemais is found in the same insolation cycle.

We start our correlation where the lithological cycles are most pronounced: around the Cochiti Subchron in the Notio member and around the Thvera Subchron in the lower half of the Kyrio member. The polarity reversals provide a first order correlation to the insolation time series. The lithological cycles around the Cochiti Subchron, for example, should be recognised in the insolation pattern around  $\sim 4.25$  Ma (Fig. 5a).

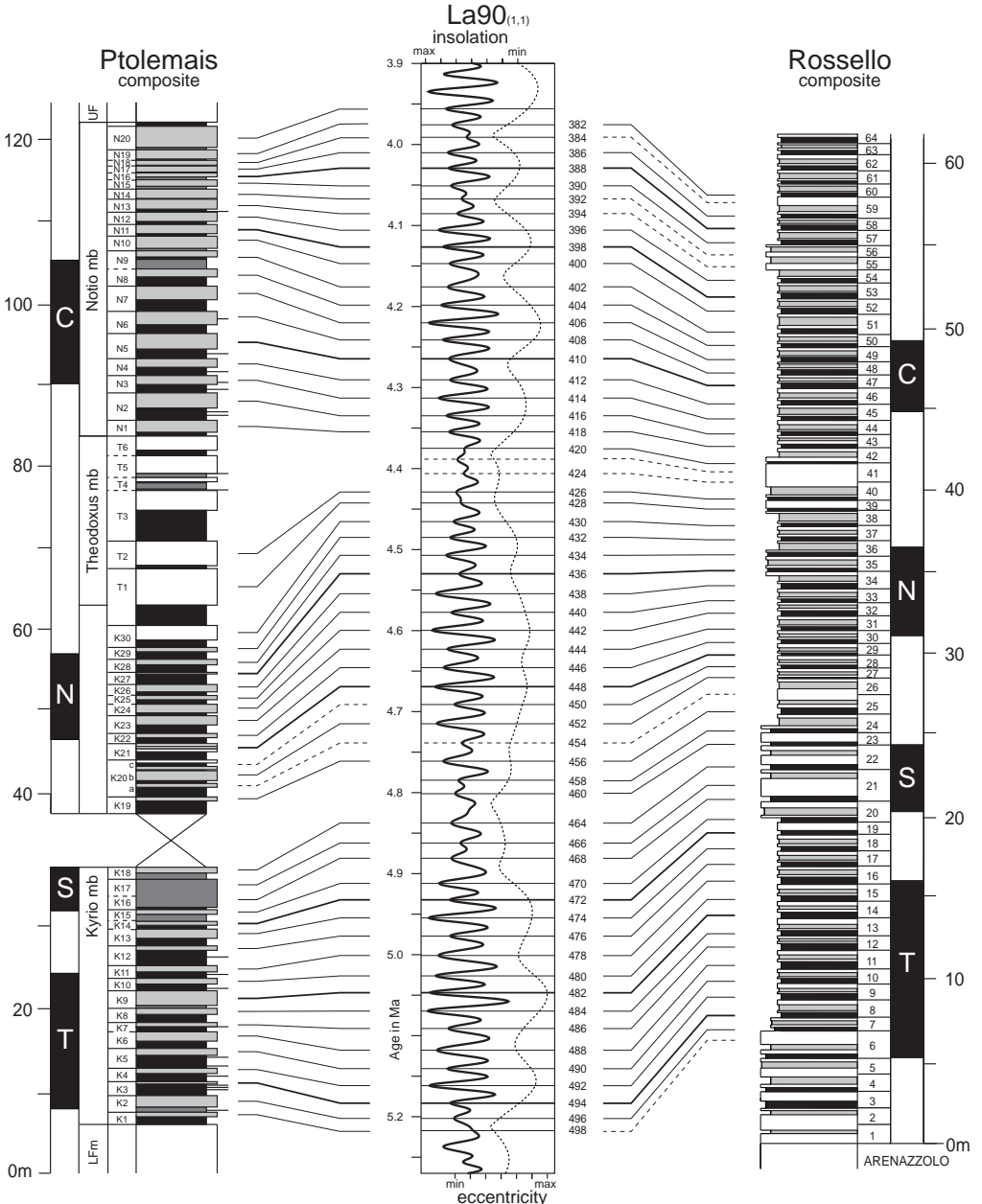
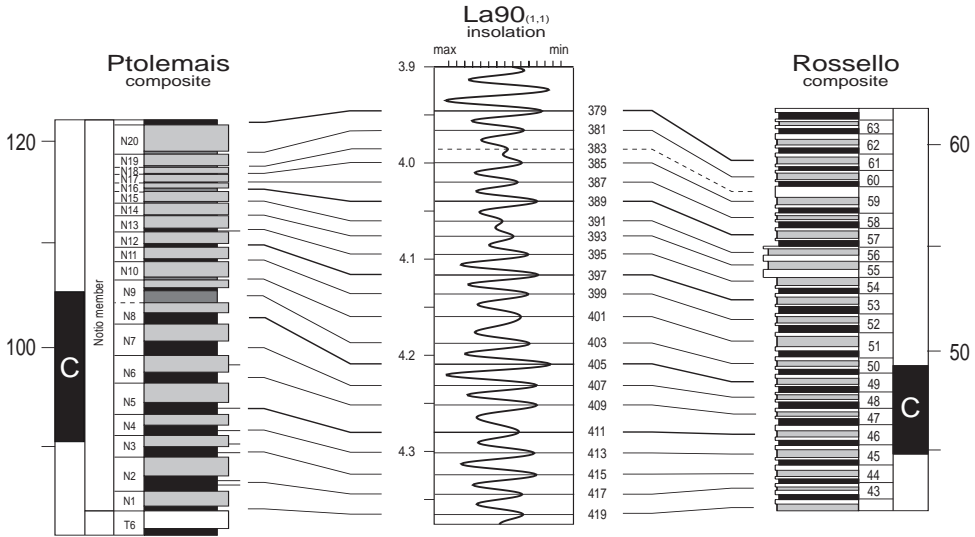


Figure 5. (a) Magnetostratigraphy, stratigraphic names, cycle numbers and lithology of the Ptolemais composite section (see also caption to Figure 3) correlated to 65°N summer insolation, eccentricity (dotted) and the marine Rossello composite section; i-cycle codification of insolation peaks, indicated on the right hand side, after Lourens (1996). T, S, N and C denote the Thvera, Sidufjall, Nunivak and Cochiti Subchrons respectively. In the lithological

column of the Rosello section, black (shaded) indented beds denotes grey (beige) marls, and white protruding beds denote white carbonate-rich marls. (b) Enlargement of the tuning of the Notio member. Correlation lines connect lignites in Ptolemais, insolation minima and the corresponding beige layers in the Rosello composite.



### Tuning of cycles N1-19

The first eight cycles of the Notio member are very regular, but cycle N9 and the lignite phase of N10 are not well developed (Figure 5a, b). An alternation of thin lignite and marl layers represents these cycles in Tomea Eksi, while in Vorio a thin lignite and a dark clay can be recognised as the lignite phases of N9 and 10 respectively. Since cycle N1 contains the first regular lignite phase above the a-typical Theodoxus member, this lignite is correlated to i-cycle 419, i.e. the first insolation minimum with a relatively high amplitude after a series of low-amplitude oscillations (caused by a 400 kyr eccentricity minimum). In the Rosello section a transition from double, high-carbonate cycles (Rc 40-41) to regular cycles occurs at the same level (Rc-cycle 42). Cycles N2-8 are then correlated to consecutive insolation peaks, and cycle N9 and the lignite of N10 to the moderate amplitude insolation peaks 403-401. The marl of cycle N5 is in most outcrops thicker than average and its top half often contains numerous thin lignite beds. In our correlation, this marl corresponds to i-cycle 410, an insolation maximum with a relatively long duration.

The uppermost cycles of the succession (N10-20) are dominated by marl and can only be distinguished by their thin lignite phases that are occasionally represented by brown clay layers rather than real lignite (Figure 5b). The lignite phases of N10, 14, 15, 17 and 19 are represented by thin clay layers; while N11, 12, 13, and also N16 and N21 have relatively thick lignites or dark clays. This pattern fits excellently with the high-amplitude minima 399, 397, 395 and with 389 and 379 and the lower amplitude cycles in between. The relatively dark N14-marl and the thin N18-marl are now correlated to the low-amplitude max-



ima 392 and 384 respectively. The only significant inconsistency with the Rossello-composite pattern is the thick beige layer in Rc 51: its equivalent is a thin dark clay layer (lignite-phase of N10), correlated with a low-amplitude, long-duration insolation minimum (401).

### *Tuning of cycles K1-18*

The Kyrio member has fairly constant and regular cycles up to cycle K14, except for the first two cycles (K1-2). Although cycles K1 and 2 are developed in Tomea Eksi only, and therefore their expression may just represent a local phenomenon, it appears that K1 has an ordinary lignite, while its marl and the overlying lignite of K2 are merged into an alternation of thin layers of lignite and marl. Despite the lack of lateral continuity, it is remarkable that the pattern of these two cycles followed by a long series of regular cycles fits very well with the insolation pattern near the 400 kyr eccentricity minimum at 5.22 Ma. Cycles K1 and K2 are thus correlated to i-cycle 499/498 and 497/496 respectively, and the overlying cycles K3-14 to insolation peaks 495-472. The only inconsistency is cycle K9, which has, despite the regular overall thickness, a relatively thin and less pronounced lignite, overlain by a thicker marl. The transition between the lignite and the marl is gradual, and an erroneous position of this boundary may explain the different thickness ratio. It remains conspicuous, however, that in our correlation this less pronounced lignite K9 corresponds to the highest amplitude insolation minimum between 4 and 5 Ma (i-cycle 483), especially since this cycle is not prominent in the Rossello composite section (Rc 13).

The lignite phases of cycles K15 and 18 contain many thin marl beds, while K17 does not even have a lignitic interval. The thickness of the combined marl bed of K16-17 led to the interpretation of K17 as a separate cycle. The less pronounced or absent lignites in this interval are correlated to the low amplitude insolation minima connected with the eccentricity minimum at 4.9 Ma. Similar considerations for the marl beds (the intercalation of thin lignite layers throughout the marl of K16-17) lead to correlation to the low amplitude i-cycles 468-466. Supportive for this correlation are the similarities between the cyclic patterns of the Ptolemais and Rossello sections. The absent beige layers in Rc 19 and double cycle Rc 21 in the Rossello composite correspond very well to the less pronounced lignite K15 and absent lignite K17 in Ptolemais.

### *Tuning of cycles K19-30*

With the detailed correlation so far, the reversal horizons corresponding with the upper Thvera and lower Sidufjall as well as with the upper and lower Cochiti in Ptolemais coincide with those in the Rossello composite section (and thus with the reversals in the APTS) within an interval of less than one cycle (or less than 21 kyr) (Table 1). It seems therefore reasonable to expect the same small difference for the Nunivak reversal horizons, even despite a possible difference in delayed remanence acquisition. The most remarkable feature in the Nunivak interval is the very thin or sometimes even absent marl of cycle K27. Either insolation maximum 436 (with very low amplitude) or 440 (with relatively low amplitude, caused by the high amplitude of neighbouring maxima 442 and 438) is the best candidate for correlation to cycle K27. The marl of K25 is also thinner than average, and marl K29 was found to be very thin in Tomea Eksi, but average in Komanos and in a (not published)

outcrop near the Vorio field. For the equivalent of a high-amplitude insolation maximum (438 and 442) we expect a marl enhanced in thickness and/or in appearance. Marl K24 has both, marl K26 is thicker than average, and marl K28 is in some outcrops enhanced, in others not. Altogether, the preferred correlation for this interval connects thin or absent marl K27 to the lowest-amplitude maximum 436, which means that enhanced marls K24 and K26 are correlated to high-amplitude maxima 442 and 438 respectively, and marls K25 and K29 to i-cycles 440 and 432 respectively. The correlation is extended straightforwardly downwards to cycle K21 and upwards to K30.

For the interval K19–20, the correlation with the insolation time series is not unambiguous, because there is no distinct or typical cyclic pattern, and the connection with underlying cycles is disturbed by the inferred hiatus. While cycle K19 appears to be a regular cycle, K20 has a thick heterogeneous marl phase and might be composed of two or even three cycles. We estimated earlier that the hiatus probably represents three cycles. Exactly three insolation cycles above the insolation maximum (i-cycle 464) correlated to the uppermost marl below the hiatus, K18, a prominent, normal-amplitude insolation cycle is present (i-cycles 457–456). We correlate K19 to this cycle. That leaves three cycles for K20, of which the upper- (450) and lowermost (454) maxima and the lowermost minimum (455) have reduced amplitude. For reasons of consistency cycle K20 is thus divided into three cycles (a, b and c), and correlated to the three insolation cycles. Considering the appearance of this interval in the Rossello composite (Figure 5a), where i-cycle 454 lacks expression, we suggest that the marl of K20a might be absent, and that the increased number of thin lignite layers just below the top of the thick marl phase of K20 marks lignite K20c.

### *Tuning of cycles T1–6*

The Theodosius member is now confined to the insolation peaks between i-cycles 429 and 420. As mentioned earlier, the bed thickness is laterally variable; a metres thick marl layer can disappear over a distance of only 100 m. The only constant beds are thin lignite T2, thick lignites T1 and T3 and the two ash layers in cycles T4 and T5. The extraordinarily thick lignite of T3 is correlated to the relatively high-amplitude minimum 425. T1 and T2 are thus necessarily correlated to the double insolation maximum 426–428 and the upper part of the Theodosius member should correspond to the remaining two and a half insolation cycles. This upper part, however, was interpreted as three and a half lithological cycles (marl phase of T3 and T4–6), but the cyclic pattern is difficult to recognise in this particular interval. In the Rossello composite, the beige layer (Rc 40) corresponding to the extra thick lignite T3 is very thick, while the beige below (Rc 39) is absent. The number of cycles in the Rossello-equivalent of cycles T3–6 corresponds to the number of insolation peaks, although these (double) cycles are again difficult to recognise.

### *Alternative correlation of cycles K19–T6*

To explore the discrepancy between the number of insolation peaks and the apparent number of lithological cycles in the Theodosius member, an alternative correlation has been examined (Figure 6). In this alternative correlation, all lithological cycles between K19 and T6 are correlated to two insolation cycles older than in the previously discussed correlation.

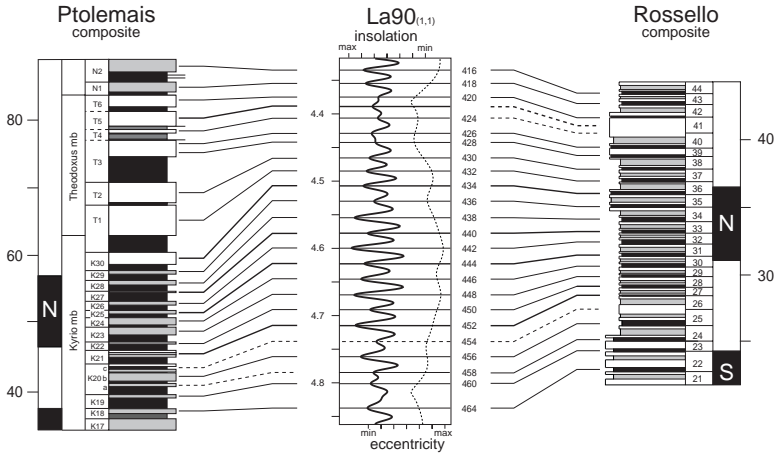


Figure 6. Alternative correlation in the interval 4.6-4.4 Ma. The tuning of cycles to insolation is only slightly less consistent than in the preferred correlation, but a major disparity with the Rosello composite is introduced by the discrepant position of the Nunivak reversal boundaries. See also caption to Figure 5a

The marl of thick cycle T<sub>3</sub> is correlated to the double insolation maximum 426-428, introducing one extra lithological cycle. I-cycle 425 should then represent an enhanced lignite phase, but it does not. The marls of K<sub>29</sub> and K<sub>28</sub> (both with varying thickness) are then correlated to the lowest-amplitude maximum 436 and to the high-amplitude maximum 438 respectively, and the enhanced marl of K<sub>24</sub> is correlated to the relatively low-amplitude i-cycle 446. When this alternative correlation is extended downwards, assuming that cycle K<sub>20</sub> indeed represents three insolation cycles, it follows that the hiatus between K<sub>18</sub> en K<sub>19</sub> is reduced to one (low-amplitude) insolation cycle (463/462). Since, moreover, this insolation cycle could well be incorporated in K<sub>19</sub>, the hiatus would be eliminated.

In addition to the inconsistencies between the lithological and insolation pattern, the alternative correlation makes the Nunivak Subchron significantly too old. This can only be explained by a two-cycle delayed acquisition of magnetic remanence in this specific interval in the Rossello composite, which is unlikely considering the consistency of the APTS with other studies (Shackleton et al., 1995; Wilson, 1993; Renne et al., 1994; Hall and Farrell, 1995; Clement et al., 1997).

*Phase relation between lithology and insolation*

Lignite was previously argued to correspond to an insolation minimum, with cool summers, and marl to an insolation maximum, with warm summers. This preferred phase relation is particularly clear in intervals with alternating high- and low-amplitude insolation peaks, occurring at times of low eccentricity minima. The precession amplitude is then reduced, resulting in a relatively larger effect of obliquity on insolation. Such interference patterns are for example observed at ~ 4.45 Ma and 4.53 Ma. In these intervals, relatively high-amplitude minima and maxima are correlated to the thick lignites of T<sub>1</sub> and T<sub>3</sub> and to the thick marls of T<sub>1</sub> and T<sub>2</sub> respectively, and low-amplitude minima and maxima to the

thin lignite of T<sub>2</sub> and to the thin or absent marl of K<sub>27</sub> respectively. No matching lithological and insolation patterns would be found in this interval if the inverse phase relation were used. The same holds for cycles K<sub>14-17</sub> and N<sub>13-16</sub>, where some lignite and marl beds are more prominent or thicker than others and can only be correlated to insolation if the preferred phase relation is used.

In conclusion, organic material was preserved during periods with cooler summers (insolation minima), whereas marl was preferentially deposited during periods with warmer summers (insolation maxima). Combined sedimentological observations and gastropod assemblages (Steenbrink et al., 1999) and preliminary palynological data (van Hove, pers. comm.) all suggest that lignite corresponds to a reed swamp environment, and marl to a relatively deeper lake. Hence, the lake level was higher at times of increased summer insolation and lower at times of reduced summer insolation, implying that the amount of precipitation and related run-off dominated evaporation in controlling the lake level. This is in agreement with the inferred precipitation increase in the eastern Mediterranean northern borderlands during an insolation maximum, i.e. when the Earth resided in perihelion during boreal summer (Rossignol-Strick, 1987; Rohling and Hilgen, 1991). A similar humidity-temperature relation was found for marine environments in the Mediterranean during the Pliocene (de Visser et al., 1989; van Os et al., 1994; Tzedakis, 1993).

### *Eccentricity*

The influence of precession on the lithology is evident in the Ptolemais sequence, but an expression of 100-kyr eccentricity is only found in the typical clustering of the uppermost ten cycles of the Notio member. A few other 100-kyr minima can be recognised as cycles with anomalous thickness and/or expression fitting the insolation curve (caused by the increased relative importance of obliquity). Expression of the 100-kyr cycles is especially lacking within the 400-kyr maxima around 5.05 and 4.6 Ma. In these intervals, the eccentricity time series shows little variation and/or relatively high minima (Figure 5a), caused by a ~2 Myr-eccentricity cycle with a minimum at ~4.65 Ma.

The most pronounced 400 kyr minima in the Rossello composite section are found around 5.25 and 4.4 Ma. The very same intervals have an unusual lithology in Ptolemais: beige marls around 4.4 Ma and the lacustrine marls of the Lower Formation around 5.25 Ma. The Lower Formation marls, however, continue further downwards and are still found well below the 400-kyr eccentricity minimum, so, in addition to astronomically forced climate, other factors must have influenced the long-term changes in lithology.

### *Lower Thvera discrepancy*

The polarity reversal horizons in Ptolemais typically deviate less than one i-cycle (i.e. less than half a lithological cycle) from the APTS, except for the lower Thvera, which differs three i-cycles, i.e.  $1\frac{1}{2}$  lithological cycle (Table 1). Its position could be determined from the Tomea Eksi section as well as from the Komanos section. Although in the latter section the cyclic pattern was unclear below cycle K<sub>4</sub>, the reversal was recorded just above the volcanic ash layer dividing cycles K<sub>1</sub> and 2, and well below the ash layer in lignite K<sub>3</sub>, thus confining the position to K<sub>2</sub>.

Since the Ptolemais age of the reversal is too young compared to the APTS, delayed acquisition in Ptolemais cannot explain the discrepancy. Therefore, we argue that the position of the lower Thvera in the Rossello composite might be too old. A close look at the results of van Hoof and Langereis (1992) from their detailed lower Thvera record in the Rossello composite, reveals that their two uppermost samples are reversed, indicating that the actual reversal horizon could be located higher in the stratigraphy than they interpreted.

## Conclusions

A reliable magnetostratigraphy of the lacustrine deposits of Ptolemais has been established. Despite the occurrence of delayed acquisition of magnetic remanence, the difference in the positions of the reversal horizons between Ptolemais and the APTS/Rossello composite is less than half a lithological cycle (~10 kyr), except for the lower Thvera. The resulting time frame proves that astronomical forcing of climate determines the continental lacustrine environment, in particular through the influence of climatic precession.

The most important result of this study is the unprecedented accuracy of the correlation of continental (*i.c.* lacustrine) sequences to the marine realm through tuning to the insolation time series, a correlation we consider reliable on a bed-to-bed scale. Typical patterns co-occur in the same cycles and in the same climatic phases in both the continental and marine records, implying that the argued phase relation is correct, *i.e.* that lignites were deposited in dryer periods with cooler summers, and marls in more humid periods with warmer summers.

Thus, the results provide a highly accurate time frame, which will enable detailed and comparative palaeoclimate studies in both marine and continental environments.

## Acknowledgements

We thank Prof. dr. E. Velitzelos and prof. dr. C.S. Doukas for arranging necessary contacts and for their pleasant co-operation in the field. The field assistance and fruitful discussions with Marloes van Hoeve, Hans de Bruin, Hendrik-Jan Bosch, Konstantin Theocharopoulos, Wout Krijgsman and Mark Dekkers are much appreciated. We are grateful to the employees of the Public Power Company ( $\Delta\text{EH}/\text{AKP-A}$ ) for providing us with the freshest possible outcrops and digging 'staircases' to reach these outcrops. We thank N.J. Shackleton, W.A. Berggren and an anonymous reviewer for their valuable comments. The investigations were supported by the Netherlands Geosciences Foundation (GOA) with financial aid from the Netherlands Organisation for Scientific Research (NWO). This work was conducted under the programme of two Dutch national research schools: the Vening Meinesz Research School of Geodynamics (VMSG) and the Netherlands Research School of Sedimentary Geology (NSG).

## References

- Berger, A., and Loutre, M.F., 1991. Insolation values for the climate of the past 10 m.y. *Quat. Sci. Rev.* 10, 297-317.
- Bottema, S. 1974. Late Quaternary vegetation history of Northwestern Greece, *PhD Thesis* Groningen University, 190 p.
- Clement, B. M., Swisher, C. C., Rodda, P. 1997. New magnetostratigraphic and  $^{40}\text{Ar}/^{39}\text{Ar}$  dating results from the Suva Marl, Fiji: Calibration of the Early Pliocene geomagnetic polarity time scale. *Earth Planet. Sci. Lett.* 151, 107-115.
- Ehlers, E., 1960. Bericht über die die bisher im Rahmen der Expertise Ptolemais durchgeführten geologischen und paläontologischen Untersuchungen. *Bundesanst. Geowiss. & Rohst. Hannover*, 1-36.
- Gramann, F., 1960. Die Fossilien des Braunkohlenbeckens von Ptolemais-Komanos. *Bundesanst. Geowiss. & Rohst Hannover*, 37-49.
- Hall, C. M. and Farrell, J. W., 1995. Laser  $^{40}\text{Ar}/^{39}\text{Ar}$  ages of tephra from Indian Ocean deep-sea sediments: Tie points for the astronomical and geomagnetic polarity time scales. *Earth Planet. Sci. Lett.* 133, 327-338.
- Hilgen, F.J., 1987. Sedimentary cycles and high-resolution chronostratigraphic correlations in the Mediterranean Pliocene. *Newsl. Stratigr.* 17, 109-127.
- Hilgen, F.J., 1991a. Astronomical calibration of Gauss to Matuyama sapropels in the Mediterranean and implication for the Geomagnetic Polarity Time Scale. *Earth Planet. Sci. Lett.* 104, 226-244.
- Hilgen, F.J., 1991b. Extension of the astronomically calibrated (polarity) time scale to the Miocene/Pliocene boundary. *Earth Planet. Sci. Lett.* 107, 349-368.
- Hilgen, F.J., Lourens, L.J., Berger, A. and Loutre, M.F., 1993. Evaluation of the astronomically calibrated time scale for the late Pliocene and earliest Pleistocene. *Paleoceanography* 8, 549-565.
- Hilgen, F.J., Krijgsman, W., Langereis, C.G., Lourens, L.J., Santarelli, A., Zachariasse, W.J., 1995. Extending the astronomical (polarity) time scale into the Miocene. *Earth Planet. Sci. Lett.* 136, 495-510.
- van Hoof, A.A.M. and Langereis, C.G., 1991. Reversal records in marine marls and delayed acquisition of remanent magnetization. *Nature* 351, 223-225.
- van Hoof, A.A.M. and Langereis, C.G., 1992. The upper and lower Thvera sedimentary geomagnetic reversal records from southern Sicily. *Earth Planet. Sci. Lett.* 114, 59-76.
- Kaouras, G., 1989. Kohlenpetrographische, Palynologische und Sedimentologische Untersuchungen der Pliozänene Braunkohle von Kariochori bei Ptolemais/NW-Griechenland. *Thesis Universität Göttingen*.
- Kent, D.V., Olsen, P.E. and Witte, W.K., 1995. Late Triassic-earliest Jurassic geomagnetic polarity sequence and paleolatitudes from drill cores in the Newark rift basin, eastern North America. *J. Geophys. Res.* 100, 14.965-14.998.
- Langereis, C.G. and Hilgen, F.J., 1991. The Rossello composite: A Mediterranean and global reference section for the Early to early Late Pliocene. *Earth Planet. Sci. Lett.* 104, 211-225.
- Langereis, C.G., Dekkers, M.J., de Lange, G.J., Paterne, M., van Santvoort, P.J.M., 1997. Magnetostratigraphy and astronomical calibration of the last 1.1 Myr from an eastern Mediterranean piston core and dating of short events in the Brunhes. *Geophys. J. Int.* 129, 75-94.
- Laskar, J., 1990. The chaotic motion of the solar system: A numerical estimate of the size of the chaotic zones. *Icarus* 88, 266-291.
- Loh, H., 1992. Die Genese und Fazies der quartären Torf-Lagerstätte von Agras (Griechisch-Mazedonien) als Hintergrund der Braunkohlen-Mazeral- und Lithotypen-Bildung. *Dissertation thesis*, Georg-August-Universität, Göttingen, 61 p.

- Lourens, L.J., Antonarakou, A., Hilgen, F.J., van Hoof, A.A.M., Vergnaud-Grazzini, C., Zachariasse, W.J., 1996. Evaluation of the Plio-Pleistocene astronomical time scale. *Paleoceanography* 11, 391-413.
- Mercier, J.L., Sorel, D., Vergely, P., 1989. Extensional tectonic regimes in the Aegean basins during the Cenozoic. *Basin Research* 2, 49-71.
- Olsen, P.E., Kent, D.V., Cornet, B., Witte, W.K. and Schlische, R.W., 1996. High-resolution stratigraphy of the Newark rift basin (early Mesozoic, eastern North America). *Geol. Soc. Am. Bull.* 108, 40-70.
- van Os, B.J.H., Lourens, L.J., Beaufort, L., Hilgen, F.J., de Lange, G.J., 1994. The formation of Pliocene sapropels and carbonate cycles in the Mediterranean: diagenesis, dilution and productivity. *Paleoceanography* 9, 601-617.
- Papakonstantinou, A., 1979. Die hydrogeologischen Verhältnisse im Raum der Ptolemais-Senke und die westlichen Vermiongebirges in Griechisch-Mazedonien. *Berliner geowiss. Abh.* 13, 1-79.
- Pavlidis, S.B. and Mountrakis, D.M., 1986. Neotectonics of the Florina-Vegoritiss-Ptolemais Neogene basin (NW Greece): an example of extensional tectonics of the greater Aegean area. *Ann. Geol. Pays Hell.* 33, 311-327.
- Renne, P.R., Deino, A.L., Walter, R.C., Turrin, B.D., Swisherr, C.C., Becker, T.A., Curtis, G.H., Sharp, W.D., Jaouni, A.R., 1994. Intercalibration of astronomical and radioisotopic time. *Geology* 22, 783-786.
- Rohling, E.J. and Hilgen, F.J., 1991. The eastern Mediterranean climate at times of sapropel formation: a review. *Geol. en Mijnb.* 70, 253-264.
- Rosignol-Strick, M., 1983. African monsoons, an immediate climate response to orbital insolation. *Nature* 304, 46-49.
- Rosignol-Strick, M., 1987. Rainy periods and bottom water stagnation initiating brine accumulation and metal concentrations: 1. The Late Quaternary. *Paleoceanography* 2, 333-360.
- Shackleton, N.J., Crowhurst, S., Hagelberg, T., Pisias, N.G. and Schneider, D.A., 1995. A new late Neogene time scale: Application to Leg 138 sites. *Proc. Ocean Drill. Program Sci. Results* 138, 73-101.
- Shackleton, N.J., Crowhurst, S., 1997. Sediment fluxes based on an orbitally tuned time scale 5 Ma to 14 Ma, Site 926. *Proc. Ocean Drill. Program Sci. Results* 154, 69-82.
- Steenbrink, J., van Vugt, N., Hilgen, F.J., Wijbrans, J.R. and Meulenkaamp, J.E., 1999. Sedimentary cycles and volcanic ash beds in the lower Pliocene lacustrine succession of Ptolemais (NW Greece): Discrepancy between  $^{40}\text{Ar}/^{39}\text{Ar}$  and astronomical ages. *Palaeogeogr. Palaeoclimatol. Palaeoecol.* 152, 283-303.
- Tzedakis, P.C., 1993. Long-term tree populations in northwest Greece through multiple Quaternary climatic cycles. *Nature* 364, 437-440.
- Vergnaud-Grazzini, C., Ryan, W.B.F., Cita, M.B., 1977. Stable isotope fractionation, climatic change and episodic stagnation in the eastern Mediterranean during the late Quaternary. *Mar. Micropaleont.* 2, 353-370.
- de Visser, J.P., Ebbing, J.H.J., Gudjonsson, L., Hilgen, F.J., Jorissen, F.J., Verhallen, P.J.J.M., Zevenboom, D., 1989. The origin of rhythmic bedding in the Pliocene Trubi Formation of Sicily, Southern Italy. *Palaeogeogr., Palaeoclimatol., Palaeoecol.* 69, 45-66.
- van de Weerd, A., 1978. Early Ruscinian rodents and lagomorphs (Mammalia) from the lignites near Ptolemais (Macedonia, Greece). *Proc. K. Ned. Akad. Wet.* B82, 127-170.
- Wilson, D.S., 1993. Confirmation of the astronomical calibration of the magnetic polarity time scale from sea-floor spreading rates. *Nature* 364, 788-790.

# Sedimentary cycles and volcanic ash beds in the lower Pliocene lacustrine succession of Ptolemais (NW Greece): Discrepancy between $^{40}\text{Ar}/^{39}\text{Ar}$ and astronomical ages

## Abstract

A high-resolution cyclostratigraphy for the rhythmically bedded lignite-marl sequences of the lower Pliocene Ptolemais Formation is combined with  $^{40}\text{Ar}/^{39}\text{Ar}$  dating results of intercalated volcanic ash beds. Detailed field reconnaissance in three open-pit lignite mines reveals three end-member sediment types: lignites, composed primarily of organic material; grey marls, a mixture of carbonate and organic material; and beige marls, almost exclusively composed of carbonate. These lithologies are arranged in two basic types of sedimentary cycles: lignite-grey marl and lignite-beige marl cycles. A cyclostratigraphic composite section comprising 56 lignite-marl cycles is constructed which combines the consistent cycle patterns from three parallel sections. The concordant positions of 20 volcanic ash beds in these sections confirm the cyclostratigraphic correlations and indicate that the lignite-marl cycles result from regional, basin-wide forcing rather than lateral facies migrations.

$^{40}\text{Ar}/^{39}\text{Ar}$  ages on sanidine and biotite separates from nine volcanic ash beds were obtained by multiple total fusion and incremental heating experiments. The  $^{40}\text{Ar}/^{39}\text{Ar}$  ages range between  $5.00 \pm 0.05$  and  $4.04 \pm 0.04$  Ma and are, in general, consistent with the stratigraphic order. A least square linear regression using the measured  $^{40}\text{Ar}/^{39}\text{Ar}$  ages gives an average duration of  $21.8 \pm 0.8$  kyr per lignite-marl cycle. Evidently, the lignite-marl cycles in the Ptolemais Formation are linked to the precessional variation in the Earth's orbit through its influence on Mediterranean climate. For the first time,  $^{40}\text{Ar}/^{39}\text{Ar}$  dating results, totally independent from any other dating and or tuning technique, confirm the astronomical theory of climate change.

The  $^{40}\text{Ar}/^{39}\text{Ar}$  ages of the volcanic ash beds show a constant  $\sim 200$  kyr ( $\sim 4.5\%$ ) age discrepancy with the astronomical ages of the same ash beds. This inconsistency remains difficult to explain. The discrepancy is unlikely to have resulted from erroneous astronomical ages, through incorrectness in the astronomical tuning, inaccuracies of the magnetostratigraphic data or the orbital time-series used, and/or errors in the APTS. The  $^{40}\text{Ar}/^{39}\text{Ar}$  dating results neither give clear indications for a possible source of error. From the excellent data set it is evident that neither loss of radiogenic  $^{40}\text{Ar}$ , nor an underestimation of the contribution of Ca- and K-derived Ar isotopes could have caused the discrepancy. Moreover, the discrepancy is also beyond the errors in the systematic variables, like the decay constants of  $^{40}\text{K}$  or the ages for the neutron fluence monitors.

*This chapter is published as: Steenbrink, J., van Vugt, N., Hilgen, F.J., Wijbrans, J.R. and Meulenkamp, J.E., 1999. Cyclostratigraphy and  $^{40}\text{Ar}/^{39}\text{Ar}$  dating of lower Pliocene lacustrine sequences of the Ptolemais Basin, NW Greece, *Palaeogeography, Palaeoclimatology, Palaeoecology* 152, 283-303.*



## Introduction

It has long been realised that marine sedimentary cycles may reflect climate oscillations that are controlled by the Earth's orbital cycles (Gilbert, 1895; Barrell, 1917). During the last decades, deep-sea oxygen isotope records fully confirmed that Pleistocene glacial cycles are driven by orbitally controlled variations in the solar radiation reaching the earth surface (Emiliani, 1955; Shackleton and Opdyke, 1973; Hays et al., 1976; Imbrie et al., 1984). More recently, the astronomical forcing and geochronological application of Milankovitch-type sedimentary cycles in deep marine Pliocene and Miocene records in the Mediterranean have been explored in detail (Hilgen, 1991; Krijgsman et al., 1995; Lourens et al., 1996). The tuning of such astronomically induced sedimentary sequences to computed time series of past variations in the Earth's orbit (or to derived target curves, e.g. insolation or ice sheet volume) has led to the construction of an astronomically calibrated polarity time scale (APTS) for the marine record which has been extended back to 12 million years (Hilgen et al., 1995; Krijgsman et al., 1995; Shackleton et al., 1995).

Orbital influences are not restricted to open marine systems, but are found in all types of sedimentary environments, including lacustrine successions (Bradley, 1929; Van Houten, 1964; Fischer, 1980; Anderson, 1982). Ideally, sections with a continuous cyclic pattern and good time control are used in studying the role of orbital forcing. Cyclostratigraphic studies on lacustrine sediments are hampered by a large degree of lateral variability, the scarcity of long continuous outcrops and the general lack of direct and precise time control. Yet, the complete and almost undisturbed lacustrine sequences of the lower Pliocene Ptolemais Formation in the intermontane Ptolemais Basin (NW Greece) are an exception. These successions are excellently exposed in open-pit lignite mines and show an often prominent alternation of lignite-marl cycles. Intercalated volcanic ash beds throughout the entire Ptolemais Formation serve as important time marker horizons for stratigraphic correlations.  $^{40}\text{Ar}/^{39}\text{Ar}$  dating of these volcanic ash beds provides significant time calibration points for the record and concomitant magnetostratigraphic studies (Van Vugt et al., 1998) give accurate time control as well.

In this paper, the cyclostratigraphic properties of the Ptolemais Formation will be discussed along with  $^{40}\text{Ar}/^{39}\text{Ar}$  dating results on nine intercalated volcanic ash beds. The  $^{40}\text{Ar}/^{39}\text{Ar}$  ages will be compared with astronomical ages for the same volcanic ash beds. The former ages are based on the radioactive decay of  $^{40}\text{K}$ . The latter ages were independently obtained by magnetostratigraphic calibration to the APTS and subsequent correlation of the sedimentary cycles to computed astronomical target curves by Van Vugt et al. (1998). Their paleomagnetic data, combined with the cyclostratigraphic framework and  $^{40}\text{Ar}/^{39}\text{Ar}$  dating results presented in this paper, provide the necessary high-resolution time frame for further paleoclimate and paleoenvironment studies on the Ptolemais area.

## Geological setting and stratigraphy

The elongated intermontane Ptolemais Basin is part of a NNW-SSE trending graben system that extends over a distance of 250 km from Bitola in the Former Yugoslavian Republic of Macedonia (F.Y.R.O.M.) to the village of Servia, south-east of Ptolemais, Greece (Fig. 1). The depression is filled with a 500-600 m thick succession of upper Miocene to lower Pleistocene, predominantly lacustrine sediments with intercalated lignite seams and fluvial deposits, schematically indicated in Fig. 1.

The basin is bounded by two fault systems, which can be related to two extensional episodes (Pavlidis and Mountrakis, 1986; Mercier et al., 1989). The first, Late Miocene episode resulted in the origin of the basin in response to NE-SW extension. The second, Pleistocene episode of NW-SE extension resulted in the development of a

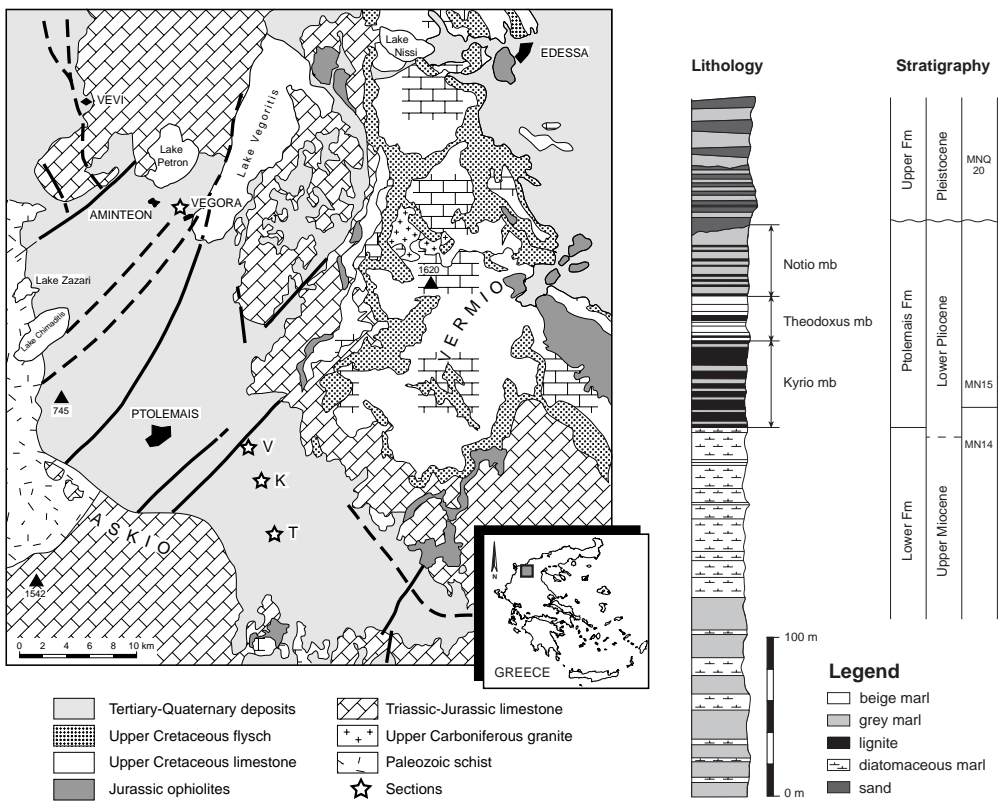


Figure 1: Left: Simplified geological map of the Ptolemais Basin in NW Greece showing the location of the Vorio (V), Komanos (K) and Tomea Eksi (T) sections (modified after Papakonstantinou, 1979). Right: Generalised stratigraphy of the Neogene sedimentary sequence in the Ptolemais area. Lithology slightly modified after Anastopoulos & Koukouzas (1972); Formations and members after Ehlers (1960); MN and MNQ (micro-mammal) zones from Van de Weerd (1979), Koufos and Pavlidis (1988).

sequence of sub-basins. Currently, the basin is situated about 700 metres above sea level. The depression is surrounded by the mountain-ranges of Vermio (2052 m) to the east and Askio (2111 m) to the west, which are mainly composed of Palaeozoic schists and Mesozoic limestones (Brunn, 1956; Kaouras, 1989) (Fig. 1).

Following previous investigations (Ehlers, 1960; Anastopoulos and Koukouzas, 1972) three basin-wide lithostratigraphic units can be recognised in stratigraphic order: the Lower Formation, the Ptolemais Formation and the Upper Formation (Fig. 1). The Lower Formation is approximately 300 metres thick and unconformably overlies the pre-Neogene basement. Information is mainly derived from drillings. It is predominantly composed of lacustrine (sometimes diatomaceous) marls with some prominent intercalated lignite seams. Plant remains from the middle part of the Lower Formation point to a late Miocene age (Gregor and Velitzelos, 1995).

The next higher Ptolemais Formation, with a thickness of approximately 110 metres, has been subdivided into the Kyrio, Theodoxus and Notio members (Fig. 1). The lowermost Kyrio member consists of rhythmic alternations of lignite and grey marl beds (Fig. 2a). These alternations pass laterally into a succession predominantly composed of lignite with only minor intercalations of marls and/or sand lenses. The base of the Kyrio member reflects the onset of Pliocene lignite accumulation in the Ptolemais Basin. The first abundant occurrence of the characteristic freshwater gastropod *Theodoxus macedonicus* defines the base of the next-higher unit. The middle Theodoxus member includes two predominantly beige-coloured marl intervals, separated by a prominent lignite bed (Fig. 2b). The distinctive change in colour from beige to grey marls marks the transition towards the next-higher unit. This uppermost unit, the Notio member, is composed of lignite-grey marl rhythmites (Fig. 2c). In the upper part of this unit, the



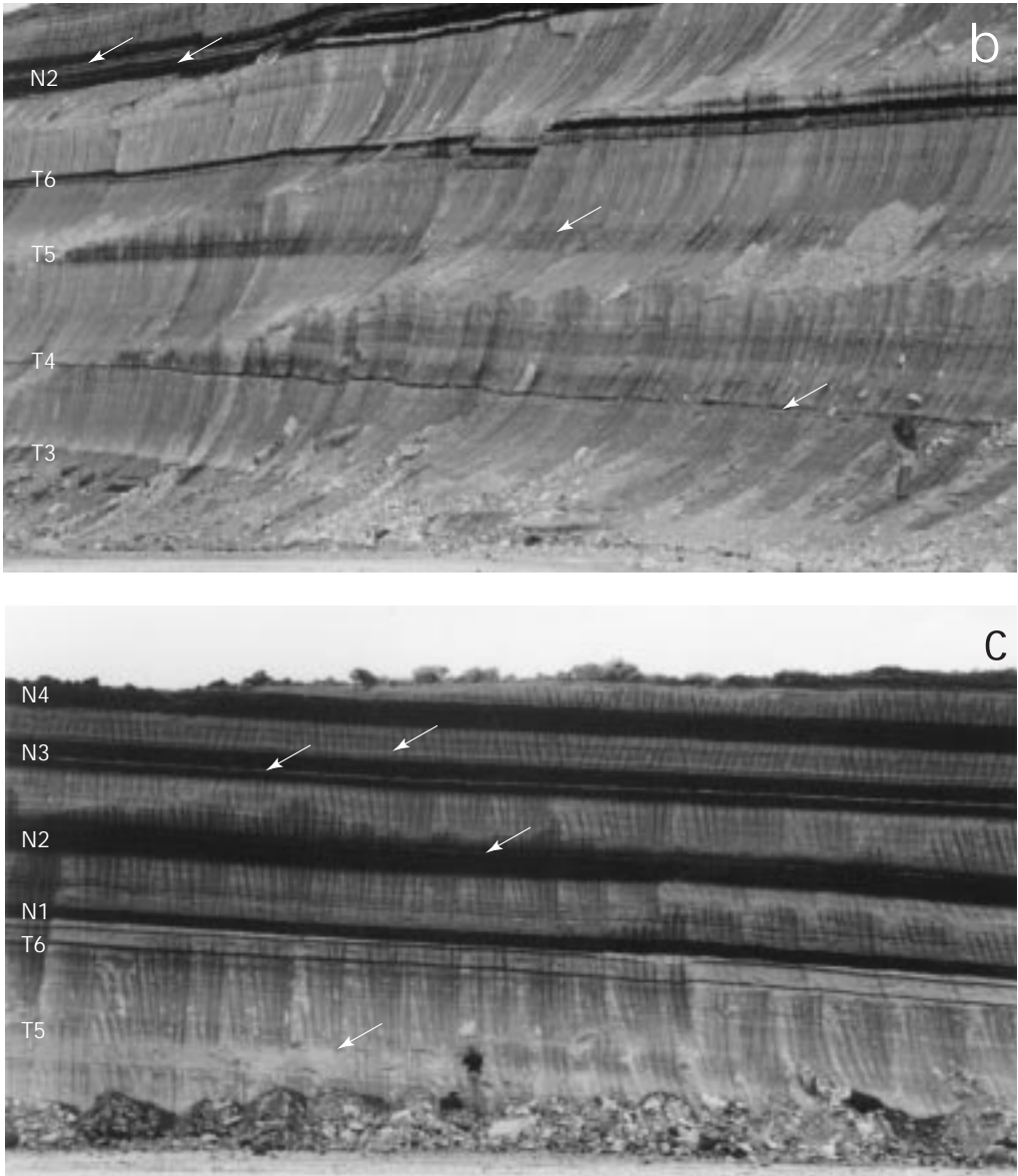


Figure 2: a) (previous page) Komanos open pit mine. Lignite-grey marl cycles K5 to K11 of the Kyrrio member. Arrows denote positions of the volcanic ash beds in cycles K5, K7 - the so-called layer 9 (Van de Weerd, 1983) -, K10 and K11. b) Vorio open pit mine. Lignite-beige marl cycles T3 to T6 of the Theodosus member, and lignite-grey marl cycles N1 (poorly developed) and N2 from the Notio member. Arrows denote positions of the volcanic ash beds in cycles T4, T5 and N2. c) Tomea Eksi open pit mine. Lignite-beige marl cycles T5 and T6 of the Theodosus member, and lignite-grey marl cycles N1 to N4 of the Notio member. Arrows denote positions of the volcanic ash beds in cycles T5, N2 and N3.

lignite-grey marl rhythmites pass laterally into banded xylite. Pollen, mollusc and micro-mammal studies indicate an early Pliocene age for the Ptolemais Formation (Vetoulis, 1957; Gramann, 1960; Van de Weerd, 1979).

The Upper Formation unconformably overlies the Ptolemais Formation; it consists of up to 200 metres of fluvio-lacustrine marls with intercalated clay, sand and conglomerate beds (Fig. 1). The succession includes a vertebrate fauna of Pleistocene age (Velitzelos and Schneider, 1973; Koufos and Pavlides, 1988).

In this contribution, we will only consider the cyclostratigraphy and  $^{40}\text{Ar}/^{39}\text{Ar}$  dating results for the Ptolemais Formation. In a forthcoming paper, we will discuss the stratigraphic framework for the Lower Formation.

## **Sediment types and cyclostratigraphy**

Ideally, continuous cyclic successions are used in studying the role of orbital forcing. Such ideal conditions do not exist everywhere in the Ptolemais record. The sediments show a considerable degree of lateral variability. Moreover, in some parts of the sequence, the occurrence of fossiliferous lenses and discontinuous channel fills may reflect periods of erosion and non-deposition. Both the lateral variability and local presence of minor gaps in the sedimentary record hamper a straightforward interpretation of the succession in terms of sedimentary cycles.

Detailed field reconnaissance in three open-pit lignite mines (Fig. 1) reveals that the successions in each open-pit contain both intervals in which the cyclic alternations of lignites and marls is very prominent, and intervals where indications for cyclic sedimentation are less obvious or even absent. We logged representative sections in the three open-pits, focusing on the rhythmic lignite-marl patterns. Through careful comparison of outcrops all over the mining area, local features could be separated from consistent (i.e. laterally continuous) patterns. The results will be discussed below. Firstly, the sedimentological characteristics of the three main sediment types constituting the rhythmic alternations - lignite, grey marl and beige marl - will be considered. Secondly, the two basic types of sedimentary cycles, i.e. lignite-grey marl and lignite-beige marl cycles, will be dealt with. Finally, the cyclic patterns of alternating lignite and marl beds are discussed for each stratigraphic unit, thus providing the basis for a cyclostratigraphic composite section showing an 'ideal' succession of cycles for the Ptolemais Basin.

### *End-member sediment types*

The Ptolemais Formation contains two major sediment types: dark-coloured lignites and light-coloured marls. Considering colour, composition and fossil content, grey and beige marls can further be distinguished. For this study, the terminology of Bates and Jackson (1987) is used, defining marl as a soft, earthy material, largely composed of carbonate precipitated in freshwater lakes and ponds. The three sediment types - lignite, grey marl and beige marl - are so-called end-members; i.e. they form the primary components of a variety of lithologies. One of the general characteristics of the three sedi-

ment types is the low concentration of non-combustible material such as terrigenous clastics or siliceous microfossils (diatoms). In contrast, organic and carbonate components together constitute generally more than 95% by weight. Of primary interest in this study are the rhythmic alternations of lignite and marl beds in the Ptolemais Formation. Therefore, only the sedimentological properties of these sediment types will be discussed in the following section.

**Lignites.** The lignites of the Ptolemais Formation are primarily composed of fine-grained organic material. Larger fragments of fossil plant tissue (mainly reed and root remains) are common, wood remains are rare. Both massive lignites without macroscopic structure and finely bedded lignites occur. The lignite beds contain fossiliferous levels mostly in lags with small mammal associations, fish remains, freshwater pelecypods and gastropods. The total organic matter content is around 90%. As a rule individual lignite beds of lignite-marl cycles are some dm to 2 m thick (Figs. 2a, c and 3). Thin (cm-scale) lignite layers are present within most marl beds.

The extensive character of the lignite beds, their composition as well as the faunal content of the associated strata suggest formation in a reed swamp environment. Van de Weerd (1983) came to the same interpretation based on palynological studies. This is in accordance with the classification of the lignites as huminite-rich brown coals by Cameron et al. (1984) and Kaouras (1989).

**Grey marls.** The grey marls represent a mixture of predominantly homogeneous carbonate and organic plant debris. Bioturbation, chiefly by roots, is pervasive. The rich biota is dominated by shallow-water lacustrine gastropods (e.g. *Planorbis planorbis*, *Valvata cristata* and *Lymnea stagnalis*) and ostracods, and furthermore characterised by the near-absence of aquatic macrophytes. Seeds of typical reed plants are abundant. The samples contain up to 30% of organic matter and between 70 and 95% of carbonate by weight. Individual grey marl beds, often with thin lignite interbeds, are up to 2 m thick, and can generally be traced from one section to another. Such beds are only found in the Kyrio and Notio members (Figs. 2a, c and 3).

The lateral extent, composition and gastropod assemblages of the grey marl beds point to deposition in a flat marginal, shallow lacustrine environment with abundant plant growth. This is also indicated by the intense bioturbation and general absence of aquatic macrophytes, which prefer more open lacustrine conditions (Dean and Fouch, 1983).

**Beige marls.** The beige marls contain as much as 95% carbonate and only a few percent of organic matter. Calcite is the predominant carbonate mineral. The organic fraction is dominated by aquatic plant fragments. The biota is dominated by lacustrine bottom-dwelling gastropods (e.g. *Theodoxus macedonicus* and *Valvata hellenica*) and stem encrustations of the chlorophyte *Chara*. Root imprints are generally absent. Individual beige marl beds have a thickness between 0.2 and 2 metres, showing large lateral thickness variations both within and between the open-pit mines studied. The beige marl beds are mainly found in the *Theodoxus* member (Figs. 2b and 3).

The gastropods *Theodoxus macedonicus* and *Valvata hellenica* prefer open lacustrine conditions devoid of bottom vegetation (Gramann, 1960). The chlorophyte *Chara* thrives in littoral lacustrine conditions, with a lower limit of deposition normally between four

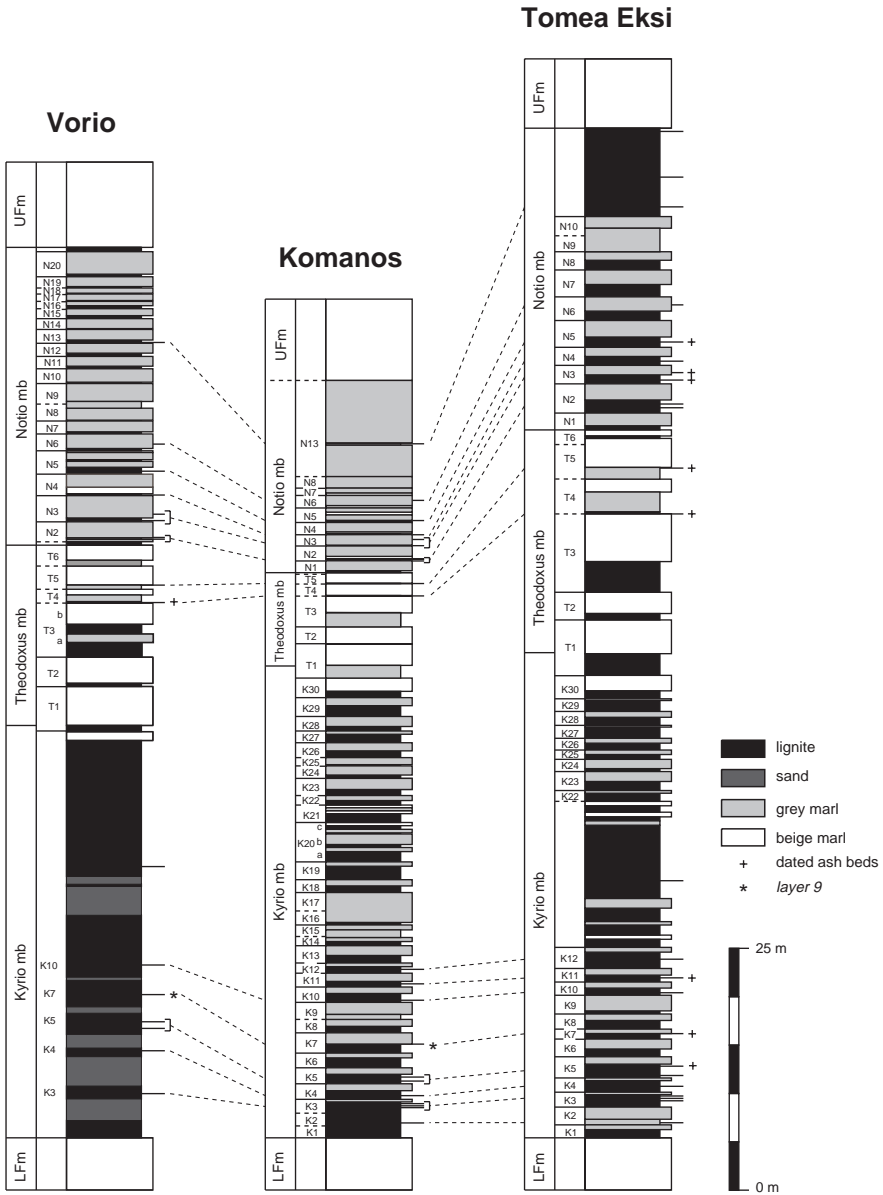


Figure 3: Lithostratigraphy and cyclostratigraphy of the Vorio, Komanos and Tomea Eksi sections. In the lithological column, black (grey) indented beds denote lignite (marly equivalent of lignite) beds, grey (white) protruding beds denote grey (beige) marl beds, thin extra protruding layers denote volcanic ash beds and dark grey indented layers in the basal part of Vorio denote sand lenses. Dashed lines correlate individual ash beds. The sedimentary cycles have been numbered from base to top for each member where 'K' refers to the Kyrrio member (cycles K1-30), 'T' to the Theodoxus member (cycles T1-6) and 'N' to the Notio member (cycles N1-20).

and six metres below lake level (Dean and Fouch, 1983). The absence of lamination suggests shallow, oxygenated conditions. Comparison with recent analogues (Murphy and Wilkinson, 1980) leads us to suggest that the Ptolemais beige marls were deposited on the marl bench platform and/or slope. The observed large lateral variability of individual beige marl beds is consistent with this interpretation.

### *Basic types of sedimentary cycles*

The occurrence on various scales of alternating dark-coloured lignites and light-coloured marl beds is the most obvious characteristic of the Ptolemais Formation (Figs. 2 and 3). These sedimentary colour couplets represent rhythmic lignite and marl alternations. On a metre scale two basic types of sedimentary cycles can be distinguished: lignite-grey marl and lignite-beige marl cycles.

*Lignite-grey marl cycles.* The bipartite lignite-grey marl cycles display black-grey colour alternations. This type of cycle ranges in thickness from 1.1 to 2.5 m and consists of some dm to 2 m of black-coloured lignite at the base followed by a grey marl bed, usually with cm-thick lignite interbeds (Figs. 2a, c). Lignite-grey marl cycles are clearly developed in the Kyrio and Notio members (Fig. 3). The lignite and marl segments of individual cycles display considerable lateral variations in thickness. For instance, the cycles in the Notio member of the Tomea Eksi section have considerably thicker lignite beds than those in the Vorio section (Fig. 3). The grey marl segments of the same cycles show an opposite trend, that is, thicker in the Vorio section with respect to the Tomea Eksi section.

*Lignite-beige marl cycles.* Individual bipartite lignite-beige marl cycles display black or brown and beige colour alternations and range in thickness from 1.0 to 5.5 m. Such cycles are most pronounced in the Theodoxus member and consist of a basal black lignite or dark-coloured marl bed topped by a beige marl bed (Figs. 2b and 3). The beige marl beds display a subtle colour banding. The lignite-beige marl cycles show considerable lateral variation between the sections, both in cycle-thickness and in thickness of individual lignite and beige marl beds (Fig. 3).

### *Cyclostratigraphic framework*

Evidently the cyclicity is not uniform throughout the entire sequence; specific intervals show quite regular lignite-marl cycles, whereas others are composed of less well developed cycles. In addition, the type of cyclicity, i.e. lignite-grey marl or lignite-beige marl is confined to specific intervals. The cyclostratigraphic details will be presented below in stratigraphic order for each member, where 'K' refers to Kyrio, 'T' to Theodoxus and 'N' to Notio. The sedimentary cycles have been numbered from base to top for each member: K1-30 for the Kyrio member, T1-6 for the Theodoxus member and N1-20 for the Notio member (Figs. 2 and 3).

### **Kyrio member**

Considering the expression and lateral consistency of the alternating lignite and marl beds, the Kyrio member was subdivided into three stratigraphic intervals. The lower



interval, spanning cycles K<sub>1</sub> to K<sub>12</sub>, consists of clear lignite and marl alternations in at least one section. The same holds for the upper interval, cycles K<sub>23</sub> to K<sub>30</sub>. The sedimentary expression of lignite and marl alternations in the middle interval, which contains cycles K<sub>13</sub> to K<sub>22</sub>, is less pronounced in the studied sections.

**Cycles K<sub>1</sub> to K<sub>12</sub>.** Cycles K<sub>1</sub> to K<sub>12</sub> are apparent as rhythmic alternations of lignite and grey marl beds in the Tomea Eksi section (Fig. 3). In the Komanos section, cycles K<sub>4</sub> to K<sub>12</sub> show essentially the same cyclic lignite–grey marl alternations (Figs. 2a and 3). The occurrence and number of volcanic ash layers in both sections in the cycles K<sub>2</sub>, K<sub>3</sub> (three ash beds), K<sub>4</sub>, K<sub>5</sub> (two ash beds), K<sub>7</sub>, K<sub>10</sub>, K<sub>11</sub> and K<sub>12</sub> confirm the cyclostratigraphic correlations, and show that the rhythmic alternations are synchronous. Additional evidence for the proposed correlation between the two sections is provided by cycle K<sub>9</sub>, which has a poorly developed basal lignite bed in contrast to the other cycles in this part of the sequence. The general lack of grey marl beds in the Vorio section impedes the recognition of individual cycles. However, the unusually thick volcanic ash layer in cycle K<sub>7</sub> – the so-called layer 9 (Van de Weerd, 1983)– as well as the consistent presence of additional, particular, mm-thick volcanic ash beds below and above this ash bed enables a detailed correlation with the corresponding interval of the pronounced cyclically bedded Komanos and Tomea Eksi sections.

**Cycles K<sub>13</sub> to K<sub>22</sub>.** The cyclostratigraphic interpretation of this interval is not very straightforward. Only the Komanos section comprises alternating lignite and grey marl beds. In the Vorio and Tomea Eksi sections the corresponding interval consists of an extensive, thick lignite seam with only a few, subordinate marl intercalations; abundant fossiliferous lenses suggest episodes of erosion and/or non-deposition. Even in the Komanos section, the expression of the sedimentary cyclicity is not very distinct. The basal lignite layers of cycles K<sub>15</sub>, 17 and 18 alternate with thin grey marl beds. This holds in particular for cycle K<sub>17</sub>, which contains alternating thin lignite and marl layers extending from marl K<sub>16</sub> to lignite K<sub>18</sub>. The thickness of the combined marl bed of K<sub>16</sub>–17 led to the interpretation of K<sub>17</sub> as a separate cycle. The interval between K<sub>19</sub> and K<sub>21</sub> lacks a clear cyclicity. It contains a distinct basal lignite bed, followed by alternating lignite, grey and beige marl beds. The banded interval is approximately three times thicker than the average cycle thickness. Therefore, it might represent three cycles (K<sub>20a</sub>, b, and c), but the lack of distinct lignite layers hampers an unambiguous cycle definition for this interval.

**Cycles K<sub>23</sub> to K<sub>30</sub>.** Cycles K<sub>23</sub> to K<sub>29</sub> in Komanos and Tomea Eksi are apparent as rhythmic alternations of lignite and grey marl beds. The expression of the cyclicity is clearer in Tomea Eksi due to the presence of more prominent basal lignite beds as compared to Komanos. Notable is the fact that the marl segments of cycles K<sub>27</sub> and K<sub>29</sub> in Tomea Eksi are very thin or sometimes even absent in contrast to the other cycles which have a ‘normal’ marl segment. In Komanos the marl segments of cycles K<sub>25</sub> and K<sub>27</sub> are thinner than average. Cycle K<sub>30</sub> comprises a pronounced beige marl bed. The general lack of marl beds in the Vorio section prevents a clear recognition of sedimentary cycles in the corresponding interval of cycles K<sub>23</sub> to K<sub>30</sub>.

### Theodoxus member

The Theodoxus member consists of two beige marl beds with thin lignite intercalations, separated by a prominent lignite bed. The lower marl bed is separated in two by a thin lignite bed and therefore interpreted to comprise two lignite-beige marl cycles, T<sub>1</sub> and T<sub>2</sub> (Fig. 3). The upper part of the Theodoxus member includes a banded beige marl bed with some two to four thin lignite seams. However, the lack of distinct lignite beds and the great lateral changes in bed-thickness hinder an unambiguous cyclostratigraphic interpretation for this interval. In the Vorio section, the expression of the cyclicity is most clear, showing three light-dark alternations (Fig. 2b). Therefore, this upper beige marl interval is interpreted to portray cycles T<sub>4</sub>, T<sub>5</sub> and T<sub>6</sub> (Fig. 3). The prominent lignite bed in Vorio separating the lower and upper beige marl bed contains a grey marl bed, which might suggest that it includes an extra cycle. Therefore cycle T<sub>3</sub> is numbered as T<sub>3a</sub> and T<sub>3b</sub> (Fig. 3). The volcanic ash beds in cycles T<sub>4</sub> and T<sub>5</sub> confirm our cyclostratigraphic correlations, showing that these lignite-marl cycles in the different sections are synchronous.

### Notio member

In view of the expression and lateral continuity of the lignite and marl alternations, the Notio member was subdivided into two parts. The lower interval, spanning cycles N<sub>1</sub> to N<sub>10</sub>, consists of clear lignite and marl alternations in all three sections. Alternating lignite and marl beds in the upper interval, spanning cycles N<sub>11</sub> to N<sub>22</sub>, are only found in the Vorio section.

*Cycles N<sub>1</sub> to N<sub>10</sub>.* In all three studied sections, this interval displays a clear rhythmic alternation of lignite and primarily grey marl beds (Fig. 3). Ten complete lignite-grey marl cycles are recorded in the Tomea Eksi and Komanos sections. In the Vorio section, the first cycle (N<sub>1</sub>) is poorly developed or missing. In Vorio and Komanos, the basal lignite beds are generally thinner than in Tomea Eksi. Consequently, the cyclicity is more distinct in the latter section. Again, the occurrence, position and number of volcanic ash layers in cycles N<sub>2</sub> (two ash beds), N<sub>3</sub> (two ash beds), N<sub>4</sub>, N<sub>5</sub> and N<sub>6</sub> confirm our correlations between the different sections, and show that the lignite-marl cycles are time-equivalent. Additional evidence is provided by the relatively thick grey marl bed of cycle N<sub>5</sub> and the lack of a distinct basal lignite bed in cycles N<sub>9</sub> and N<sub>10</sub>.

*Cycles N<sub>11</sub> to N<sub>20</sub>.* In the Vorio section, ten additional lignite-grey marl cycles have been recorded. In these cycles, grey marl beds alternate with thin lignite beds. Some characteristic cycle patterns can be distinguished in addition to the basic cycle repetition. Cycles with distinct lignite (N<sub>11</sub> to N<sub>13</sub>, and N<sub>16</sub>) alternate with cycles in which lignites are weakly developed (N<sub>14</sub>, N<sub>15</sub>, and N<sub>17</sub> to N<sub>19</sub>). In the Tomea Eksi section, lignite predominates above cycle N<sub>10</sub>, whereas in the Komanos section grey marl predominates, which in both cases impedes a further recognition of sedimentary cycles for this interval.

## Argon geochronology

We performed both incremental heating and laser total fusion  $^{40}\text{Ar}/^{39}\text{Ar}$  dating on the Ptolemais volcanic ashes complementing our cyclostratigraphic study. Nine ash beds were analysed, three from each stratigraphic member (Fig. 3). Isotopic dating focused on the sanidine populations of these ash beds, because of the generally good preservation and high K-content of the individual crystals. In general, the biotite crystals have been partially altered to chlorite and are therefore less suitable for dating. The only exception is the ash bed in cycle T5 in the Theodoxus member, which contains fresh and unaltered biotite crystals. Because of their continuity and uniform thickness, the ash beds are interpreted as primary fall-outs, with only limited post-depositional transport. All but one appear as a few-mm to three-cm thick partings. Ash bed K7 - the so-called *layer 9* (Van de Weerd, 1983) - about 10 m above the base of the Ptolemais Formation, has a thickness of about 25 cm. Explosive acid volcanic activity is common in the area from Miocene to Recent, and thought to be related to subduction related magmatism (Kolios et al., 1980).

### Methods

Bulk samples with a weight of ca. 1 kg were washed and sieved to separate the  $> 125 \mu\text{m}$  fraction. An optimum sieve fraction between  $125 \mu\text{m}$  and  $500 \mu\text{m}$  was selected for further separation. Mineral separates of sanidine and biotite were concentrated by standard heavy liquid and magnetic separation techniques, and finally by hand-picking the clear (fresh) phenocrysts under a binocular microscope. Sample purity and mineralogy of the sanidine separates was assessed by non-destructive X-ray fluorescence (XRF) analyses on the actual separates. The K/Ca ratios for all separates were  $\sim 10$ , which is indicative for the K-feldspar sanidine.

$^{40}\text{Ar}/^{39}\text{Ar}$  analyses were performed in 1996 and 1997 (irradiation runs VU16 and VU21) on the argon laser-probe facility (VULKAAN) at the Free University in Amsterdam, the Netherlands. A detailed description of techniques is given by Wijbrans et al. (1995). Approximately 50-mg aliquots of the purified mineral separates were wrapped in Al foil and loaded in 5 mm ID quartz reactor vials. Irradiation with fast neutrons was done in the Oregon State University TRIGA reactor in the cadmium shielded CLICIT facility for 2 hrs (VU16) and 7 hrs (VU21). To monitor the variation in neutron flux over the entire length of the irradiation vials, neutron fluence monitors were loaded at the top and bottom positions of the tube and between each set of four or five unknowns. The monitor mineral used in VU16 was sanidine DRA from the trachite from Drachenfels, Germany (Wijbrans et al., 1995). The age used for this standard has been determined by intercalibration against Taylor Creek Ryolite sanidine (sample TCR 85G003 of Dalrymple et al., 1988). The error-weighted mean age of 48 analyses vs. an age of 27.92 Ma for TCR was  $24.99 \pm 0.14$  Ma for DRA (Wijbrans et al., 1995). The age of TCR is relative to a K-Ar age of 162.9 Ma of the primary standard SB-3 biotite (Lanphere, 1990). VU21 was monitored with DRA, TCR and FCT sanidines. An internally consistent J-curve was calculated from multiple analyses, using an age of 27.92 Ma for

TCR, 24.99 Ma for DRA and 27.62 Ma for FCT. The age of 27.62 Ma for FCT is based on unpublished, internal calibrations of multiple irradiation runs with TCR and DRA.

Subsequent to irradiation, the samples were transferred into 2 mm diameter wells in a copper sample holder for laser fusion, placed in an ultra-high-vacuum extraction line and preheated to 200 °C for 24 hrs in order to remove undesirable large quantities of atmospheric argon from the line. The samples were fused using a focused continuous ion laser beam (max. 18W), applied for 60 to 90 seconds. After an additional 5-min of clean-up, the isotopes of the purified argon gas were measured using a Mass Analyser Products LTD 215-50 noble gas mass spectrometer. Beam intensities were measured in peak jumping mode over the mass range 40-36 on a secondary electron multiplier and regressed to the height at the time of the inlet. The laser incremental heating experiments consisted of 8 to 14 individual steps, degassing approximately 50 grains. We defocused the laser beam and increased the power of the laser for each subsequent step. In the laser total fusion experiments, five separate splits of approximately 25 grains were analysed. Here, we used a focused laser beam.

Each analysis was corrected for mass discrimination and a total system blank at the five Ar mass positions. System blanks were measured between every five steps. Mass discrimination during this study as monitored by aliquots of air from an on-line air pipette system was 1.0029 per mass unit for VU16 and 1.0038 for VU21. The total system blanks for this project were in the range 1.1-6.0 exp-17 moles for m/e=40, 0.4-4.3 exp-19 moles for m/e=39, 1.1-5.3 exp-19 moles for m/e=38, 1.7-2.5 exp-18 moles for m/e=37 and 3.3-7.9 exp-19 moles for m/e=36. The neutron fluence parameter J was calculated from five to twelve replicate total fusion analyses of 10 to 15 grains of the monitor standards. J for each point in the quartz tube was determined using a second order polynomial regression between individual standards, what resulted in best-fit curves with R<sup>2</sup> of 0.98 (VU16) and 0.93 (VU21). Reproducibility of each monitor point along the J curve suggests that errors in the J value are around 0.3%; this error was propagated into the age calculations for each analysis. MSWD calculations were also made to test for scatter about the mean. Ages were calculated using the decay constants of Steiger and Jaeger (1977). All the error assignments throughout this paper are  $\pm 2\sigma$ .

## Results

The results from the incremental heating experiments are presented in age spectrum diagrams (Fig. 4). Age plateaux are reported in this study, because the uniformly high radiogenic Ar yields of individual gas fractions (90-99.9%) generally precluded regression in isotope correlation diagrams. Plateau gas fractions were selected from age spectra using the criteria of Fleck et al. (1977), whereby a plateau consists of at least three successive incremental heating steps, showing consistency within  $2\sigma$  error and carrying >50% of the total  $^{39}\text{Ar}$  gas released. The apparent ages calculated for each step are internally concordant; all age spectra are essentially flat and satisfy the plateau criteria. They yielded plateaux for 90.3-99.8% of the total released  $^{39}\text{Ar}$  (Table 1), which is typical for thermally undisturbed volcanic sanidine (Duffield and Dalrymple, 1990). Discordant gas

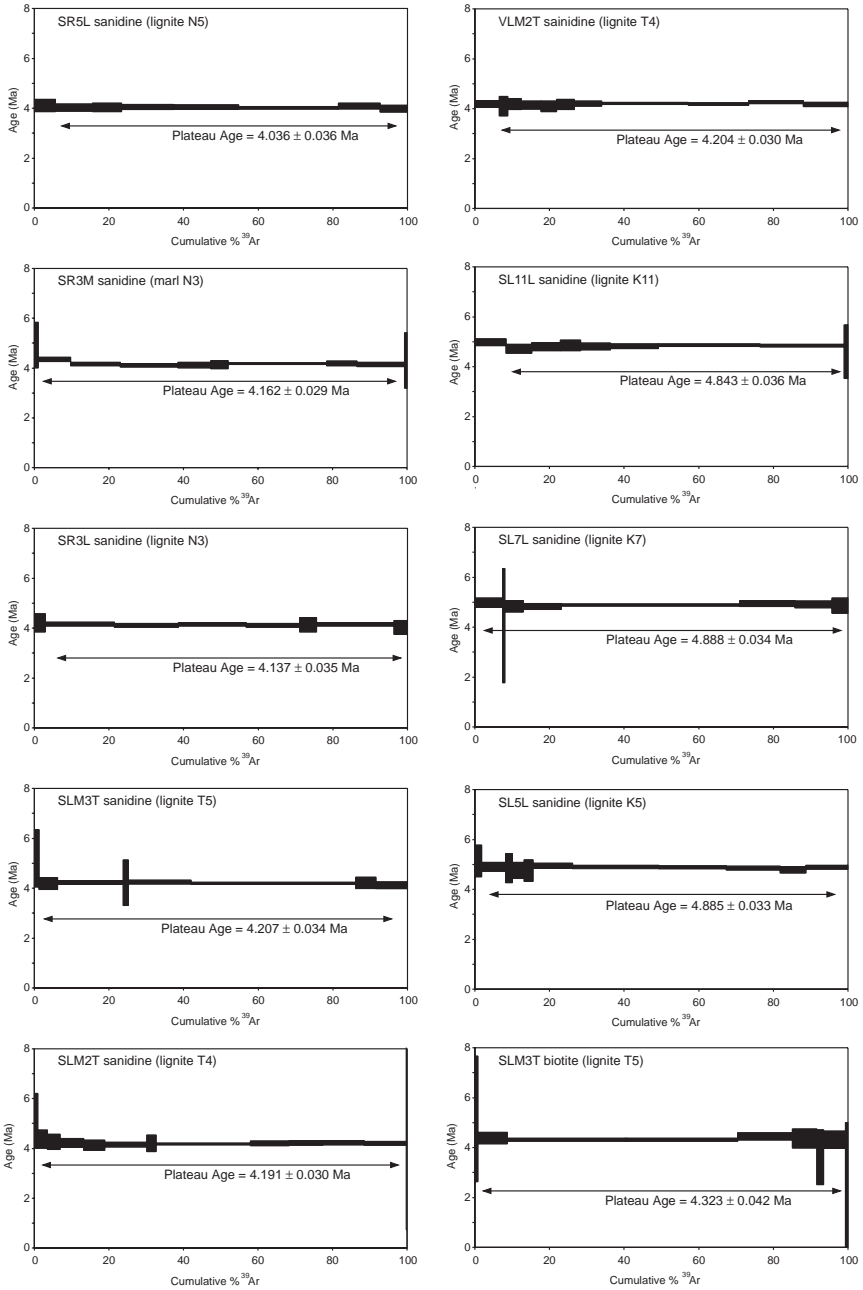


Figure 4:  $^{40}\text{Ar}/^{39}\text{Ar}$  laser incremental-heating spectra for sanidine and biotite separates from nine of the Ptolemais volcanic ash beds. Plateau definitions are as described by Fleck et al. (1977). For the location of the ash beds see Fig. 3. All errors shown are listed at the 2s level, internal precision.

fractions are limited to initial increments showing high variance and low radiogenic argon yields. Weighted mean ages based on inverse variances were calculated for the plateaux, demonstrating that the main part of the Ptolemais Formation spans an interval from approximately 5.0 to 4.0 Ma (Table 1). The plateau ages are generally consistent with stratigraphic position.  $^{40}\text{Ar}/^{39}\text{Ar}$  ages of the volcanic ash beds from the lower Kyrio member are systematically older than those from the middle Theodosius member, while the volcanic ash beds from the upper Notio member have the youngest ages. Even within the three members, the ages are generally in agreement with the stratigraphic order. Noteworthy is that the biotite separate of sample SLM<sub>3</sub>T yielded an ~120 kyr older plateau age than the sanidine separate of the same sample.

All nine sanidine separates were also analysed via single-step total fusion. The results are summarised in Table 1. From all but three sanidine separates, all individual replicate analyses are concordant within the error limits of their weighted mean value. Their apparent  $^{40}\text{Ar}/^{39}\text{Ar}$  ages are in excellent agreement with their stratigraphic order. For sanidine VLM<sub>2</sub>T, 4 out of 5 total fusion ages are indistinguishable at the 95% confidence level. The remaining run has a 60 kyr younger apparent age. Sanidine SL<sub>5</sub>L and SL<sub>7</sub>L gave less reliable  $^{40}\text{Ar}/^{39}\text{Ar}$  dating results. Two individual runs of SL<sub>5</sub>L gave ~80 kyr older ages than the weighted mean value. Total fusion experiments on SL<sub>7</sub>L gave rather divergent results, with only three concordant analyses out of five after irradiation run VU<sub>16</sub>. Of the remaining two runs of SL<sub>7</sub>L one age was ~80 kyr older, while the other was ~540 kyr older. Analogous to the first experiment, individual analyses for SL<sub>7</sub>L after irradiation run VU<sub>21</sub> showed considerable scatter around the mean with ages ranging between 4.989 and 5.119 Ma and a MSWD value of 16.38 (Table 1).

The volcanic ash bed from cycle T<sub>4</sub> yielded two independent age estimates from samples collected at two localities, SLM<sub>2</sub>T and VLM<sub>2</sub>T. Both the single fusion and incremental heating experiments gave  $^{40}\text{Ar}/^{39}\text{Ar}$  ages, which were not statistically different at the 95% confidence level. For all samples, single fusion and incremental heating experiments yielded ages that were indistinguishable (Table 1). Moreover, laser total fusion experiments on sanidine separate SLM<sub>2</sub>T yielded concordant weighted mean ages after irradiation runs VU<sub>16</sub> and VU<sub>21</sub> (Table 1). These experiments altogether have demonstrated the good reproducibility of the dating experiments.

## Discussion and conclusions

### *Ptolemais composite section*

All sections exposed in the Vorio, Tomea Eksi and Komanos open-pit mines contain both intervals in which rhythmic alternations of lignites and marls are very prominent, and intervals where indications for rhythmic sedimentation is less obvious or absent. The uniform presence of volcanic ash beds in these sections confirms the cyclostratigraphic correlations and indicates that the lignite-marl rhythmites represent regional, basin-wide sedimentary cycles rather than lateral facies migrations. Intervals without a clear expression of cyclicity often contain discontinuous fossiliferous levels or sand lenses, indicating

AGE SPECTRUM																
Sample	Cycle	Material	APTS age (Ma)	$^{40}\text{Ar}/^{39}\text{Ar}$ age <sup>1</sup> (Ma) (TCR=27.92)	K/Ca	$^{39}\text{Ar}$ (%)	n1	MSWD	$\Delta$ (Ma)	$\Delta$ (%)	$^{40}\text{Ar}/^{39}\text{Ar}$ age <sup>2</sup> (Ma) (TCR=28.34)	$\Delta$ (Ma)	$\Delta$ (%)	$^{40}\text{Ar}/^{39}\text{Ar}$ age <sup>3</sup> (Ma) (TCR=28.16)	$\Delta$ (Ma)	$\Delta$ (%)
Irradiation VU16																
SR5L	N5	sanidine	4.280	4.036 ± 0.036	41.0	94.4	7	0.42	0.244	6.0	4.097	0.183	4.5	4.070	0.210	5.2
SR3M	N3	sanidine	4.308	4.162 ± 0.029	45.0	90.3	8	0.66	0.146	3.5	4.225	0.083	2.0	4.197	0.111	2.7
SR3L	N3	sanidine	4.324	4.137 ± 0.035	48.1	97.0	7	0.44	0.187	4.5	4.199	0.125	3.0	4.172	0.152	3.7
SLM3T	T5	sanidine	4.387	4.207 ± 0.034	97.9	98.8	7	0.45	0.180	4.3	4.270	0.116	2.7	4.243	0.144	3.4
SLM2T	T4	sanidine	4.408	4.191 ± 0.030	70.6	99.1	12	0.39	0.217	5.2	4.254	0.154	3.6	4.227	0.181	4.3
VLM2T	T4	sanidine	4.408	4.204 ± 0.030	62.1	93.5	10	0.79	0.204	4.9	4.267	0.141	3.3	4.240	0.168	4.0
SL11L	K11	sanidine	5.015	4.843 ± 0.035	39.0	91.6	8	0.54	0.172	3.6	4.916	0.099	2.0	4.884	0.131	2.7
SL7L	K7	sanidine	5.099	4.888 ± 0.034	35.2	99.8	8	0.59	0.211	4.3	4.962	0.137	2.8	4.929	0.170	3.5
SL5L	K5	sanidine	5.146	4.885 ± 0.033	20.6	98.2	10	0.73	0.261	5.3	4.958	0.188	3.8	4.926	0.220	4.5
Irradiation VU21																
SLM3T	T5	biotite	4.387	4.323 ± 0.042	21.8	98.6	7	0.93	0.063	1.5	4.388	-0.002	0.0	4.481	0.027	0.6
TOTAL FUSION																
Sample	Cycle	Material	APTS age (Ma)	$^{40}\text{Ar}/^{39}\text{Ar}$ age <sup>1</sup> (Ma) (TCR=27.92)	K/Ca	n2	MSWD	D (Ma)	D (%)	$^{40}\text{Ar}/^{39}\text{Ar}$ age <sup>2</sup> (Ma) (TCR=28.34)	D (Ma)	D (%)	$^{40}\text{Ar}/^{39}\text{Ar}$ age <sup>3</sup> (Ma) (TCR=28.16)	D (Ma)	D (%)	
Irradiation VU16																
SR5L	N5	sanidine	4.280	4.083 ± 0.023	37.5	5	1.32	0.197	4.8	4.144	0.136	3.3	4.118	0.162	4.0	
SR3M	N3	sanidine	4.308	4.122 ± 0.026	35.5	5	2.35	0.186	4.5	4.184	0.124	3.0	4.157	0.151	3.7	
SR3L	N3	sanidine	4.324	4.132 ± 0.026	45.0	5	0.63	0.192	4.6	4.194	0.130	3.1	4.167	0.157	3.8	
SLM3T	T5	sanidine	4.387	4.158 ± 0.024	51.8	5	0.02	0.228	5.5	4.221	0.166	3.9	4.193	0.193	4.6	
SLM2T	T4	sanidine	4.408	4.178 ± 0.023	53.3	5	2.02	0.230	5.5	4.241	0.167	3.9	4.213	0.195	4.7	
VLM2T	T4	sanidine	4.408	4.224 ± 0.019	50.1	4	0.42	0.184	4.4	4.288	0.120	2.8	4.260	0.148	3.5	
SL11L	K11	sanidine	5.015	4.888 ± 0.031	49.5	5	2.39	0.127	2.6	4.962	0.053	1.1	4.929	0.086	1.7	
SL7L	K7	sanidine	5.099	4.862 ± 0.029	38.1	3	0.33	0.237	4.9	4.932	0.164	3.3	4.903	0.196	4.0	
SL5L	K5	sanidine	5.146	4.841 ± 0.025	40.6	3	0.59	0.305	6.3	4.914	0.232	4.7	4.882	0.264	5.5	
Irradiation VU21																
SLM2T	T4	sanidine	4.408	4.222 ± 0.023	50.9	12	1.19	0.186	4.4	4.286	0.122	2.9	4.258	0.150	3.6	
SL7L	K7	sanidine	5.099	5.002 ± 0.051	36.1	12	16.38	0.097	1.9	5.077	0.022	0.4	5.044	0.055	1.1	

Table 1: All samples are from the Tomea Eksi section, except VLM2T which is from the Vorio section (see also Fig. 3). Cycle number is from base of the Ptolemais Formation. APTS (astronomical) ages were obtained by linear interpolation of the sedimentation rate between astronomically dated calibration points, i.e. the lignite midpoints (see Van Vugt et al., 1998).  $^{40}\text{Ar}/^{39}\text{Ar}$  ages<sup>1</sup> are quoted against TCR sanidine of 27.92 Ma (Wijbrans et al., 1995) and  $^{40}\text{Ar}/^{39}\text{Ar}$  ages<sup>2</sup> against TCR sanidine of 28.34 Ma (Renne et al., 1998), both calculated with  $\lambda = 5.543310 \cdot 10^{-10} \text{ yr}^{-1}$  and  $^{40}\text{K}$  isotopic abundance of 0.01167 % (Steiger and Jaeger, 1977).  $^{40}\text{Ar}/^{39}\text{Ar}$  ages<sup>3</sup> are quoted against TCR of 28.16 Ma, calculated using the intercalibration coefficients between GA-1550, FCT and TCR of Renne et al. (1998), the branching coefficients of Endt (1990) and isotopic abundance of  $^{40}\text{K}$  of 0.01167 % (Garner, 1975).  $^{39}\text{Ar}(\%)$  is the percentage of total released  $^{39}\text{Ar}$  used in the plateau age.  $n1$  and  $n2$  are the number of increments and single fusion experiments used for the plateau and total fusion ages, respectively. MSWD is the mean squared weighted deviation.  $\Delta$  is the difference between the APTS and  $^{40}\text{Ar}/^{39}\text{Ar}$  ages. Isotope interference corrections from measurements of  $\text{CaF}_2$  and Fe-doped K-silicate glass were  $(^{36}\text{Ar}/^{37}\text{Ar})_{\text{Ca}} = 0.000264 \pm 0.0000017$ ;  $(^{39}\text{Ar}/^{37}\text{Ar})_{\text{Ca}} = 0.000673 \pm 0.0000037$ ;  $(^{40}\text{Ar}/^{39}\text{Ar})_{\text{K}} = 0.00086 \pm 0.00007$ . Errors are reported at  $2\sigma$  analytical precision. Copies of the full  $^{40}\text{Ar}/^{39}\text{Ar}$  data set are available on the first authors' request.

a dominance of local (e.g. topography) over regional (e.g. climatically induced) control. To demonstrate that the lignite-marl cycles in the Ptolemais basin are linked to orbital variations one must minimise these local effects. Any single section in the studied open-pit mines does not fulfil this purpose. In contrast to most deep-marine environments, local control generally plays an important role on facies development in shallow lacustrine deposits (Platt and Wright, 1992). Fortunately, the regular and consistent (i.e. laterally continuous) cyclic patterns for a particular stratigraphic interval are always present in at least one of the sections. The cyclostratigraphic Ptolemais composite section incorporates those intervals and thus shows an 'ideal' succession of lignite-marl cycles for the Ptolemais Basin.

Altogether, the Ptolemais composite section reveals 56 sedimentary cycles; 30 cycles in the Kyrio member (K1-30), 6 cycles in the Theodoxus member (T1-6) and 20 cycles in the Notio member (N1-20). From the Tomea Eksi section, cycles K1-12, K22-30 and N1-10 have been incorporated in the composite section. Cycles K13-21 are taken from the Komanos section. All cycles from the Theodoxus member (T1-6) and the upper 11 cycles from the Notio member (N11-20) in the composite section are selected from the Vorio section (Fig. 5).

### *Precessional origin of lignite-marl cycles*

The positions of the volcanic ash beds are well defined within the cyclostratigraphic composite section, and hence their  $^{40}\text{Ar}/^{39}\text{Ar}$  ages provide the age-control necessary for calculating the average duration of a lignite-marl cycle. From each of the nine volcanic ash beds dated, we used both the plateau ages from the incremental heating experiments and the weighted mean ages from the total fusion experiments. We plotted these versus the cumulative sedimentary cycle numbers from the base towards the top of the Ptolemais composite section (Fig. 6). The slope of a linear best-fit line through the data points equals the average duration of a lignite-marl cycle. A least square linear regression using all 22 radiometric ages gives an average duration of  $21.8 \pm 0.8$  kyr for the deposition of a lignite-marl cycle. This duration is in excellent agreement with the 21.7 kyr average periodicity of astronomical precession. Evidently, the lignite-marl cycles in the Ptolemais Formation are linked to the precessional variation in the Earth's orbit



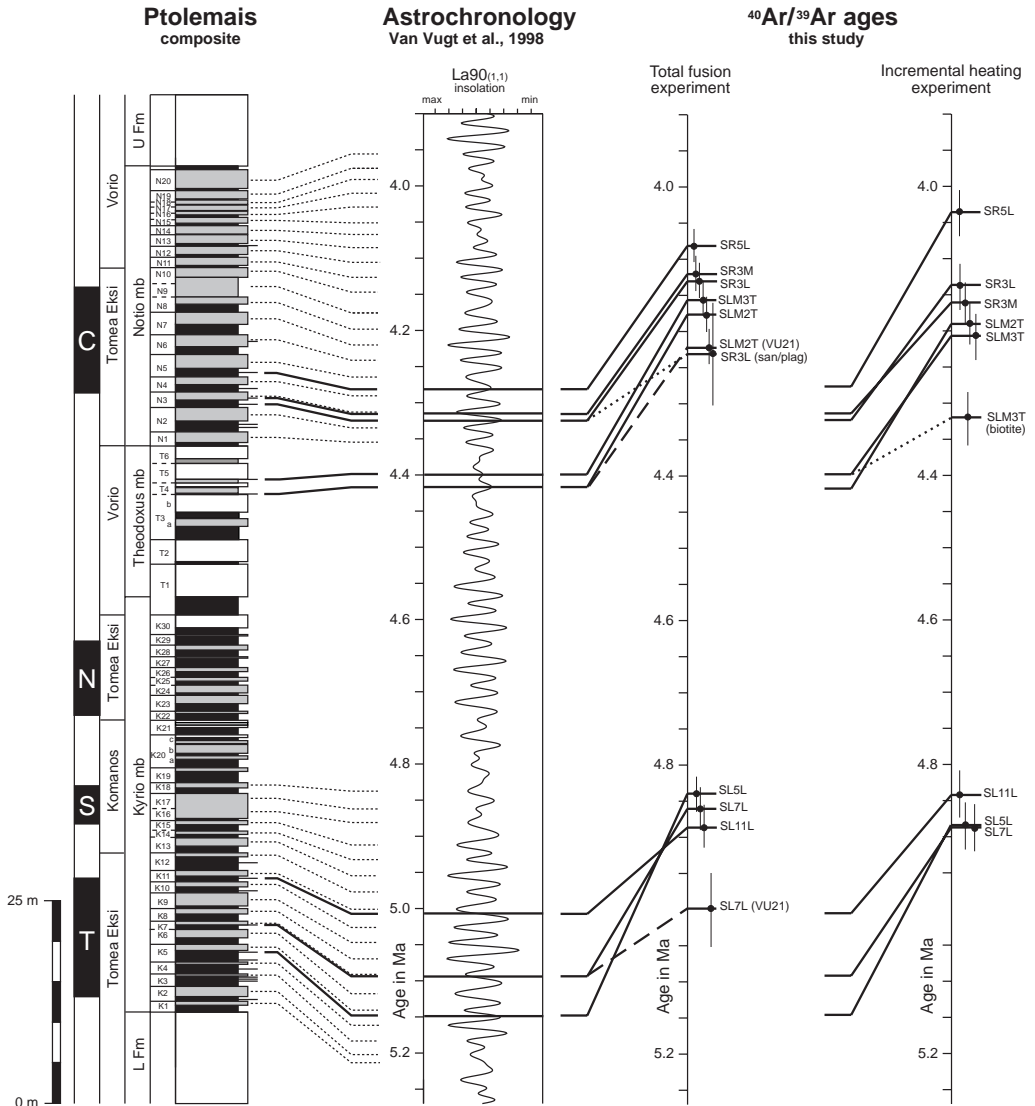


Figure 5: Composite section showing the succession of lignite-marl cycles in the Ptolemais Formation. Magnetic polarity and partial sections are indicated to the left of the sedimentary cycle numbers and stratigraphic members. In the polarity column, black (white) indicates normal (reversed) polarity. T, S, N and C indicate the Thvera, Sidufjall, Nuniavak and Cochiti Subchrons, respectively (for details see Van Vugt et al., 1998). Also shown is the comparison of incremental-heating and total fusion  $^{40}\text{Ar}/^{39}\text{Ar}$  ages of nine volcanic ash beds with astronomical ages for the same beds. Astronomical ages were obtained by linear interpolation of the sedimentation rate between astronomically dated calibration points, i.e. the lignite midpoints (Van Vugt et al., 1998). Solid lines, which connect astronomical and  $^{40}\text{Ar}/^{39}\text{Ar}$  ages, represent the VU16 sanidine separates. Dashed lines mark the VU21 sanidine separates, and dotted lines the VU21 biotite and VU10 mixed sanidine/plagioclase separates, respectively. All errors in the  $^{40}\text{Ar}/^{39}\text{Ar}$  ages are at 2s analytical precision.

through its influence on Mediterranean climate. To our knowledge, this is the first time that  $^{40}\text{Ar}/^{39}\text{Ar}$  dating results - totally independent from any other dating and or tuning technique - confirm the astronomical theory of climate change.

Independently from our method, an astronomical control on the deposition of the sedimentary cycles has also been suggested by Van Vugt et al. (1998). They correlated the magnetic polarity sequence of the Ptolemais succession to the Astronomical Polarity Time Scale (APTS) and found an average duration of the lithological cycles of  $21.6 \pm 0.5$  kyr.

### Comparison of $\text{Ar}/\text{Ar}$ and astronomical ages

The correlation of individual lignite-marl cycles to computed astronomical target curves by Van Vugt et al. (1998) resulted in astronomical ages for all sedimentary cycles - and thus for the intercalated volcanic ash layers. These astronomical ages have been obtained totally independent from our radioisotopic chronology. These two age estimates for the volcanic ash beds are compared in Table 1 and Fig. 5. It is striking that all  $^{40}\text{Ar}/^{39}\text{Ar}$  ages are significantly younger than the corresponding astronomical ages. For the sanidine separates, the discrepancies between the two ages are close to 200 kyr ( $\sim 4.5\%$ ). Such an age difference is beyond stated uncertainties, and so the astronomical ages must either be too old, or the  $^{40}\text{Ar}/^{39}\text{Ar}$  ages too young (or both). Below, we will evaluate the possible sources of error in both age estimates.

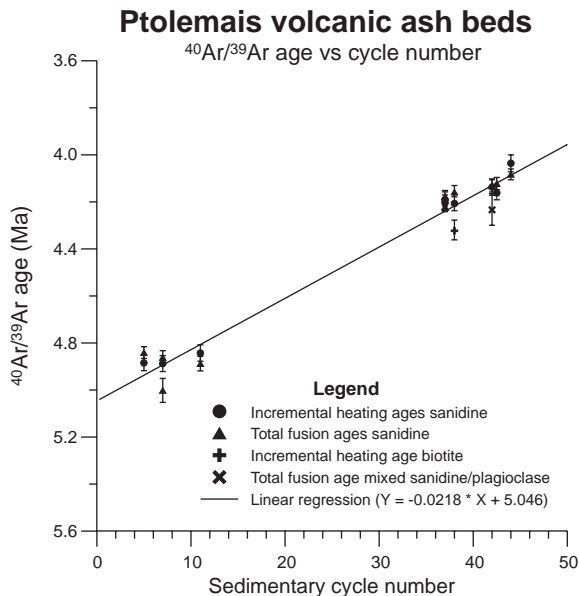


Figure 6: Laser incremental-heating and total fusion  $^{40}\text{Ar}/^{39}\text{Ar}$  ages of Ptolemais volcanic ash beds plotted vs. their corresponding cumulative sedimentary cycle number from the base of the Ptolemais Formation. Simple linear regression yields an average period of  $21.8 \pm 0.8$  kyr for a lignite-marl cycle, which is in excellent agreement with the average periodicity of astronomical precession.

The accuracy in the orbitally tuned chronology depends ultimately on (1) the correctness of the tuning, (2), the accuracy of the magnetostratigraphic data of the sedimentary succession studied, (3) accuracy of the orbital time-series used, and (4) errors in the APTS.

The orbitally tuned chronology used the magnetostratigraphy and biostratigraphy of the Ptolemais composite and the age of the corresponding reversal boundaries in the astronomically dated Rossello composite section (Langereis and Hilgen, 1991) for a first order calibration; see Van Vugt et al., 1998. Sedimentary cycles in the Rossello section were calibrated to the summer insolation time series by Lourens et al. (1996), thus providing astronomical ages for the magnetic reversal boundaries as well. The thus obtained astronomical ages for the magnetic reversal boundaries served as approximate tie-points for the astronomical tuning of the sedimentary cycles in the Ptolemais composite. Subsequent tuning to insolation resulted in astronomical ages for all the sedimentary cycles in the Ptolemais succession. The tuning shows a good-fit between insolation and typical sedimentary cycle patterns, like the well developed cycles in the Notio member or the absence of an apparent cyclicity in the Theodoxus member. Furthermore, the positions of the reversal boundaries generally appear within the same lithological cycle as in the APTS/Rossello composite (Van Vugt et al., 1998). Consequently, we consider the orbital tuned chronology to be accurate within one precession cycle, that is less than 21 kyr, and believe that the discrepancy unlikely originated from incorrectness in the orbital tuning.

The alternative is that the magnetostratigraphy of the Ptolemais succession is subject to error. The Ptolemais magnetostratigraphy reveals a dominantly reversed polarity with four normal intervals (Fig. 5). Given its early Pliocene age (Van de Weerd, 1979), these normal intervals have been correlated to the four normal Subchrons of the Gilbert Chron; see Van Vugt et al. (1998) for details. A possible source of error might be delayed acquisition of the magnetic remanence. However, delayed acquisition of the magnetisation in the Ptolemais sequence cannot explain the discrepancy between  $^{40}\text{Ar}/^{39}\text{Ar}$  and astronomical ages. This would result in older astronomical ages for the volcanic ash beds rather than younger ages. Again, support for the correctness of the magnetostratigraphy comes from the fact that the positions of the reversal horizons generally appear within the same lithological cycle as in the APTS/Rossello composite (Van Vugt et al., 1998). Thus, errors in the Ptolemais magnetostratigraphy cannot explain the age discrepancy.

Inaccuracy of the orbital time series will not result in a 200-kyr difference between the astronomical and radioisotopic ages at 4 or 5 Ma. Continuing improvements of the astronomical calculations resulted in a solution that is very accurate for at least the last 3 Ma (Quinn et al., 1991). Because of its complexity, the error in the astronomical solution is difficult to estimate. It is believed to be less than  $\sim 0.03$  radians for the Earth's longitude and pole position at 3.0 Ma, which is of the order of only a few 100 yr. Thus, inaccuracy in the orbital solutions can at most generate a negligible error in the astronomical age estimates.

As explained above, Van Vugt et al. (1998) use the astronomical ages of the magnetic

reversal boundaries in the Rossello section - on which the APTS is based - as approximate tie-points for the orbital tuning of the sedimentary cycles in Ptolemais. These astronomical ages were derived from correlation of a detailed record of carbonate cycles to astronomical time series (Hilgen, 1991; Lourens et al., 1996). Therefore, the discrepancy might be explained by too old astronomical ages for the reversal boundaries in the Rossello section. This might result from delayed acquisition of magnetisation or by an incorrect correlation of the sedimentary cycles to the astronomical time series. Both options seem unlikely. Detailed magnetostratigraphic studies of the Rossello section (Van Hoof and Langereis, 1991; Langereis and Hilgen, 1991) limit the influence of delayed acquisition to less than two sedimentary cycles, that is less than 42 kyr. Independent support for the correlation of the carbonate cycles to the astronomical time series came from GRAPE density (Shackleton et al., 1990, 1995) and dust flux (Tiedemann et al., 1994) oscillations in deep-sea records. Further confirmation for the APTS came from a study by Wilson (1993), who showed that the astrochronology resulted in a more consistent and steady history of sea floor spreading rates. Consequently, a systematic error in the age of the reversal boundaries in the Rossello composite section seems unlikely.

Thus, it is tentatively concluded that the discrepancy between the astronomical and isotopic ages for the Ptolemais volcanic ash beds cannot be explained by systematically too old astronomical ages. In addition to errors in the orbitally tuned chronology, the other option might be that the  $^{40}\text{Ar}/^{39}\text{Ar}$  age estimates are systematically too young. Too young isotopic ages may result from (1) partial loss of radiogenic  $^{40}\text{Ar}$ , (2) an underestimation of the contribution of Ca- and K-derived Ar isotopes, (3) uncertainties in the age of the neutron-fluence monitor or primary standards, and/or (4) errors in the values of the decay constants of  $^{40}\text{K}$ .

Neither loss of radiogenic  $^{40}\text{Ar}$ , nor an underestimation of the contribution of Ca- and K-derived Ar isotopes are likely causes for the discrepancy. Incremental heating experiments allow for evaluation of the possible influence of radiogenic argon loss. The generally uniform distribution of the  $^{40}\text{Ar}/^{39}\text{Ar}$  ratios (Fig. 4) suggests a closed system with no influence of post-depositional alteration or thermal disturbances (Hess and Lippolt, 1986). The low coalification stage of the lignites (Cameron et al., 1984; Kaouras, 1989) also argues against possible thermal disturbances. The contribution of neutron produced Ar isotopes from Ca and K is not a significant source of error in this study either, as indicated by the uniformly high K/Ca ratios of the dated separates (Table 1).

In addition, too young  $^{40}\text{Ar}/^{39}\text{Ar}$  ages may result from errors in the ages of the (primary and secondary) standards.  $^{40}\text{Ar}/^{39}\text{Ar}$  dating is a relative dating method, i.e.  $^{40}\text{Ar}/^{39}\text{Ar}$  ages are quoted relative to primary standards whose ages are determined by the  $^{40}\text{K}/^{40}\text{Ar}$  method, or on secondary standards whose ages are based on  $^{40}\text{Ar}/^{39}\text{Ar}$  intercalibration with primary standards. Recent intercalibrations of several internationally used standards have eliminated intercalibration of standards as a significant source of error in  $^{40}\text{Ar}/^{39}\text{Ar}$  dating (Baksi et al., 1996; Renne et al., 1998). Until now however, the absolute ages of  $^{40}\text{Ar}/^{39}\text{Ar}$  monitor standards remain an unresolved issue. In our age calibration we have used an age for the monitor standard TCR sanidine of 27.92 Ma,

quoted relative to a K-Ar age of 162.9 Ma of the primary standard SB-3 biotite (Lanphere et al., 1990). Baksi et al. (1996) reported an age for TCR sanidine of 28.0 Ma, cited relative to a similar age for SB-3 biotite. Renne et al. (1998) obtained a total fusion age of 28.34 Ma for TCR, based on 54 isotopic measurements. Their age for TCR is quoted relative to a  $^{40}\text{Ar}/^{40}\text{K}$  age of  $98.79 \pm 0.96$  Ma for the primary standard GA-1550. It should be noted that this age is somewhat older than but statistically indistinguishable from the age of  $97.9 \pm 0.9$  Ma calculated from the original data of McDougall and Roksandic (1974). Using the equation of Dalrymple et al. (1993), we have recalculated our  $^{40}\text{Ar}/^{39}\text{Ar}$  ages with an age of  $28.34 \pm 0.28$  Ma for TCR as suggested by Renne et al. (1998). This reduces the 4.5% age discrepancy by  $\sim 1.5\%$  (Table 1), to a still significant  $\sim 3\%$  discrepancy.

Inaccuracies in the values of the decay constants might also be a source of error for our  $^{40}\text{Ar}/^{39}\text{Ar}$  ages. Beckinsale and Gale (1969) summarised the available determinations of the specific activities for the various decay modes of  $^{40}\text{K}$ . These data were combined with a new atomic abundance for  $^{40}\text{K}$  (Garner et al., 1975) to calculate the decay constants recommended by Steiger and Jaeger (1977). These calculations gave a total decay constant  $\lambda$  of  $^{40}\text{K}$  of  $(5.543 \pm 0.010) \times 10^{-10}$  year, and a half life of  $(1.250 \pm 0.002) \times 10^9$  year. We have used these values in our age calculations. It is noteworthy that these values are at odds with values used since 1973 by the nuclear physics and chemistry communities. Endt (1990) cites a half-life of  $(1.277 \pm 0.008) \times 10^9$  year for  $^{40}\text{K}$ , based on branching coefficients of 89.33% for  $\beta^-$  decay and 10.67% for electron capture decay, and a value of  $(1.178 \pm 0.004) \times 10^{-2}$  % for the  $^{40}\text{K}$  abundance. The value for the isotopic  $^{40}\text{K}$  abundance was based on measurements done by Nier (1950) and Reuterswärd (1956). It deviates significantly from the generally accepted isotopic abundance value for  $^{40}\text{K}$  of  $(1.167 \pm 0.0004) \times 10^{-2}$  % as determined by Garner et al. (1975). The latter value, which was calculated from standards of known composition, prepared by gravimetrically mixing, is probably more accurate than the ones by Nier (1950) and Reuterswärd (1956), who used older, less accurate techniques. Therefore, we have used the value of Garner (1975) in our work. We have recalculated the age of GA-1550 of Renne et al. (1998), using only the branching coefficients of Endt (1990) and neglecting the isotopic abundance value for  $^{40}\text{K}$  as reported in Endt (1990). Instead we take the isotopic abundance for  $^{40}\text{K}$  of Garner et al. (1975), the  $^{40}\text{K}$  concentration of Renne et al. (1998) and the  $^{40}\text{Ar}^*$  measurements of McDougall and Roksandic (1974). The age of GA-1550 is recalculated to 98.23 Ma. With this value for GA1550 and the intercalibration factors for GA1550, FCT and TCR of Renne et al (1998) the age of TCR is recalculated to 28.16 Ma. We have again recalculated our own  $^{40}\text{Ar}/^{39}\text{Ar}$  ages with this value for TCR (Table 1). This resulted in a reduction of the age discrepancy of  $\sim 1\%$  compared to the original values (Table 1), but still leaving an  $\sim 3.5\%$  (140-175 kyr) discrepancy.

The mineral sanidine is generally believed to be the ideal mineral for  $^{40}\text{Ar}/^{39}\text{Ar}$  dating, because of its high  $\text{K}_2\text{O}$  content and resistance against weathering (McDougall and Harrison, 1988). Therefore, we have focussed on the sanidine populations in the  $^{40}\text{Ar}/^{39}\text{Ar}$  experiments. In general, the biotite crystals in the Ptolemais ashes have been (partially) altered to chlorite, and are, consequently, less suitable for dating. The only

exception is the ash in cycle T<sub>5</sub> in the Theodoxus member, which contains fresh and unaltered biotite crystals. For comparison, we have also dated a biotite separate of this ash (sample SLM<sub>3</sub>T), which yielded a ~120 kyr older plateau age than the sanidine separate of the same sample (Table 1, Fig. 5). Therefore, the biotite separate SLM<sub>3</sub>T resulted in an (uncorrected)  $^{40}\text{Ar}/^{39}\text{Ar}$  age that is in closer agreement with the astronomical age than the experiment on pure sanidine separates. However, given the fact that from one ash only biotite and sanidine minerals have both been dated, and considering the uncertainties in the corrections discussed above, no far reaching consequences can be drawn from this inconsistency. Moreover, the literature is replete with examples to the contrary (e.g. Spell and McDougall, 1992; Turrin et al., 1994; Izett and Obradovich, 1994; Smith et al., 1996; Hilgen et al., 1997).

In conclusion, the ~200 kyr age discrepancy between the astronomical and  $^{40}\text{Ar}/^{39}\text{Ar}$  ages of the volcanic ash beds in the Ptolemais composite remains difficult to explain. The discrepancy is beyond the errors in both the astronomical and the  $^{40}\text{Ar}/^{39}\text{Ar}$  ages. Possible sources of error in the astronomical ages include incorrectness of the tuning, inaccuracies of the magnetostratigraphic data or the orbital time-series used, and/or errors in the Rossello section – on which the APTS is based. However, none of these seems to have significantly contributed to the ~200 kyr discrepancy. The other option is that the  $^{40}\text{Ar}/^{39}\text{Ar}$  age estimates are systematically too young. From the excellent  $^{40}\text{Ar}/^{39}\text{Ar}$  data set it is evident that neither loss of radiogenic  $^{40}\text{Ar}$ , nor an underestimation of the contribution of Ca- and K-derived Ar isotopes are significant sources of error. Moreover, only part of the discrepancy might result from the use of erroneously young ages for the neutron fluence monitors, and/or incorrect values for the decay constants of  $^{40}\text{K}$ . Clearly, as noted by Renne et al. (1998), improved determination of decay constants and absolute ages of monitor standards are necessary to increase the accuracy of the  $^{40}\text{Ar}/^{39}\text{Ar}$  method. Our ongoing research aims at a more robust inter-calibration of  $^{40}\text{Ar}/^{39}\text{Ar}$  and astronomical time using astronomically dated volcanic ash beds in both marine and continental successions.

## Acknowledgements

Prof. Dr. C.S. Doukas and Prof. Dr. E. Velitzelos (University of Athens, Greece) are greatly acknowledged for arranging necessary contacts and for co-operation in the field. We are grateful to the Public Power Corporation (Δ.Ε.Η. / Α.Κ.Π.-Α.) for permission to work in the mines and to the corporation's employees for their hospitality and assistance in the field. The authors thank Hendrik-Jan Bosch, Mark Dekkers, Marloes van Hoeve, Cor Langereis, Rob Satter, Konstantin Theocharopoulos and Wout Krijgsman for their interesting discussions and assistance in the field. We thank the reviewers T.C. Johnson and P.R. Renne for their valuable comments on an earlier version of the manuscript. This work was partly supported by the Netherlands Geosciences Foundation (GOA) with financial aid from the Netherlands Organisation for Scientific Research (NWO grant to J.S. and N.V.V.). This is NSG publication 990105.

## References

- Anastopoulos, J., and Koukouzas, C.N., 1972. Economic geology of the southern part of the Ptolemais lignite basin (Macedonia, Greece). *Geol. Geophys. Res.* 16(1), 1-189.
- Anderson, R.Y., 1982. A long geoclimatic record from the Permian. *J. Geophys. Res.* 87(C9), 7285-7294.
- Baksi, A.K., Hoffman, K.A., and McWilliams, M., 1993. Testing the accuracy of the geomagnetic polarity time-scale (GPTS) at 2-5 Ma, utilizing  $^{40}\text{Ar}/^{39}\text{Ar}$  incremental heating data on whole-rock basalts. *Earth Planet. Sci. Lett.* 118, 135-144.
- Baksi, A.K., Archibald, D.A. and Farrar, E., 1996. Intercalibration of  $^{40}\text{Ar}/^{39}\text{Ar}$  dating standards. *Chem. Geol.* 129, 307-324.
- Barrell, J., 1917. Rhythms and the measurements of geologic time. *GSA Bulletin* 28, 745-904.
- Bates, R.L., and Jackson, J.A.e., 1987. *Glossary of geology*. American Geological Institute, Alexandria -Virginia.
- Beckinsale, R.D. and Gale, N.H., 1969. A reappraisal of the decay constants and branching ratio of  $^{40}\text{K}$ . *Earth Planet. Sci. Lett.* 6, 289-294.
- Bradley, W.H., 1929. The varves and climate of the Green River epoch. *U.S. Geol. Surv. Prof. Pap.* 158E, 87-110.
- Brunn, J.H., 1956. Étude géologique du pinde serpetional et de la Macedoine occidentale. *Ann. Géol. Pays Hellen.* 7, 1-358.
- Cameron, A.R., Kalkreuth, W.D., and Koukouzas, C., 1984. The petrology of Greek brown coals. *Int. J. Coal Geol.* 4, 173-207.
- Dalrymple, G.B. and Duffield, W.A., 1988. High precision  $^{40}\text{Ar}/^{39}\text{Ar}$  dating of Oligocene rhyolites from the Mogollon-Datil volcanic field using a continuous laser system. *Geophys. Res. Lett.* 15(5), 463-466.
- Dalrymple, G.B., Izett, G.A., Snee, W. and Obradovich, J.D., 1993.  $^{40}\text{Ar}/^{39}\text{Ar}$  age spectra and total-fusion ages of tektites from Cretaceous-Tertiary boundary sedimentary rocks in the Beloc Formation, Haiti. *U.S. Geological Survey Bulletin* 2065, 1-20.
- Dean, W.E., and Fouch, T.D., 1983. Lacustrine environments. In P.A. Scholle, D. Bebout, and D. Moore, Eds. Carbonate depositional environments, *Am. Assoc. Pet. Geol. Mem.* 33, 97-130.
- Duffield, W.A., and Dalrymple, G.B., 1990. The Taylor Creek Rhyolite of New Mexico: a rapidly emplaced field of lava domes and flows. *Bull. Volcan.* 52, 475-478.
- Ehlers, E., 1960. Bericht über die bisher im Rahmen der Expertise Ptolemais durchgeführten geologischen und paläontologischen Untersuchungen. *Bundesanst. Geowiss. & Rohst.* Hannover, 1-36.
- Emiliani, C., 1955. Pleistocene temperatures. *J. Geol.* 63, 538-578.
- Endt, P.M., 1990. Energy levels of  $A = 21-44$  nuclei. *Nucl. Phys. A* 521, 1-830.
- Fischer, A.F., 1980. Gilbert - Bedding rhythms and geochronology. *GSA Special paper* 183, 93-104.
- Fleck, R.J., Sutter, J.F., and Elliot, D.H., 1977. Interpretation of discordant  $^{40}\text{Ar}/^{39}\text{Ar}$  age-spectra of Mesozoic tholeiites from Antarctica. *Geochem. Cosmochem. Acta* 41, 15-32.
- Gilbert, G.K., 1895. Sedimentary measurement of geological time. *J. Geol.*, 3, 121-127.
- Garner, E.L., Murphy, T.J., Gramlich, J.W., Paulsen, P.J. and Barnes, I.L., 1975. Absolute isotopic abundance ratios and the atomic weight of a reference sample of potassium. *J. Res. Natl. Bur. Stand.* 79A, 713-725.
- Gramann., 1960. Die Fossilien des Braunkohlenbeckens von Ptolemais-Komanos. *Bundesanst. Geowiss. & Rohst. Hannover* 37-49.
- Gregor, H.J., and Velitzelos, E., 1995. Facies development of Greek browncoals - dependant on tectonic movements. *Ann. Géol. Pays Hellen.* 36.

- Hall, C.M., and Farrell, J.W., 1995. Laser  $^{40}\text{Ar}/^{39}\text{Ar}$  ages of tephra from Indian Ocean deep-sea sediments: Tie points for the astronomical and geomagnetic polarity time scales. *Earth Planet. Sci. Lett.* 133, 327-338.
- Hays, J.D., Imbrie, J., and Shackleton, N.J., 1976. Variations in the Earth's orbit: pacemaker of the ice ages. *Science* 194, 1121-1132.
- Hess, J.C., and Lippolt, H.J., 1986.  $^{40}\text{Ar}/^{39}\text{Ar}$  ages of tonstein and tuff sanidines: New calibration points for the improvement of the Upper Carboniferous time scale. *Chem. Geol. (Isot. Geosci. Sect.)* 59, 143-154.
- Hilgen, F.J., 1991. Extension of the astronomically calibrated (polarity) time scale to the Miocene/Pliocene boundary. *Earth Planet. Sci. Lett.* 107, 349-368.
- Hilgen, F.J., Krijgsman, W., Langereis, C.G., Lourens, L.J., Santarelli, A., and Zachariasse, W.J., 1995. Extending the astronomical (polarity) time scale into the Miocene. *Earth Planet. Sci. Lett.* 136, 495-510.
- Hilgen, F.J., Krijgsman, W. and Wijbrans, J., 1997. Direct comparison of astronomical and  $^{40}\text{Ar}/^{39}\text{Ar}$  ages of ash beds: Potential implications for the age of mineral standards. *Geophys. Res. Lett.* 24, 2043-2046.
- Imbrie, J., Hays, J.D., Martinson, D.G., McIntyre, A., and Mix, A.C., 1984. The orbital theory of Pleistocene climate: support from a revised chronology of the marine  $\delta^{18}\text{O}$  record. In A. Berger, J. Imbrie, J. Hays, G. Kukla, and B. Saltzman, Eds. *Milankovitch and climate* 1, p. 510. Reidel, Dordrecht/Boston/Lancaster.
- Izett, G. and Obradovich, J., 1994.  $^{40}\text{Ar}/^{39}\text{Ar}$  age constraints for the Jaramillo normal subchron and the Matuyama-Brunhes geomagnetic boundary. *J. Geophys. Res.* 99, 2925-2934.
- Kaouras, G., 1989. Kohlenpetrographische, Palynologische und Sedimentologische Untersuchungen der Pliozänen Braunkohle von Kariochori bei Ptolemais / NW Griechenland. Mathematisch-Naturwissenschaftlichen Fachberieche, *Ph.D. Thesis*, Georg-August-Universität, Göttingen, Germany.
- Kolios, N., Innocenti, F., Manetti, P., Peccerillo, A., and Giliani, O., 1980. The Pliocene Volcanism of the Voras Mts (Central Macedonia, Greece). *Bull. Volcan.* 43, 553-568.
- Koufos, G.D., and Pavlides, S.B., 1988. Correlation between the continental deposits of the lower Axios Valley and the Ptolemais Basin. *Bull. Geol. Soc. Greece* 20, 9-19.
- Krijgsman, W., Hilgen, F.J., Langereis, C.G., Santarelli, A., and Zachariasse, W.J., 1995. Late Miocene magnetostratigraphy, biostratigraphy and cyclostratigraphy in the Mediterranean. *Earth Planet. Sci. Lett.* 136, 475-494.
- Langereis, C.G., and Hilgen, F.J., 1991. The Rossello composite: a Mediterranean and global reference section for the Early to early Late Pliocene. *Earth Planet. Sci. Lett.* 104, 211-225.
- Lanphere, M.A., Dalrymple, G.B., Fleck, R.J. and Pringle, M.S., 1990. Intercalibration of mineral standards for K-Ar and  $^{40}\text{Ar}/^{39}\text{Ar}$  measurements. *EOS, Trans. Am. Geophys. Union* 71, 1658.
- Lourens, L.J., Antonarakou, A., Hilgen, F.J., Van Hoof, A.A.M., Vergnaud-Grazzini, C., and Zachariasse, W.J., 1996. Evaluation of the Plio-Pleistocene astronomical timescale. *Paleoceanography* 11, 391-413.
- McDougall, I. and Roksandic, Z., 1974. Total fusion  $^{40}\text{Ar}/^{39}\text{Ar}$  ages using HIFAR reactor. *J. Geol. Soc. Aust.* 21, 81-89.
- McDougall, I. and Harrison, T.M., 1988. Geochronology and thermochronology by the  $^{40}\text{Ar}/^{39}\text{Ar}$  method. *Oxford Monographs on Geology and Geophysics* 9. Oxford University Press, New York, 212 pp.
- Mercier, J.L., Sorel, D., and Vergely, P., 1989. Extensional tectonic regimes in the Aegean basins during the Cenozoic. *Basin Research* 2, 49-71.
- Murphy, D.H., and Wilkinson, B.H., 1980. Carbonate deposition and facies distribution in a central Michigan marl lake. *Sedimentology* 27, 123-135.
- Nier, A.O., 1950. A redetermination of the relative abundances of the isotopes of carbon, nitrogen, oxygen, argon, and potassium. *Phys. Rev.* 77, 789-793



- Pavlidis, S.B., and Mountrakis, D.M., 1986. Neotectonics of the Florina-Vegoritiss-Ptolemais Neogene Basin (NW Greece): an example of extensional tectonics of the greater Aegean area. *Ann. Géol. Pays Hellen.* 33, 311-327.
- Platt, N.H., and Wright, V.P., 1992. Palustrine carbonates and the Florida Everglades: Towards an exposure index for the fresh-water environment. *J. Sed. Petrol.* 62, 1058-1071.
- Quinn, T.R., Tremaine, S. and Duncan, M., 1991. A three million year integration of the Earth's orbit. *Astron. J.* 101, 2287-2305.
- Renne, P.R., Deino, A.L., Walter, R.C., Turrin, B.D., Swisherr, C.C., Becker, T.A., Curtis, G.H., Sharp, W.D., and Jaouni, A.-R., 1994. Intercalibration of astronomical and radioisotopic time. *Geology* 22, 783-786.
- Renne, P.R. et al., 1998. Intercalibration of standards, absolute ages and uncertainties in  $^{40}\text{Ar}/^{39}\text{Ar}$  dating. *Chem. Geol.* 145, 117-152.
- Reuterswärd, 1956. On the isotopic constitution of potassium: A study of mass discrimination in a hot anode ion source. *Ark. Fys.* 11, 1-54.
- Shackleton, N.J., Berger, A., and Peltier, W.R., 1990. An alternative astronomical calibration of the lower Pleistocene timescale based on ODP site 677. *Transactions of the Royal Society of Edinburgh, Earth Sciences* 81, 251-261.
- Shackleton, N.J., Crowhurst, S., Hagelberg, T., Pisias, N.G., and Schneider, D.A., 1995. A new Late Neogene time scale: application to leg 138 sites. *Proc. Ocean Drill. Prog., Sci. Results* 138, 73-97.
- Shackleton, N.J., and Opdyke, N.D., 1973. Oxygen isotope and paleomagnetic stratigraphy of Pacific core V28-238: oxygen and isotope temperatures and ice volumes on a 105 and 106 year scale. *Quaternary Research* 3, 39-55.
- Smith, P.E., York, D., Chen, Y. and Evensen, N.M., 1996. Single crystal  $^{40}\text{Ar}/^{39}\text{Ar}$  dating of a Late Quaternary paroxysm on Kos, Greece: Concordance of terrestrial and marine ages. *Geophys. Res. Lett.* 23, 3047-3050.
- Spell, T.L. and McDougall, I., 1992. Revisions of the age of the Brunhes-Matuyama boundary and the Pleistocene Geomagnetic Polarity Timescale. *J. Geophys. Res.* 19, 1181-1184.
- Steiger, R., and Jaeger, E., 1977. Subcommittee on geochronology: convention on the use of decay constants in geo- and cosmochronology. *Earth Planet. Sci. Lett.* 36, 359-362.
- Tiedemann, R., Sarnthein, M. and Shackleton, N.J., 1994. Astronomical timescale for the Pliocene Atlantic  $\delta^{18}\text{O}$  and dust flux records of the Ocean Drilling Program site 659. *Palaeoceanography* 9, 619-638.
- Turrin, B.D., Donnelly-Nolan, J.M. and Hearn, B.C.J., 1994.  $^{40}\text{Ar}/^{39}\text{Ar}$  ages from the rhyolite of Alder Creek, California: Age of the Cobb Mountain normal-polarity subchron revisited. *Geology* 22, 251-254.
- Van de Weerd, A., 1979. Early Ruscinian rodents and lagomorphs (Mammalia) from the lignites near Ptolemais (Macedonia, Greece). *Proc. Kon. Akad. v. Wetensch.-Amsterdam B* 82, 127-170.
- Van de Weerd, A., 1983. Palynology of some Upper Miocene and Pliocene Formations in Greece. *Geologisches Jahrbuch*, B 48, 3-63.
- Van Houten, F.B., 1964. Cyclic lacustrine sedimentation, Upper Triassic Lockatong Formation, Central New Jersey and adjacent Pennsylvania. *Kansas Geol. Survey Bull.* 169, 497-531.
- Van Hoof, A.A.M., and Langereis, C.G., 1991. Reversal records in marine marls and delayed acquisition of remanent magnetization. *Nature* 351, 223-225.
- Van Vugt, N., Steenbrink, J., Langereis, C.G., Hilgen, F.J., and Meulenkamp, J.E., 1998. Magnetostratigraphy-based astronomical tuning of the early Pliocene lacustrine sediments of Ptolemais (NW Greece) and bed-to-bed correlation with the marine record. *Earth Planet. Sci. Lett.* 164, 535-551.
- Velitzelos, E., and Schneider, H., 1973. Beiträge zur Geologie West-Makedoniens 1. Elephantiden-Reste aus dem Pleistozän der Provinz Florina. *Ann. Mus. Goulandris* 1, 251-256.
- Vetoulis, D.G., 1957. Beiträge zur Kenntnis der Geologie des Ptolemais-Beckens, Mazedoniens. *Ann. Géol. Pays Hellen.* 8, 48-79.

- Wijbrans, J.R., Pringle, M.S., Koppers, A.A.P., and Scheveers, R., 1995. Argon geochronology of small samples using the Vulkaan argon laserprobe. *Proc. Kon. Akad. v. Wetensch.-Amsterdam* 98, 185-218.
- Wilson, D.S., 1993. Confirmation of the astronomical calibration of the magnetic polarity time scale from sea-floor spreading rates. *Nature* 364, 788-790.



# Magneto- and cyclostratigraphy and mammal-fauna's of the Pleistocene lacustrine Megalopolis Basin, Peloponnesos, Greece

## Abstract

The Pleistocene Megalopolis basin contains lacustrine silt, clay and marl with regularly intercalated lignite seams. Mammal fauna's that were collected from four levels indicate a late Early to Late Biharian age (middle Pleistocene). The magnetostratigraphic study revealed the Matuyama-Brunhes boundary in the section. Reversal excursions were not recorded or indistinguishably overprinted by delayed acquisition of magnetic remanence.

The regular pattern of lignite seams is argued to be related to 100 kyr eccentricity, with the lignite intervals corresponding to eccentricity maxima. Smaller-scale lignite cycles are correlated to insolation maxima. This interpretation leads to the conclusion that organic material was preserved during warm and humid periods, while predominantly detrital material was deposited during relatively cool and dry intervals.

Generally,  $\delta^{18}\text{O}$  minima correspond to eccentricity maxima in the Pleistocene. However, the interglacial oxygen isotope stages 19 and 11, which correspond to very low-amplitude eccentricity maxima, have a normal amplitude. Interestingly, the pattern of lignite seams in Megalopolis corresponds much better to the eccentricity curve than to the  $\delta^{18}\text{O}$  record. This suggests that environmental/climatic changes on the Mediterranean continent are forced by a mechanism different from the one that forces glaciations as reflected by marine  $\delta^{18}\text{O}$  records.

## Introduction

Sediments are a natural archive for the Earth's climate. The many studies on Mediterranean sedimentary sections have provided a wealth of palaeoclimatic information. A multi-disciplinary research programme on continental-marine correlations in the Mediterranean aims to study different non-marine Neogene sedimentary environments. High-resolution time frames for such deposits, established through correlation with marine reference sections and/or astronomical target curves, are the basis for various detailed studies that enhance our understanding of the coupling between astronomical parameters, palaeoclimate and palaeoenvironment in different realms. Miocene floodplain and distal alluvial environments from the western Mediterranean are currently being investigated (Abdul Aziz et al., 2000; Krijgsman et al., 1994), as well as a Pliocene shallow lacustrine carbonate-lignite system from northern Greece (Steenbrink et al., 1999; van Vugt et al., 1998). A study on much younger (Pleistocene) lacustrine deposits is presented here.

The lignite-containing lacustrine sediments in the Megalopolis basin have been studied for geological and mining purposes since 1962 (Lüttig and Marinos, 1962; Vinken, 1965). More recently, various studies in the Megalopolis lignite mines have contributed to the Pleistocene palaeoclimate records (Benda et al., 1987; Nickel et al., 1996, among others). The detailed study by Nickel et al. suggests that lignites were formed during an interglacial or interstadial, thus hinting at a cyclic origin for the groups of lignite seams. The present study aims at identifying such a cyclic origin, finding the periodicity and correlating the cycles to an astronomical solution. Palaeontology and magnetostratigraphy provide the first-order time control.

## Geological background

The intramontane lacustrine Megalopolis Basin is located in the middle of the Peloponnesos peninsula in southern Greece (Figure 1), at the boundary between Mesozoic limestones of the Pindos zone and Eocene flysch of the Tripolitza Group (Vinken, 1965). The eastern margin of the basin is formed by NE-SW trending normal faults, that have been active since the Late Miocene.

Upper Pliocene lacustrine and fluvial units overly the limestone and flysch basement, followed by Pleistocene fluvial conglomerates of the Apiditsa Formation in the western and central part of the basin (Figure 1). The overlying Choremi Formation, especially its Marathousa Member, with lacustrine clay, silt, lignite, and some sand beds in the centre of the basin, and fluvial sediments at the margins is of main interest to this study. Fluvial terraces and braided channel deposits constitute the top of the Pleistocene basin fill (Vinken, 1965).

Three open pit lignite mines provide large, unweathered exposures of the Marathousa Member. The lignite has previously been divided into three major coal seams (Löhnert and Nowak, 1965), divided by clay, silt and sand partings of 5–30 m thick. This classifi-

cation is in close agreement with the cyclic pattern distinguished in the Marathousa member (see below). Based on this cyclic interpretation, we prefer to arrange the lignite seams into four groups: I-IV (Figure 2), of which groups III and IV belong to Löhnert's uppermost (Panagiatis) group.

The lignite layers exposed in the mines are thickest in the western part of the mines and wedge out towards the east, as opposed to the detrital layers, that are thickest in the east

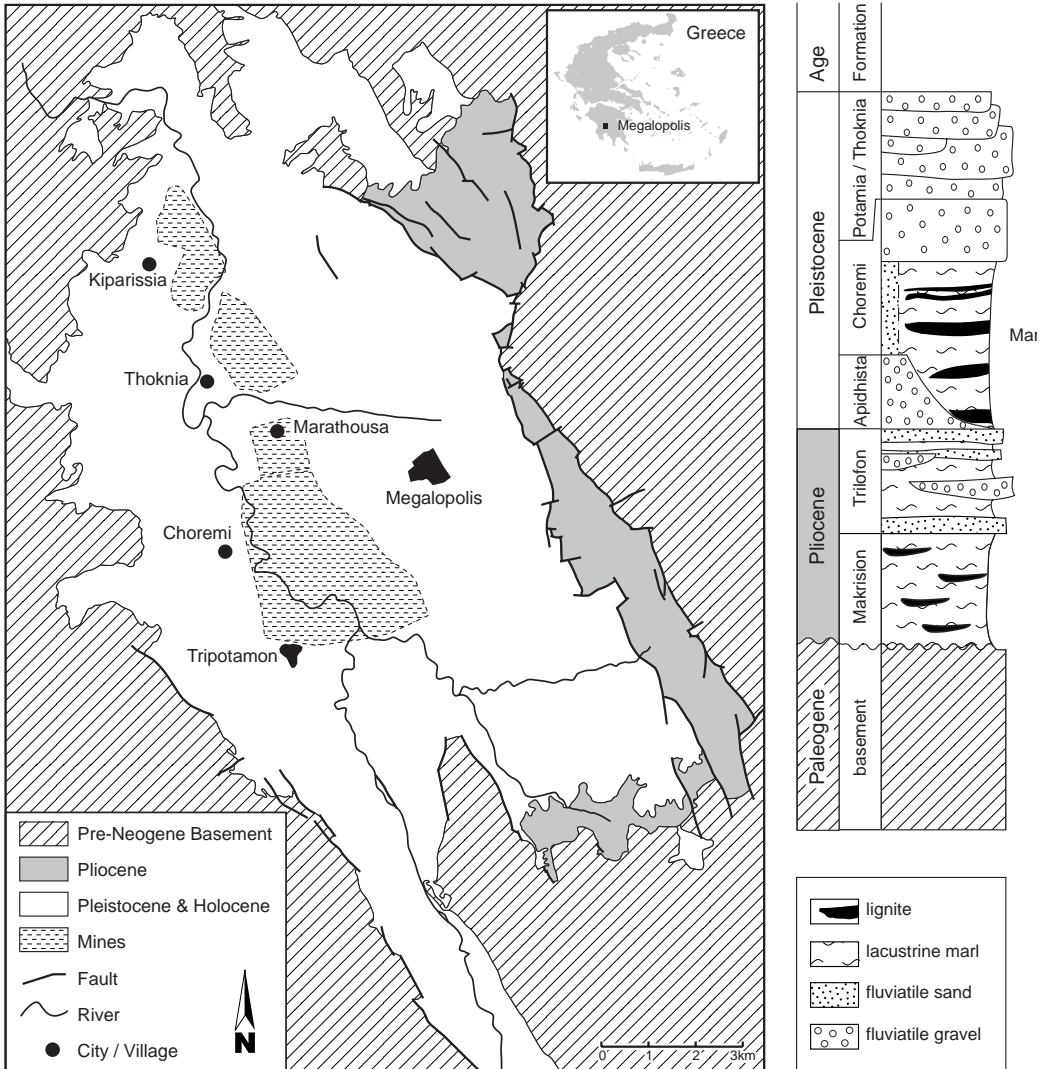


Figure 1: Geological sketch map of the Megalopolis basin and stratigraphic column of the basin fill (not to scale).

and become thinner towards the west. This is in accordance with the half-graben configuration of the basin, with major subsidence along the steep faults in the east, providing accommodation space for the abundant detrital sediment from the steep relief. Along the western margin, where subsidence was moderate, the lake bottom dipped gently, enabling swamps to accumulate organic material for prolonged periods of time. The northernmost mine, the Kiparissia field, is closest to the western margin of the basin. Here, the Marathousa Member is represented by a single massive lignite without detrital interbeds.

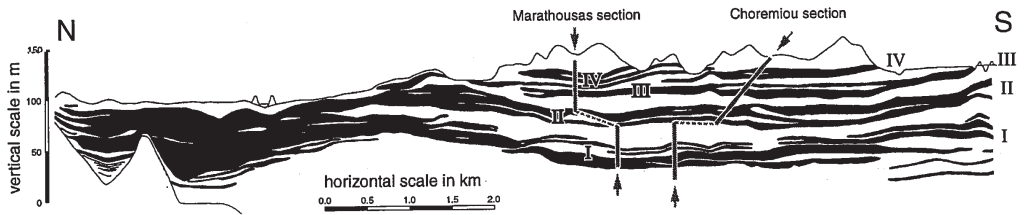


Figure 2: Schematic cross section through the Megalopolis basin. Roman numerals indicate the major coal seams, arrows indicate the positions of the two samples sections.

## Vertebrate remains from the Marathousa Member

The occurrence of mammalian fossils in deposits exposed in the Megalopolis Basin has been mentioned in several papers published in the 19<sup>th</sup> century or in the first half of the 20<sup>th</sup> century. Melentis described the Pleistocene larger mammal remains excavated from six different localities near the village of Megalopolis in a series of papers (1961; 1963a; 1963b; 1965a; 1965b; 1965c; 1965d; 1965e). The fossils came from six fossiliferous horizons ranging in age from the Early to the Late Pleistocene (Melentis, 1961). The stratigraphical position of these finds is not clear and the faunal data can therefore not be used to date the deposits (Vinken, 1965). In 1962 and 1963 a team of German geologists collected mammal fossils from the Marathousa Beds during a detailed geological survey of the Megalopolis Basin. The faunal remains were described by Sickenberg (1975) who identified eleven species of larger mammals (carnivores, *Mammuthus meridionalis*, *Hippopotamus antiquus*, four different cervids including *Praemegaceros verticornis*, a water buffalo, a horse and *Stephanorhinus etruscus*). He referred the fauna to the Early Biharian. A remarkable specimen in the fossil assemblage from the Marathousa Member is an upper M<sub>3</sub> of a hominid. The oldest evidence for the presence of hominids in Europe, according to Sickenberg (1975).

Sickenberg's opinion about the stratigraphical position of the Marathousa Member was modified by Benda et al. (1987), who assumed a late Villanyian age for the lower lignite bed exposed in the Thoknia open cast lignite mine, on the basis of its smaller mammals. In the early eighties, de Bruijn and van der Meulen took samples from four levels in the same mine (Thoknia 1-4), all these yielded an unpublished, small collection of fossil

	CHO 1	CHO 2	CHO 3	CHO 4
Pisces (Cyprinidae)	x	x	x	x
Aves indet.			4	1
Amphibia:				
<i>Rana (ridibunda)</i> sp.		11	42	11
Reptilia:				
<i>Emys orbicularis</i>		3	9	5
cf. <i>Coronella austriaca</i>			1	
<i>Elaphecf. E. longissima</i>			1	
<i>Natrix</i> sp.		47	94	40
<i>Natrix natrix</i>		2		2
<i>Vipera berus</i> group				1
Mammalia:				
Soricidae indet.	1			1
<i>Castor fiber</i>		1	12	1
<i>Sciurus</i> cf. <i>Vulgaris</i>			1	
<i>Pliomys</i> aff. <i>episcopalis</i>			4	
<i>Miomys</i> aff. <i>savini</i>	30	30	43	36
<i>Miomys</i> sp.		1		1
<i>Apodemus</i> cf. <i>sylvaticus</i>			1	
<i>Apodemus</i> sp.				15
<i>Mus</i> cf. <i>spretus</i>				39
<i>Mus</i> sp.			1	
Muridae gen. et p. indet.			1	
Mustelidae indet.	1		1	
<i>Hippopotamus</i> sp.			1	
Cervidae indet.			3	1

Table 1: List of taxa represented in the levels CHO 1, 2, 3 and 4 and the number of specimens. Please note that the fauna CHO 1 has not yet been investigated for the presence of amphibians and reptiles.

vertebrates. The Marathousa Member was sampled again for mammalian remains in the Choremiou section in 1995 by Doukas, Theocharopoulos and de Bruijn to contribute to the discussion on the stratigraphical position. Six hundred kg of matrix was screen washed from four different levels with mammalian remains; the two lowermost faunas (CHO 1 and CHO 2) come from lignite I, CHO 3 from the base of lignite II and CHO 4 from lignite III (Figure 6). The samples are rich in both botanical and faunal remains; mammalian fossils are, however, not very abundant. The identified specimens from the four levels are listed in Table 1.

Fish remains such as pharyngeal teeth of carp-like fish (Cyprinidae) are numerous in the four different levels. The bird remains (referred to as Aves indet.) represent various species which clearly differ in size. Frogs, turtles and snakes are most abundant among the herpetofauna of CHO 2, 3 and 4 (Holman & Van Kolfschoten, in prep.). Insectivore remains are rare; in the assemblage CHO 1 there is only the labial part of an upper P4 dext. and in CHO 4 a lower m2 dext. Both specimens closely resemble the



corresponding elements of the living *Crocidura suaveolens*. The beaver teeth from Choremi are rather small in comparison to the living north European *Castor fiber*, but hardly differ from those from the Middle Pleistocene of Mauer (Germany) (Mai, 1979).

*Voles*

There are three different voles represented in the Choremi faunas. *Pliomys* aff. *episcopalis*, characterized by rooted, high crowned molars and by the absence of crown-cementum in the re-entrant angles occurs only in fauna CHO 3. The occlusal pattern of the *Pliomys* molars (Plate 1: Figure 1a) as well as the height of the enamel free areas (Plate 1: Figure 1b) resembles that of *Pliomys episcopalis*. The molars are, however, larger than the type material from Betfia (length m1 from CHO 3 3.04 – 3.15, length of m1 from Betfia + 2.8 mm.). Other *Pliomys* species such as *Pl. simplicior* and *Pl. hollitzeri* are smaller. The large size of the molars from CHO 3 assigned to *Pliomys* aff. *episcopalis* may be an endemic feature.

A large vole characterized by high-crowned molars with roots and crown-cementum in the salient angles is the most abundant vole in all four assemblages. The upper M3 and the lower m1 do not show the presence of a *Mimomys* islet; one molar shows the presence of a *Mimomys* ridge (which disappears towards the base of the crown). The molars show a negative enamel differentiation. In size the m1 is similar to *M. ostramosensis* (Table 2); the morphology of the M3 from Choremi, however, differs (Plate 1: Figure 2). The molars have a much deeper posterior lingual re-entrant angle which results in two isolated triangles. The posterior dentine triangle of the upper M3 of *M. ostramosensis* is broadly confluent with the posterior loop.

Another large vole is *Mimomys rex*. Characteristic for this species is the morphology of the anteroconid with a deep lingual as well as buccal re-entrant angle. The occlusal pattern of most of the teeth from Choremi does not show these characteristics. The buccal re-entrant angle of these molars is very shallow, the lingual angle is more prominent (Plate 1: Figure 3) but still less well-developed than in the molars of *Mimomys rex*. However, in CHO 2 and CHO 4 there are a few molars with better developed re-entrant angles in the anteroconid (Plate 1: Figure 4). These molars resemble the molars from Thoknia, described and figured by Benda et al. (1987). They assigned the specimens from Thoknia to *Mimomys rex* because of their large dimensions and the morphology of the anteroconid. In the assemblages from Choremi, only a minority have this morphology; the occlusal pattern of most of the larger m1 resembles that of *Mimomys*

	N	range	X
CHO 1	4	3.45 - 3.82	3.68
CHO 2	2	3.61 - 3.67	3.64
CHO 3	6	3.38 - 4.01	3.74
CHO 4	2	3.34 - 3.40	3.37

Table 2: Length of the m1 of *Mimomys* aff. *savini* from CHO 1-4.

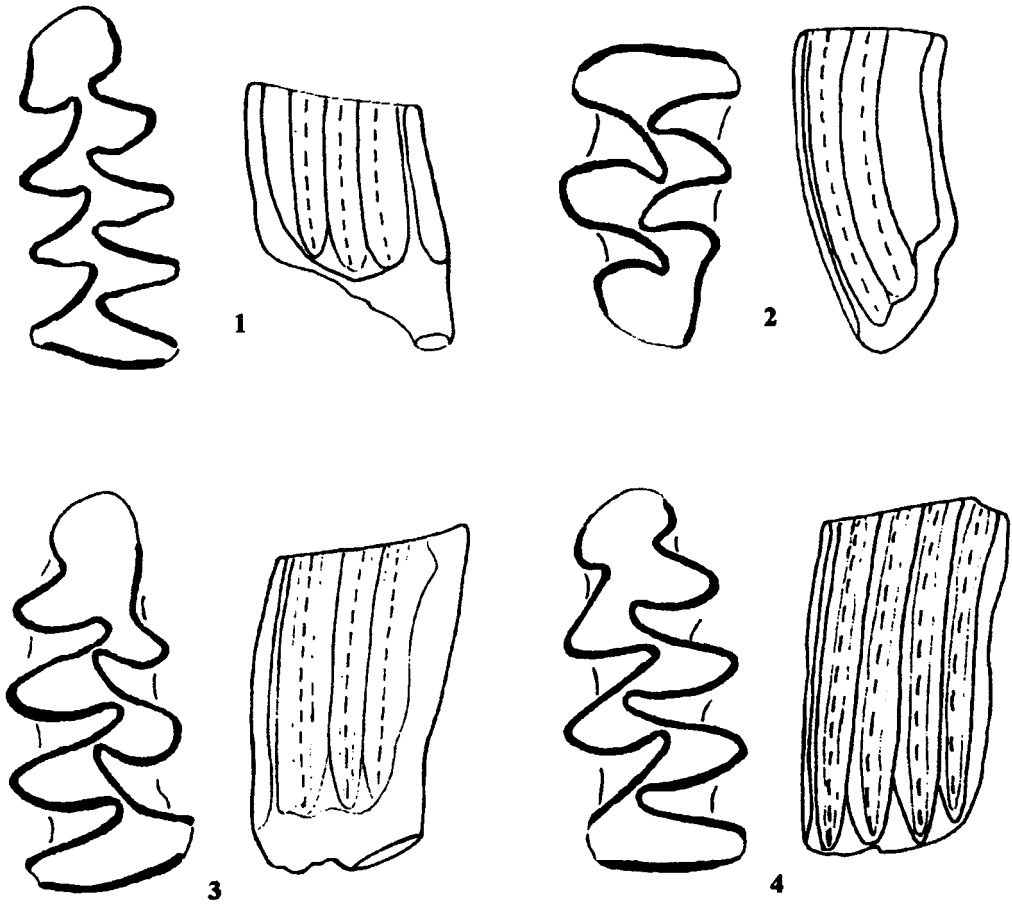


Plate 1: Voles from Choremi (Megalopolis Basin, Peloponnesos). Figure 1: *Pliomys* aff. *episcopalis* m1 sin. (Ch 3-39); Figure 2-4: *Mimomys* aff. *savini*; Figure 2: M3 sin. (Ch 1-23); Figure 3: m1 dext. (Ch 3-31); Figure 4: m1 sin. (Ch 2-31). a: occlusal surface; b: lingual view. All figures approximately x25

*savini*. The Choremi molars are, however, larger than the type material of *M. savini* from West Runton (England) (length m1: 3,08 – 3,56 mm; x 3.33 mm) (Table 2). Because of the large size of the molars we prefer to assign the material to *Mimomys* aff. *savini*, assuming that the larger voles represent a single species. We include the *Mimomys rex* morphotypes into the population of *Mimomys* aff. *savini*. A medium-sized *Mimomys* species could be identified in the assemblages CHO 2 (M1) and CHO 4 (m2). These two molars have a *Mimomys* pattern, are rooted and show the presence of crown-cementum in the re-entrant angles. They are, however, too small to be assigned to *Mimomys* aff. *savini*.

*Mus*

The isolated cheek teeth of a species of *Mus* from Choremi are morphologically and metrically similar to extant *Mus spretus* (Plate 2, Table 3). similar teeth are present in the uppermost sample taken from the Thoknia section (Th 4) and in the associations collected from the base of cycle II (CHO 3) and from the lignite of cycle III (CHO 4). This suggests that the immigration of this species is documented within the Marathousa member. The main interest of these occurrences is that they date the FAD of *Mus* in Greece between 700 and 750 thousand years before present (see cyclo-magnetostratigraphic discussion below). This is considerably later than the first record of the genus in N. Africa (Pliocene of Ichkeul, (Jaeger, 1975)), but may be roughly coeval with the oldest known occurrences from the Carpathian basin (Tarkö; Janossy, 1986) and from the South of France (Le Vallonet; Chaline, 1971).

Tooth position	Species	Length		N	Width	
		range	mean		mean	range
M1	<i>Mus spretus</i> (extant)	16.8-19.0	18,2	12	11,1	10.5-11.6
	<i>Mus cf. spretus</i> (TH 4)	16.9-18.3	17,8	3	11,1	10.8-11.6
	<i>Mus cf. spretus</i> (CHO 4)	17.9-18.5	18,1	–	10,5	10.2-10.8
M2	<i>Mus spretus</i> (extant)	9.5-11.8	11	12	10	8.0-10.7
	<i>Mus cf. spretus</i> (TH 4)	10.3-11.6	10,9	4	10,1	10.0-10.2
	<i>Mus cf. spretus</i> (CHO 4)	22.0-12.0	11,4	5	9,8	9.7-10.0
M3	<i>Mus spretus</i> (extant)	5.9-7.0	6,6	4	7,3	6.8-7.5
	<i>Mus cf. spretus</i> (TH 4)	- -	--	-	--	- -
	<i>Mus cf. spretus</i> (CHO 4)	- -	6	1	6,3	- -
m1	<i>Mus spretus</i> (extant)	14.8-16.0	15,5	10	9,3	8.8-10.0
	<i>Mus cf. spretus</i> (TH 4)	14.8-15.8	15,3	5	9,4	9.2-9.5
	<i>Mus cf. spretus</i> (CHO 4)	14.7-15.7	15,3	7	9,2	8.9-9.5
m2	<i>Mus spretus</i> (extant)	9.8-11.3	10,4	10	9,1	8.7-9.7
	<i>Mus cf. spretus</i> (TH 4)	10.0-11.4	11	6	9,2	8.7-9.5
	<i>Mus cf. spretus</i> (CHO 4)	9.0-10.9		14	9,2	8.7-9.8
m3	<i>Mus spretus</i> (extant)	6.7-7.9	7,2	5	6,3	6.0-6.8
	<i>Mus cf. spretus</i> (TH 4)	- -	--	-	--	- -
	<i>Mus cf. spretus</i> (CHO 4)	6.7-8.0	7,3	9	6,6	6.3-6.8

Table 3: Length and width of the cheek teeth of extant *Mus spretus* from Paradision (island of Rhodes) and of the Pleistocene material from the Megalopolis Basin (Peloponnesos); TH 4 indicates the sample Thoknia 4 from De Bruijn and Van der Meulen (unpublished), CHO 4 is from this study.

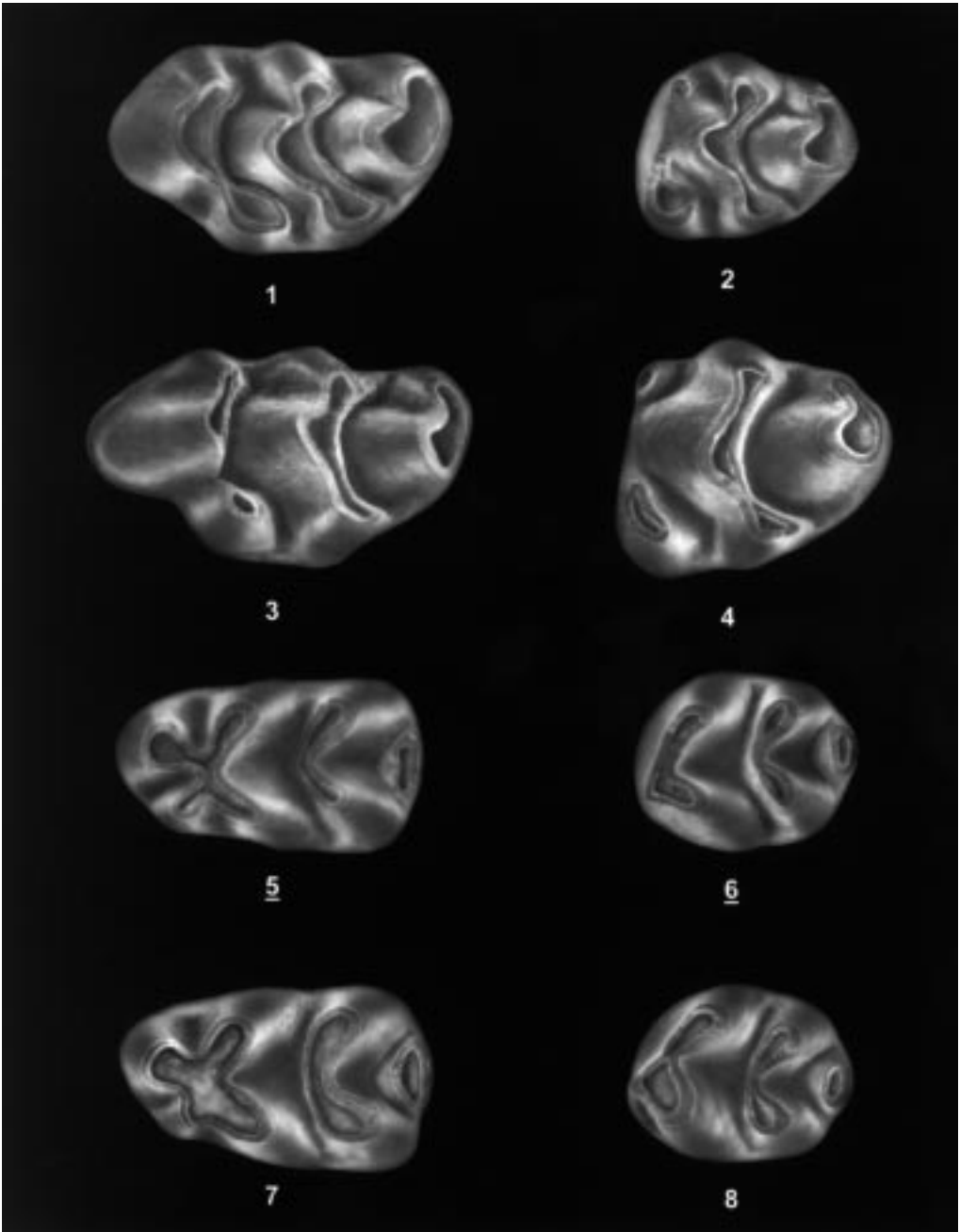


Plate 2: *Mus spretus* from Paradise Rhodes (extant), Figure 1: M1 sin., Figure 2: M2 sin., Figure 5: m1 dext. (reversed), Figure 6: m2 dext. (reversed). *Mus cf. spretus* from CHO 4, Figure 3: M1 sin., Figure 4: M2 sin., Figure 7: m1 sin., Figure 8: m2 sin. All figures approximately x35

Since the dental morphology of different fossil and extant species of *Mus* is very similar, identification of our material to species level would require a detailed analysis of all the material available, a job that is out of the scope of this study (for a review of fossil occurrences of *Mus* see Auffray et al., 1990). Using the criteria that were developed by Darviche and Orsini (1982) on the basis of biochemically screened specimens of *Mus spretus* and *Mus musculus* from the South of France shows that the material from the Megalopolis basin is very similar to extant *Mus spretus*. The only difference detected is that the anterolabial cinquulum of the M2 is better developed in our material than in the reference material of *M. spretus* from the island of Rhodes. We therefore identify the specimens from Megalopolis as *Mus* cf. *spretus*.

Other than the material of *Mus* cf. *spretus* the levels II and IV of the Thoknia section and the levels III and IV of the Choremiou section yielded some isolated cheek teeth of *Apodemus*. Judging by size there seems to be more than one species represented. One *Apodemus* M2 from Th II lacks the t9 entirely and may therefore be referable to *A. maasrichtiensis* (van Kolfschoten, 1985) from the Middle Pleistocene of Maastricht-Belvédère.

#### *Larger mammals*

Two fossils (a fragment of an upper M2 in CHO 1 and a lower p3 in CHO 3) indicate the presence of a medium-sized mustelid. *Hippopotamus* sp. is represented by an upper tusk found in CHO 3. Three molar-fragments and an incisor indicate the occurrence of a deer (Cervidae indet.) in size intermediate between the extant roe deer (*Capreolus capreolus*) and the red deer (*Cervus elaphus*).

#### *Environmental conclusions*

The mollusc associations from the four samples CHO 1 to 4, identified by W. Kuyper (Leiden University), consist of freshwater species; remarkable is the absence of terrestrial species. The herpetofauna is also dominated by (semi)aquatic species and indicates, just as the mollusc-fauna, a permanent, quiet body of water with abundant aquatic vegetation. Peripheral to the aquatic setting there has been a marshy area with some forest.

#### *(Bio)stratigraphical conclusions*

The only species that is well represented in the four Choremi faunal assemblages, *Mimomys* aff. *savini*, does not show any difference in morphology or size between different levels, suggesting that the four faunas do not differ much in age. This supports the assumption that there is no major stratigraphical hiatus in the Choremiou sequence. The biostratigraphical position of the four faunal assemblages is, however, not very clear. The biostratigraphically important genus *Microtus* is absent and the other voles are difficult to identify with certainty since we most probably deal with populations with some endemic characteristics. The genus *Mus*, occurring in the in the uppermost assemblages (CHO 3 and 4), however, indicates that, for the upper part of the sequence, we are dealing with Late Biharian deposits. *Mus* appears in Central Europe during the Middle Pleistocene; since the genus is known from Late Biharian faunas such as Tarkö and Le Vallonet.

*Mus cf. spretus* is also present in the fauna Thoknia 4 together with the Late Biharian *Microtus arvalidens*. Based on the assumed continuity in the section we conclude that the entire Marathousa Member either dates from the Late Biharian, or that the lower part of the sequence has a late Early Biharian and the upper part a Late Biharian age. This conclusion slightly modifies earlier (bio)stratigraphical correlations, in particular that published by Benda et al. (1987). They assume a Late Villanyian age for the Marathousa Member because of the presence of *Mimomys rex* and the absence of *Microtus* in the fauna from the lower part of the Thoknia sequence. The assignment of the larger voles to *Mimomys rex* has been questioned above. What remains is the absence of *Microtus*. It is important to realize that the number of specimens is restricted and that there are only three species of voles represented in the fauna. This might explain the absence of the genus *Microtus*. However, there might be a taphonomical explanation. The complete absence of terrestrial molluscs in the faunas CHO 1 to 4 and the dominance of aquatic species in the herpetofauna indicate specific environmental conditions, that are unfavorable for the terrestrial voles such as *Microtus*.

Sickenberg's (Sickenberg, 1975) conclusion that the Marathousa Member dates from the Early Biharian is based on the correlation between the larger mammal fauna from the Megalopolis Basin and other European faunas with an Early or Middle Pleistocene age. The Biharian is a biozone based on smaller mammals. The correlation of the smaller mammal biozonation to the larger mammal biozonation is still unsatisfactory, which makes a correlation of a larger mammal fauna to the smaller mammal biozonation problematic in some cases. Moreover, Sickenberg's definition of the Biharian differs from the original definition used by e.g. Kretzoi (1965) and van der Meulen (1973). Faunas with an early Middle Pleistocene age (e.g. Voigtstedt) date, according to Sickenberg (1975), to the Early Biharian. This indicates that there is no contradiction between Sickenberg's and our results.

On the basis of the mammalian record, the sedimentary cycles II and III have a Late Biharian age and cycle I with the faunas CHO 1 and CHO 2 is only slightly older and has a late Early Biharian or a Late Biharian age. This conclusion confirms that the palaeomagnetic reversal indicated in deposits in between cycle I and II can be correlated with the Matyama/Brunhes transition.

## Palaeomagnetic sampling and laboratory methods

Two sections were sampled for palaeomagnetic analysis: one in the Marathousas mine, and a second one in the Choremiou mine. The Marathousas section begins at the base of lignite I and ends 65 m higher, above a series of dark clay bands overlying lignite IV (Figures 2 and 4a). The sample spacing in this first section was ~2 m, with 51 samples in total. The more detailed Choremiou section starts ~20 m below lignite I and ends ~20 m above lignite IV (Figures 2 and 4b). Samples (380 in this section) were generally taken every ~0.4 m, but were as closely spaced as 6 cm in intervals where reversals or excursions were expected (based on the results from the parallel Marathousas section).

An electrical drill was used to take oriented rock samples with a diameter of 2.5 cm. In the laboratory, these cores were cut into specimens with a length of 2.2 cm. The samples below the first lignite were obtained from a vertical core with a diameter of 10 cm, drilled by the Greek national mining company, and could only be oriented in a vertical sense (up/down). Non-lignite lithology was preferred, because pure lignite usually does not give meaningful palaeomagnetic results (van Vugt et al., 1998). Sand occurs often in lenses that incise underlying sediments, so they represent discontinuities in the succession. Therefore, sand was avoided, where possible, by shifting the sampling/logging track sideways. The outcrops in the mines were less than a year old, so digging was hardly necessary to reach the fresh rock. The Marathousas section was primarily logged to enable identification of the sample positions, not for cyclostratigraphic purposes, therefore the presentation of Marathousas shows less detail than that of Choremioiu.

The natural remanent magnetisation (NRM) was measured on a 2G squid cryogenic magnetometer. The non-lignitic samples were thermally demagnetised with temperature increments of 30 and 50°C, up to 600°C. The lignitic samples were progressively demagnetised along three axes in a static alternating field (AF) up to 130 mT. At high alternating fields, the samples acquired a gyroremanent magnetisation (GRM) (Dankers and Zijdeveld, 1981; Stephenson, 1993), concealing the NRM. Therefore, above fields of 50 mT, we followed the method of Dankers and Zijdeveld (1981), in which the samples are initially demagnetised along two orthogonal axes, without measuring residual remanence, followed by demagnetisation along the third orthogonal axis and the first two axes, with measurement of the residual remanence along the demagnetised axis after each treatment.

### **Cyclostratigraphic frame for the Marathousa member**

The lignite occurrences in Megalopolis are concentrated in 10–20 metre-thick seams, which alternate with 12–25 metres-thick layers that contain clay, silt and sand. This alternation is regular in the stratigraphic section as well as in a lateral sense, so we interpreted them as sedimentary cycles (roman numerals I–IV in Figures 2 and 4). The clay-silt-sand sequence between lignites I and II is approximately twice as thick as the other detrital units. Lignite V is very clear, but does not necessarily represent a full cycle, because it is much thinner than the other lignite cycles. Above lignite V, the clay-silt unit is thicker than average. In the top of the Choremioiu section, no cycles could be distinguished above lignite IV, where the sediment contains many small carbonate concretions, and layers are indistinct. The cyclostratigraphy for the upper part is therefore based on the Marathousas section only.

Smaller scale cycles are also present. These are defined by the regular occurrence of lignite or dark brown clay layers in the detrital phase of the larger-scale cycles. These layers are generally made of lignite in the western part of the basin, and pass into thinner and/or less organic layers towards the east. The regularly intercalated and laterally continuous detrital layers in coal seam IV were also interpreted as small-scale cycles. The

small-scale cycles were discovered during the second field study, when the lower half of the Marathousas section could not be reached anymore because of mining activities. Therefore, the cyclic pattern in the detrital layers between I and III is based on the Choremiou section only.

In the detrital unit between I and II, six sub-cycles (a-f) could consistently be distinguished at regular stratigraphic intervals (Figure 6). Cycles a and c have genuine lignite beds; the other cycles are lignitic towards the west, but characteristically consist of dark clay. Cycle f seems thinner than average, but the boundary with the overlying lignite (II) is transitional. The detrital unit between II and III contains one prominent lignite bed, signifying at least one cycle (g), but there might be more cycles present in this unit. Between lignite III and IV, two distinct lignite layers occur (h and j), with h being consistently thinner than j. Lignite j contains a thin tephra layer, thus confirming the cyclostratigraphic correlation between both sections. This tephra layer is in all places located in the top part of the lignite layer, indicating that the lignite-detrital alternations represent synchronous palaeo-environmental changes rather than lateral facies shifts. Above lignite IV, more or less regular lithological alternations exist in the detrital units, but the pattern was not apparent. There generally are three prominent lignites or dark layers that we interpreted as small-scale cycles k, l and m (l might be a large-scale cycle and is also called V). within the lignites I, II and III, there are many interbeds; some of them are lenticular (not drawn in Figure 4), but others are continuous over the length of the outcrop (~3 km). These non-lignite (clay, silt and occasionally marl/carbonate) layers occur irregularly, thus inhibiting cyclic interpretation. Only lignite IV is consistently divided into cyclic parts: the small-scale cycles  $\alpha$ ,  $\beta$  and  $\gamma$  (Figure 4).

## Palaeomagnetic results

The NRM intensities vary between nearly zero and  $\sim 10^5 \mu\text{Am}^{-1}$ ; clay and silt have generally higher intensities than organic-rich lithologies. A small, randomly oriented viscous component is in all cases completely removed at 15 mT or 200°C, and from the samples with reversed polarity it can be seen that there is hardly any present-day-field component present in these unweathered rocks (Figure 3b). The separate-axis measurement method after alternating field demagnetisation removes the largest part of the gyroremanent magnetisation, but directions still tend to move away from the stable (15–50 mT) direction, so some remaining influence cannot be excluded. Therefore, only the data points acquired at fields between 15 and 50 mT are used to obtain the direction of the characteristic remanent magnetisation (ChRM). Thermal demagnetisation also has a limitation, at 390°C. Some samples have reached their maximum unblocking temperature at 390°C, but most were not yet fully demagnetised, while both the intensity and direction of the remanence sometimes showed drastic changes above this temperature. Rock magnetic investigations (van Vugt et al., 2000b) have shown that when the intensity of the characteristic component in samples from Megalopolis is higher than  $10^3 \mu\text{Am}^{-1}$ , the sample is dominated by secondary greigite. These samples were discarded in



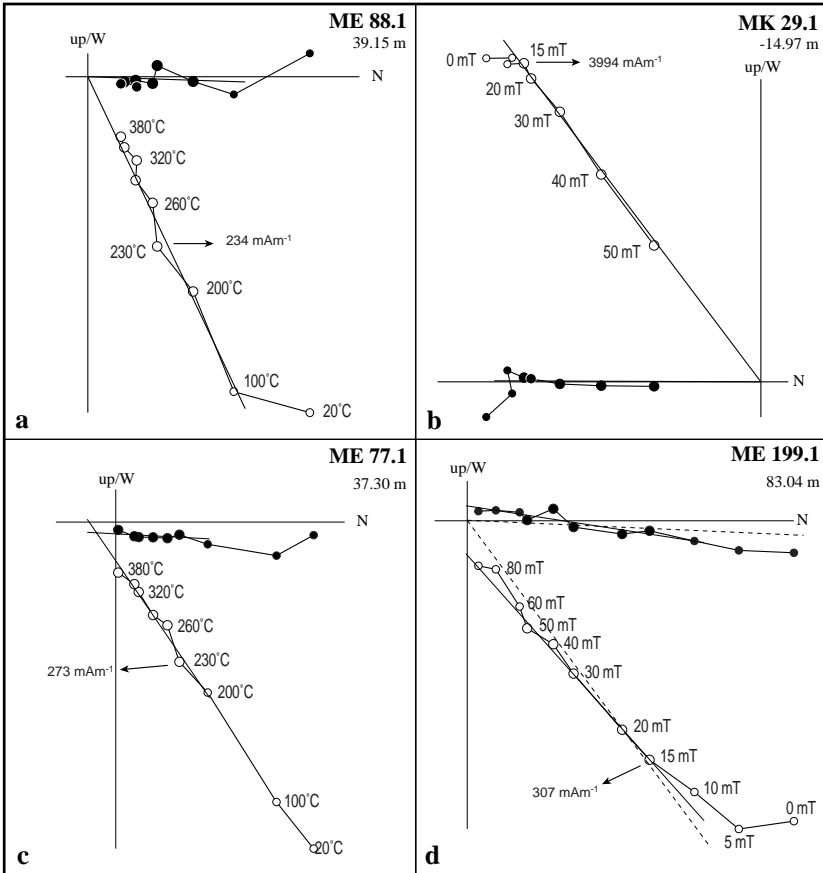


Figure 3: Demagnetisation diagrams Figures a and b show unambiguous normal and reversed polarity, respectively; c is clearly missing the origin, d might pass the origin, but is uncertain.

this study. The samples that were used probably contain a mixture of magnetite and a ferrimagnetic iron sulphide (van Vugt et al., 2000b). Low-intensity data are more sensitive to disturbances. In order to reduce the risk of interpreting noise, the samples with intensities  $<100 \mu\text{Am}^{-1}$  were not used for magnetostratigraphy.

The Zijdeveld diagrams have been divided into three categories: a line straight towards the origin, either from a reversed or from a normal direction (Figure 3a, b); a line clearly missing the origin (Figure 3c); and an uncertain group (Figure 3d). The samples from the core (between  $-20$  and  $0$  m) were interpreted based on their inclination only. Interpretation of the samples from the first group was straightforward, and the directions are plotted in Figure 4 as black dots connected with a line. The directions indicated by the straight lines clearly missing the origin were interpreted as secondary, with the primary magnetic polarity being opposite (large white circles). With the great circle

method the primary directions were approximated (large asterisks). The directions calculated from the third group of samples (small grey circles) are considered to be not very reliable, but a great circle analysis was used as a very rough estimation of the possible primary direction (small asterisks).

## Discussion

### *Magnetostratigraphy*

Both the Marathousas and Choremiou sections recorded reversed polarity at the base, and normal polarity in the rest of the section (Figure 4). In the Choremiou section there are many samples near the reversal with a normal (low-T/low-Field) component and a probably or possibly reversed primary remanence remaining after 50 mT or 390°C. This indicates that (part of) the magnetic remanence was acquired some time after deposition. This delayed acquisition causes the position of a polarity reversal to be at least as high as the highest sample that recorded the pre-reversal polarity. The position of the reversed-to-normal polarity transition in this section is therefore at least higher than 23 m, but there is a single, possibly reversed sample at 37.3 m (ME 77, see Figure 3c). This could be an indication for a reversal excursion, but remanence acquisition is so much delayed that the chance of recording a very short polarity event is negligible. We therefore regard the polarity between 23 and 38 m (lower half of the detrital interval above lignite I) to be uncertain. In the Marathousas section, there are no indications for reversed polarity above 12 m (middle of lignite I), but the sample spacing was much larger. These two sections are exactly parallel, so, according to the principle of delayed acquisition, the reversal is positioned at the highest possible level, i.e. the level from the Choremiou section.

Since previous palynological and palaeontological data (Benda et al., 1987; Lüttig and Marinos, 1962; Vinken, 1965) point to a middle Pleistocene age for the studied sediments, the normal interval can theoretically represent the Olduvai, Jaramillo or Brunhes (sub)Chron. The Jaramillo lasts only 80 kyr, the Olduvai 157 kyr. If the normal polarity interval in Megalopolis would represent a part of the Olduvai subchron, the sedimentation rate would be at least 57 cm/kyr, which is extremely high for lignite deposits. Moreover, since the present palaeontological study indicates a late Early Biharian or a Late Biharian age for lignites I and II, the normal interval is considered to represent the lower part of the Brunhes Chron (the only prolonged normal polarity period in the Pleistocene), and the recorded reversal the Matuyama-Brunhes boundary.

### *Phase relationship*

In their pollen analysis of (the lowermost) lignite I of Megalopolis, Nickel et al. (1996) found the palaeoclimate to change from a temperate intermediate to a (warmer) Mediterranean climate from the base of the lignite upwards, and a possible opposite trend towards the top of lignite I, but their section was too short to certify this last

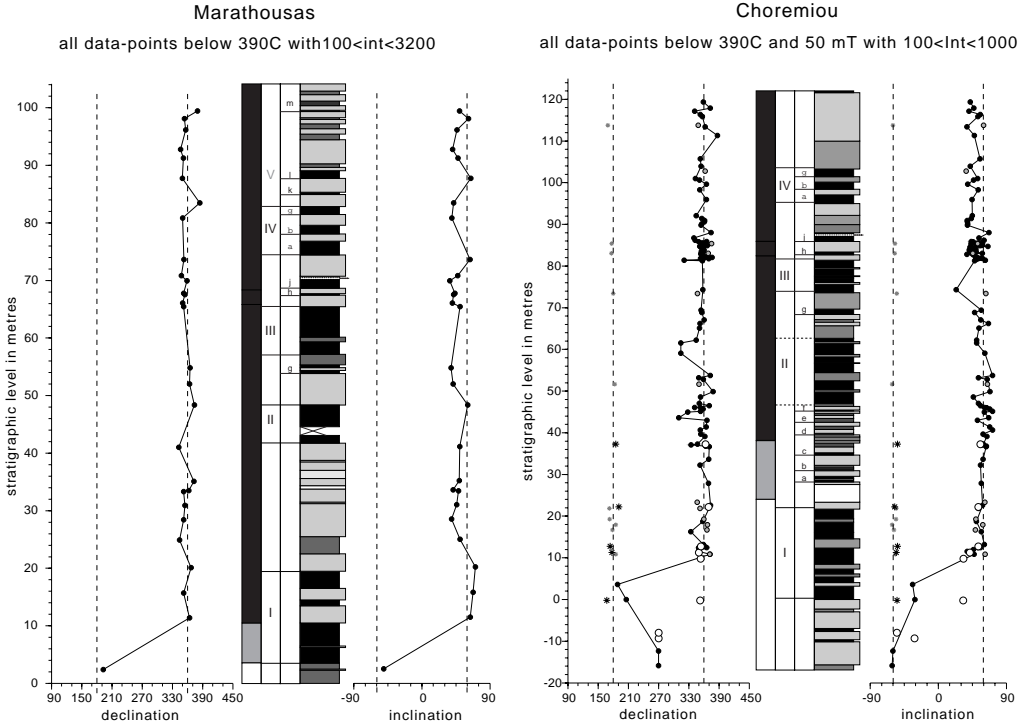


Figure 4: Palaeomagnetic results, polarity zones, large-scale cycles (roman numerals), small-scale cycles (letters) and lithology of the Megalopolis sections. Black dots denote primary magnetic directions; large white circles denote overprinted directions with the primary direction being opposite, asterisks denote approximations of these primary directions derived from the great circle method; small grey circles and asterisks belong to the uncertain group (see text). In the polarity column, black (white) indicates normal (reversed) polarity, while shaded indicates undetermined polarity. In the lithological column, black (shaded) indented beds denote lignite (dark-clay equivalent of lignite), shaded (white) protruding beds denote detrital (sand) layers, and the +++line indicates the position of the volcanic ash layer.

observation. They interpreted a lignite to represent an interglacial or interstadial. In a similar sedimentary setting in Lupoia (Romania) from the lower Pliocene, with more time control points (Radan and Radan, 1996; Radan and Radan, 1998; van Vugt et al., 2000a), the alternation of lignite and detrital beds was found to have an average period of ~100 kyrs, with the lignites corresponding to eccentricity maxima (van Vugt et al., 2000a).

A new palynological study (Okuda, in prep.) in Megalopolis on a 70-metre section that contains lignites II to V shows a typical alternation between *Quercus* (oak) and *Artemisia* pollen (Figure 5). *Artemisia*, indicative for cold and dry conditions, is abundant in the detrital intervals. *Quercus*, representative for a relatively warm and humid climate, occurs mainly in the lignites. The lignite–detrital alternation thus coincides with an alternation between warm/humid and cold/arid climate respectively. This leads

to the interpretation that the lignite seams in Megalopolis represent the warm phase in a cyclically changing climate. These warm periods could be either interglacials or interstadials, as Nickel et al. (1996) suggested already.

Smaller scale cycles may tentatively be recognised in the pollen diagram, but the sample resolution is generally too low to confirm them. Only in the lignite of small-scale cycle g two samples were taken, which both have a high arboreal pollen content, indicating a warm and humid phase. Also within lignite II, where small-scale cycles could not be distinguished in the lithology, there is some suggestion for small-scale cyclicity in the pollen record. At 60 and 53 m, a minor drop in *Quercus* that coincides with a peak in *Artemisia* suggest two short cold and arid periods in an otherwise warm and humid period. Further palynological research on a higher-resolution sample set is needed to confirm these small-scale variations.

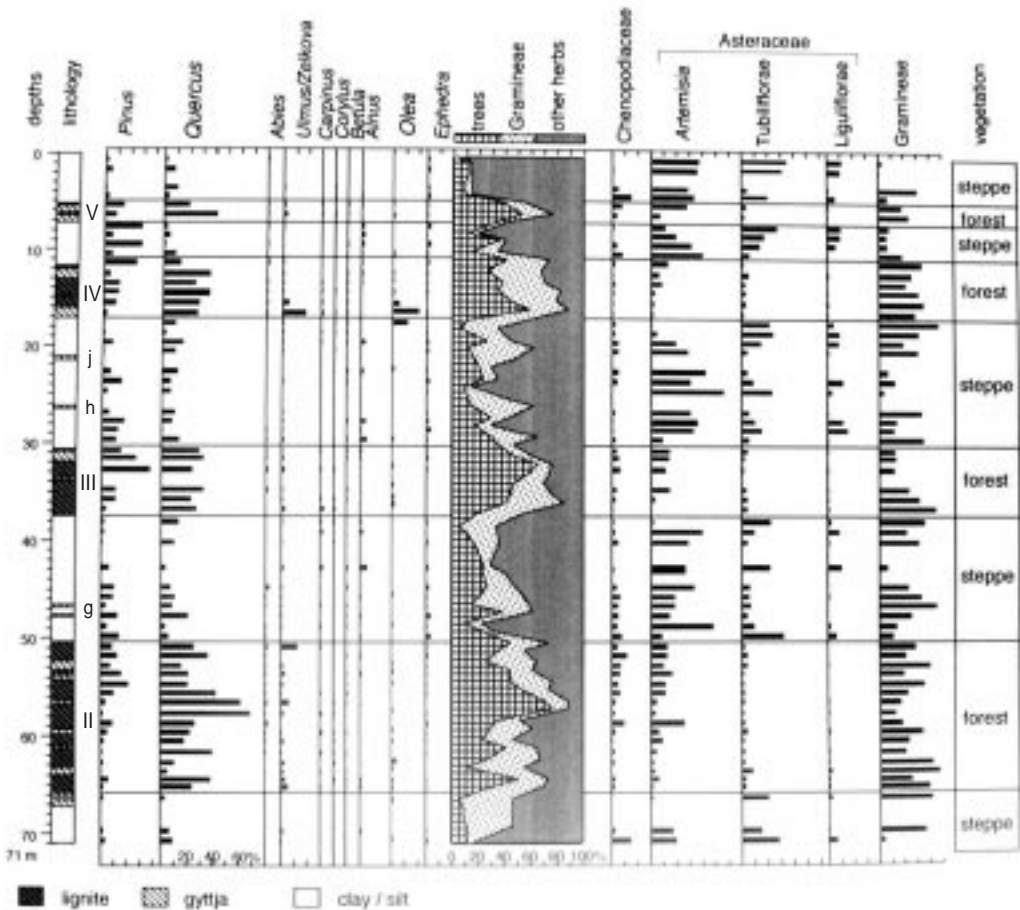


Figure 5: Simplified pollen diagram, after (Okuda, in prep.).

If the large scale cycles represent glacial-interglacial alternations, which would be quite logical considering the regularity and the omnipresent quasi-periodic (~100 kyr) occurrence of ice ages during the late Pleistocene (e.g., Imbrie et al., 1993; Imbrie et al., 1984; Raymo, 1997b and references therein), the average sedimentation rate would be 21 cm/kyr. If, on the other hand, the lignite seams would represent interstadials, which are approximately precession-related (~20 kyr) in the late Pleistocene, the average sedimentation rate would be 105 cm/kyr. This seems too high for such a lacustrine-marsh environment. For comparison, the sedimentation rate in the lignite-carbonate Ptolemais basin (N Greece) is 10 cm/kyr (van Vugt et al., 1998), and in the lignite-clastic Lupoia succession (Romania) it is 18 cm/kyr (van Vugt et al., 2000a). Therefore, we interpret the large-scale cycles to be caused by eccentricity-forced climate changes, and the small-scale cycles to represent precessional cycles. Both types have lignite as the warm/humid phase in the climate cycle, and the detrital beds as the cold/arid phase.

The phase relationship between lithology and astronomical parameters must be established independently and can never be assumed based on the results in other continental basins. This is illustrated by the fact that lignite formation in the Pliocene Ptolemais basin in N. Greece happened during the opposite phase than in Megalopolis, i.e. during insolation minima (cool and dry climate). The carbonate-lignite alternation in Ptolemais is primarily caused by lake level fluctuations as a result of precipitation variations (van Vugt et al., 1998; van Hove, pers. comm.). In other words, when humidity increased, the Ptolemais lake level rose and marsh vegetation drowned, enabling carbonate precipitation to increase; during more arid conditions, the lake level lowered and the lake was overgrown by reed swamp vegetation, creating anoxic conditions in which organic material was preserved. The forcing mechanism for Megalopolis is not clear yet, but a possible explanation is that during cold and dry periods, vegetation around the basin and/or along the lake margins that could trap the sediment was scarce, so erosional products could be transported far into the basin, where they formed the detrital beds. When the climate became warmer and more humid, conditions for vegetation improved, and large quantities of organic material were preserved. Detailed studies (palynology, organic petrology and/or sedimentology) within the current cyclostratigraphic frame will be needed to further test this hypothesis.

### *Astronomical tuning*

#### **Preferred tuning based on the sedimentary pattern**

Recognition of the typical pattern caused by superposition of the 400 kyr cycles on 100 kyr-eccentricity would make the presumed relation between the large-scale cycles and eccentricity more credible. The Matuyama-Brunhes boundary is recorded in the extra-thick detrital interval above lignite I. This interval could well correspond to the 400 kyr minimum at 0.78 Ma, around the Matuyama-Brunhes boundary (Figure 6). The regular pattern formed by lignites II-IV and the detrital intervals in-between matches the three prominent eccentricity maxima at 0.7, 0.6 and 0.5 Ma. Lignite I (V) is much thinner,

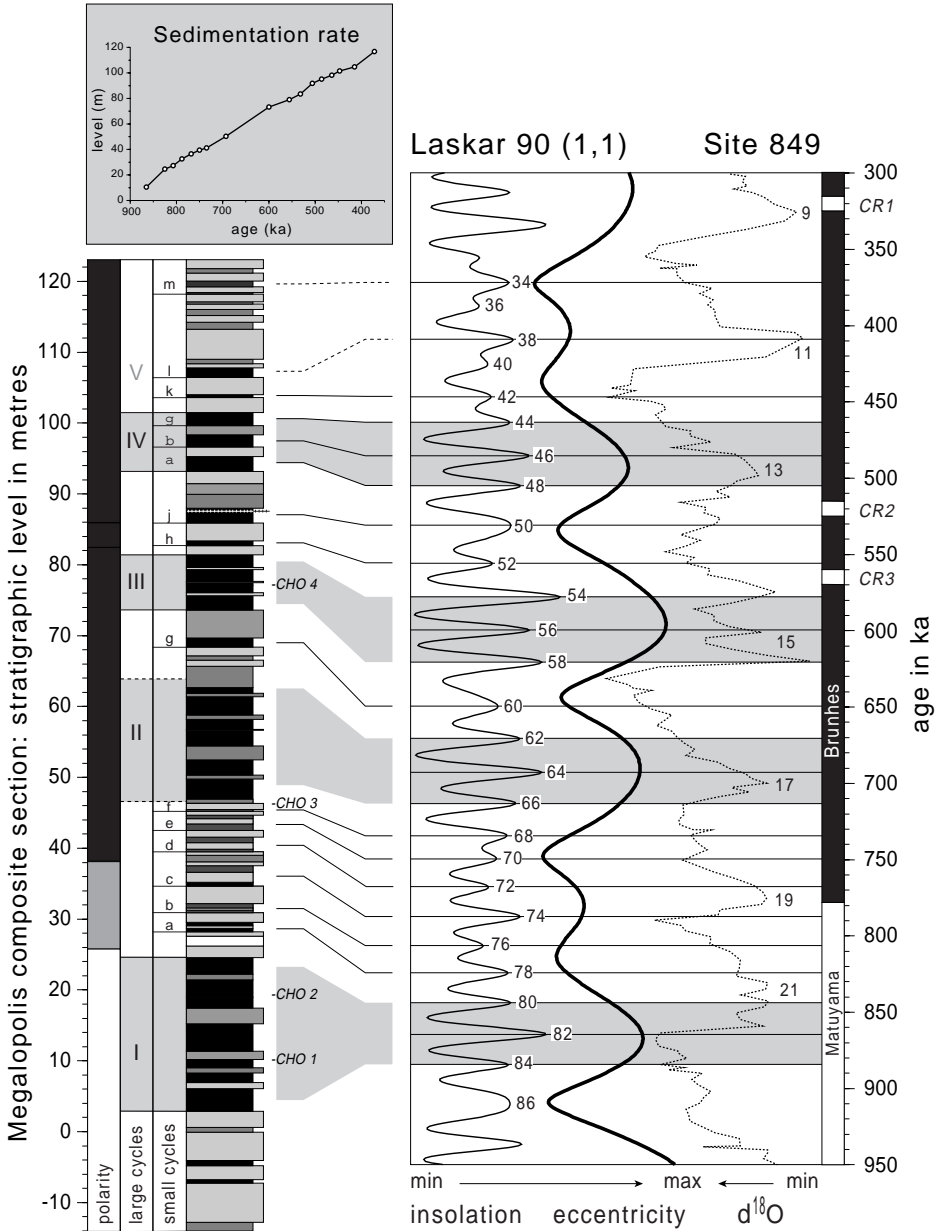


Figure 6

Figure 6: Megalopolis composite section (polarity, cyclostratigraphy and lithology; see also caption to Figure 4) correlated with insolation (i-cycle codification after (Lourens et al., 1996)) and eccentricity (Laskar, 1990).  $\delta^{18}O$ -record from site 849 (Mix et al., 1995; Raymo, 1997a) plotted to the GSS97 timescale (Raymo, 1997b) with selected isotope stages labelled and magnetic polarity timescale with excursions labelled in italics (Langereis et al., 1997). CHO 1-4 indicate small-mammal faunas. Inset: sedimentation rate resulting from this correlation.

which is in agreement with the low-amplitude 100 kyr-maximum at 0.4 Ma. In conclusion, the large-scale coal seam pattern correlates well with the eccentricity pattern between 0.9 and 0.35 Ma.

In the Mediterranean, the best fitting target curve for the Pliocene and Pleistocene is generally considered to be the 65°N summer insolation (average of June and July) as calculated by Laskar (1990), because it best matches the marine geological record (Lourens et al., 1996). The small-scale cycles are correlated to this insolation curve as illustrated in Figure 6. The thick lignitic part of cycle c is correlated with high-amplitude i-cycle 74, and the very thin non-lignitic phase of cycle e is connected to the very low-amplitude insolation minimum 69. The interval between lignites II and III appears to contain only one small-scale cycle (g), that is correlated to long-duration i-cycle 60. Cycles h (thin) and j (thick) are correlated to the consecutive low and relatively high amplitude i-cycles 52 and 50, respectively. I-cycle 50 also has a long duration. In this correlation, the lignite seams are supposed to represent two insolation minima, consistent with the two colder phases observed in the pollen record of lignite II.

The stratigraphic levels of the midpoints of all lignites are plotted versus their astronomically tuned age (Figure 6, inset). The resulting sedimentation rate is fairly constant throughout the section, without any sudden changes or outliers that would imply erosion and major hiatuses.

#### Alternative tuning based on palynological data

The pollen record of Okuda (in prep.) shows a distinct peak in *Olea* (Olive trees) in three samples around the base of lignite IV. This could be interpreted as a short period that was distinctly warm, and possibly warmer than any other sampled interval. Based on the pollen record alone, it would seem valid to correlate this peak to the warm interglacial stage 11. The consequence of correlating the underlying lignite seams with subsequently older eccentricity maxima or interglacial stages is that the Brunhes–Matuyama boundary below lignite II then has an age that is one cycle too young. This would imply a considerable hiatus in the record, which is of course possible in a continental environment. The most likely position for such an unconformity would be the lower boundary of lignite II. This boundary is formed by an irregular transition zone that is locally cut by the overlying lignite. The rich CHO 3 fauna was found in this transition zone, indicating a, possibly prolonged, period of non-deposition.

Correlation of the sedimentary cycles with the insolation curve – based on the assumption that one large-scale cycle is missing below lignite II – does neither result in a good fit for the small-scale cycles g–j, nor for the cycles  $\alpha$ – $\gamma$ . Therefore, the first correlation is preferred.

#### Consequences

The details in the pattern of lignites and lignite seams matches very well with the astronomical target curves of insolation and eccentricity. The correlation with  $\delta^{18}\text{O}$  curves or stacks (Bassinot et al., 1994; Imbrie et al., 1984) or ice volume curves (Imbrie and Imbrie, 1980; Paillard, 1998), however, reveals some important differences (Figure 6).

We compare the Megalopolis section to the Pacific  $\delta^{18}\text{O}$  record from ODP core 849, because this is generally considered to be a very detailed record. The critical features are the same in all marine  $\delta^{18}\text{O}$  records, including those from the Mediterranean Sea. Prominent interglacial stage 19 (~780 ka) is not represented by a prominent lignite in Megalopolis (interval between lignite I and II). The same holds for stage 11 and corresponding lignite V. Stage 17 (~680 ka) is significantly less pronounced than stage 15 (~600 ka) in the  $\delta^{18}\text{O}$  records, whereas the corresponding lignites (II and III, respectively) show hardly any difference within the width of the outcrops (~3 km). Apparently, the pattern of lignite seams in Megalopolis was forced by eccentricity and not by (whatever forced) the glacial-interglacial cycles as recorded in the world oceans by stable oxygen isotopes.

The oxygen isotope variations in the world oceans are mainly a reflection of the global ice volume. Isotope records from the Mediterranean basin document regional climate changes superimposed on the global signal. The much higher amplitude of  $\delta^{18}\text{O}$  variations in Mediterranean records is associated with reduction in surface-water salinity as a regional response to global increase in ice volume and decrease of temperature (Ganssen and Troelstra, 1987; Howell et al., 1998; Thunell et al., 1990; Vergnaud-Grazzini et al., 1986; Williams et al., 1978, among others). Apart from differences in amplitude, the Mediterranean isotope records of Sites 963, 964 and 967 from the eastern Mediterranean are comparable with oceanic oxygen isotope records at the critical stages 19 and 11 (Howell et al., 1998; Kroon et al., 1998). So, either the forcing of the regional (continental) Mediterranean climate was different from the eccentricity forcing of the lignite pattern in Megalopolis, or, more probably, the Mediterranean marine isotope records are influenced more by global factors than by regional climate.

## Conclusions

The Megalopolis section is dated as Pleistocene with magnetostratigraphy (lower Brunhes) and palaeontology (Late Biharian). Subsequent astronomical tuning of the lignite pattern gave ages of ~900 ka for the base of the section and ~350 ka for the top. Each lignite seam represents an eccentricity maximum, individual lignites represent insolation maxima. Not all the astronomical cycles are recognised in the lithology. Most notable is that low-amplitude eccentricity maxima lack expression as lignite seams, although they are recorded as normal interglacial stages in the marine oxygen isotope records (from both the Mediterranean Sea and the open oceans). Apparently, the regional Mediterranean climate was either forced by a different mechanism than the one determining the lignite–detrital alternations in Megalopolis, or the Mediterranean marine isotope records are influenced much more by global factors than by the regional climate.



## Acknowledgements

Dr. Masaaki Okuda from Japan courteously provided his palynological data and scientific opinions. We thank him for his permission to use them in this thesis. This research was much advanced by the fruitful discussions with Joris Steenbrink and Christian Mulder. Field assistance by Joris Steenbrink, Erik Snel, Marloes van Hoeve, Hendrik-Jan Bosch, Johan Meulenkamp, Constantin Doukas, Constantin Theocharopoulos and several Greek miners was much appreciated. The co-operation of the Greek Public Power company (AEI) was essential for collecting our samples. The investigations were supported by the Netherlands Council for Earth and Life Sciences (ALW), part of the Netherlands Science Foundation (grant to NvV). This work was conducted under the programme of the Dutch Vening Meinesz Research School of Geodynamics (VMSG).

## References

- Abdul Aziz, H., Hilgen, F.J., Krijgsman, W., Sanz-Rubio, E. and Calvo, J.P., 2000. Astronomical forcing of sedimentary cycles in the Miocene continental Calatayud Basin (NE Spain). *Earth and Planetary Science Letters*, in press.
- Auffray, J.-C., Vanlerberghe, F. and Britton-Davidian, J., 1990. The house mouse progression in Eurasia: a palaeontological and archaeozoological approach. *Biol. Journ. of the Linnean Society* 41, 13-25.
- Bassinot, F.C. et al., 1994. The astronomical theory of climate and the age of the Brunhes-Matuyama magnetic reversal. *EPSL* 126, 91-108.
- Benda, L., van der Meulen, A.J., Meyer, K.J. and van de Weerd, A., 1987. Biostratigraphic correlations in the Eastern Mediterranean Neogene: 8. Calibration of sporomorph- and rodent-associations from the Megalopolis Basin (Peloponnesus, Greece). *Newsl. Stratigr.* 17, 129-141.
- Chaline, J., 1971. La microfaune du Vallonet (A.-M.) et le problème des corrélations micromammifères à la limite Pleistocène inférieur-moyen. *Bulletin du Musée d'Anthropologie Préhistorique de Monaco* 17, 65-69.
- Dankers, P.H.M. and Zijdeveld, J.D.A., 1981. Alternating field demagnetization of rocks, and the problem of gyromagnetic remanence. *Earth and Planetary Science Letters* 53, 89-92.
- Darviche, D. and Orsini, P., 1982. Critères de différenciation morphologique et biométrique de deux espèces de souris sympatriques: *Mus spretus* et *Mus musculus domesticus*. *Mammalia* 46, 205-217.
- Ganssen, G.M. and Troelstra, S.R., 1987. Paleoenvironmental change from stable isotopes in planktonic foraminifera from Eastern Mediterranean sapropels. *Marine Geology* 75, 210-218.
- Howell, M.W. et al., 1998. Stable isotope chronology and paleoceanographic history of Sites 963 and 964, Eastern Mediterranean Sea. *Proceedings of Ocean Drilling Program, Scientific Results* 160, 167-180.
- Imbrie, J. et al., 1993. On the structure and origin of major glaciation cycles, 2, The 100,000-year cycle. *paleoceanography* 8, 699-735.
- Imbrie, J. et al., 1984. The orbital theory of Pleistocene climate: support from a revised chronology of the marine  $\delta^{18}\text{O}$  record. In: A. Berger, J. Imbrie, J. Hays, G. Kukla and B. Saltzman (Eds.), *Milankovitch and climate, part I*, pp. 269-305, Plenum Reidel, Dordrecht.
- Imbrie, J. and Imbrie, J.Z., 1980. Modeling the climatic response to orbital variations. *Science* 207, 943-953.
- Jaeger, J.J., 1975. The mammalian faunas and hominid fossils of the Middle Pleistocene of the Maghreb. In: K.W.

- Butzer and G.U. Isaac (Eds.), *After the Australopithecines.*, pp. 399-418.
- Janossy, D., 1986. Pleistocene Vertebrate Faunas of Hungary. *Elsevier Science Publishers.*
- Kretzoi, M., 1965. Die Nager und Lagomorphen von Voigtstedt in Thüringen und ihre chronologische Aussage. *Paläont. Abh.* 2, 587-660.
- Krijgsman, W., Langereis, C.G., Daams, R. and van der Meulen, A.J., 1994. Magnetostratigraphic dating of the middle Miocene climate change in the continental deposits of the Aragonian type area in the Calatayud-Teruel basin (Central Spain). *Earth and Planetary Science Letters* 128, 513-526.
- Kroon, D. et al., 1998. Oxygen isotope and sapropel stratigraphy in the eastern Mediterranean during the last 3.2 million years. Proceedings of the Ocean Drilling Program, *Scientific Results* 160, 181-189.
- Langereis, C.G., Dekkers, M.J., de Lange, G.J., Paterne, M. and van Santvoort, P.J.M., 1997. Magnetostratigraphy and astronomical calibration of the last 1.1 Myr from an eastern Mediterranean piston core and dating of short events in the Brunhes. *Geophysical Journal International* 129, 75-94.
- Laskar, J., 1990. The chaotic motion of the solar system: A numerical estimate of the size of the chaotic zones. *Icarus* 88, 266-291.
- Löhnert, E. and Nowak, H., 1965. Die Braunkohlenlagerstaette van Khoremi im Becken von Megalopolis/Peloponnes. *Geologisches Jahrbuch* 82, 847-867.
- Lourens, L.J. et al., 1996. Evaluation of the Plio-Pleistocene astronomical timescale. *paleoceanography* 11, 391-413.
- Lüttig, G.W. and Marinos, G., 1962. Zur Geologie des neuen Griechischen Braunkohlen-Lagerstaette von Megalopolis. *Braunkohle* 14, 222-231.
- Mai, H., 1979. Die Biberarten Castor und Trogontherium aus den altpleistozänen Schichten von Mauer an der Elsenz. *Schr. Naturw. Ver. Schlesw.-Holst.* 49, 35-46.
- Melentis, J.K., 1961. Die Dentition der pleistozänen Proboscidiere des Beckens von Megalopolis im Peloponnes (Griechenland). *Ann. Géol. d. Pays Helléniques* 12, 153-262.
- Melentis, J.K., 1963a. Die Osteologie der pleistozänen Proboscidiere des Beckens von Megalopolis im Peloponnes (Griechenland). *Ann. Géol. d. Pays Helléniques* 14, 1-107.
- Melentis, J.K., 1963b. Über Equus abeli aus dem Mittelpleistozän des Beckens von Megalopolis im Peloponnes (Griechenland). *Ann. Géol. d. Pays Helléniques* 16, 507-519.
- Melentis, J.K., 1965a. Die pleistozänen Cerviden des Beckens von Megalopolis im Peloponnes (Griechenland). *Ann. Géol. d. Pays Helléniques* 16, 1-92.
- Melentis, J.K., 1965b. Studien über fossile vertebraten Griechenlands. 4. Die pleistozänen Nashörner des Beckens von Megalopolis im Peloponnes (Griechenland). *Ann. Géol. d. Pays Helléniques* 16, 363-402.
- Melentis, J.K., 1965c. Studien über fossile vertebraten Griechenlands. 5. Über Hippopotamus antiquus Desmarest aus dem Mittelpleistozän des Beckens von Megalopolis im Peloponnes (Griechenland). *Ann. Géol. d. Pays Helléniques* 16, 403-435.
- Melentis, J.K., 1965d. Studien über fossile vertebraten Griechenlands. 6. Sus scrofa L. aus dem Jungpleistozän des Beckens von Megalopolis im Peloponnes (Griechenland). *Ann. Géol. d. Pays Helléniques* 16, 436-445.
- Melentis, J.K., 1965e. Studien über fossile vertebraten Griechenlands. 7. Die Boviden des Jungpleistozäns des Beckens von Megalopolis im Peloponnes (Griechenland). *Ann. Géol. d. Pays Helléniques* 16, 446-472.
- van der Meulen, A.J., 1973. Middle Pleistocene Smaller Mammals from the Monte Peglia (Orvieto, Italy) with Special Reference to the Phylogeny of Microtus (Arvicolidae, Rodentia). *Quaternaria* XVII, 1-144.
- Mix, A.C., Le, J. and Shackleton, N.J., 1995. Benthic foraminiferal stable isotope stratigraphy of Site 846: 0-1.8 Ma. *Proc. Ocean Drill. Program, Sci. Results* 138, 839-854.
- Nickel, B., Riegel, W., Schonherr, T. and Velitzelos, E., 1996. Environments of coal formation in the Pleistocene

- lignite at Megalopolis, Peloponnesus (Greece) - reconstruction from palynological and petrological investigations. *N. Jb. Geol. Palaont. A.* 200, 201-220.
- Paillard, D., 1998. The timing of Pleistocene glaciations from a simple multiple-state climate model. *Nature* 391, 378-381.
- Radan, S. and Radan, M., 1996. Magnetostratigraphy as a technique of nomination and correlation of coal beds: two examples from western Dacic basin (Romania). *Geologica Carpathica* 47, 174-176.
- Radan, S.C. and Radan, M., 1998. Study of the geomagnetic field structure in the tertiary in the context of magnetostratigraphic scale elaboration. I - the Pliocene. *Anuarul Institutului Geologic al Romaniei* 70, 215-231.
- Raymo, M.E., 1997a. Major Climate Terminations Data. *IGBP PAGES/World Data Center-A for Paleoclimatology Data Contribution Series # 97-024*.
- Raymo, M.E., 1997b. The timing of major climate terminations. *paleoceanography* 12, 577-585.
- Sickenberg, O., 1975. Eine Säugetierfauna des tieferen Biharium aus dem Becken von Megalopolis (Peloponnes, Griechenland). *Ann. Géol. d. Pays Helléniques* 27, 25-73.
- Steenbrink, J., van Vugt, N., Hilgen, F.J., Wijbrans, J.R. and Meulenkamp, J.E., 1999. Cyclostratigraphy and  $^{40}\text{Ar}/^{39}\text{Ar}$  dating of lower Pliocene lacustrine sequences of the Ptolemais Basin, NW Greece. *Palaeogeography, Palaeoclimatology, Palaeoecology* 152, 283-303.
- Stephenson, A., 1993. Three-axis static alternating field demagnetization of rocks and the identification of natural remanent magnetization, gyroremanent magnetization and anisotropy. *Journal of geophysical research* 98, 373-381.
- Thunell, R., Williams, D., Tappa, E., Rio, D. and Raffi, I., 1990. Pliocene-Pleistocene stable isotope record for Ocean Drilling Program Site 653, Tyrrhenian Basin: implications for paleoenvironmental history of the Mediterranean Sea. *Proceedings ODP, Scientific Results* 107, 387-399.
- van Kolfschoten, T., 1985. The Middle Pleistocene (Saalian) and Late Pleistocene (Weichselian) mammal faunas from Maastricht, Belvédère (Southern Limburg, The Netherlands). *Med. Rijks Geol. Dienst* 39, 45-74.
- van Vugt, N., Langereis, C.G. and Hilgen, F.J., 2000a. Dominant expression of eccentricity versus precession in the lithology of Mediterranean continental (lacustrine) deposits. *Geological Utrajectina* 189, Chapter 4.
- van Vugt, N., Langereis, C.G. and Dekkers, M.J., 2000b. Rock-magnetic properties of lignite-bearing lacustrine sediments from the Megalopolis and Ptolemais Basins as possible climate proxies. *Geologica Utrajectina* 189, Chapter 7.
- van Vugt, N., Steenbrink, J., Langereis, C.G., Hilgen, F.J. and Meulenkamp, J.E., 1998. Magnetostratigraphy-based astronomical tuning of the early Pliocene lacustrine sediments of Ptolemais (NW Greece) and bed-to-bed correlation with the marine record. *Earth and Planetary Science Letters* 164, 535-551.
- Vergnaud-Grazzini, C., Devauz, M. and Znaidi, J., 1986. Stable isotope "anomalies" in Mediterranean Pleistocene records. *Mar. Micropaleontol.* 10, 35-69.
- Vinken, R., 1965. Stratigraphie und Tektonik des Beckens von Megalopolis (Peloponnes, Griechenland). *Geologisches Jahrbuch* 83, 97-148.
- Williams, D.F., Thunell, R.C. and Kennett, J.P., 1978. Periodic freshwater flooding and stagnation of the eastern Mediterranean Sea during the late Quaternary. *Science* 201, 252-254.

# Dominant expression of eccentricity versus precession in the lithology of Mediterranean continental (lacustrine) deposits

## Abstract

Milankovitch forcing of climate is expressed in the sedimentary record as lithological cycles that can have one or more of four typical periods related to precession (21 kyr), obliquity (41 kyr) and eccentricity (100 and 400 kyr). In several Mediterranean continental successions that have recently been studied, striking differences in the expression of particularly precession and eccentricity appear. In this paper, we present the results of an additional upper Pliocene lacustrine section from Lupoiaia (southern Romania). We compare the cyclic expression in this lignite-detrital basin in detail with the time-equivalent lignite-carbonate basin of Ptolemais (northern Greece), the middle Pleistocene lignite-detrital basin of Megalopolis (southern Greece) and the Miocene carbonate-clay basin of Orera (north eastern Spain). From this comparison, it appears that carbonate basins dominantly express precession, while detrital basins dominantly express eccentricity in their lithological cycles. This can be explained by a more linear response to insolation forcing in carbonate basins than in detrital basins. Alternatively, it can be explained by the low amplitude of 100-kyr eccentricity at the times the carbonate sections were deposited. This reduced 100-kyr amplitude is caused by minima in the 2.35-Myr eccentricity cycle, that co-occurred with the deposition in both carbonate basins. Finally, the expression of 100-kyr eccentricity appears to be independent of glacial cyclicity.

*This chapter is submitted as: van Vugt N., Langereis, C.G. and Hilgen, F.J. Dominant expression of eccentricity versus precession in the lithology of Mediterranean continental (lacustrine) deposits, to Palaeogeography, Palaeoclimatology, Palaeoecology.*

## Introduction

Lithological cycles in sediments are now widely accepted as having been caused by astronomically forced climate cycles. Precession has a pronounced influence on seasonal contrast and has an opposite effect on each hemisphere. It can change monsoon systems that can in turn affect depositional systems. Obliquity causes fluctuations in the seasonal contrast between summer and winter and its effect increases towards higher latitudes, simultaneously on both hemispheres. Obliquity may enhance the climatic effect of precession on one hemisphere, while it reduces the effect on the other hemisphere. Eccentricity mainly modulates the effect of precession, it has itself very little effect (<0.1%) on the incoming solar radiation. The classic Milankovitch target curve of summer insolation incorporates all these effects and its frequency spectrum is dominated by precession, but obliquity is clearly discernible as well; eccentricity is virtually absent. Yet, the periods of eccentricity (100 and 400 kyr) are clearly expressed in many geological records (e.g. Imbrie et al., 1984; Fischer et al., 1991; Hilgen, 1991a; Olsen and Kent, 1996). This can be explained by non-linear response mechanisms, such as the asymmetric response mechanism of Clemens and Tiedemann (1997) that preferentially introduces variance into the climate system during the warmer portions of the eccentricity cycle. The spectral peaks at the eccentricity-frequencies of their truncated insolation curve are comparable to those in oxygen-isotope records, demonstrating that eccentricity can indeed cause strong 100 and 400-kyr lithological cycles. Another type of non-linear response is used in Paillard's ice-age model with multiple steady states and predefined insolation-related rules (Paillard, 1998). This model can successfully simulate late Pleistocene  $d^{18}O$  time series, which occurred approximately every 100 kyrs. Alternatively, a combination of truncated response and post-depositional effects such as bioturbation may smear the precession cycles and transfer nearly all power from the precession frequencies to eccentricity (Fischer et al., 1991).

Recently, many Neogene Mediterranean records from widely different continental environments have been studied: from alluvial to lacustrine (Krijgsman et al., 1997; van Vugt et al., 1998; Steenbrink et al., 1999; Abdul Aziz et al., 2000; van Vugt et al., 2000). In this paper we present the results from one more continental section from southern Romania. In all these successions, Milankovitch-type cyclicity is expressed in the lithology. The most apparent astronomical periods in these successions are precession and eccentricity, but generally one of them is dominant. We will compare three of these continental sections in detail, all lignite bearing lacustrine successions; two of them are overlapping in time. It will become apparent that the dominant astronomical period expressed in these records is not necessarily related to the geological era and its predominant climate type in which they were deposited. Instead, the sedimentary environment or basin setting seems to be crucial for whether eccentricity or precession is the dominant astronomical period. Finally, similarities and differences with the other Mediterranean continental records will be discussed.

## Geological backgrounds

The three successions discussed here were all deposited in lacustrine basins and are now exposed in open-pit lignite mines (see Figure 1 for locations). The first is the lower Pliocene Ptolemais composite section from the elongated intra-montane basin between Kozani and Florina in northern Greece (van Vugt et al., 1998; Steenbrink et al., 1999). The 100 m thick succession consists of a rhythmic alternation of metre-scale lignite and carbonate layers, that can be recognised and correlated across the basin. Intercalated volcanic ash layers serve as isochrons, and prove that the rhythmic lithological changes are synchronous. These sedimentary cycles occur in a regular pattern, except in a 10 m thick interval in the middle of the succession, where the expression of the cycles is less clear. The sediment is almost solely formed by either carbonate or organic material; the detrital fraction is generally less than a few percent.



Figure 1: Map of the northern border of the eastern Mediterranean. Capital cities (dots) and locations of studied sections (squares) are indicated.

The second succession is the middle Pleistocene Megalopolis section that was deposited in the half-graben near Megalopolis, southern Greece (van Vugt et al., 2000). This 135 m thick succession contains four 5–30 m thick lignite seams in otherwise detrital sediments (clay, silt, sand). The lignite seams can be correlated over a large part of the basin, and a volcanic ash layer confirms that the lithology changes are synchronous. In addition to the large-scale cyclicity, smaller scale cycles were observed within the detrital intervals as 0.5–2 m thick lignite or organic-rich clay layers alternating with clay, silt and/or sand.

The third succession is the lower Pliocene Lupoia section from the Oltenia basin near the city of Motru, south-west Romania. This section belongs to the Motru coal complex, a member of the Jiu-Motru Formation, that consists of several thick coal seams (~5 m) that are labelled with roman numerals by the mining company. These lignites are separated by ~15 m thick intervals of clay, silt and sand. Most lignite seams occur in this regular alternating pattern, and therefore a lignite and overlying detrital interval are called a sedimentary cycle. In the Lupoia mine, lignite seams V to XV are exposed, but our study focussed on an interval with a clear cyclic expression: the 80-metre long section between lignites V and IX. Subdivision of lignites V and IIX might point to an additional small-scale cyclicity, but lateral continuity of these small-scale cycles should be verified outside the single studied mine before defining these as sedimentary cycles. The magnetostratigraphy for the complete exposed succession was performed by (Radan and Radan, 1998), below we discuss the results of the interval between lignites V and IX.

## Magnetostratigraphy of Lupoia

The palaeomagnetic analysis of the Lupoia section is based on the analysis of 78 magnetostratigraphic sites, cored in the field with an electrical portable drill. The natural remanent magnetisation (NRM) was studied in the laboratory by means of standard stepwise thermal demagnetisation procedures and measured on a 2G Enterprises horizontal DC SQUID magnetometer. A selection of samples was exposed to a pulse field to acquire an IRM and subsequently thermally demagnetised.

The samples generally have a viscous component that is completely removed at 210°C. Several samples have a component that is removed between ~200 and 300–330°C: the low temperature (LT) component (Figure 2a and b). Most samples have a stable higher-temperature component that generally fully unblocks at 390° or 420°C (Figure 2a and c); maximum unblocking temperatures higher than 450°C are rarely observed (figure 2b). The LT component can be anti-parallel to the HT component or have an intermediate direction (Figure 2a and b respectively), but mostly, only one of these components could be reliably determined in a single sample (Figure 2c).

In both the IRM acquisition and demagnetisation diagrams two types of behaviour can be distinguished. The first type shows a steep increase in IRM at low fields, but saturation is not reached until ~600 mT. The IRM strongly decreases on heating up to

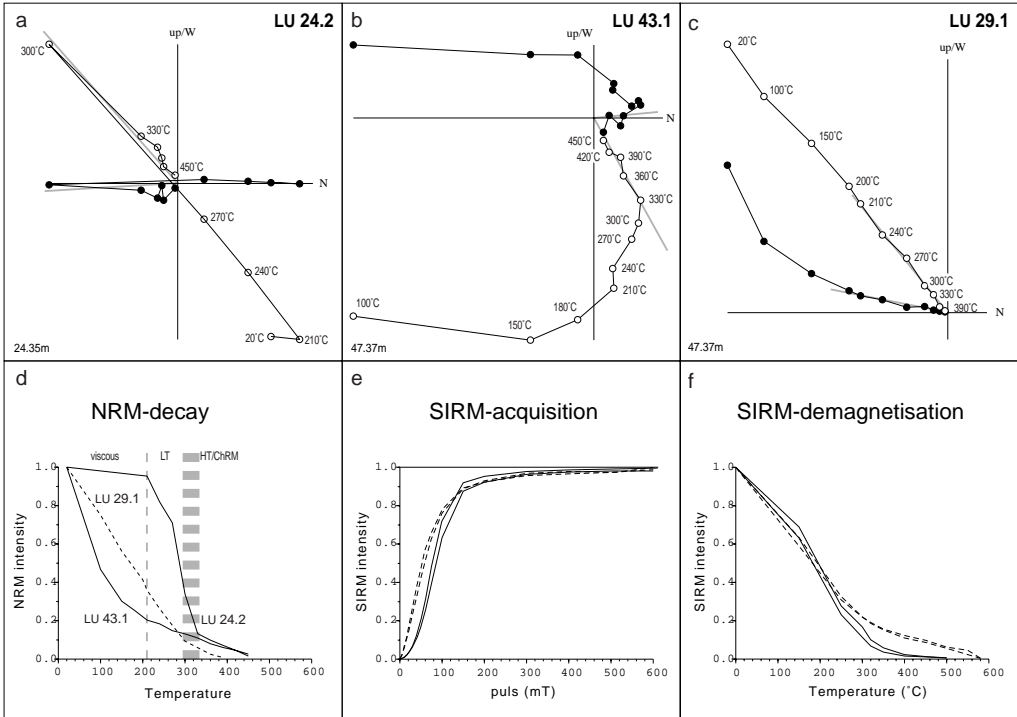


Figure 2: upper panel: Thermal demagnetisation diagrams of typical samples; black (white) dots indicate horizontal (vertical) projection. a) LT ( up till 300 °C) and Ch component (300-420 °C) have opposite polarities. b) LT (up till 330 °C) and Ch component (330-450 °C) are not opposite. c) only Ch component distinguishable. Lower panel: d) normalised intensity plot of NRM during thermal demagnetisation; SIRM acquisition (e) and thermal demagnetisation (f); dashed line: magnetite + iron sulphide, solid line: greigite.

~300°C and total unblocking occurs at 580°C. These samples are interpreted to contain magnetite and a ferrimagnetic iron sulphide. The IRM of the second type increases slowly at low fields and saturation is reached at ~600 mT. The maximum unblocking temperature of 400°C points to a ferrimagnetic iron sulphide carrying the IRM, probably greigite, which is very common in fresh-water sediment.

The maximum unblocking temperature of the LT component (300-330°C) indicates that this remanence is probably carried by a ferrimagnetic iron sulphide. Since greigite decomposes upon heating between 270 and 350°C and the Curie temperature for pyrrhotite is 325°C (Torii et al., 1996), they could both be the carrier of this component. These iron sulphides commonly form as an authigenic phase, i.e. they are formed after deposition, and the moment of remanence acquisition is therefore uncertain. Furthermore, the LT component changes polarity almost every other sample. Hence, we do not use this component for magnetostratigraphy.

The HT component unblocks at higher temperatures (390-420°C or higher), which indicates that magnetite could be the remanence carrier, but the chemical reaction of



iron sulphides upon heating to  $\sim 400^{\circ}\text{C}$  obscures the typical magnetite Curie temperature that was indeed observed in the IRM experiment. Since the directional results of these samples provide a sensible polarity pattern, we take this component as the characteristic remanent magnetisation (ChRM). It is assumed to be of (near) primary origin. The lowermost part of the section (lignite V), and the interval from lignite VII up to IIX have a normal polarity (Figure 3). The middle and uppermost parts are reversed. From previous work in the Lupoia mine (Radan and Radan, 1998), it is known that the uppermost reversed interval continues at least up till lignite XV (Figure 3).

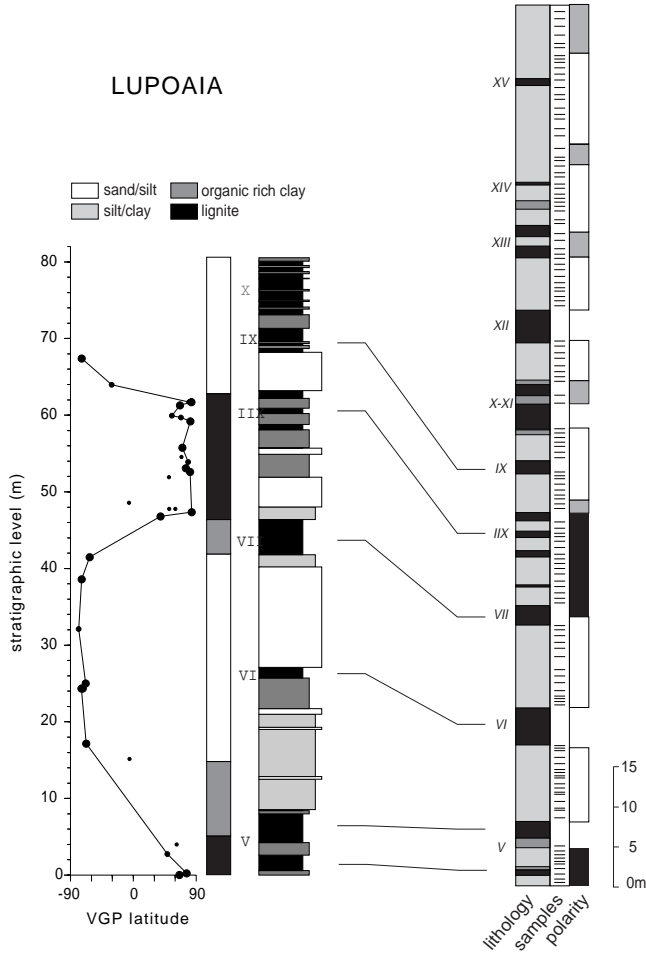


Figure 3: Lupoia section with the magnetic polarity pattern. Left hand side: latitude of the virtual geomagnetic pole (larger dots = more reliable data); inferred magnetic polarity (black = normal, white = reversed, grey = uncertain); cycle numbers and lithology from this study. Right hand side: lithology; sample positions and inferred polarity as reported by [Radan, 1998 #261].

Assuming an on average constant sedimentation rate, this section represents consecutively part of a normal polarity period, two short periods with subsequently reversed and normal polarity, and a reversed interval that lasted at least three times as long as the short periods. Since the Dacian-Romanian stage boundary occurs in this section, it is assigned a Pliocene age (Andreescu, 1981; Alexeeva and al., 1983). Then there are only two possible subchrons to correlate the long reversed interval to: the top of the Gilbert Chron or the base of the Matuyama Chron. The reversed upper Gilbert is preceded by several short normal subchrons (Cochiti, Nunivak, Sidufjall and Thvera subchrons). Since our polarity pattern is not consistent with the base of the Matuyama, we conclude that the polarity pattern in Lupoia represents the upper part of the reversed Gilbert Chron, and the normal intervals can be correlated to the Nunivak and Cochiti subchrons.

### Astronomical forcing and tuning of the sedimentary cycles in Lupoia

Astronomical forcing of sedimentary cycles can be demonstrated by analysing the average duration of the cycles, provided that age calibration points such as polarity reversals are available. When the average period of the cycles in the time domain is constant and identical to one of the known Milankovitch periods, astronomical forcing is a likely cause. Figure 4 (after van Vugt et al., 1998) illustrates how the 7 well-defined polarity reversals from Ptolemais were used in this way to show that the sedimentary cycles have the same average duration ( $21.6 \pm 0.5$  kyr) as the climatic precession cycle (21.7 kyr, (Berger, 1984)).

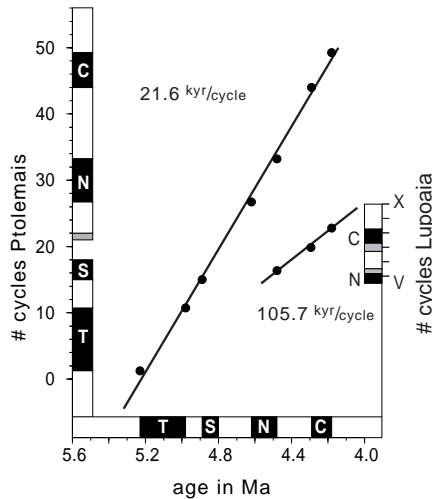
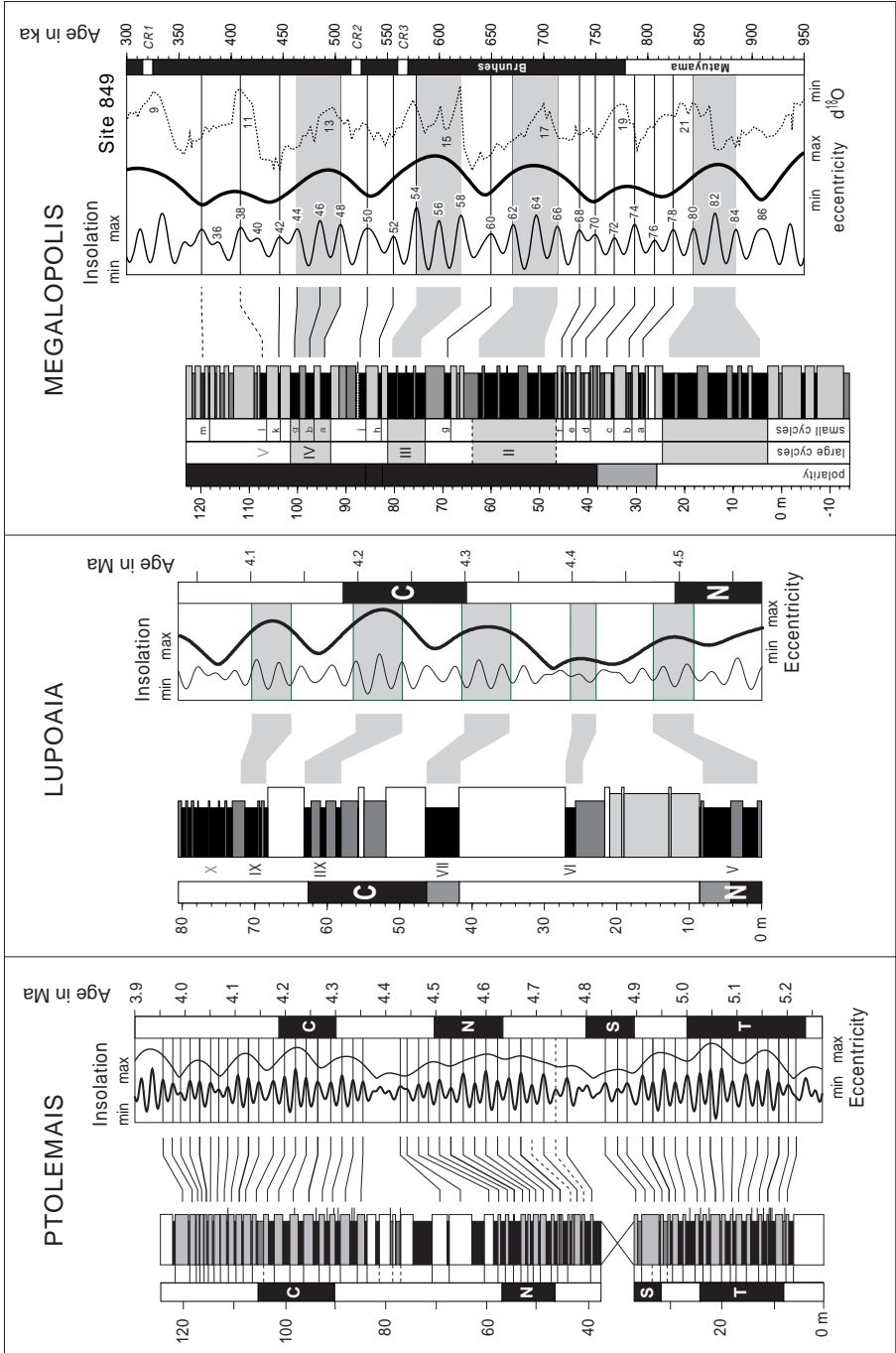


Figure 4: Polarity column of Ptolemais (left hand side) and Lupoia (right hand side) in number of cycles versus age (APTS). T = Thvera, S = Sidufjall, N = Nunivak, C = Cochiti subchron. The lines indicate the average duration of a sedimentary cycle: 21.8 kyr for Ptolemais and 105.7 kyr for Lupoia.



Similarly, the three polarity reversals in the Lupoia section enable examination of the average duration of the sedimentary (lignite) cycles. In Figure 4, the number of sedimentary cycles and their polarity is plotted versus the astronomical polarity time scale (APTS). The three age calibration points are linearly related, suggesting a constant duration for the sedimentary cycles. The slope of the regression line gives an average duration of  $105.7 \pm 5.6$  kyr for a sedimentary cycle if a lignite – although stratigraphically thinner than a detrital interval – is assumed to represent half a cycle. If a lignite is assumed to represent a lesser amount of time (i.e. less than half a cycle), the slope of the regression line does not significantly decrease. This period is in accordance with the  $\sim 100$  kyr period of eccentricity, and strongly suggests a causal relation that allows astronomical tuning of the cycles. We can then construct an age model which has sufficient resolution for an accurate correlation with other successions.

The Nunivak and Cochiti reversals are astronomically dated (Lourens et al., 1996) and their positions with respect to eccentricity are thus determined (Figure 5b). Correlation of the Lupoia polarity pattern with the Astronomical Polarity Time Scale (APTS), shows that the lignites correspond to eccentricity maxima, as is the case in the similar Megalopolis basin (van Vugt et al., 2000). This assumes that NRM acquisition is not significantly delayed. Part of the NRM is recorded in authigenic ferrimagnetic sulphides, but this component was not used to determine the direction of the ChRM, and thus to determine the polarity pattern. Indications for systematic delayed acquisition were not observed in either the LT or HT components. Moreover, it is not likely that any delay amounts to more than  $\sim 50$  kyr in this succession. If the NRM acquisition were untraceably delayed, this would occur much sooner in the organic-rich layers than in the detrital layers, because (partial) oxidation of abundant organic material often causes the magnetic mineralogy to change. Since all three reversals in this section are recorded in a lignite, any untraceable delay of that amount would have to have occurred in the detrital beds.

The phase relationship between lithology and eccentricity is therefore established: the lignites correlate to maxima, the detrital intervals to minima in eccentricity. Tuning of the succession is straightforward (Figure 5b): lignite V contains the top of the Nunivak and is correlated to the eccentricity maximum around 4.50 Ma and thin lignite VI corresponds to the low-amplitude eccentricity maximum around 4.41 Ma. Lignites VII and IIX, which contain the lower and upper Cochiti reversals respectively, are correlated to the maxima around 4.32 Ma and 4.22 Ma, and lignite IX is correlated to the maximum around 4.12 Ma. Correlation of lignites X and higher in the Lupoia mine is not as straightforward, and we have refrained from doing so.

Figure 5: Astronomical tuning of the discussed lacustrine sections. Left hand panel: Ptolemais [van Vugt, 1998 #124]. Lithology: black (shaded) indented beds = lignite (marly equivalent of lignite); white (shaded) protruding beds = white (grey) carbonate. Carbonate layers are correlated with insolation maxima. Central panel: Lupoia. Lithology: see caption to Figure 3. Lignite seams are correlated with eccentricity maxima. Right hand panel: Megalopolis [van Vugt, in prep. #249]. Lithology: black (shaded) indented beds = lignite (organic-rich equivalent of lignite); shaded (white) protruding beds = clay or silt (sand) layers. Large-scale cycles are indicated by roman numerals, small-scale cycles by arabic numerals. Lignite seams are correlated with eccentricity maxima, small-scale lignites with insolation maxima. The numbers in the  $\delta^{18}O$  record indicate oxygen isotope stages.

In summary, we argue that the lower Pliocene cyclic deposits from Lupoia are forced by eccentricity, with lignite representing the eccentricity maxima. During the Pleistocene, eccentricity maxima corresponded to warm periods (interglacials), while glacial periods occurred during eccentricity minima (Hays et al., 1976). In the (early) Pliocene, however, there was no eccentricity-related glacial-interglacial climatic regime. The suppressed amplitude of the insolation cycles during eccentricity minima is likely to have resulted in a generally colder climate, but without further data from this succession (e.g. pollen), a palaeoclimatic interpretation must remain tentative.

## Orbital forcing in continental records

### *a. Lignite dominated lacustrine basins*

The lower Pliocene Ptolemais section (northern Greece) was deposited during the Gilbert Chron. The upper half of the section has recorded the Nunivak and Cochiti subchrons (Figure 5a) and overlaps with the Lupoia section. The sections are very different, however, in two ways: the lithology and the dominant astronomical period. Although both sections contain lignite, the other lithology consists mainly of carbonate in Ptolemais, as opposed to detrital clay, silt and sand in Lupoia. Furthermore, the lignite-carbonate cycles from Ptolemais are 2 m thick, whereas the lignite-detrital cycles from Lupoia are ~20 m thick. As demonstrated in Figure 4, the sedimentary cycles in Ptolemais are related to precession (21.7 kyr). The cyclic pattern fits with summer insolation when lignite is correlated with insolation minima and carbonate with maxima (van Vugt et al., 1998), but eccentricity (100 kyr) is hardly expressed. In Lupoia, however, precession is not unambiguously recognised, whereas eccentricity is dominantly expressed in the lithology. In marine Mediterranean records of the same age, both precession and eccentricity are clearly expressed in the sedimentary record (e.g. Hilgen, 1991b). Apparently, the response of these continental basins to astronomically forced climatic changes is different for each continental environment and different than in marine environments.

An answer to what determines this response may be found in the Pleistocene Megalopolis basin in southern Greece. It has a similar lithology as Lupoia: fluvio-lacustrine sands, silts and clays alternating with lignite seams of 7-20 metres thickness, which were defined as sedimentary cycles (van Vugt et al., 2000). In addition to these prominent cycles, thinner lignite or organic-rich clay layers (up to 2 m) could be recognised as small-scale cycles in several intervals (Figure 5c). The Matuyama-Brunhes boundary was recognised near the base of the section, but apart from this single polarity boundary, no other accurate age control point was found. The pollen signal showed that the large-scale cycles are climatically induced, similar to glacial-interglacial phases, with the lignite representing the warm and humid phase. The large-scale cycles were assumed to be related to eccentricity, and the small-scale cycles to precession. The hypothesis of 100-kyr eccentricity forcing was supported by a good fit of the prominent large-scale cyclic pattern with the typical 400-kyr minimum in the 100-kyr eccentricity cycles, and of the

small-scale cycles with insolation. Furthermore, the age model provided a realistic and constant sedimentation rate throughout the succession. It appeared that the lignite seams represent eccentricity maxima, the detrital intervals eccentricity minima, while the small-scale lignite or organic-rich clay layers are correlated to precession minima (summer insolation maxima). In summary, the cycles in Megalopolis look very similar to those in Lupoia and they are dominated by the same astronomical period and moreover have the same phase relationship. Contrary to Lupoia, which was deposited during a warm (early Pliocene) period, Megalopolis was deposited during the middle Pleistocene ice age regime, when 100 kyr (eccentricity) became the dominant astronomical (quasi-)period controlling glacial cyclicity (Hays et al., 1976; Imbrie et al., 1984).

Although the cyclic pattern in Megalopolis fits closely with the eccentricity curve, it is strikingly distinct from typical open-ocean  $d^{18}O$  records, which reflect the variation of global ice volume (van Vugt et al., 2000). During low-amplitude 100-kyr eccentricity maxima (due to 400-kyr eccentricity minima), the lignite cycles in Megalopolis are restrained or underdeveloped, whereas every 100-kyr eccentricity cycle is expressed as a glacial-interglacial alternation in the marine  $-^{18}O$  records, regardless of eccentricity amplitude (*the '400-kyr or Stage-11 problem'* (Imbrie and Imbrie, 1980)). The sapropel pattern in Mediterranean Sea cores shows a similar contrast with  $d^{18}O$  records. The (ghost) sapropels formed at 20-kyr insolation maxima, but generally not during low eccentricity periods (e.g. Langereis et al., 1997; Kroon et al., 1998; Passier et al., 1998). The oxygen isotope stages corresponding to these low 100-kyr eccentricity maxima (OIS 19 and 11) are clearly recognisable, and neither suppressed nor less well developed in the available  $d^{18}O$  records from these cores (Langereis et al., 1997; Kroon et al., 1998). Thus, the Mediterranean oxygen isotope records mainly follow changes in global ice volume. Evidently, not the ice ages (glacial-interglacial alternation), but a mechanism more directly related to orbital (eccentricity) forcing of regional climate determined the prominence of the sedimentary cycles in both the Mediterranean Sea and the continental Megalopolis basin (van Vugt et al., 2000).

In conclusion, eccentricity is not expressed in the lignite-carbonate cycles of Ptolemais, which is unlike the time-equivalent marine records. In the overlapping Lupoia section, only eccentricity is clearly expressed, which is also in contrast to the marine records. The Megalopolis section is dominantly forced by 100-kyr eccentricity, roughly similar to time-equivalent marine records. Strikingly, both Megalopolis and Lupoia have the same type of sedimentary cycles (lignite-detrital) and are dominantly forced by the same astronomical parameter. The type of sedimentary setting, rather than the global climatic regime, apparently determines by which astronomical parameter the system is dominantly forced. From these three case studies, it would appear that lacustrine carbonate basins are dominantly forced by precession, whereas lacustrine detrital basins are dominantly forced by eccentricity. Maybe carbonate basins are more sensitive to small (threshold) changes, and detrital basins need larger fluctuations to change their sedimentary environment.

### *b. Other Mediterranean continental basins*

Does this observed relation between lithology (i.e. type of sedimentary cycles) and dominant astronomical period also apply to continental basins without lignite? Several (fluvio-)lacustrine records from the Mediterranean are described in the literature, but astronomically forced sedimentary cycles are not always recognised and rarely reported. A perfect example of a cyclical succession is the magnetostratigraphically dated Miocene Orera section from the Calatayud Basin in NE Spain. It contains a cyclic alternation between lacustrine carbonate and marl/clay layers, with a period of 19–23 kyr, which is likely precession-related (Abdul Aziz et al., 2000). In addition, larger-scale 400-kyr cyclicity could be distinguished and – less clear – a 5-cycle clustering in the lower and upper part of the succession, that is probably related to 100-kyr eccentricity. Both the lithology (carbonate) and the dominant astronomical period (20 kyr) in the Orera section are thus more or less similar to those in Ptolemais.

A second example is the Miocene Armantes section from the Calatayud Basin in NE Spain. This section contains very pronounced asymmetric large-scale (10 m) cycles of reddish silt (red bed) that gradually changes into an indurated bed of whitish (groundwater) caliches with a relatively sharp top. Magnetostratigraphy (Krijgsman et al., 1994) has shown that the average period of these cycles is 111 kyr, suggesting that it is related to the 100-kyr eccentricity cycle (Krijgsman et al., 1997). Large-scale cycles contain up to five pink (silty) caliche beds, more closely spaced towards the top of each large-scale cycle, suggesting a precessional origin. Based on palaeoclimatic reasons, the prominent large-scale white limestone beds are correlated to eccentricity maxima, the small-scale pink limestones to precession minima (summer insolation maxima). Although this section contains carbonate, it is mainly formed by precipitation from groundwater, as opposed to the lacustrine carbonate in Ptolemais and Orera. There is a large detrital component (silt), similar as in Megalopolis and Lupoiaia, although it is on average finer grained. The most obvious astronomical period is eccentricity, but precession is locally well-expressed. The strong saw-tooth like asymmetry in the carbonate content of the cycles in Armantes is different from the other Mediterranean sections and reminds of the asymmetric Late Pleistocene glacial cycles. They might therefore, like the glacial cycles, be caused by a highly non-linear response mechanism.

The Pliocene fluvio-lacustrine Apolakkia Formation on Rhodes has a very high sedimentation rate (80–140 cm/kyr, based on magnetostratigraphy) and a large detrital input. The section contains some limestone beds of mainly pedogenic origin. Van Vugt and Langereis. (submitted) reported that the thick (~25 m) sedimentary cycles have approximately the same period as precession. So, although the section contains coarse-grained detrital sediment, the dominant period is not eccentricity but precession.

Finally, there are the loess sequences, which are not really Mediterranean, but we mention them because they are important continental successions for palaeoclimate studies. The most famous loess sequences are no doubt from the Chinese loess plateau, but nearer to the Mediterranean, loess is found in central Europe. The magnetic susceptibility records of the Late Pleistocene Chinese and European loess are broadly in good agreement with the marine  $d^{18}O$  record, revealing 100-kyr as the dominant period. The

coherence implies a strong causal relation between climatic forcing of northern hemisphere ice sheets and Chinese loess deposition/soil formation (Maher and Thompson, 1999).

### *c. Possible explanations*

The dominant expression of eccentricity in the detrital Megalopolis and Lupoia basins must be explained by some non-linear response to insolation forcing. The mechanism of (Fischer et al., 1991), that invokes bioturbation to diminish the expression of precession in favour of eccentricity is not applicable here, because of two reasons. Firstly, the sedimentation rate is three to four hundred times higher here than it was in their deep marine core, so bioturbation could hardly mix the sediment as deep as the thickness of a precession cycle. Secondly, precession cycles are typically absent from the lignite seams in Megalopolis, that were deposited in an anoxic lake where burrowing animals could not live and deep-rooting plants such as trees did not grow (Mulder et al., submitted). The dominance of eccentricity might be explained by a mechanism somewhat similar to Paillard's model (Paillard, 1998), that was designed to explain the late Pleistocene ice ages. The 100-kyr cycles in the middle to late Pleistocene Megalopolis section could – because of their deposition during the global ice age regime – be related to the glacial-interglacial cycles. However, van Vugt and others (2000) showed that the pattern of these cycles did not match ice-volume-related  $d^{18}O$  records, but was instead similar to the eccentricity curve. This suggests that those cycles were not related to the 100-kyr glacial cycle. The 100-kyr cycles in the Lupoia section cannot have been influenced by glacial cycles, because the early Pliocene was a warm period during which only minor, obliquity-controlled, glacial cycles intermittently occurred. Nevertheless, Paillard's idea of multiple steady states could be used for a model with two sedimentary-environment states (a lignite-accumulating swamp versus a fluvio-lacustrine basin that deposits detrital sediment), which respond non-linearly to insolation. An additional feature of this model should be that the depositional environment has a memory, which requires the system to remain in one steady state for a certain amount of time before it can pass back to the other state. This amount of time should exceed the duration of half an eccentricity cycle to explain the dominance of eccentricity in our detrital basins. An additional eccentricity effect could be introduced into such a model by using a truncated insolation response (Clemens and Tiedemann, 1997).

A feasible geological explanation for such a mechanism could be that the weathering of source rock to produce abundant detrital sediment during warm and humid periods requires a long time (say 40 kyr). After such a prolonged, densely-vegetated period, the local climate became colder and dryer and the weathered material was eroded and deposited in the basin. During cold and dry intervals following short vegetated periods (i.e. during insolation minima in an eccentricity maximum), there might not have been enough detrital material available to bury the swamp vegetation (in the whole basin), and organic material was still preserved in the lignite seams. Occasionally, detrital material was deposited during eccentricity maxima, but only in lenticular sediment bodies or when the basin was nearly filled up (e.g. as observed in cycle IV in Megalopolis).



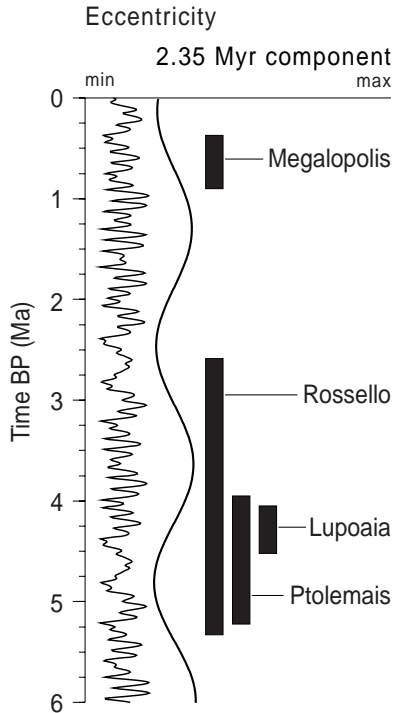


Figure 6: Eccentricity [Laskar, 1990 #150] and its filtered 2.35-Myr component; the amplitude of the 100-kyr eccentricity cycle is reduced during 2.35-Myr minima. The largest part of the Ptolemais section was deposited during a 2.35-Myr minimum, as opposed to the Lupoia and Megalopolis sections. The marine Rossello section [Hilgen, 1991 #12] covers a whole 2.35-Myr cycle: its largest part was deposited during a period with large-amplitude 100-kyr cycles, which are clearly expressed in the lithology. The lower part, which corresponds to a 2.35-Myr minimum, lacks expression of the 100-kyr cycle in the lithology, like the parallel Ptolemais section.

The lacustrine calcium carbonate systems of Ptolemais and Orea apparently responded more linear to insolation forcing, because precession is so distinctly expressed. However, the lack of a – dominant – expression of the 100-kyr cycle can also be explained otherwise. Both the Ptolemais section and the largest part of the Orea section were deposited during a period that the amplitude of the 100-kyr eccentricity cycle was reduced. Low 100-kyr amplitudes regularly occur because there is – apart from the well-known 100 and 400-kyr eccentricity cycles – also a 2.35 Myr eccentricity cycle that periodically reduces the magnitude of the 100-kyr cycle. Coincidentally, the Ptolemais section and the middle part of the Orea section were deposited during such a 2.35-Myr eccentricity minima (Figure 6, Orea not shown). The top of the Ptolemais section correlates with an interval with clear 100-kyr cycles, but the fact that the basin was nearly filled up may explain why this period is not clearly expressed in the lithology. This means that there might still be some non-linear response mechanism in lacustrine calcium carbonate basins, but that cannot be checked in these two basins.

## Acknowledgements

We gratefully acknowledge the co-operation with Maria and Sorin R\_dan. Their extensive palaeomagnetic studies in the Oltenia lignite mines led us to the Lupoia section in the first place and working with them in the mine was great fun, even despite the horrible weather. Field assistance of Marloes van Hoeve, Joris Steenbrink and Johan Meulenkamp was also greatly appreciated. Scientific discussions with Wout Krijgsman and Hayfaa Abdul Aziz furthered our understanding of several Mediterranean successions beyond what publications alone could have provided. Finally, we thank the Romanian mining company and her employees for their friendly permission and service.

## References

- Abdul Aziz, H., Hilgen, F.J., Krijgsman, W., Sanz-Rubio, E. and Calvo, J.P., 2000. Astronomical forcing of sedimentary cycles in the Miocene continental Calatayud Basin (NE Spain). *Earth and Planetary Science Letters*, in press.
- Alexeeva, L.I. and al., e., 1983. Correlations of the Pliocene and Lower Pleistocene deposits in the Dacic and Euxinic Basins. *Annuaire de l'Institut de Géologie et de Géophysique*, 59: 143-152.
- Andrescu, I., 1981. Middle-Upper Neogene and Early Quaternary chronostratigraphy from the Dacic Basin and correlations with neighbouring areas. *Ann. Géol. Pays Hellén.*, tome hors série, 4: 129-138.
- Berger, A.L., 1984. Accuracy and frequency stability of the earth's orbital elements during the Quaternary. In: A.L. Berger, J. Hays, G. Kukla and B. Saltzman (Editors), *Milankovitch and climate*, NATO ASI Ser C. Riedel, Dordrecht, pp. 3-39.
- Clemens, S.C. and Tiedemann, R., 1997. Eccentricity forcing of Pliocene-Early Pleistocene climate revealed in a marine oxygen-isotope record. *Nature*, 385: 801-804.
- Fischer, A.G., Herbert, T.D., Napoleone, G., Premoli Silva, I. and Ripepe, M., 1991. Albian pelagic rhythms (Piobbico core). *Journal of sedimentary petrology*, 61(7): 1164-1172.
- Hays, J.D., Imbrie, J. and Shackleton, N.J., 1976. Variations in the Earth's orbit: pacemaker of the Ice Ages. *Science*, 194: 1121-1132.
- Hilgen, F.J., 1991a. Astronomical calibration of Gauss to Matuyama sapropels in the Mediterranean and implication for the Geomagnetic Polarity Time Scale. *Earth and Planetary Science Letters*, 104: 226-244.
- Hilgen, F.J., 1991b. Extension of the astronomically calibrated (polarity) time scale to the Miocene/Pliocene boundary. *Earth and Planetary Science Letters*, 107: 349-368.
- Imbrie, J. et al., 1984. The orbital theory of Pleistocene climate: support from a revised chronology of the marine  $d^{18}O$  record. In: A. Berger, J. Imbrie, J. Hays, G. Kukla and B. Saltzman (Editors), *Milankovitch and climate*, part I, pp. 269-305, Plenum Reidel, Dordrecht.
- Imbrie, J. and Imbrie, J.Z., 1980. Modeling the climatic response to orbital variations. *Science*, 207: 943-953.
- Krijgsman, W., Delahaije, W., Langereis, C.G. and de Boer, P.L., 1997. Cyclicity and NRM acquisition in a continental red bed sequence (Miocene, Spain): potential for an Astronomical Polarity Time Scale. *Geophys. Res. Lett.*, 24: 1027-1030.
- Krijgsman, W., Langereis, C.G., Daams, R. and Meulen, A.J.v.d., 1994. Magnetostratigraphic dating of the middle

- Miocene climate change in the continental deposits of the Aragonian type area in the Calatayud-Teruel basin (Central Spain). *Earth and Planetary Science Letters*, 128: 513-526.
- Kroon, D. et al., 1998. Oxygen isotope and sapropel stratigraphy in the eastern Mediterranean during the last 3.2 million years. Proceedings of the Ocean Drilling Program, *Scientific Results*, 160: 181-189.
- Langereis, C.G., Dekkers, M.J., Lange, G.J.d., Paterne, M. and Santvoort, P.J.M.v., 1997. Magnetostratigraphy and astronomical calibration of the last 1.1 Myr from an eastern Mediterranean piston core and dating of short events in the Brunhes. *Geophysical Journal International*, 129: 75-94.
- Laskar, J., 1990. The chaotic motion of the solar system: A numerical estimate of the size of the chaotic zones. *Icarus*, 88: 266-291.
- Lourens, L.J. et al., 1996. Evaluation of the Plio-Pleistocene astronomical timescale. *paleoceanography*, 11: 391-413.
- Maher, B.A. and Thompson, R., 1999. Palaeomonsoons I: the magnetic record of palaeoclimate in the terrestrial loess and palaeosol sequences. In: B.A. Maher and R. Thompson (Editors), Quaternary climates, environments and magnetism. *Cambridge University Press*, Cambridge, pp. 81-125.
- Mulder, C., Sakorafá, V., Burrigato, F. and Visscher, H., submitted. Ecohydrological perspective of phytogenic organic and inorganic components in Greek lignites: a quantitative reinterpretation. *Earth and Planetary Science Letters*.
- Olsen, P.E. and Kent, D.V., 1996. Milankovitch climate forcing in the tropics of Pangaea during the Late Triassic. *Palaeogeography, Palaeoclimatology, Palaeoecology*, 122: 1-26.
- Paillard, D., 1998. The timing of Pleistocene glaciations from a simple multiple-state climate model. *Nature*, 391: 378-381.
- Passier, F.H., Dekkers, M.J. and Lange, G.J.d., 1998. Sediment chemistry and magnetic properties in an anomalously reducing core from the eastern Mediterranean sea. *Chemical Geology*, 152: 287-306.
- Radan, S.C. and Radan, M., 1998. Study of the geomagnetic field structure in the tertiary in the context of magnetostratigraphic scale elaboration. I - the Pliocene. *Anuarul Institutului Geologic al Romaniei*, 70: 215-231.
- Steenbrink, J., Vugt, N.v., Hilgen, F.J., Wijbrans, J.R. and Meulenkaamp, J.E., 1999. Cyclostratigraphy and  $^{40}\text{Ar}/^{39}\text{Ar}$  dating of lower Pliocene lacustrine sequences of the Ptolemais Basin, NW Greece. *Palaeogeography, Palaeoclimatology, Palaeoecology*, 152: 283-303.
- Torii, M., Fukuma, K., Horng, C.-S. and Lee, T.-Q., 1996. Magnetic discrimination of pyrrhotite- and greigite-bearing sediment samples. *Geophysical Research Letters*, 23(14): 1813-1816.
- van Vugt, N., Steenbrink, J., Langereis, C.G., Hilgen, F.J. and Meulenkaamp, J.E., 1998. Magnetostratigraphy-based astronomical tuning of the early Pliocene lacustrine sediments of Ptolemais (NW Greece) and bed-to-bed correlation with the marine record. *Earth and Planetary Science Letters*, 164(3-4): 535-551.
- van Vugt, N., de Bruijn, H., van Kolfschoten, M., Langereis, C.G. and Okuda, M., 2000. Magneto- and cyclostratigraphy and mammal-fauna's of the Pleistocene lacustrine Megalopolis Basin, Peloponnesos, Greece. *Geologica Ultrajectina*, 189: Chapter 3.
- van Vugt, N. and Langereis, C.G., submitted. Magnetostratigraphic dating and the recognition of astronomically forced sedimentary cycles in a Pliocene fluvio-lacustrine succession on Rhodes (Greece). *Palaeogeography, Palaeoclimatology, Palaeoecology*.

# Improved precision of the Messinian APTS from sedimentary cycle patterns in the lacustrine Lava section (Servia Basin, NW Greece)

## Abstract

A high-resolution cyclostratigraphy and magnetostratigraphy is presented for the upper Messinian lacustrine Lava section from the Servia Basin in Northwest Greece. The section contains fifteen distinct sedimentary cycles of alternating dark and light-coloured marls, while the gamma-ray attenuation record reveals an additional five to six cycles. The cycles in the lower half of the section are on average 5.3 m thick, as opposed to the cycles in the upper part that have an average thickness of 3.1 m. Palynological results point to a common cause for these cycles and define the lithological alternations in terms of periodic changes in humidity, where the light marls represent the humid periods and the dark marls the relatively dry periods.

Field evidence and shifts in average gamma-ray values point to a rather abrupt decrease in sedimentation rate, which coincides with the decrease in cycle thickness. This is confirmed by the magnetostratigraphy, which recorded four reversals that – given the biostratigraphic constraints from the Lava locality – could be correlated unambiguously to subchrons C<sub>3</sub>An.1n and C<sub>3</sub>An.2n of the geomagnetic polarity time scale. With this magnetostratigraphic time control, the average duration of the cycles can be calculated to be constant in the entire section, and similar to precession. The astronomical origin of the cycles is confirmed by the results of spectral analyses of gamma-ray and susceptibility time series.

The sedimentary cycles in the upper part of the Lava section are unambiguously tuned to insolation; there are two options for tuning the cycles in the lower part. The tuning results in accurate ages for the sedimentary cycles and polarity reversals that confirm the astronomical tuning of (Krijgsman et al., 1999), but define more precisely the astronomical polarity time scale.

*This chapter is submitted as: Steenbrink, J., van Vugt, N., Kloosterboer, M.L. and Hilgen, F.J. Improved precision of the Messinian APTS from sedimentary cycle patterns in the lacustrine Lava section (Servia Basin, NW Greece), to Earth and Planetary Science Letters.*

## Introduction

The astronomical theory of climate change, according to which climatic oscillations are linked to perturbations in the Earth's orbit (Adhémar, 1842; Croll, 1864; Milankovitch, 1941), is at present widely accepted. During the last decades, deep-sea oxygen isotope records have convincingly demonstrated that Pleistocene glacial cycles are driven by orbitally controlled variations in solar radiation (Emiliani, 1955; Shackleton and Opdyke, 1973; Hays et al., 1976; Imbrie et al., 1984). More recently, the recognition of Milankovitch cycles in sedimentary records of especially marine deposits has enabled in the development of very accurate time scales for the entire Neogene marine record, and in combination with magnetostratigraphy this has resulted in an astronomically tuned polarity time scale (APTS) (Lourens et al., 1996; Hilgen et al., 1997; Shackleton and Crowhurst, 1997; Shackleton et al., 1999). For the Messinian, the APTS is based on the integrated stratigraphy of several marine sections in the Mediterranean (Krijgsman et al., 1999). The astronomical tuning of these sections is confirmed by open-ocean calcareous nannofossil biochronology from ODP Sites 853 and 926 and by their implications for sea-floor spreading rates (see Krijgsman et al., 1999, Table 1). The magnetostratigraphic data were derived from the Spanish Sorbas Basin (Krijgsman et al., 1999) and the Cretan Faneromeni section (Krijgsman et al., 1994). Because of the moderate quality of the palaeomagnetic signal in these sections, the astronomical ages of the polarity reversals in the APTS are not well constrained (uncertainties of 20 to 60 kyr). Not only marine, but also continental sediments provide important archives of environmental and climatic change in the geological past. In fact, continental settings are expected to register orbitally induced climate changes more directly because they are not influenced by complex oceanographic processes which include linear and non-linear feed-back mechanisms. Until now, the role of astronomically induced climate variations in the deposition of sedimentary cycles in continental settings has often been underestimated. Sedimentary cycles are often linked to autocyclic processes such as tectonics and base-level change. However, Bradley (1929) already suggested that varves and sedimentary cycles in the Eocene Green River Formation are climatically linked and astronomically controlled. Since then, orbital forcing has been demonstrated for several continental deposits. The best known example is the Triassic lacustrine succession of the Newark Basin (Olsen and Kent, 1996; Kent and Olsen, 1999). Long and continuous cyclically-bedded continental successions are also present in the Mediterranean area. Recent studies demonstrated a strong orbital control on sedimentation for the late Miocene marginal lacustrine-floodplain sequences in the Calatayud Basin in Spain (Abdul Aziz et al., accepted), for the lower Pliocene lignite-marl alternations in the central part of the Ptolemais Basin in northern Greece (van Vugt et al., 1998; Steenbrink et al., 1999), and for the middle Pleistocene lignite seams in the Megalopolis basin (van Vugt et al., 2000). In this paper, we present the results of an integrated study on the cyclically bedded Messinian lacustrine Lava section. Astronomical tuning of the sedimentary cycle pattern combined with a reliable magnetostratigraphy offers a unique opportunity to confirm and define more precisely the APTS ages in the Messinian.

## Geological setting

The intramontane lignite-bearing Servia basin is located approximately 100 km southwest of Thessaloniki and is part of an elongated NNW-SSE trending graben system that extends over a distance of 120 km from Bitola in former Yugoslavia (F.Y.R.O.M.) to Servia in northern Greece (Figure 1). The graben system belongs to the Pelagonian Zone, which is the westernmost zone of the Internal Hellenides (Brunn, 1956) and developed in the late Miocene by late-Alpine NE-SW extensional movements. A Pleistocene episode of NW-SE extension resulted in the development of several sub-basins, e.g., the basins of Florina, Ptolemais and Servia (Pavlidis and Mountrakis, 1987). The basins are flanked by mountain ranges that are primarily composed of Mesozoic limestones, Upper Carboniferous granites and Palaeozoic schists (Brunn, 1956) (Figure 1). The basin fill comprises a ~600 m thick late Miocene to late Pleistocene succession of predominantly lacustrine sediments with intercalated lignite seams and fluvial deposits, which can be divided into a number of basin-wide lithostratigraphic units (Ehlers, 1960; Anastopoulos and Koukouzas, 1972) (Figure 1).

In this study, we focus on part of the lower Komnina Formation, which was dated as late Miocene (Turolian, lower part of mammal zone MN 13) on the basis of palaeontological data from small mammals (de Bruijn et al., 1999), plant remains (Velitzelos and Gregor, 1990) and charophytes (Antoniadis and Rieber, 1997). The Komnina Formation is ~300 m thick, unconformably overlies the pre-Neogene basement and is predominantly composed of lacustrine (diatomaceous) marls and clays, with some intercalated lignite seams, fluvial sands and conglomerates. This subsurface information is mainly derived from drillings and from outcrops in open-pit lignite mines in the Florina basin (Achlada and Vevi mines), Ptolemais basin (Vegora mine) and Servia basin (Lava and Prosilion mines) (Figure 1).

## Studied section and sampling

The Lava section is exposed in a private lignite open-pit, situated a few kilometres south of Servia and close to the deserted village of Lava in the footwall block of a major fault system that runs ENE-WSW and forms the southern margin of the Servia basin (Figure 1). The Lava depression has a NNW-SSE orientation and is bounded by basement faults, which strike in the same direction.

We selected the Lava mine for this study for a number of reasons. It has the most complete succession of the Komnina Formation. The sediments that crop out in the Lava mine display a distinct sedimentary cyclicity and, in contrast to some of the other mines, are all fine-grained, which is preferred for our palaeomagnetic study. Moreover, a biostratigraphic age constraint to calibrate these palaeomagnetic data is provided by a fossiliferous level with small mammal remains (de Bruijn et al., 1999).

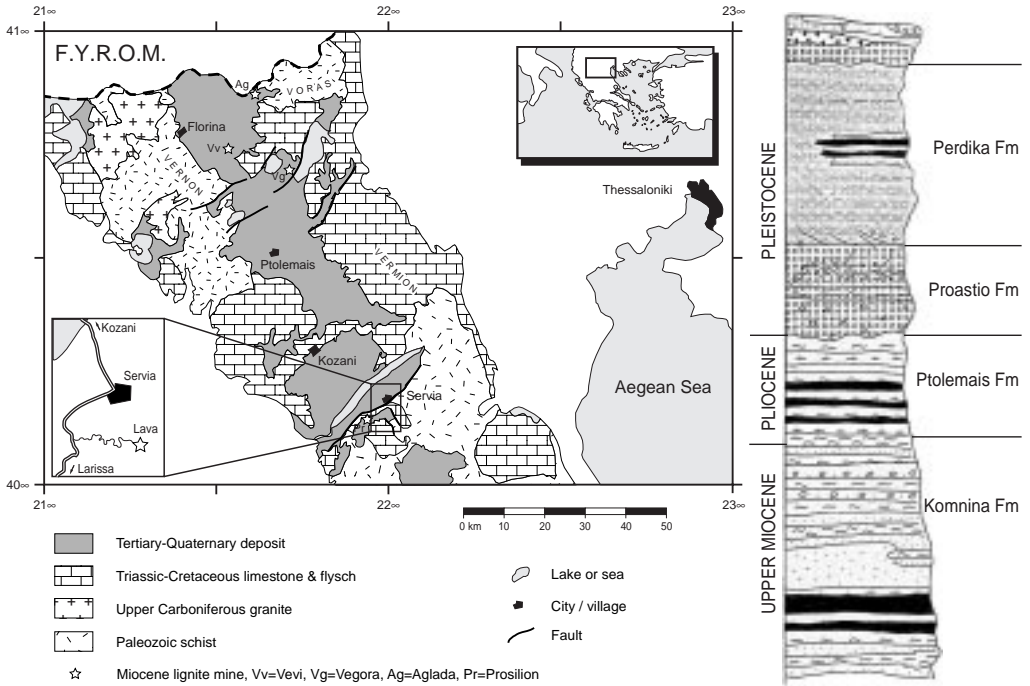


Figure 1: Geological map of the Florina, Ptolemais and Servia basins. The inset shows the exact location of the Lava mine. Sketched stratigraphic column of the basin fill after IGME Geological map of Greece, Ptolemais sheet 62, 1997.

The Lava section has a thickness of 130 m (Figure 2). The basal ~20 m of the section contains two (xylite-type) lignite seams, which are separated by homogeneous clays and laminated marls with abundant charophyte oogonia and freshwater gastropods. The upper ~110 m consists chiefly of lacustrine marls and clays with abundant leafs (among which the characteristic late Miocene *Glyptostrobos europaeus* (Velitzelos and Gregor, 1986)), freshwater diatoms and ostracods, and show a distinct cyclicality. Rather abrupt changes towards more clayey and organic-rich sediments occur twice in the lithology, namely between 60 and 67 m and between 85 and 88 m in the section. At 41.6 m in the section, a 5 cm thick bed full of gastropods is found (key-bed I) and at 73.2 m, a 5 cm thick clay bed is found with abundant fish teeth and vertebrae (key-bed II). These two layers have a constant thickness over the entire mining area and were also recognised in the five km westerly situated Prosilion mine, which supports their potential use as marker-beds.

Detailed logging and sampling of the Lava section was done in two campaigns. In 1994 we logged and sampled the section from the base up to 115 m, an upward extension was done in 1997. We took oriented palaeomagnetic samples, cored with a portable drill at 194 levels over a stratigraphic interval of 130 meters, which corresponds to an average spacing of 67 cm (resulting in an average temporal spacing of ~3.5 kyr). Additional non-

oriented samples were taken at the same levels for chemical and pollen analyses. During the 1994 sampling campaign, the gamma-ray signal was measured seven-fold at each sampling level with a UG135 differential gamma spectrometer, a portable apparatus equipped with a NaI crystal. Data were measured in the TC2-mode, detecting all energies above 400 kea. The low-field bulk magnetic susceptibility of the samples was measured in the laboratory on a KLY-2 susceptibility bridge. The natural remanent magnetisation (NRM) was studied in the laboratory by means of standard stepwise thermal demagnetisation procedures and measured on a 2G DC SQUID magnetometer.

## Cyclostratigraphy of the Lava section

The lacustrine marl succession that constitutes the upper ~110 m of the Lava section shows a marked succession of an alternating pattern of light- and dark-coloured marls on various scales. The dark-coloured marl beds are faintly laminated, enriched in organic matter and/or clay. The light-coloured marl beds are homogeneous and enriched in carbonate. The most prominent colour variations occur on a scale of 3 to 5 metres. We defined a basic sedimentary cycle as one such 3 to 5 metres thick dark-light marl couplet. We numbered the distinct dark marl beds, which we defined as the base of a sedimentary cycle, in ascending order from the base of the Lava section upward. Faintly developed (or very thin) dark-coloured marl beds are also present in different parts of the section (see below), but these were not numbered.

The Lava section contains 15 distinct sedimentary cycles. Sedimentary cycles are not present throughout the entire section, but are found primarily in two intervals. The first interval forms the lower part of the marl succession, it starts from ~20 m in the section, just above the second lignite, and continues up to ~60 m in the section. It contains seven regular cycles (cycles 1 to 7) of alternating dark- and light coloured marl beds, which have an average thickness of  $5.1 \pm 0.7$  metres. The dark-coloured marl bed of cycle 5 is the most prominent one in this interval. Within the light-coloured marl beds of cycle 6, which is very carbonate-rich and distinctly yellowish coloured, two additional thin dark-coloured marl beds are present. The dark-coloured marl bed of cycle 7 is composed of one thin, and two thicker dark-coloured marl beds (Figure 2).

The second interval is found in the upper part of the section, between roughly 90 and 120 m and contains eight cycles that are arranged in two clusters. The lower cluster comprises four well-developed cycles (cycle 8 to 11), with an average thickness of  $3.3 \pm 0.6$  metres. Especially the dark marl beds of cycles 10 and 11 are very distinct and clay-rich. The upper cluster contains four sedimentary cycles (cycles 12 to 15), of which the three lower cycles (cycles 12 to 14) are very regular both in thickness (~3.3 metres) and appearance, and have prominent dark-coloured clay beds. Cycle 15 is relatively thin (2.3 metres), its dark marl bed is strongly lignitic and the light marl segment of this cycle contains abundant freshwater gastropods and is composed almost exclusively of carbonate. In between these two clusters lies a more homogeneous interval in which a few cm-thick dark-coloured clay beds are intercalated: four at around 105 m and one at



around 108 m, suggesting that two more cycles might be present in this interval (Figure 2). The two intervals with well-developed sedimentary cycles are separated by an interval that runs from ~60 to 90 m in the section and lacks an obvious lithological cyclicity. This interval is not homogeneous, but the difference between the dark- and light coloured marl beds is less pronounced. This makes subdivision into sedimentary cycles arbitrary. There are a few prominent dark-coloured marl beds, but these are very thin (<10 cm) and not regularly spaced (Figure 2).

### Gamma-ray and susceptibility

The gamma-ray intensity and low-field magnetic susceptibility records of the Lava section were measured to quantify the subtle light-dark colour variations that we observed in the field. Moreover, spectral analysis of these records in either the depth or time domain enables an objective estimate of periodic characteristics. The gamma-ray (GR) intensity is mainly a function of the Uranium-content (ten Veen and Postma, 1996) and Uranium tends to be more abundant in both detrital minerals and organic-rich sediments. The low-field susceptibility ( $\kappa$ ) is positively influenced by the concentration of ferri-magnetic and paramagnetic (clay) minerals and negatively by diamagnetic material (carbonate). Both gamma-ray and susceptibility are thus good parameters to describe the alternation of organic-rich clay layers and carbonate-rich marl layers.

The GR and  $\kappa$  records are marked by a high variability showing a close correlation with the lithological variation (Figure 2). More precisely, they reveal relatively high values in the dark-coloured clay-rich beds and low values in the light-coloured carbonate-rich beds. The GR record reflects all sedimentary cycles as recognised in the field. In addition, the GR recorded another five or six minima and maxima in the interval between ~60 and ~90 m, where no distinct sedimentary cyclicity was observed. These maxima correspond to thin darker (clay) layers, which suggests that cyclicity is present in this interval as well, but less distinct than in the rest of the section. Sedimentary cycles 2–7 and 9–16 can be recognised as peaks in the  $\kappa$  record, but  $\kappa$  does not show any regular minima and maxima in the non-cyclic interval. The GR record shows a much smoother curve than the  $\kappa$  record, because  $\kappa$  is measured on discrete samples, while the gamma spectrometer measures the GR intensity of a sphere with a diameter of 25 cm. Two sharp increases in the mean GR value between 60 and 67 m and between 85 and 88 m co-occur with two earlier described lithological changes towards more clayey and organic-rich sediments. The  $\kappa$  record, on the other hand, does not show any pronounced change in its mean value.

The variance spectra of the GR and  $\kappa$  records in the depth domain show that power is concentrated in two broad bands (Figure 2). One is centred at ~5.4 metres and the other at ~3.1 metres. These two values are indistinguishable from the average cycle thickness in the lower and upper part of the section, which arrived at  $5.1 \pm 0.7$  and  $3.3 \pm 0.6$  metres, respectively. Further confirmation of cyclicity in both the GR and  $\kappa$  records with periods close to those of the sedimentary cyclicity is given by applying a Gaussian

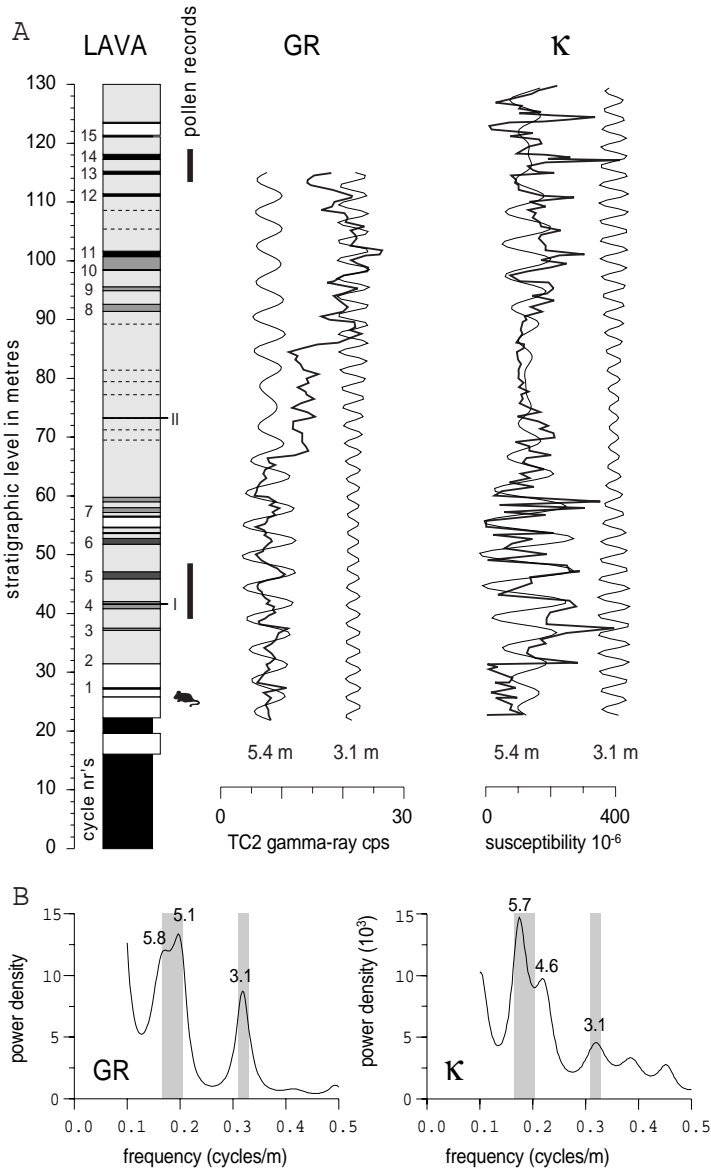


Figure 2: A: Schematic lithological column of Lava with sedimentary cycle numbers: black indented = lignite, white = carbonate, light shaded = marl, intermediate (dark) shaded = dark (-er) marl, black = clay. I and II denote key beds; mouse denotes small-mammal fauna (de Bruijn et al., 1999) and vertical lines indicate the position of the two palynological records. Dashed lines indicate thin dark marl beds. Gamma-ray and magnetic susceptibility records with their filtered components (thin lines) in the distance domain. B: Maximum entropy variance spectra of the GR (length of filter is 16.6 % of the series) and K records (length of filter is 14.9 % of the series), computed with the Analysseries program (Paillard et al., 1996), investigated in the frequency range 0.1 to 0.5 cycle/m. The cycle length (m) is indicated, the shaded bands indicate the band widths of the 5.4 and 3.1 m filters.

bandpass filter to the GR and  $\kappa$  records (centred at 5.4 and 3.1 m). The filtered records centred at 5.4 m follow the GR and  $\kappa$  records – and thus the lithological cyclicity – best in the lower half of the section, while the filtered records centred at 3.1 m reproduce the cyclicity best in the upper part of the section (Figure 2). The shift from a dominantly 5.4 m-scale cyclicity towards a 3.1 m-scale cyclicity is especially obvious from the filtered GR record and occurs between 60 and 67 m, coinciding with the first increase of the mean GR values. The question remains, however, whether these two types of cyclicity are forced by two different mechanisms or a single one? The thickness-ratio of the two cycle types is close to the ratio of the dominant periods of obliquity and precession. So, if the cycles are astronomically controlled, the thicker cycles might be related to obliquity, and the thinner ones to precession. Alternatively, both scales of cycles are controlled by the same (orbital forcing) mechanism and thus have the same duration. This second scenario implies a decrease in sedimentation rate.

### Palynology of sedimentary cycles

To determine whether a single mechanism is at work during the formation of the lower and upper cycles of the Lava section, we conducted a palynological study on two cycles from the lower part of the section and two from the upper part (Figure 2). From the palynological data, vegetational changes throughout the different cycles can be reconstructed, giving information on forcing mechanisms. The palynological data are expressed as percentages of a pollensum including all spores and pollen, and excluding fungi and algae (Figure 3).

For all cycles investigated, mixed deciduous/coniferous forests appear to have been widespread in the mid-altitude uplands surrounding the intramontane sedimentary basin. Montane forests with *Pinus*, *Cedrus*, *Abies* and *Fagus* dominated at higher elevations. Lowland elements, characteristic for fringing swamp vegetation around the lake, are mainly represented by *Taxodium*.

The available palynological evidence points to continuously wet and warm-temperate climatic conditions. This is notably apparent from the records of conifer pollen. *Cathaya* presently occurs in mid-altitude forests in China where annual precipitation is in excess of 2000 mm (Farjon, 1990). *Tsuga* is nowadays restricted to mountainous regions in Asia and North America where similarly high precipitation is available throughout the growing season (Farjon, 1990). An annual precipitation between 1000–1500 mm in higher altitudes can be inferred from the occurrence of *Cedrus* (Farjon, 1990). *Cedrus* forests nowadays occur only in high mountains around the eastern Mediterranean basin. Humid warm-temperate conditions were also inferred from studies on macroflora of the Lava mine (Velitzelos and Gregor, 1986). Additional evidence that conditions may have been generally moister than at present is provided by the conspicuous absence of dry-tolerant sclerophyllous evergreen-species of *Quercus*, characteristic of modern Mediterranean vegetation. The subordinate presence of *Juniperus* may be controlled more by substrate than by (low) precipitation.

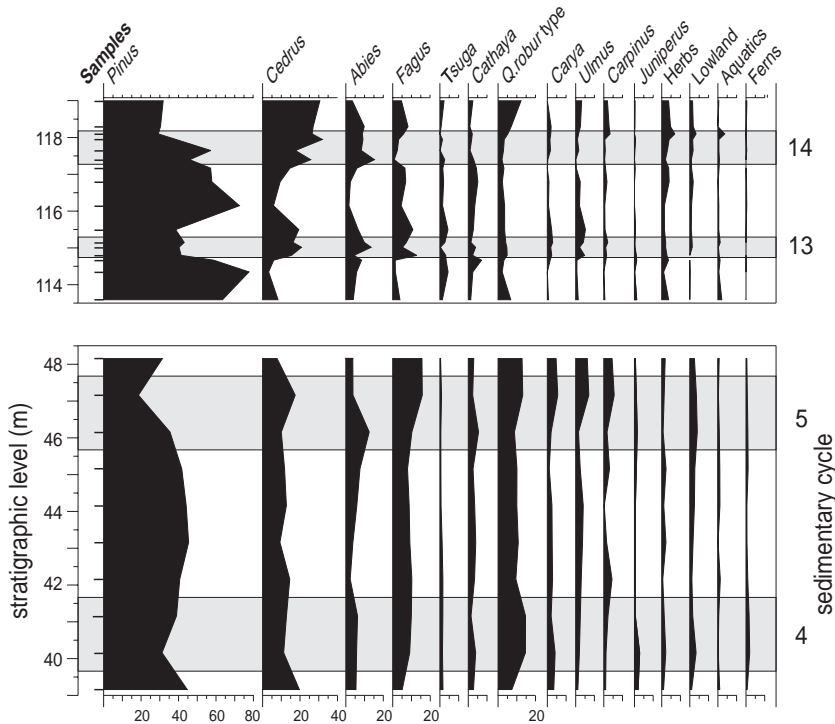


Figure 3: Pollendiagram of cycles 4, 5, 13 and 14 from Lava. The results are presented as percentages of a pollen-sum including all pollen and spores, excluding fungi and algae. The grey bands indicate dark marls. Herbs are a sum of mainly Poaceae, Asteraceae and Chenopodiaceae; Lowland consists of *Taxodium* and some *Salix* and *Alnus*; Aquatics are a sum of Cyperaceae, *Nuphar* and *Ceratophyllum*; Ferns are a sum of Polypodiaceae and *Osmunda*. *Quercus robur* type consist only of deciduous species of *Quercus*.

Superimposed on these generally wet conditions, palynological data for cycles 13 and 14 indicate periods of relatively increased precipitation that more or less coincide with the deposition of the light-coloured marls. Analogous to Holocene vegetation development in the eastern Mediterranean region (van Zeist and Bottema, 1982), a marked spread of *Pinus* at the expense of *Cedrus* can be interpreted as an increase in precipitation at higher elevations, resulting in downward expansion of *Pinus* into the mid-altitude deciduous forests. Similarly, increased montane humidity may also be responsible for an expansion of *Fagus* at the cost of *Abies*.

The pollen spectra of cycles 4 and 5 have generally higher amounts of *Fagus* and *Quercus* compared to the upper cycles. This may be due to higher (winter) temperatures in the lower cycles. Cyclic changes in precipitation are less obvious in the pollen records of these lower cycles than in cycles 13 and 14, which is in agreement with the less-pronounced lithological changes in these lower cycles. Apparently, climate was more equable during deposition of these lower cycles. Yet, careful inspection of the pollen curves suggests similar patterns for the relation between *Pinus* and *Cedrus*, as well as *Fagus* and *Abies*.

Palynological data of both the lower and upper cycles indicate that climate was generally humid and warm-temperate, but cyclic changes in precipitation could be inferred. Periods with increased precipitation occurred during deposition of the light marls, both in the lower as well as in the upper cycles. The results suggest that the sedimentary cycles in the Lava section are forced by a single mechanism. Comparison with results from the cyclically-bedded Ptolemais formation indicates that dominantly precession-controlled variations in regional climate are the most likely cause for the formation of the Lava cycles (van Vugt et al., 1998; Steenbrink et al., 1999)

### Palaeomagnetic analysis

A high-resolution chronology is a prerequisite for studying the role of orbital forcing on sedimentation patterns and may confirm our hypothesis of a single mechanism causing the formation of the sedimentary cycles. A number of methods is used to construct a high-resolution chronology in continental sections: 1) magnetic polarity reversal stratig-

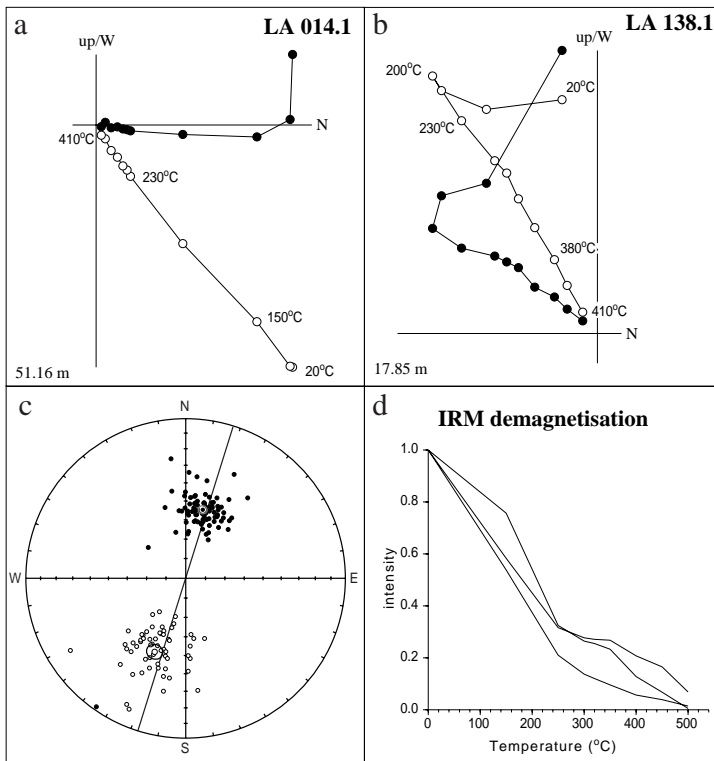


Figure 4: A and B) Representative demagnetisation diagrams. C) Stereographic projection of palaeomagnetic directions: black (white) circles indicate downward (upward) projection. D) Thermal IRM demagnetisation.

raphy. (Heller and Liu, 1982; van Vugt et al., 1998; Kent and Olsen, 1999); 2) a closely spaced  $^{40}\text{Ar}/^{39}\text{Ar}$  data set of intercalated volcanic ash beds (McDougall, 1985; McDougall et al., 1992; Steenbrink et al., 1999), or 3) varve countings of the sediments under study (Bradley, 1929; Anderson, 1984). Only a very limited part of the Lava section is (annually) laminated, and no volcanic ash layers were found, so the last two methods, varve counting and  $^{40}\text{Ar}/^{39}\text{Ar}$  dating, could not be used to build our time frame. The fine-grained sediments have a good potential, however, for the use of magnetostratigraphy.

Thermal demagnetisation reveals a two-component NRM (Figure 4a-b). The low-temperature (up to 200°C) component generally has a random direction, but it may be approximately parallel to the present-day field in the slightly weathered uppermost part of the section. The characteristic remanent magnetisation is isolated above 200°C and shows both normal and reversed polarities. These normal and reversed ChRM directions are almost antipodal (Figure 4c). Above ~400°C, both direction and intensity of the remanence change in many samples, indicating the presence of iron-sulphides (pyrite). To find the maximum unblocking temperatures, some samples were given an IRM that was thermally demagnetised. The samples have a maximum unblocking temperature of 500°C or higher, indicating magnetite (Figure 4d).

The declinations and inclinations of the ChRM compose a well-defined magnetic polarity pattern in the Lava section, with two reversed and two normal intervals (Figure 5). Given the constraint that the mammal assemblage from Lava belongs to the lower part of MN<sub>13</sub> (de Bruijn et al., 1999), we find a unique correlation with the geomagnetic polarity time scale, in which the lower normal polarity interval represents C<sub>3</sub>An.2n, and the upper normal interval C<sub>3</sub>An.1n (Figure 5).

## Astronomical forcing of the sedimentary cycles

Recently, two new time scales have been proposed for this interval by Krijgsman and others (1999), one astronomically tuned and one based on sea-floor spreading rates. Although the spreading-rate (SR) ages are statistically indistinguishable from the astronomically tuned ages (APTS), there is a notable difference in the duration of the polarity intervals (Table 1). The APTS and SR ages are significantly older than those from previous time scales, which were based on marine magnetic anomaly spacings in the South Atlantic and on ~10 Myr spaced age calibration points (Cande and Kent, 1992; Cande and Kent, 1995). These earlier time scales were presented 'pending further refinements such as the results of high-precision radiometric and astronomical dating methods', as stated by the authors. Since these refinements are now presented by Krijgsman and others (1999), we will not use the CK95 ages in this discussion, but prefer the SR ages; the results of our calculations based on ages from the –statistically similar – APTS as well as on those from the CK95 ages (Cande and Kent, 1995) are listed in Table 1.

With the magnetostratigraphic time control, the average sedimentation rates in the two complete polarity zones in Lava can be calculated. As expected from other observations, the sedimentation rate in the lower interval is higher than in the upper interval. There is

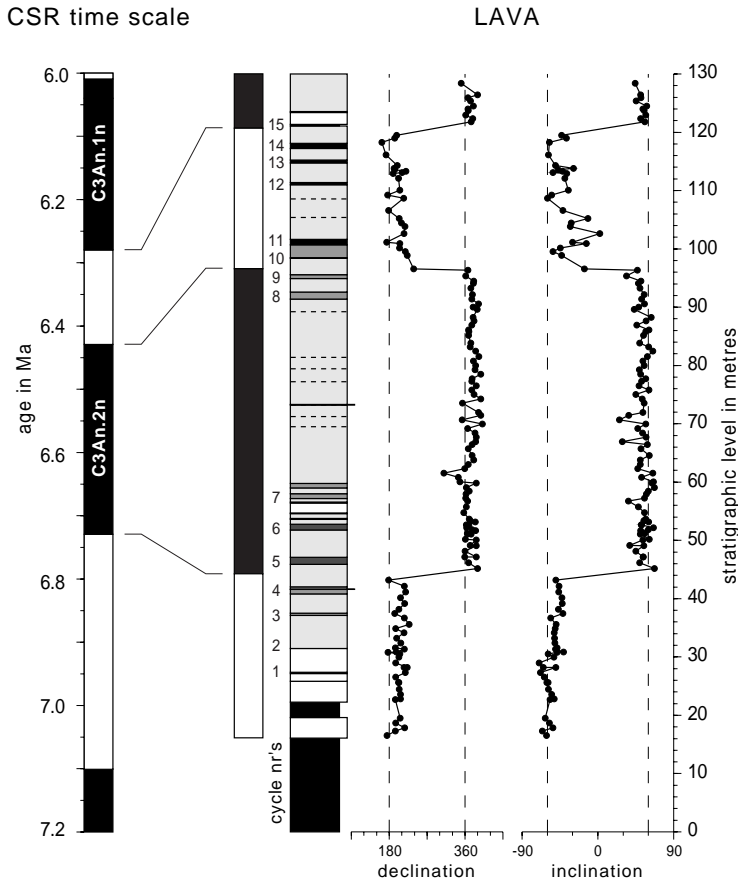


Figure 5: Palaeomagnetic directions of the Lava section and correlation of the polarity pattern to the constant spreading rate time scale (Krijgsman et al., 1999). For explanation of the lithological column see Figure 2.

no reason to assume that this shift in sedimentation rate co-occurs with a polarity reversal, in fact, the shift is probably located between 60 and 67 m, where there is a shift in both the thickness of the cycles and the average GR attenuation. We assume that the shift is located at 60 m, because this resulted in more consistent cycle periods than higher positions. The sedimentation rate for the reversed polarity zone was extrapolated downwards to 60 m. This yields a new, virtual age control point, with which the average sedimentation rate for the lower part of the normal polarity zone is determined. Combining these sedimentation rates with the average length of the sedimentary cycles in each interval results in an average duration for the cycles of  $19.9 \pm 5.4$  to  $23.0 \pm 3.1$  kyr for the thin sedimentary cycles, and  $22.8 \pm 4.0$  kyr for the thick cycles (Table 1). When we assume that the shift in sedimentation rate is located at 67 m, the duration of

the thick cycles changes to  $25.8 \pm 3.3$  kyr. This value is within error to the period based on the sedimentation-rate change at 60 m. The periods of the thin cycles (in the middle and upper part of the section) are unaffected. The similarity of the periods of the thin and thick cycles confirms the hypothesis that the cycles have the same cause, and the average duration strongly suggests that the cycles were forced by precession. This confirms the palynological results and their comparison with the Ptolemais Formation. Moreover, a dominant precession forcing as early as 6.8 Ma is in agreement with the theory of Schenau and others (1997) that primarily precession-induced dry-wet oscillations controlled the Mediterranean climate during (at least) the last 10 Myr.

Using the APTS ages results in a longer duration for the reversed interval. Extrapolation of the corresponding sedimentation rate leaves a negative amount of time for the lowermost part of the (shorter) normal zone, and therefore a highly inconsistent average duration of the cycles (Table 1). Assuming the sedimentation-rate shift at 67 m results in a very small amount of time for the lowermost part of the normal zone and consequently a short cycle duration (9 kyr). The CK95 time scale results in an even more inconsistent average duration. Since we had already strong, independent indications for a single duration of the cycles, these data support the SR time scale of Krijgsman and others (1999).

Table 1: palaeomagnetic age models for the Lava section

Reversal	Position	Lava section APTS age	KRIJ99 SR age		KRIJ99 APTS age		CK95 GPTS age	
C3An.1n (o)	120.1 ± 0.8	6.273 ± 0.005	6.28		6.26 ± 0.02		6.137	
C3An.2n (y)	96.4 ± 0.1	6.433 ± 0.001	6.43		6.44 ± 0.01		6.269	
C3An.2n (o)	44.2 ± 1.4	6.699 ± 0.005*	6.73		6.71 ± 0.03 6.731 ± 0.010*		6.567	
Polarity interval	Length	Cycle thickness	Duration	Sed rate	Duration	Sed rate	Duration	Sed rate
C3An.1r	23.6 ± 0.9	3.1 ± 0.8	150	0.16 ± 0.01	180 ± 22	0.13 ± 0.02	132	0.18 ± 0.01
C3An.2n	52.3 ± 1.4	4.3 ± 1.0	300	0.17 ± 0.01	270 ± 32	0.19 ± 0.02	298	0.18 ± 0.01
Polarity interval	Length	Cycle thickness	Sed rate	Period	Sed rate	Period	Sed rate	Period
C3An.1r	23.3	3.1 ± 0.8	0.16 ± 0.01	19.9 ± 5.4	0.13 ± 0.02	23.8 ± 7.1	0.18 ± 0.01	17.5 ± 4.8
C3An.2n (from 60 m up)	36.4	3.6 ± 0.5	0.16 ± 0.01	23.0 ± 3.1	0.13 ± 0.02	27.6 ± 5.0	0.18 ± 0.01	20.2 ± 2.7
C3An.2n (from 60 m down)	15.9	5.3 ± 0.5	0.23 ± 0.04	22.8 ± 4.0	-2.2	-	0.17 ± 0.02	31.3 ± 4.7

Table 1: Upper panel: Palaeomagnetic age models for the Lava section. Position (m) of reversal horizons in the Lava section and ages (Ma) of the corresponding reversals based on spreading rates (SR), astronomical tuning (APTS) both from (Krijgsman et al., 1999), and sea-floor anomalies (GPTS) from (Cande and Kent, 1995). The error estimates in the astronomical ages refer to the uncertainty in the exact stratigraphic position of the magnetic polarity reversal with respect to the astronomically dated cycles. \* Correspond to the two astronomical ages for C3An.2n(o), related to the two correlation options (Figure 7). Middle panel: Length (m) of and average cycle thickness (m) in the polarity intervals. Duration (kyr) of and average sedimentation rate (m/kyr) in these intervals according to the different time scales. Note the difference in sedimentation rate between the two polarity intervals for both the SR and APTS time scales. Lower panel: As middle panel, with the sedimentation rate from subchron C3An.1r extrapolated down to 60 m. Note the similarity of the average cycle periods and the period of precession for the SR age model, and divergent periods for the other age models.



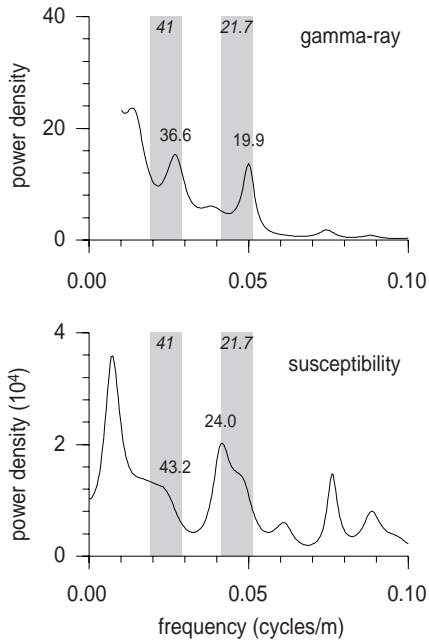


Figure 6: Maximum entropy variance spectra of the GR (length of filter is 12.8% of the series) and  $\kappa$  time series (length of filter is 11.2% of the series), computed with the Analseries program (Paillard et al., 1996) and investigated in the frequency range  $10^{-2}$  to  $10^{-1}$  cycle/kyr. The time series are generated from the SR ages for the reversals and our virtual age control point (see text), and re-sampled with 2.5-kyr intervals. The shaded areas indicate the width of the obliquity and precession frequency bands, as used for the filtered records in Figures 7 and 8. Numbers indicate cycle periods (kyr).

Spectral analysis of proxy records provides an objective estimate of periodic properties in time series of data. To be useful in testing the orbital hypothesis, the data must be transformed into geological time series. We constructed GR and  $\kappa$  time series by linear interpolation between and extrapolation beyond the control points, provided by — in our case — the SR ages of the palaeomagnetic reversals of Krijgsman and others (1999) and the extra age control point that we calculated for the 60-m level in the section (Table 1). The original data set was re-sampled with an interval of 2.5 kyr to obtain a regular sampling desirable for processing the signal.

The variance spectra of the GR and  $\kappa$  records vs. age are given in Figure 6. Both the spectra reveal peaks in two frequency bands. The first frequency band includes periodicities close to the obliquity period of 41 kyr and is located at 38.0 kyr in the GR and 44.0 kyr in the  $\kappa$  record. The second frequency band includes periodicities close to the precession periods of 23 and 19 kyr. A 20.3-kyr periodicity is present in the GR record and the  $\kappa$  spectrum reveals a prominent peak at a period of 23.0 kyr. These results indicate that both the GR and  $\kappa$  records, and thus the sedimentary cyclicity, have a strong orbital control that is dominated by precession and to a lesser extent by obliquity.

## Astronomical tuning of the sedimentary cycles of Lava

The sedimentary cycles of Lava are now proven to be related to precession. Moreover, the pollen study has shown that the dark-coloured marl beds correspond to relatively dry periods, while the light-coloured marl beds correspond to humid periods. In the Mediterranean area, relatively humid (and warm) climate occurred during summer insolation maxima, while the opposite regime occurred during insolation minima (Rohling and Hilgen, 1991). The dark-coloured marls can thus be correlated to insolation minima and the light coloured marls to an insolation maximum (Figure 7).

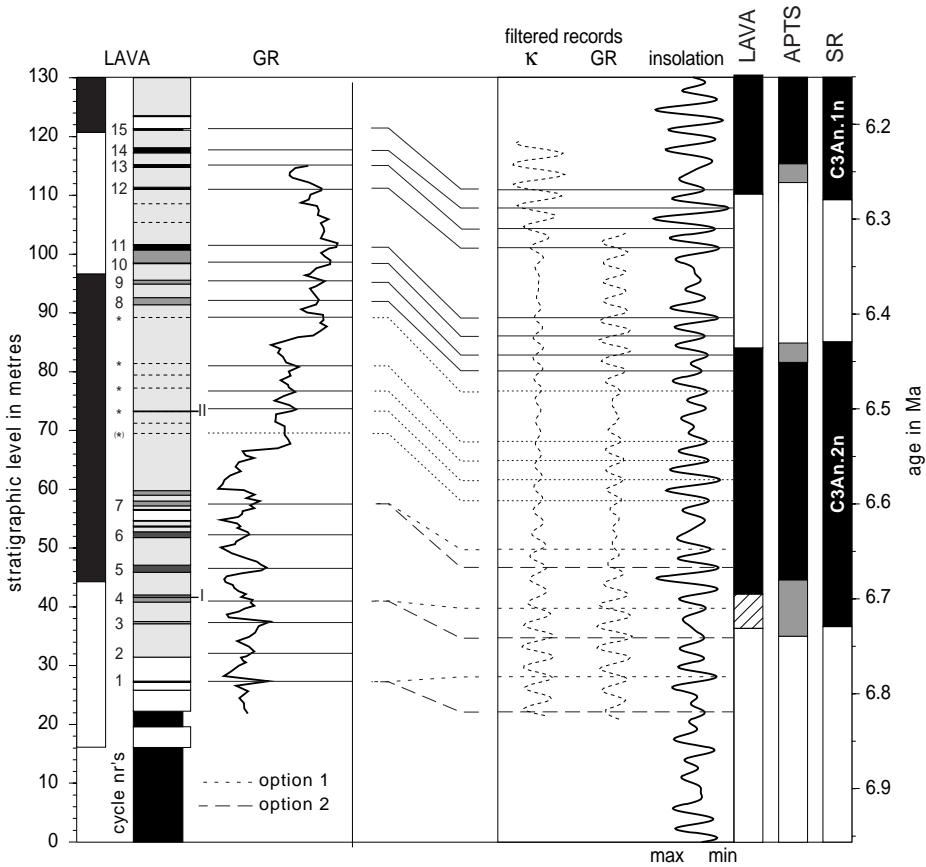


Figure 7: Tuning of the sedimentary cycles in Lava to 65°N summer insolation (Laskar, 1990; Laskar et al., 1993). Cycles that were not expressed in the lithology, but were clearly present in the GR or K record are indicated with an asterisk. The correlation of the lower cluster (cycles 1-7) is not certain, two likely options are indicated. The filtered precession components of GR and K are shown for comparison. The polarity pattern in the time domain is derived from our tuning and compared with the APTS and SR time scales (Krijgsman et al., 1999).

Considering that the sedimentary cycles are related to precession, typical clusters of 3–4 cycles, as observed in the upper part of the section (cycles 8–11 and 12–14), portray maxima in 100-kyr eccentricity cycle. With the upper two magnetic polarity reversals as approximate tie-points we can now tune these clusters to groups of high-amplitude insolation cycles related to the eccentricity maxima at  $\sim 6.4$  and  $\sim 6.3$  Ma.

Next, individual sedimentary cycles can be tuned to insolation. Cycle 11 has the most prominent organic-rich layer, and the underlying dark marl beds are alternately reduced and enhanced in GR and, to a lesser extent,  $\kappa$ . Therefore, cycle 11 is correlated to the high-amplitude minimum at 6.4 Ma, and the underlying cycles to consecutively older minima. The dark marls of cycles 12 to 14 are very prominent, they are therefore correlated to the cluster of three high-amplitude insolation minima around 6.3 Ma.

In the middle of the section, no cycles were recognised in the lithology nor in the  $\kappa$  record. The GR record, however, showed several distinct cycles in this interval, that are indicated in the column by an asterisk (Figure 7). These cycles are correlated to a series of relatively high-amplitude insolation minima between 6.55 and 6.6 Ma, with the most prominent dark clay bed (key bed II) corresponding to the highest amplitude insolation minimum. The GR peak immediately below cycle 8 is very wide, and likely covers two cycles (see also filtered record, Figure 2). In that case, an extra correlation line could tentatively be drawn below the one indicated in Figure 7.

The cycles in the lower part of the section (1–7) show no typical clustering, and they can thus not be tuned using the eccentricity modulation of insolation. Therefore, we suggest two likely correlations for cycles 1 to 7. Cycles 5, 6 and 7 have the most pronounced lithological expression. The first option assumes two cycles between 60 and 70 m (each  $\sim 5$  m thick, similar to the average thickness of the thick cycles) and correlates cycles 5–7 to three consecutive insolation minima with slightly higher amplitudes than the minimum below ( $\sim 6.71$  Ma). Cycles 1 to 4 are correlated to consecutive insolation minima. The second option assumes three cycles between 60 and 70 m (each  $\sim 3$  m thick, similar to the average thickness of the thin cycles) and correlates cycles 2–7 to one insolation cycle older than the first option. In this option, the prominent light-coloured carbonate bed of cycle 6 is correlated to the high-amplitude insolation maximum at  $\sim 6.68$  and the carbonate lithology of cycle 1 and below is correlated to the high-amplitude insolation maximum at  $\sim 6.79$  and 6.85 Ma.

The filtered precession components of GR and  $\kappa$ , plotted for comparison in Figure 7, generally fit with insolation. Small differences most probably originate from errors in the SR age model.

The quality of the correlation can be tested by applying a Gaussian bandpass filter centred at 41 kyr to the GR record. Since the Lava record was tuned to the dominantly precession-related peaks of insolation, and thus independent of obliquity, a good fit between the filtered record and obliquity would suggest that the tuning is correct. The GR record was filtered twice, once for either age model (based on both tuning options) (Figure 8). The filtered components are almost identical in the uppermost part of the records, where the age models are identical, and they are in phase with obliquity, indicating that the tuning in this interval is correct. The lowermost parts of the two filtered

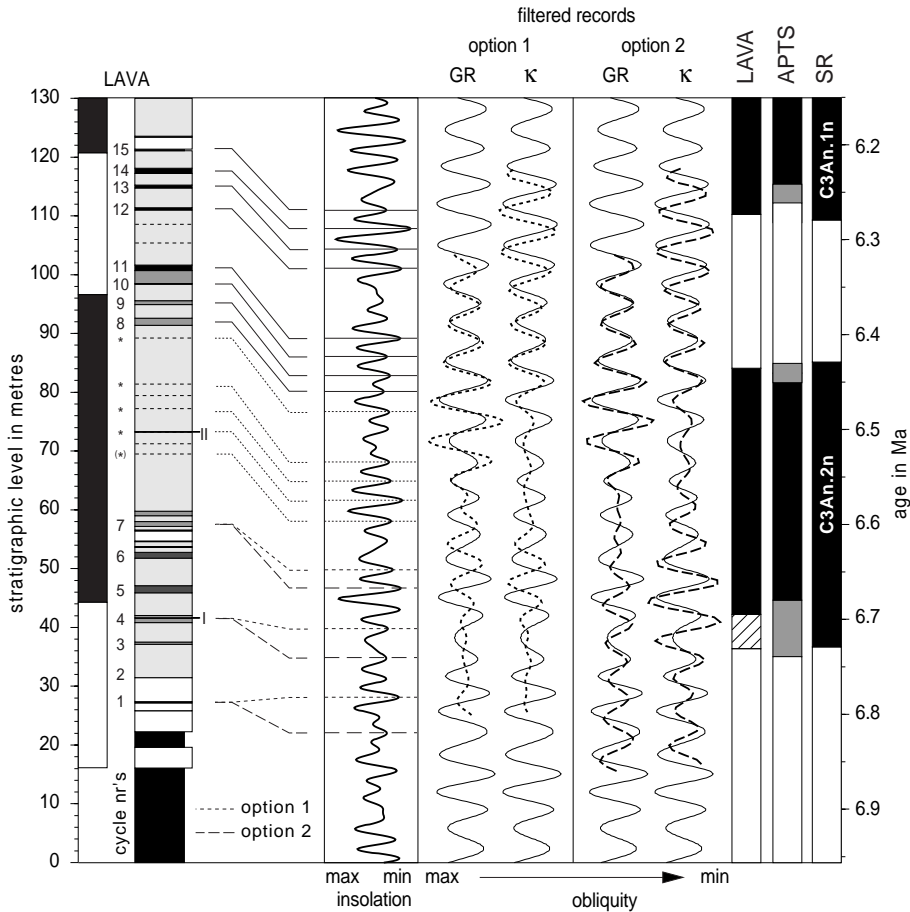


Figure 8: Filtered GR and  $\kappa$  records with a broad Gaussian bandpass filter centred around 41 kyr, plotted on top of obliquity (Laskar, 1990; Laskar et al., 1993). Two different age models were applied, according to the two correlation options of cycles 1-7 in the Lava section. The filtered components are almost identical and in phase with obliquity in the upper part of the records. The first option results in negligible amplitude in the lowermost parts; the second option shows higher amplitudes, that are almost in phase with obliquity, and is thus preferred.

records are clearly distinct: the first option (left-hand side in Figure 8) results in negligible amplitude for the 41-kyr component in this interval, so the phase cannot be compared; the second option (right-hand side in Figure 8) results in a higher amplitude, and the cycles are almost in phase with obliquity. Obliquity filtering of the  $\kappa$  records showed the same pattern (not shown). Therefore, we have a strong preference for the second correlation option.

We can now assign astronomical ages to the polarity reversals of the Lava section (Table 1). The positions of all the reversals are well-defined (Figure 3 and Table 1), and the unambiguous astronomical tuning of cycles 8-15 results in high-precision ages for the

C<sub>3</sub>An.2n(y) and C<sub>3</sub>An.1n(o) reversals. The two correlation options for cycles 1-7 results in two possible astronomical ages for reversal C<sub>3</sub>An.2n(o), the older of which is preferred. Comparison with the APTS ages shows that all our reversals are within the error limits of the APTS ages, but have a higher precision (Table 1). The SR ages of the upper two reversals cannot be distinguished from our astronomical ages; the SR age of the lower reversal is within the error limits of our preferred tuned age.

## Conclusions

A reliable magnetostratigraphy is established for the late Messinian Lava section, which results in an age of ~6.9 Ma for the base and ~6.2 Ma for the top of the section. The cycles in the Lava section, as expressed in the lithology, gamma-ray attenuation and susceptibility records have the same duration and are forced by climatic precession. Palynological records indicate that dark marls were deposited during summer insolation minima (drier periods with cooler summers), and light marls in maxima (more humid periods with warmer summers). Astronomical tuning of the cycles yields absolute ages for the polarity reversals that confirm and define more precisely the APTS ages of Krijgsman and others (1999).

## Acknowledgements

Prof. Dr. C.S. Doukas (University of Athens, Greece) is greatly acknowledged for arranging necessary contacts and for co-operation in the field. We are grateful to the Larko Mining Corporation for permission to work in their quarry and the corporation's employees for their hospitality and assistance in the field. The authors thank Wout Krijgsman, Johan Meulenkamp, Rob Satter, Erik Snel and Konstantin Theocharopoulos for various discussions and assistance in the field. We thank Cor Langereis, Johan Meulenkamp and Henk Visscher for their valuable comments on an earlier version of the manuscript. The investigations were supported by the Netherlands Council for Earth and Life Sciences (ALW), part of the Netherlands Science Foundation (grant to JS, MK and NvV).

## References

- Abdul Aziz, H., Hilgen, F.J., Krijgsman, W., Sanz, E. and Calvo, J.P., accepted. Astronomical forcing of sedimentary cycles in the Miocene continental Calatayud Basin (NE Spain). *Earth Planet. Sci. Lett.* .
- Adhémar, J.A., 1842. Révolutions de la mer. *privately published*, Paris.
- Anastopoulos, J. and Koukoulas, C.N., 1972. Economic geology of the southern part of the Ptolemais lignite basin (Macedonia, Greece). *Geol. Geophys. Res.* 16, 1-189.
- Anderson, R.Y., 1984. Orbital forcing of evaporite sedimentation. In: A. Berger, J. Imbrie, J. Hays, G. Kukla and B. Saltzman (Eds.), *Milankovitch and Climate*. Reidel, Dordrecht/Boston/Lancaster, pp. 147-162.
- Antoniadis, P.A. and Rieber, E., 1997. Zum Fossilinhalt Kohlegenese und Startigraphie des Kohlebeckens von Lava in Nordgriechenland. *Acta Palaeobot.* 37, 61-80.
- Bradley, W.H., 1929. The varves and climate of the Green River epoch. U.S. *Geol. Surv. Prof. Pap.* 158E, 87-110.
- Brunn, J.H., 1956. Étude géologique du pinde serpetional et de la Macedoine occidentale. *Ann. Geol. Pays Hellen* 7, 1-358.
- Cande, S.C. and Kent, D.V., 1992. A New Geomagnetic Polarity Time Scale for the Late Cretaceous and Cenozoic. *Geophysical Research Letters* 97, 13917-13951.
- Cande, S.C. and Kent, D.V., 1995. Revised calibration of the Geomagnetic Polarity Time Scale for the Late Cretaceous and Cenozoic. *Geophysical Research Letters* 100, 6093-9095.
- Croll, J., 1864. On the physical cause of the change of climate during geological epochs. *Philosophical Magazine* 28, 121-137.
- de Bruijn, H., Saraç, G., van den Hoek Ostende, L. and Roussiakis, S., 1999. The status of the genus name *Parapodemus* Schaub, 1938; new data bearing on an old controversy.
- Ehlers, E., 1960. Bericht über die bisher im Rahmen der Expertise Ptolemais durchgeführten geologischen und paläontologischen Untersuchungen, *Bundesanst. Geowiss. & Röhst.*, Hannover.
- Emiliani, C., 1955. Pleistocene temperatures. *J. Geol.* 63, 538-578.
- Hays, J.D., Imbrie, J. and Shackleton, N.J., 1976. Variations in the Earth's orbit: pacemaker of the ice ages. *Science* 194, 1121-1132.
- Heller, F. and Liu, T.S., 1982. Magnetostratigraphical dating of loess deposits in China. *Nature* 300, 431-433.
- Hilgen, F.J., Krijgsman, W., Langereis, C.G. and Lourens, L.J., 1997. Breakthrough made in dating of the geological record. EOS transactions, *American Geophysical Union* 78, 285-289.
- Imbrie, J., Hays, J.D., Martinson, D.G., McIntyre, A. and Mix, A.C., 1984. The orbital theory of Pleistocene climate: support from a revised chronology of the marine  $\delta^{18}\text{O}$  record. In: A. Berger, J. Imbrie, J. Hays, G. Kukla and B. Saltzman (Eds.), *Milankovitch and climate*. Reidel, Dordrecht - Boston - Lancaster, pp. 510.
- Kent, D.V. and Olsen, P.E., 1999. Astronomically tuned geomagnetic polarity timescale for the Late Triassic. *Journal of Geophysical Research* 104, 12,831-12,841.
- Krijgsman, W., Hilgen, F.J., Langereis, C.G. and Zachariasse, W.J., 1994. The age of the Tortonian/Messinian boundary. *Earth and Planetary Science Letters* 121, 533-547.
- Krijgsman, W., Hilgen, F.J., Raffi, I., Sierro, F.J. and Wilson, D.S., 1999. Chronology, causes and progression of the Messinian salinity crisis. *Nature* 400, 652-655.
- Laskar, J., 1990. The chaotic motion of the solar system: A numerical estimate of the size of the chaotic zones. *Icarus* 88, 266-291.
- Laskar, J., Joutel, F. and Boudin, F., 1993. Orbital, precessional, and insolation quantities for the Earth from -20 Myr to + 10 Myr. *Astron. Astrophys.* 270, 522-533.

- Lourens, L.J. et al., 1996. Evaluation of the Plio-Pleistocene astronomical timescale. *Paleoceanography* 11, 391-413.
- McDougall, I., 1985. K-Ar and  $^{40}\text{Ar}/^{39}\text{Ar}$  dating of the hominid-bearing Pliocene-Pleistocene sequence at Koobi Fora, Lake Turkana, northern Kenya. *GSA Bulletin* 96, 159-175.
- McDougall, I., Brown, F.H., Cerling, T.E. and Hillhouse, J.W., 1992. A reappraisal of the geomagnetic polarity time scale to 4 Ma using data from the Turkana basin, East Africa. *Geophysical Research Letters* 19, 2349-2352.
- Milankovitch, M., 1941. Kanon der Erdbestrahlung und seine Anwendung auf das Eiszeitenproblem. *Royal Serb. Acad. Spec. Publ.* 133, 1-633.
- Olsen, P.E. and Kent, D.V., 1996. Milankovitch climate forcing in the tropics of Pangea during the Late Triassic. *Palaeogeography, Palaeoclimatology, Palaeoecology* 122, 1-26.
- Paillard, D., Labeyrie, L. and Yiou, P., 1996. Macintosh Program Performs Time-Series Analysis. *Eos Trans. AGU* 77, 379.
- Pavlidis, S.B. and Mountrakis, D.M., 1987. Extensional tectonics of northwestern Macedonia, Greece, since the late Miocene. *Journal of Structural Geology* 9, 385-392.
- Rohling, E.J. and Hilgen, F.J., 1991. The eastern Mediterranean climate at times of sapropel formation: a review. *Geologie en Mijnbouw* 70, 252-264.
- Schenu, S. et al., 1997. Organic-rich layers in the Metochia section (Gavdos, Greece): evidence for a single mechanism of sapropel formation during the past 10 My. *Marine Geology* 153, 117-135.
- Shackleton and Crowhurst, 1997. Sediment fluxes based on an orbitally tuned time scale 5 Ma to 14 Ma, Site 926. Proceedings of the Ocean Drilling Program, *Scientific Results* 154, 69-82.
- Shackleton, N.J., Crowhurst, S.J., Weedon, G.P. and Laskar, J., 1999. Astronomical calibration of Oligocene-Miocene time. Philosophical Transactions of the Royal Society of London: Mathematical, Physical and Engineering Sciences, series A 357, 1907-1929.
- Shackleton, N.J. and Opdyke, N.D., 1973. Oxygen isotope and paleomagnetic stratigraphy of Pacific core V28-238: oxygen and isotope temperatures and ice volumes on a 105 and 106 year scale. *Quaternary Research* 3, 39-55.
- Steenbrink, J., van Vugt, N., Hilgen, F.J., Wijbrans, J.R. and Meulenkamp, J.E., 1999. Sedimentary cycles and volcanic ash beds in the lower Pliocene lacustrine succession of Ptolemais (NW Greece): Discrepancy between  $^{40}\text{Ar}/^{39}\text{Ar}$  and astronomical ages. *Palaeogeography, Palaeoclimatology, Palaeoecology* 152, 283-303.
- van Vugt, N., de Bruijn, H., van Kolfschoten, T., Langereis, C.G. and Okuda, M., 2000. Magneto- and cyclostratigraphy and mammal-fauna's of the Pleistocene lacustrine Megalopolis Basin, Peloponnesos, Greece, Utrecht University, Utrecht.
- van Vugt, N., Steenbrink, J., Langereis, C.G., Hilgen, F.J. and Meulenkamp, J.E., 1998. Magnetostratigraphy-based astronomical tuning of the early Pliocene lacustrine sediments of Ptolemais (NW Greece) and bed-to-bed correlation with the marine record. *Earth Planet. Sci. Lett.* 164, 535-551.
- ten Veen, J.H. and Postma, G., 1996. Astronomically forced variations in gamma-ray intensity: Late Miocene hemipelagic successions in the eastern Mediterranean basin as a test case. *Geology* 24, 15-18.
- Velitzelos, E. and Gregor, H.-J., 1986. Geologische Daten zu den fossilführenden Fundstellen Lava, Prosilion und Likudi (Griechenland) nebst Bemerkungen zu deren Frucht- und Samenfloren. *Documenta naturae* 29, 34-40.
- Velitzelos, E. and Gregor, H.J., 1990. Some aspects of the Neogene floral history in Greece. *Review of Palaeobotany and Palynology* 62, 291-307.

# Magnetostratigraphic dating of a Pliocene fluvio-lacustrine succession on Rhodes (Greece) and the recognition of astronomically forced sedimentary cycles

## Abstract

Astronomically forced sedimentary cycles are presently recognised in widely different sedimentary environments. Coarse grained continental sedimentary facies were so far not considered to be suitable for registration of climatic cycles. In this paper, we present a study on the fluvio-lacustrine Apolakkia Formation from Rhodes, Greece. Bio- and magnetostratigraphic results show that the succession was deposited during the middle Pliocene. The sections belong to the upper Gilbert and the Gauss Chron. Three different facies associations alternate in ~30-metre thick lithological cycles, that are forced by precession. Yet, these cycles do not permit a reliable astronomical tuning, mainly because the sedimentation rate is very high (1.09–1.41 m/kyr) and the records are not long enough to recognise the typical patterns of long-period (eccentricity) Milankovitch cycles.

*This chapter is submitted as: van Vugt, N. and Langereis, C.G. Magnetostratigraphic dating and the recognition of astronomically forced sedimentary cycles in a Pliocene fluvio-lacustrine succession on Rhodes (Greece), to Palaeogeography, Palaeoclimatology, Palaeoecology.*



## Introduction

The natural human habit of observing and trying to understand what we observe has led to a tendency in stratigraphy to classify elements as part of a recurring pattern, and subsequently study the characteristics and the underlying mechanisms of such cyclic sedimentary patterns. Generally, one favours one of two explanations for these cycles: auto-cyclic, i.e. caused by the system itself, e.g. a moving riverbed in fluvial deposits, or allo-cyclic, i.e. forced by a recurring external factor. This external forcing can be episodic, with an irregular period (e.g. tectonic events), or truly cyclic with a constant period (e.g. resulting from orbitally forced climate changes).

Orbital forcing is increasingly considered to have an important influence on the geological record in widely different sedimentary environments. This concept was first put forward by Adhémar (1842), and was elaborated by Croll (1864) and Milankovitch (1941). As already suggested by Gilbert (1895), the principle of orbital forcing is now used to measure the amount of time present in sediments, and was the basis for the high-precision astronomical time scale for the Pliocene and Pleistocene (Hays et al., 1976; Hilgen, 1991a; Hilgen, 1991b; Imbrie et al., 1984; Joyce et al., 1990; Lourens et al., 1996; Raymo et al., 1989; Shackleton et al., 1990; Shackleton et al., 1995).

The concept of astronomical cycles was used at first in deep marine deposits, but these cycles have now been recognised in turbidites (Weltje and de Boer, 1993), deep lake deposits (Olsen and Kent, 1996) and shallow lacustrine environments in humid (van Vugt et al., 1998; Steenbrink et al., 1999) and arid climate systems (Abdul Aziz et al., in press). Astronomical forcing has not been conclusively demonstrated in alluvial deposits, ultimately because accurate time control – which is essential for determining periodicities – is difficult to establish in coarse-grained sediments (Weltje et al., 1994).

This paper discusses a Pliocene fluvio-lacustrine basin-fill on Rhodes, with a high sedimentation rate. The fine grained marl layers that alternate with sand and conglomerate beds are suitable for palaeomagnetic sampling, thus providing the possibility of magnetostratigraphic time-control. The succession was surveyed for regularly recurring features, aimed at resolving whether these could be astronomically forced or not, based on the palaeomagnetic age data.

## Geological background and studied sections

The Island of Rhodes is placed at the eastern end of the Hellenic Arc. The backbone of the island is formed by a series of stacked tectonic units (Mutti et al., 1970). The Neogene sedimentary history of Rhodes has been divided into four successive phases (Meulenkamp et al., 1972). From the Miocene till the Early Pliocene, there was mainly erosion. During the Pliocene, the island was part of a large fluvial and lacustrine basin that continuously subsided, providing ample accommodation space for the large supply

of clastics from the east and northeast. The area was fragmented by block faulting in the late Pliocene, and fresh water limestone (travertine) was deposited in the south, while lagoonal and fluvial deposits from this period are found in other parts of the island. In the Pleistocene the area became separated from the mainland and open marine deposition occurred along the present coastline.

Our study focuses on the middle Pliocene basin in the southern part of the island, near the villages of Monolithos and Apolakkia (Figure 1). No lithostratigraphic formations have been officially formalised in the Neogene continental succession. We refer to (Meulenkamp et al., 1972) for their definitions. The oldest stratigraphic unit is the

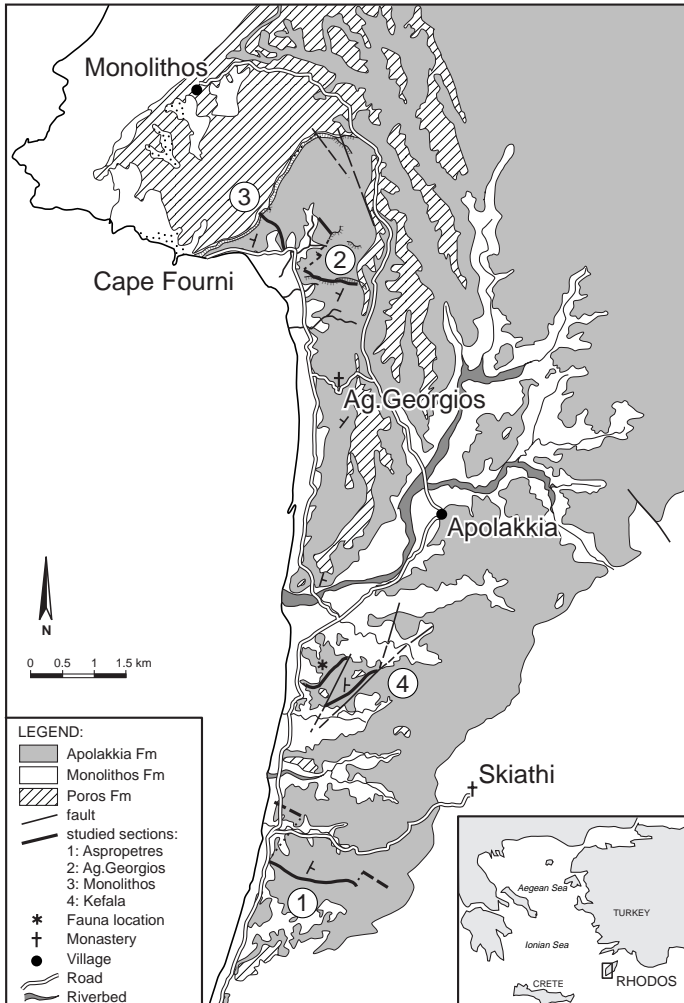


Figure 1: Geological sketch map of the Apolakkia Formation, SW Rhodes.

Istrios Formation, consisting mainly of conglomerates. The Apolakkia Formation discordantly overlies this unit (Duranti, 1997). It comprises an alternation of marl, (lignitic) clay, lignite, silt, sand and conglomerate, with abundant freshwater gastropods (Willmann, 1981) and some mammal remains. The fauna in the Apolakkia Formation is of middle and late Ruscinian age (MN zone 15, lower-middle Pliocene) (van de Weerd et al., 1982; Benda et al., 1987). The top of the Apolakkia Formation is a transition towards the travertines of the concordant Monolithos Formation. Especially the Apolakkia Formation is well exposed in the cuestas and badlands along the south-west coast of the island.

In the southern part of this area, beds are dipping  $\sim 20^\circ$  E-ESE; in the northern part they dip  $\sim 25^\circ$  WNW. Several large faults run through the area; in the south they are parallel to the coast line (N-S) or the eastern edge of the basin (NE-SW), and in the north they run NNW-SSE. We have logged and sampled four sections near the coast that are not disturbed by faults with a displacement larger than a few metres. The Kefala II section near the village of Apolakkia is 230 m long and contains 86 sampled levels. The previously studied Kefala I section (Duranti, 1997) lies to the west of Kefala II, separated by a normal fault. The stratigraphic displacement on this fault was probably less than 100 m, based on pattern recognition in both sections. Published small-mammal findings come from this section (van de Weerd et al., 1982). Twelve orientated hand samples were taken from this 230 m long section to compare the polarity with the supposedly partly parallel Kefala II section. The Aspropetres section in the south is  $\sim 600$  m long, with additional, less minutely logged, up- and downward extensions of  $\sim 200$  m each for palaeomagnetic purposes. In total, orientated hand samples were collected at 77 levels. The Agios Georgios section in the northern part of the basin is composed of two partly overlapping subsections. The composite length is 370 m, and 25 levels were sampled. The uppermost 130 m are exposed in relatively small outcrops (up to  $\sim 70$  m wide). Finally, the stratigraphically highest Monolithos section is located at the monumental Furni cliff, forming the northern boundary of the exposed basin. This 300-m section contains the uppermost part of the Apolakkia Formation, with 22 sampled levels, and the base of the Monolithos Formation (travertine). Large mammals found in this location indicate a Pliocene age (Benda et al., 1987).

## **Sedimentology/(cyclo)stratigraphy**

Essentially following the analysis of Duranti (1997), six main lithofacies are distinguished in the Apolakkia Formation (Table 1). They are: 1) light beige marl, either with lacustrine fossils (deposited in a shallow open lake) or with mud cracks (deposited in a regularly emerging lake margin), 2) dark grey silty marls with abundant organic matter or autochthonous lignite (deposited in a marginal swamp); 3) silt with root traces and nodular carbonate concretions, indicative of paleosol formation; 4) medium sand in thin sheets (typical flood plain deposit), which frequently pass laterally in 5) normally graded, internally stratified, broad lenses of pebbly sandstones, transported from the NE and

Lithofacies	Description	Facies association
1	Light beige marl with lacustrine fossils	(II), III
	Light beige marl with mud cracks	
2	dark grey silty marl with abundant organic matter autochthonous lignite	II, (III)
3	silt with roots and carbonate concretions	I, (II), III
4	medium sand in thin sheets	(II)
5	graded, internally stratified sand	I
6	unstructured conglomerate	
	lacustrine carbonate	III*
	sand lenses	
	sand with symmetric ripples	
Facies association	Contains lithofacies:	
I: delta plain	3 and 5	
II: palustrine	Mainly 2, also 1, 3 and 4	
III: shallow lacustrine	1, 3, 2 and 4 (in Monolithos also lacustrine carbonate)	

Table 1: Lithofacies and facies associations of the Apolakkia Formation. Facies associations in brackets indicate that the lithofacies is not the main constituent.

deposited by hyper-concentrated flows and flash-floods in an alluvial environment and 6) disorganised conglomerates, rarely displaying faint cross-bedding, deposited by debris flows. The debris of the latter lithofacies has an aberrant petrographic composition and was supplied from the south. Additional less abundant lithofacies are: white lacustrine silty carbonate with abundant fresh water gastropods; concave channel-fill sand lenses; and sand beds with symmetric ripples, interpreted as littoral lacustrine.

The Apolakkia Formation consists of an alternation of these lithofacies. On a large scale (tens of metres), this alternation appears to be cyclic. In order to describe this cyclicity, three facies associations are distinguished: the *delta plain*, *palustrine* and *shallow lacustrine* facies associations, after (Duranti, 1997). The sub-aerial *delta plain* association consists of graded sand, silt and calcretes (abundant carbonate concretions in palaeosols) (lithofacies 5 and 3). This coarse grained association is often distinctive in the topography as a dip slope. The *palustrine* association is dominated by dark marl and lignite (lithofacies 2), with minor intercalations of beige marls, palaeosols and sand sheets (lithofacies I, 3 and 4). The depositional environment of the palustrine facies is a regularly flooded swamp or vegetated mud flat along the margin of a lake. The *shallow lacustrine* association consists of an alternation of lacustrine marl, pedogenic carbonate (palaeosols), lignite and sand (lithofacies I, 3, 2 and 4), deposited in the margin of a large lake with varying water level, regularly causing desiccation. In the Monolithos section, this facies associa-

tion also contains lacustrine limestone and sand with ripples, and is then interpreted as less affected by alluvial supply.

In the central part of the Aspropetres section (Figure 3a and 4a), the cyclic pattern is very distinct: the (top of the) *delta plain* association generally crops out as a dip slope, followed by dark organic-rich layers of the *palustrine* facies association (often covered by low vegetation). Upwards, the thickness, frequency and darkness of these beds decrease, and the beige marl, silt and sandstone of the *shallow lacustrine* facies association predominate. This is followed by the next coarse-grained interval of the *delta plain* association, and so on. In the lower part of the Aspropetres section, the *palustrine* facies association is less well developed, but the coarse-grained layers still make dip slopes, that are followed by the *shallow lacustrine* association, occasionally with more dark beds in the basal part. These cycles are on average 36 m thick, and are also recognised in the nearby Kefala I section (Duranti, 1997) and the upper part of the Kefala II section. The upward extension of the Aspropetres section is characterised by generally coarser grained sediment, and no lithological cycles are apparent.

Thick conglomerate beds, separated by fine grained units with traces of paleosols, prevail in the Ayos Georgios section, suggesting a more proximal, alluvial environment. No regular ordering of the facies associations was apparent (Figure 3b), and lithological cycles were not defined in this section.

In the cycles from the Monolithos section (Figure 3c and 4b), the palustrine association is not always recognised, and the marginal lacustrine association can appear different because of the lacustrine limestone and sandstone beds. Nevertheless, since the regularly spaced coarse grained beds are laterally continuous over the width of the exposure (several hundreds of metres), we feel we can safely interpret these as cycles. Even more so since these distinctive coarse beds are on average 25 m apart, which is of similar magnitude as in Aspropetres and Kefala. If they indeed represent cycles forced by the same mechanism as in Aspropetres, it follows that the sedimentation rate in the Monolithos section would be lower than in the Aspropetres section.

## Palaeomagnetism

In all sections, oriented hand samples were taken from holes deeply dug below the weathered crust, to avoid overprint of the magnetisation in the palaeomagnetic samples by weathering. In the laboratory, 2.5 cm-diameter cores were drilled from these hand samples, and these cores were cut into 2.2 cm-long specimens.

### Methods

For each sample, AMS and bulk susceptibility were measured on a KLY-3 Kappa bridge. Subsequently, the NRM was measured on a 2G-SQUID magnetometer and the samples were thermally demagnetised in steps of 50°C. A series of rock magnetic experiments was carried out on selected samples, to find out which minerals carry the remanence, and whether there is a difference between weathered and fresh rocks. A selec-

tion of unheated specimens from the Agios Georgios section was therefore progressively magnetised in a DC pulse field to acquire an isothermal remanent magnetisation (IRM). After each step, the remanence of the samples was measured on a JR5 spinner magnetometer. Finally, the magnetisation as a function of temperature was measured in air on a modified horizontal translation Curie balance (Mullender et al., 1993). For this measurement, samples of 70–100 mg were used, from nine different levels. The heating and cooling rate was 10°C/min, the maximum temperature was 700°C and the applied magnetic field cycled between 150 and 300 mT.

**Results**

The AMS ellipsoids are all strongly oblate, with the minimum axis, after tilt-correction, approximately vertical. This indicates a dominantly sedimentary magnetic fabric. The maximum axis of the ellipsoid strikes 52° which is parallel to one of the sediment sup-

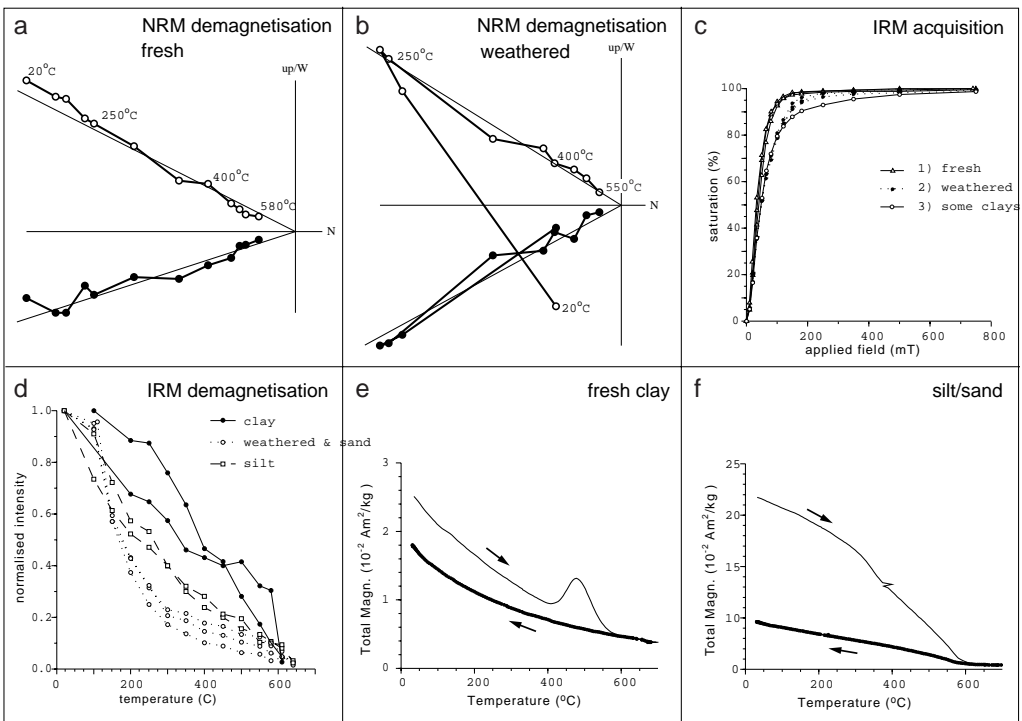


Figure 2 a & b: typical demagnetisation diagrams of a fresh (a) and a weathered (b) sample. Dots (circles) indicate the horizontal (vertical) projection of the magnetic direction. c: Relative magnetisation versus applied field in an IRM acquisition experiment. Three groups can be distinguished: open triangles indicate fresh samples, dots indicate weathered samples and open circles indicate an example of a fresh clay sample that does not saturate below 800 mT. d: IRM intensity decrease during stepwise heating: fresh clay samples show a linear decrease (dots), weathered samples and sand have a concave pattern (circles), and fresh silt shows intermediate behaviour (squares). e & f: Curie-balance experiment. During heating, the fresh clay sample has a peak above 400 °C (e), whereas the coarser grained and weathered samples show no such increase in magnetisation (f).

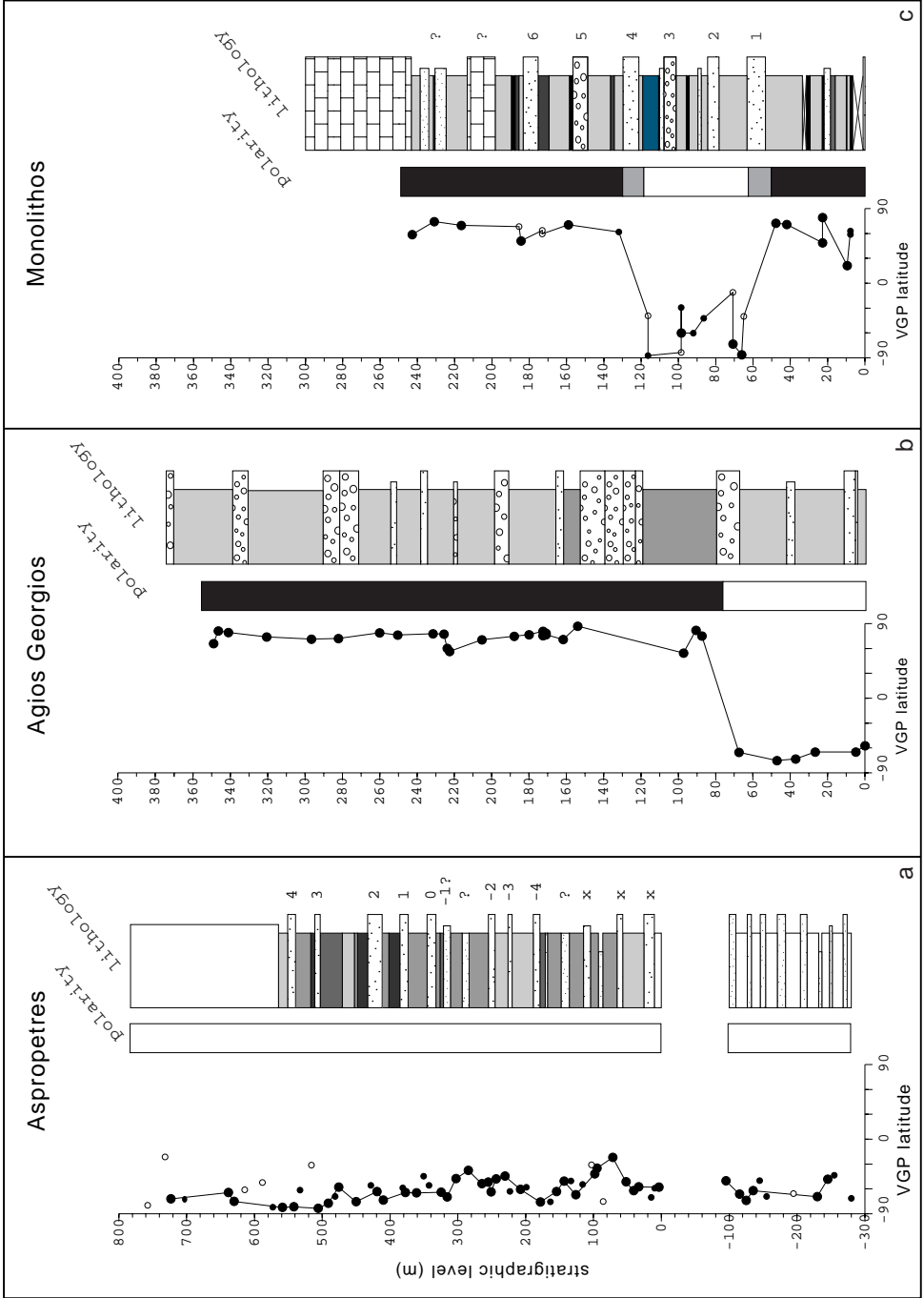


Figure 3: Schematic representation of the Aspropetres (a), Agios Georgios (b) and Monolithos sections (c). Dots (circles) indicate reliable (less reliable) palaeomagnetic directions, and white (black) indicates reversed (normal) polarity. The lithological column shows coarse grained beds from the delta plain facies association (dip slopes in Aspropetres) as protruding. Dotted indicates sand or conglomeratic sand, circles indicate coarse conglomerate. Light shading indicates marginal lacustrine facies association, dark shaded is palustrine facies association.

ply directions (NE), but also parallel to the current extension direction of the Hellenic arc in this area (Duermeijer et al., in press). The bulk susceptibility ranges between 200 and  $3000 \cdot 10^{-6}$  SI units, with an average of  $750 \cdot 10^{-6}$  SI units.

The NRM-intensity varies between 100 and 70 000  $\mu\text{Am}^{-1}$ , with an average of 3000  $\mu\text{Am}^{-1}$  in the Aspropetres and Monolithos sections and 17 000  $\mu\text{Am}^{-1}$  in the generally coarser-grained Agios Georgios section. The demagnetisation diagrams of unweathered material show generally one component, which is fully demagnetised after heating till 500–650°C (Figure 2a). The samples from weathered rocks have an additional low-temperature component, that is completely removed after 250°C (Figure 2b). Occasionally, samples having below-average intensities acquire a magnetisation in the final steps of the demagnetisation process that deviates from the characteristic, stable direction. Data from those steps were not used for calculating the characteristic component. The Kefala and Aspropetres sections have recorded only reversed polarities, the Agios Georgios and Monolithos sections show both normal and reversed polarities (Figure 3).

The IRM acquisition typically shows three types of behaviour (Figure 2c): 1) saturation at ~200 mT in fresh sandstone, limestone and some of the fresh clay samples, indicative of magnetite; 2) saturation between 300 and 500 mT in all weathered rock samples, probably caused by an additional high coercive mineral derived from oxidation (weathering); and 3) no saturation below 800 mT in the other fresh clay samples, indicative of ferrimagnetic sulphides. Thermal demagnetisation of the SIRM shows two end-type intensity decay curves, both having a maximum unblocking temperature above 600°C (Figure 2d). The first type shows a decay with a significant portion of the SIRM still present just below the maximum unblocking temperature, and occurs in fresh clay and limestone samples. The second type already decreases strongly at low temperatures and only slightly above ~400°C, and occurs in weathered rock samples and sandstone. Silt and silty clay samples have an intermediate intensity decay curve. The Curie balance results for fresh clay samples show a peak in the heating curve starting at 390°C, which is typical for the alteration of pyrite into magnetite. The Curie point is 580°C, identifying magnetite (Figure 2e). The other lithologies have no such pyrite peak, and the Curie point lies at 580°C (magnetite) for fresh silt, and slightly higher, up till 610°C for coarser material and weathered rocks. This is typical for cation-deficient (magnetised) magnetite (de Boer, 1999).

From these experiments we conclude that the fresh samples contain magnetite, a stable carrier for NRM directions. In addition, iron sulphides are occasionally present in fresh clay. Weathering has caused (partial) oxidation of the magnetite, especially in coarser-grained samples. The weathering overprint – is present – is easily removed at 250°C and has not obscured the primary NRM.



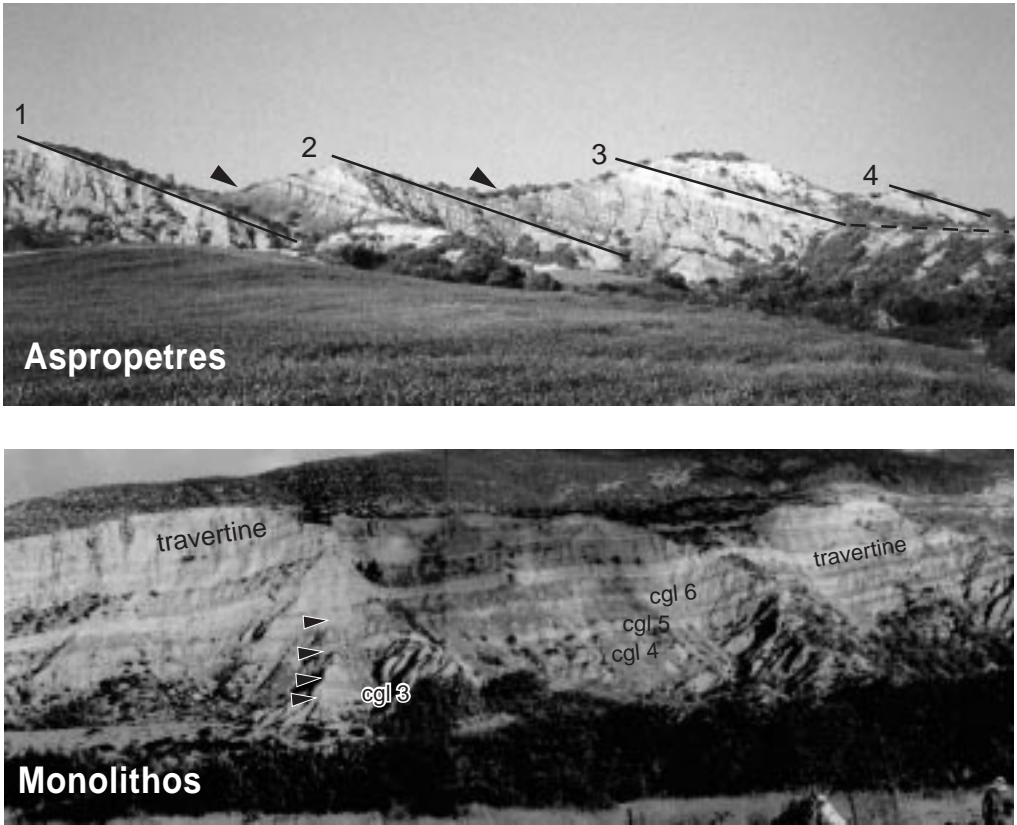


Figure 4: a) Part of the Aspropetres section clearly showing the regular sequence of dip slopes, indicated by lines and numbers (cf. Figure 3), and the dark palustrine facies (arrows). b) The Monolithos section with the coarse beds (indicated by arrows and 'cgl') and travertine in light shades.

## Discussion

### *Magnetostratigraphy*

The 800-metres long Aspropetres section is completely reversed, as are the downward extension and the nearby Kefala I and II sections. The Agios Georgios section has reversed polarity at the base and normal polarity in the rest of the section. The stratigraphical distance covered by the unexposed interval between the Agios Georgios and Monolithos sections is estimated – with a topographical map and average bedding orientation – to be 200–350 m. The Monolithos section contains the upper boundary of the Apolakkia Formation, and is therefore the youngest of the studied sections. The polarity is normal at the base and at the top, with a reversed interval of ~70 m in between.

A first order age estimate for the Apolakkia Formation comes from mammal palaeontology. Remains of *Miomys occitanus* that were found in the Kefala section led to the correlation of this formation to MN 15 and is thus of upper Ruscinian age (van de Weerd et al., 1982; Benda et al., 1987; Opdyke et al., 1997) correlate MN 15 to the reversed upper part of the Gilbert Chron (4.2-3.6 Ma), based on data from Spain. In addition, de Bruin (pers. comm.) found that the fauna from the lower part of the Ptolemais basin in N. Greece belongs to MN 14 (Lower Ruscinian), which was correlated to the lowermost normal subchrons in the Gilbert Chron (~5 Ma) (van Vugt et al., 1998). The long reversed interval from the Aspropetres section can thus only represent the top of the Gilbert Chron (Figure 5). The Monolithos section is younger, but still Pliocene (Benda et al., 1987), and the normal-polarity intervals in that section must therefore represent part of the Gauss Chron. Since the Agios Georgios section lies stratigraphically a few hundreds of metres below the Monolithos section, the normal interval in Agios

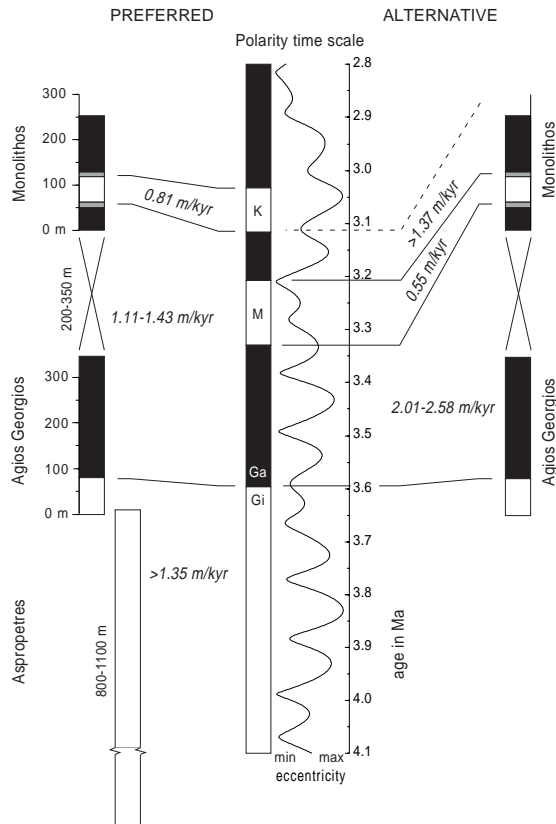


Figure 5: The polarity patterns of the studied sections on a single scale correlated to the polarity time scale (Lourens et al., 1996). On the left-hand side is the preferred option (see text) on the right-hand side is the alternative. Inferred sedimentation rates are indicated for each interval.

Georgios must also be part of the Gauss Chron. The completely reversed Kefala section is too short to be correlated to a specific polarity interval, but might overlap with the Aspropetres section.

The only complete polarity interval that is preserved here is the reversed interval in the Monolithos section. This interval could represent either the Mammoth or the Kaena subchron (Figure 5). The sedimentation rate for this interval would then be either 0.55 or 0.81 m/kyr, respectively. Additional information on sedimentation rate comes from the continuous part of the Aspropetres section. This 800 m long section represents (part of) the upper Gilbert Chron, so the minimum sedimentation rate in the Aspropetres section is 1.35 m/kyr.

The largest part of the Agios Georgios section is normal. Since this section is older than the Monolithos section, this normal interval can represent either the lowest or the middle normal subchron of the Gauss Chron. Correlation to the middle subchron would imply that the reversed interval in Monolithos represents the Kaena, and that not only the 280-metre normal interval from Agios Georgios, but also the unexposed interval and the lower normal from Monolithos together represent the 91 kyr normal subchron. This would lead to an anomalously high sedimentation rate of 5.9–7.5 m/kyr. The only alternative is thus that the normal interval from Agios Georgios must belong to the lowest normal subchron. The reversal in this record thus represents the Gilbert-Gauss boundary. If the reversed interval in Monolithos represents the Kaena subchron, the two normal intervals and the gap in between would represent the period from the base of the Gauss Chron, through the Mammoth subchron till the subsequent normal subchron (Figure 5, left-hand side). In this case, the sedimentation rate for the normal and partly unexposed interval is 1.11–1.43 m/kyr, depending on the exact stratigraphic distance between the two sections. This is approximately similar to the rates in the other intervals and consistent with the comparable types of lithology. If, on the other hand, the reversed interval in the Monolithos section represents the Mammoth subchron, the unexposed interval and the normal polarity intervals below and above would represent only the lowermost normal subchron in the Gauss Chron (Figure 5, right-hand side). This would yield an average sedimentation rate for this interval of 1.97–2.54 m/kyr, much higher than the 0.55 m/kyr for the inferred Mammoth. Moreover, the upper normal interval in the Monolithos section, that would then represent the normal subchron between the Mammoth and Kaena subchrons, would have a sedimentation rate of >1.37 m/kyr, at least twice as much as during the supposed Mammoth, which is not consistent with the observed identical lithology. In a fluvio-lacustrine system such as this, the sedimentation rate on a small scale is not at all expected to be constant. However, unless there are large scale sea level changes or important tectonic events, the sedimentation rate on a large scale (hundreds of metres) will vary only a little, or follow a trend caused, for instance, by a gradually changing rate of basin subsidence. Although the Agios Georgios section consists of generally coarser material, which indicates a more alluvial environment with possibly higher sedimentation rates than the fluvio-lacustrine facies, we prefer the correlation with the more consistent sedimentation rates, and we conclude that the reversed polarity interval in the Monolithos section must be the Kaena subchron.

*Astronomical forcing?*

To test for astronomical forcing in a geological record with regular lithological cycles, detailed time control is necessary to determine whether the average periodicity of these cycles matches one of the known astronomical frequencies. In Aspropetres, the average thickness of the observed lithological cycles is 36 m. With a minimum sedimentation rate of 1.35 m/kyr this renders a maximum average duration of 27 kyr/cycle. For Monolithos, the average duration lies between 24 and 33 kyr/cycle, depending on the exact number of cycles (3 to 3.5) in the Kaena interval (Figure 3c). The average period of the precession cycle (22 kyr) is comparable, and the number of precession cycles in the Kaena (3.5), according to the APTS (Lourens et al., 1996), is similar. We suggest that (at least in Monolithos) the lithological cycles are astronomically forced, with precession as the dominant parameter. We do refrain, however, from astronomical tuning of the cyclic patterns. First of all, the phase relation must remain speculative, since climate information (e.g. pollen) was not preserved in the sediment. Secondly, the number of cycles in the Monolithos section is too low to determine an unambiguous pattern fit. The Aspropetres section could be long enough, but there are no age calibration points. Larger scale cyclic features in the lithology, which might be caused by obliquity or eccentricity, were not recognised in the field. Looking at the lithological logs (Figure 3), however, there is a striking absence of cycles in some parts. In the top of the Aspropetres section and in the Agios Georgios section, the sediment is generally coarser (conglomerates and sands) and deposited in a more proximal environment, and lithological cycles are not apparent. This absence of sedimentary cycles was also observed in the deep marine Rossello section (Hilgen, 1991b) and the lacustrine Ptolemais section (van Vugt et al., 1998), where such intervals typically correspond to 400 kyr eccentricity minima. Intervals with an explicit expression of precessional cycles in these successions correspond to eccentricity maxima. Based on our correlation, the base of Agios Georgios and the top of Aspropetres approximately corresponds to the 400-kyr minimum around the Gilbert-Gauss boundary, but whether they overlap or not cannot be established. Monolithos and the body of Aspropetres clearly correlate with the 400-kyr maxima at 3.85 and 3.0 Ma respectively. A possible scenario to explain this observation is that during an eccentricity maximum, when the Mediterranean climate was warm and humid (Rossignol-Strick, 1983), a lake existed. When the climate became colder and more arid, during an eccentricity minimum, the lake would retreat, forcing the alluvial environment to extend. Upon return of more humid conditions, the sedimentary system would revert to (fluvio)lacustrine. This scenario is consistent with the trend towards coarser sediment in the top of the Aspropetres section, the generally more proximal sediment in the Agios Georgios section (eccentricity minimum around Gilbert-Gauss transition), and the return to fluvio-lacustrine sediments in the Monolithos section (eccentricity maximum around Kaena).

The change in lithology from the Apolakkia Formation to the travertines of the Monolithos Formation can now be estimated to have lasted 40–60 kyr (2–3 cycles). This change from detrital clastic sedimentation to chemical carbonate precipitation implies that the supply of clastics temporarily stopped, although some (pebbly) sandstone occur

between the two travertine beds and above the uppermost travertine (not shown in the log). Since we cannot think of a viable climatological explanation, the environmental transformation was probably caused by a tectonic event which must have occurred around 2.95 Ma. A phase of tectonic quiescence, for example, could have stopped the sediment supply temporarily, giving rise to carbonate precipitation in shallow, over-saturated water.

## Conclusions

The fluvio-lacustrine Apolakkia Formation was deposited during the middle Pliocene. On the basis of magnetostratigraphy in conjunction with a consistent pattern of sedimentation rates, we conclude that the Agios Georgios section contains the Gilbert-Gauss boundary. Similarly, we argue that the Monolithos section contains the Kaena subchron. From these time constraints we suggest that the 25–35 m thick regular lithological cycles in the Aspropetres and Monolithos sections are forced by precession. Other astronomical periods are too long to observe in the field, but eccentricity might have influenced the facies change from fluvio-lacustrine to more proximal and back that coincides with the presence and absence respectively of a clear expression of lithological cycles in different intervals of the Apolakkia Formation.

The transition from the fluvio-lacustrine Apolakkia Formation to the travertine Monolithos Formation around 2.95 Ma is likely tectonically induced.

## Acknowledgements

We thank Joris Steenbrink, Frits Hilgen and Poppe de Boer for stimulating discussions. The field assistance of Erik Snel, Mark Dekkers, Joris Steenbrink, Frits Hilgen and Sander Ernst was much appreciated. The people of Apolakkia will be remembered for their hospitality, especially during Greek orthodox Easter. Johan Meulenkamp is thanked for pointing out the section. The investigations were supported by the Netherlands Council for Earth and Life Sciences (ALW), part of the Netherlands Organisation for Scientific Research (NWO) (grant to NvV). This work was conducted under the programme of the Dutch Vening Meinesz Research School of Geodynamics (VMSG).

## References

- Abdul Aziz, H., Hilgen, F.J., Krijgsman, W., Sanz-Rubio, E., Calvo, J.P., Astronomical forcing of sedimentary cycles in the Miocene continental Calatayud Basin (NE Spain). *Earth and Planetary Science Letters*, in press.
- Adhémar, J.A., 1842. Révolutions de la mer. *privately published*.
- Benda, L., van der Meulen, A.J., Meyer, K.J. and van de Weerd, A., 1987. Biostratigraphic correlations in the Eastern Mediterranean Neogene: 8. Calibration of sporomorph- and rodent-associations from the Megalopolis Basin (Peloponnesus, Greece). *Newsl. Stratigr.*, 17, 129-141.
- de Boer, C.B., 1999. Rock-magnetic studies an hematite, maghemite and combustion-metamorphic rocks. *Geologica Ultrajectina*, 177. Faculteit Aardwetenschappen, Universiteit Utrecht, Utrecht, 256 pp.
- Croll, 1864. On the physical cause of the change of climate during geological epochs. *Phil. Mag.* 28, 121-137.
- Duermeijer, C.E., Meijer, P.T., Langereis, C.G. and Nijst, M. The Neogene evolution of the external Aegean arc: indications for a Pleistocene tectonic rotation phase. *Earth and Planetary Science Letters*, in press.
- Duranti, D., 1997. Il "Levantino" fluvio-lacustre dell'isola di Rodi (Grecia): sedimentologia ed analisi di bacino. *PhD thesis*, Università degli Studi di Bologna, facoltà di scienze matematiche, fisiche e naturali, pp. 110.
- Gilbert, G.K., 1895. Sedimentary measurement of geological time. *J. Geol.*, 3, 121-127.
- Hays, J.D., Imbrie, J. and Shackleton, N.J., 1976. Variations in the Earth's orbit: pacemaker of the Ice Ages. *Science* 194, 1121-1132.
- Hilgen, F.J., 1991a. Astronomical calibration of Gauss to Matuyama sapropels in the Mediterranean and implication for the Geomagnetic Polarity Time Scale. *Earth and Planetary Science Letters* 104, 226-244.
- Hilgen, F.J., 1991b. Extension of the astronomically calibrated (polarity) time scale to the Miocene/Pliocene boundary. *Earth and Planetary Science Letters* 107, 349-368.
- Imbrie, J. et al., 1984. The orbital theory of Pleistocene climate: support from a revised chronology of the marine  $\delta^{18}\text{O}$  record. In: A. Berger, J. Imbrie, J. Hays, G. Kukla and B. Saltzman (Eds.), *Milankovitch and climate*, part I., pp. 269-305, Plenum Reidel, Dordrecht.
- Joyce, J.E., Tjalsma, L.R.C. and Prutzman, J.M., 1990. High-resolution planktic stable isotope record and spectral analysis for the last 5.35 m.y.: Ocean Drilling Program site 625, northeast Gulf of Mexico. *Paleoceanography* 5, 507-529.
- Lourens, L.J. et al., 1996. Evaluation of the Plio-Pleistocene astronomical timescale. *paleoceanography* 11, 391-413.
- Meulenkamp, J.E., Mulder, E.F.J.d. and Weerd, A.v.d., 1972. Sedimentary history and paleogeography of the Late Cenozoic of the Island of Rhodos. *Z. Deutsch. Geol. Ges.* 123, 541-553.
- Milankovitch, M., 1941. Kanon der Erdbestrahlung und seine Anwendung auf das Eiszeitenproblem. *Royal Serbian Academy, Special Publication* 133, 1-633.
- Mullender, T.A.T., van Velzen, A.J. and Dekkers, M.J., 1993. Continuous drift correction and separate identification of ferrimagnetic and paramagnetic contribution in thermomagnetic runs. *Geophys. J. Int.* 114, 663-672.
- Mutti, E., Orombelli, G. and Pozzi, R., 1970. Geological studies on the Dodecanese Islands (Aegean SEa). - IX: Geological Map of the Island of Rhodes (Greece). Explanatory notes. *Ann. Geol. Pays Helleniques* 22, 77-226.
- Olsen, P.E. and Kent, D.V., 1996. Milankovitch climate forcing in the tropics of Pangaea during the Late Triassic. *Palaeogeography, Palaeoclimatology, Palaeoecology* 122, 1-26.
- Opdyke, N. et al., 1997. Continental deposits, magnetostatigraphy and vertebrate paleontology, late Neogene of eastern Spain. *Palaeogeography, Palaeoclimatology, Palaeoecology* 133, 129-148.
- Raymo, M.E., Ruddiman, W.F., Backman, J., Clement, B.M. and Martinson, D.G., 1989. Late Pliocene variation in northern hemisphere ice sheets and north Atlantic deep water circulation. *Paleoceanography* 4, 413-446.

- Shackleton, N.J., Berger, A. and Peltier, W.R., 1990. An alternative astronomical calibration of the lower Pleistocene timescale based on ODP Site 677. *Transactions of the Royal Society of Edinburgh: Earth Sciences* 81, 251-261.
- Shackleton, N.J., Crowhurst, S., Hagelberg, T., Pisias, N.G. and Schneider, D.A., 1995. A new Late Neogene time scale: application to leg 138 sites. *Proceedings of the Ocean Drilling Program, Scientific Results* 138, 73-97.
- van Vugt, N., Steenbrink, J., Langereis, C.G., Hilgen, F.J., Meulenkamp, J.E., 1998. Magnetostratigraphy-based astronomical tuning of the early Pliocene lacustrine sediments of Ptolemais (NW Greece) and bed-to-bed correlation with the marine record. *Earth and Planetary Science Letters* 164, 535-551.
- van de Weerd, A., Reumer, J.W.F. and de Vos, J., 1982. Pliocene mammals from the Apolakkia Formation (Rhodes, Greece). *Proceedings of the Koninklijke Nederlandse Akademie van Wetenschappen, Series B*, 85, 89-112.
- Weltje, G.J., van Ansenwoude, S.O.K.J. and de Boer, P.L., 1994. High-frequency detrital signals in eocene fan-delta sandstones of mixed parentage (south-central Pyrenees, Spain): a reconstruction of chemical weathering in transit. *Geologica Ultrajectina (doctorate thesis)* 121, 165-182.
- Weltje, G.J. and de Boer, P.L., 1993. Astronomically induced paleoclimatic oscillations reflected in Pliocene turbidite deposits on Corfu (Greece): implications for the interpretation of higher order cyclicity in fossil turbidite systems. *Geology* 21, 307-310.
- Willmann, R., 1981. Evolution, Systematik und stratigraphische Bedeutung der Neogenen süßwasser Gastropoden von Rhodos und Kos/Agais. *Palaeontographica A* 174, 10-235.

# Rock-magnetic properties of lignite-bearing lacustrine sediments from the Megalopolis and Ptolemais Basins (Greece) as possible climate proxies

## Abstract

Rock-magnetic parameters may be used as palaeoclimate indicators in sediments. Their interpretation is often not straightforward, however, and comparison with more conventional proxies is necessary to understand the variations in the magnetic signal. This study presents some magnetic results from two lacustrine lignite-basins that are well-known in terms of Milankovitch-scale palaeoclimate variations, to test their potential as reliable climate proxies in this type of setting.

From measurements on NRM intensity, bulk susceptibility, acquisition and demagnetisation behaviour of ARM and IRM we concluded that the alternating lignite and carbonate beds from the Ptolemais basin have magnetite as the main magnetic mineral in all lithologies except possibly pure lignite, which may contain ferri-magnetic sulphides. This could not be proven, because thermal experiments cause combustion of the lignite and destroy the samples.

Based on the same kind of experiments, with some additional Curie balance experiments, we found that the magnetic properties of the lignite and detrital sediments from the Megalopolis basin are dominated by the occurrence of authigenic greigite in clay without visible organic material, and the absence of greigite in organic-rich lithologies. The main magnetic mineral in these lithologies is probably magnetite. Although the magnetic parameters are strongly lithology-related, they show no apparent correlation with the cyclic pattern in the Megalopolis.



## Introduction

Conventional palaeoclimate and –environment data like (quantitative) palaeontological and palynological records or maceral analyses are laborious and time-demanding. Magnetic parameters may be good alternatives and have the advantage that they are quickly measurable. They can indicate different sources of sediment supply, different geochemical conditions or several phases of diagenetic alteration in the sediment, all related to changes in the sedimentary environment. Several authors suggest that the magnetic characteristics of sediments are reliable palaeoclimate and/or palaeoenvironment proxies in marine (e.g. von Dobeneck and Schmieder, 1998; Maher and Thompson, 1999) and continental (loess, lacustrine) records e.g. (Maher and Thompson, 1999). The interpretation of magnetic data in terms of climate changes is not always straightforward, however, and extensive studies that compare magnetic data with more conventional climate indicators are necessary to understand the variations in the magnetic signal.

A multi-disciplinary research programme on continental-marine correlations aimed to unravel the mechanisms of past climate changes provides an opportunity to compare various types of data from the same sections. This study reports the results of magnetic experiments on samples from two lacustrine basins with astronomically forced lignite cycles, to test how magnetic parameters compare with the climatically-induced lithological cycles. The first basin is the lower Pliocene Ptolemais basin in northern Greece, where precession dominantly forced the lignite-carbonate alternation (van Vugt et al., 1998; Steenbrink et al., 1999). The second is the middle Pleistocene Megalopolis basin from southern Greece, that has eccentricity dominated cyclic lignite seams in otherwise detrital sediment (van Vugt et al., 2000).

## Geological setting, lithology and sampling

### *Ptolemais*

The elongated intermontane Ptolemais basin in northern Greece is part of a Late Miocene NNW-SSE trending graben system that extends over a distance of 250 km, with a width of 10–20 km. The depression is filled with a 500–600 m thick succession of Upper Miocene to Lower Pliocene predominantly lacustrine sediments with intercalated lignite seams and fluvial deposits. A Pleistocene tectonic episode divided this graben into a series of sub-basins along the main basin axis, among which is the presently studied Ptolemais basin. The most important part of the stratigraphy is the Lower Pliocene Ptolemais Formation; it contains approximately 110 m of rhythmically alternating metre-scale lignite and marl beds. Four open cast lignite mines provide easy access to the sediments from this Formation. Three main lithologies were distinguished in the succession: lignite, grey marl and beige marl.

The lignite contains ~90% organic material, mostly fine grained, with some larger fragments of fossil plant tissue, but wood remains are rare. Rarely, thin (cm-scale) marl

beds are incorporated in a lignite layer. The lignite was formed in a reed swamp environment (Steenbrink et al., 1999). Organic petrology has indicated that the swamp or mire was mainly fed by meteoric or telluric water, i.e. not influenced by groundwater. (Mulder et al., submitted).

The grey marl represents a mixture of unlithified freshwater carbonate (called 'marl' (Steenbrink et al., 1999)) and organic plant debris. The amount of organic matter in the marl varies between 5 and 30%. Roots of water plants and shallow-water lacustrine gastropods and ostracods are abundant. A marl bed may contain many thin (mm- to cm-scale) lignite beds. The marl was deposited in a flat marginal shallow lacustrine environment with abundant plant growth (Steenbrink et al., 1999). Based on field observations, the lithology of each sample in these marl beds was defined as marl, lignitic marl (high organic content), lignitic clay or clayey marl. Clay or clayey is a field description and indicates that the texture of the sediment is smooth and soft like clay, but in the laboratory it turned out that 95% of the sample (by weight) was still composed of carbonate and/or organic material.

The beige marl beds occur locally or replace, in certain parts of the stratigraphy, the cyclic grey marl beds. These beige marls contain mainly calcite and only a few percent of organic material. Roots are absent and the biota is dominated by lacustrine bottom-dwelling gastropods and stem encrustations of the chlorophyte *Chara*. This beige marl was deposited in an oxygenated marl bench platform or slope (Steenbrink et al., 1999). Besides these main lithologies, there are several irregular layers and lenses of fine- to medium-grained green sand in the northernmost mine (Vorio). Apart from these, the amount of detrital material in the section is very low. The organic material mainly comes from plants that grew in the basin and the carbonate precipitated from the lake water.

The pattern of the 2-metre thick sedimentary cycles is correlated to northern hemisphere summer insolation, indicating that the cycles were mainly forced by climatic precession (period ~21 kyr), with the lignite beds corresponding to insolation minima (dry periods with cool summers) and the marl beds to insolation maxima (humid periods with warm summers) (van Vugt et al., 1998).

Three sections were previously studied (van Vugt et al., 1998) in the Ptolemais basin. For the present study, 18 standard palaeomagnetic samples from the Tomea Eksi section were used. For comparison, some of the experiments were also done on samples from the Vorio section (9) and the Komanos section (11). The sample sets used for this study were selected to represent the different lithologies present in the Ptolemais Formation.

### *Megalopolis*

The intramontane lacustrine Megalopolis Basin is located in the middle of the Peloponnesos peninsula in southern Greece, at the boundary between Mesozoic limestones of the Pindos zone and Eocene flysch of the Tripolitza Group (Vinken, 1965). The eastern margin of the basin is characterised by NE-SW trending normal faults, that have been active since the Late Miocene. The basin is filled with Upper Pliocene

to Pleistocene lacustrine and fluvial deposits. Of main interest to this study is the middle Pleistocene Marathousa Member in the Choremi Formation (Vinken, 1965), that contains lacustrine clay, silt and some sand with intercalated lignite seams. The fluvial Marathousa sediments near the basin margins were not incorporated in this study. Three open pit lignite mines facilitate large, unweathered exposures of the lacustrine part of the Marathousa Member.

The lignite occurs in 10–20 m thick seams that alternate with detrital intervals that contain clay and silt and some sand lenses. The lignite seams are interpreted as large-scale sedimentary cycles. In addition, smaller-scale sedimentary cycles occur, mainly as thin ( $\leq 2$  m) lignite or organic-rich clay layers in the large-scale detrital intervals, but also in one of the large-scale lignite seams as regular, laterally continuous (organic-rich) clay beds. The clay and silt beds can be homogeneous, or contain macroscopic plant remains. Frequently, levels with carbonate nodules occur, indicating palaeosol formation.

The palaeo-environmental interpretation for the lignite indicates a swampy recess with dynamic anastomosing channels, causing a mosaic of treeless fens and (possibly dry) forests (Mulder et al., submitted). This swamp was mainly fed by groundwater, the level of which must have been close to the surface. There is no detailed interpretation for the detrital intervals, but pollen of *gramineae* and *cyperaceae* indicate that the environment was probably still wet, but since organic material was not preserved in large quantities, this water must have been oxygenated.

The large-scale cycles have been argued to be eccentricity-forced, with the lignite representing the warm and humid 100-kyr eccentricity maxima and the detrital intervals representing cold and arid eccentricity minima. The small-scale lignite or organic-rich clay layers that occur in some intervals are correlated to insolation maxima, also representing warm and humid phases (van Vugt et al., 2000). This is opposite to the Ptolemais basin, where lignite formed during dry and cool periods.

The 28 samples used for this study were taken from three subsections of the Choremiou section, located in the southernmost field in Megalopolis. Twelve samples were taken from a lignite seam without a clear expression of small-scale cycles, six samples span nearly two small-scale cycles in a large-scale detrital interval, and a subsection of eleven samples covers 1\_ small-scale cycles within a large-scale lignite seam. Each of these subsections contains at least one sample with an anomalously high NRM intensity, flanked by samples with regular intensities.

## Laboratory methods

The used samples were standard palaeomagnetic cores (2.5 cm diameter; 2.2 cm length); low-field bulk susceptibility ( $\kappa$ ) and natural remanent magnetisation (NRM) were measured as part of the standard treatment for all samples of the Ptolemais and Megalopolis sections. The NRM was measured on a 2G Enterprises DC SQUID magnetometer (noise level  $1 \cdot 10^{-12}$  Am<sup>2</sup>),  $\kappa$  on an AGICO KLY-2 susceptibility bridge

(noise level  $4 \cdot 10^{-8}$  SI). The samples were progressively demagnetised in a magnetically shielded furnace or by the static three-axis alternating field (AF) method. To prevent concealing of the NRM by a gyroremanent magnetisation (GRM) (Stephenson, 1993) induced in many of the Megalopolis samples at alternating fields higher than 50 mT, we followed the method of (Dankers and Zijdeveld, 1981), in which the samples are brought into a cyclic state by initially demagnetising along two orthogonal axes, without measuring residual remanence, followed by demagnetisation along the third orthogonal axis and the first two axes, with single-axis measurement of the residual remanence after each treatment.

The samples from Tomea Eksi (Ptolemais) and from Megalopolis were progressively magnetised along the cylindrical axis in an alternating field up to 200 mT with a steady parallel DC bias field of 0.03 mT. This anhysteretic remanent magnetisation (ARM) was subsequently AF demagnetised in a single step (Tomea Eksi), or in 11 steps (Megalopolis) up to 200 mT. The same sample set was then progressively magnetised in a pulse field up to 2000 mT (PM<sub>4</sub> pulse magnetiser) to acquire an isothermal remanent magnetisation (IRM). After each step, the remanence of the samples was measured on an AGICO JR5 spinner magnetometer. After saturation, the Tomea Eksi samples were stepwise thermally demagnetised until maximum unblocking was reached, except for the lignite samples, which combust when heated above  $\sim 200^\circ\text{C}$ . The Megalopolis samples were also thermally demagnetised in five steps up to  $280^\circ\text{C}$ . After each demagnetisation step, the sample was saturated again in a pulse field (2000 mT) and measured, to check for a chemical reaction of the magnetic minerals. Susceptibility was measured again after heating to  $280^\circ\text{C}$ . The samples from the Vorio and Komamos sections in Ptolemais were only given a progressive IRM that was subsequently thermally demagnetised.

Finally, the magnetisation of some samples from both basins was measured in a modified horizontal translation type Curie balance (Mullender et al., 1993) during several heating and cooling runs. The results of these experiments were fully dominated by paramagnetic behaviour. Three samples from Megalopolis were qualitatively concentrated by putting a quantity comparable to approximately two specimens in 96% ethanol and ultrasonically and mechanically breaking them into small pieces. After decanting, on average ten times, the remaining material was panned on a watch glass with a hand magnet attached below it. The residue on the watch glass was dried in air for a few hours at  $35^\circ\text{C}$ , leaving approximately 0.25–0.40 g of concentrated material. Curie balance experiments were run on each of the concentrates (average sample weight: 55 mg), with five incremental heating and cooling runs between room temperature and  $350^\circ\text{C}$ , and a final run up to  $600^\circ\text{C}$  (heating/cooling rate:  $10^\circ\text{C}/\text{minute}$ ).

## Results

### Ptolemais

The results from Ptolemais are displayed per section (Figure 1, upper panel) and per lithology (Figure 1, lower panel). As can be seen from these figures, the different sections and most lithologies cannot be distinguished based on the measured values, except maybe for the lignite samples, which have distinctly lower NRM values and rather low  $k$  and IRM values.

**$\kappa$ :** The initial susceptibility for all the Ptolemais samples is on average  $(34 \pm 59) \cdot 10^{-6}$  SI units, but the samples from Vorio and Komanos have a much smaller range ( $-15 - 53$ ) than the Tomea Eksi samples ( $-8 - 239$ ). The average  $\kappa$  for Tomea Eksi is  $(56 \pm 78) \cdot 10^{-6}$ .

**NRM:** The mean NRM of the Ptolemais samples measured in this study is  $1.45 \pm 2.31$   $\text{mAm}^{-1}$ , this is comparable to the mean NRM of all the samples that were used to construct the magnetostratigraphy of the three sections in Ptolemais (van Vugt et al., 1998), which is  $\sim 1.30$   $\text{mAm}^{-1}$ . The only lithology with a distinctly low NRM intensity is lignite, there is no notable difference between the sections.

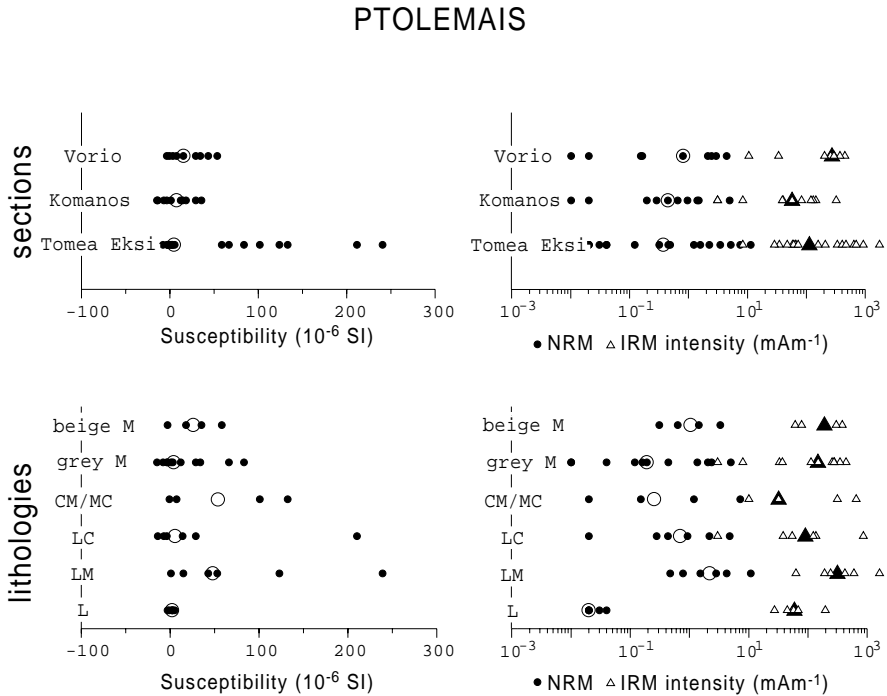


Figure 1: Susceptibility, NRM and IRM intensity of Ptolemais sorted by section (upper panel) and by lithology (lower panel). Susceptibility in  $10^{-6}$  SI units, NRM (solid dots, mean: open circle) and IRM (open triangles, mean: solid triangle) in  $\text{mAm}^{-1}$ . Lithologies: M = marl, CM/MC = clayey marl of marly clay, LC = lignitic clay, LM = lignitic marl; L = lignite.

Ptolemais		N	$\kappa(20^\circ)$	$\kappa(\text{max}/20^\circ\text{C})^*$	NRM (mA/m)	ARM (mA/m)	IRM (mA/m)	NRM/ARM	ARM/IRM (E-3)	NRM/IRM (E-3)
Tomea Eksi	mean	18	56	330%	1,81	15,23	312	0,08	43,00	4,04
	std. dev.		78	160%	3,01	21,10	411	0,05	23,60	3,69
	range		-8 - 239	100 - 640%	0.00 - 10.88	0.28 - 79	8 - 1609	0.002 - 0.17	13 - 80	0.0 - 11.3

Table 1: Results from the Tomea Eksi section from Ptolemais. N = number of samples;  $\kappa(20^\circ\text{C})$  = low-field susceptibility at room-temperature,  $\kappa(\text{max}/20^\circ\text{C})$  = maximum  $\kappa$  over initial  $\kappa$  during heating; NRM/ARM/IRM = natural/anhyseretic/isothermal remanent magnetisation.

**ARM:** The ARM was only measured on Tomea Eksi samples ( Table 1) and is on average 13 times higher than the NRM intensity. The normalised ARM acquisition curves show two types of behaviour: most samples are saturated at 80 mT, only six samples are still not saturated at 150 mT. This behaviour seems to be mainly unrelated to lithology, although many of the lignite samples have such a high coercivity.

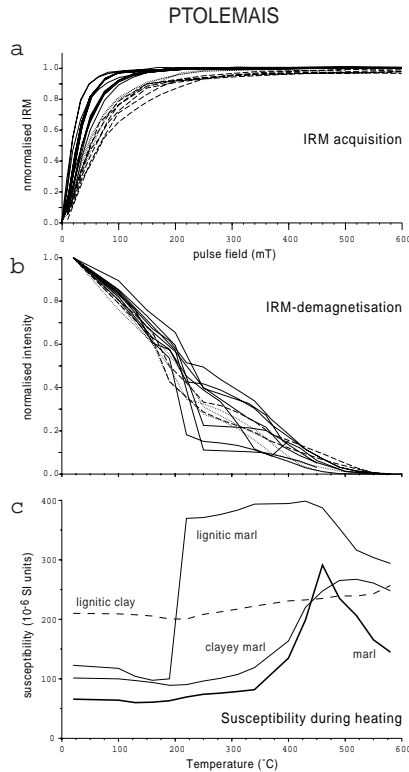


Figure 2: Normalised IRM intensity during acquisition (a) and thermal demagnetisation (b) of Ptolemais samples; solid lines: low coercivity; dashed lines: relatively high coercivity; dotted lines: intermediate coercivity; light-coloured lines suffered from combustion of organic material (see text); c) susceptibility during heating of samples from different lithologies.

**IRM:** The IRM intensity for all Ptolemais samples is on average  $225 \pm 306$  mA/m, and is approximately 140 times higher than the NRM intensity. The lignite samples have a distinctly lower than average IRM intensity, which is however very high (2500 times) compared to the NRM intensity for these samples. The normalised IRM acquisition curves show three types of behaviour (Figure 2a): saturation below 180 mT, saturation between 800 and 1500 mT (90% saturation at  $\sim 200$  mT) and an intermediate group. All the lignites belong to the (relatively) high-coercivity group, as do the two other samples that did not reach ARM saturation at 150 mT.

**Thermal demagnetisation:** Only minor differences are observed when the SIRM's are thermally demagnetised (Figure 2b). The maximum unblocking temperature of all samples lies between 500 and 560°C. Samples with a high organic content show a strong intensity decrease between 200 and 250°C, followed by a plateau, which is related to the combustion of the organic material in the furnace (lignite samples were not heated for this reason). This exothermal process heats the samples well above the set furnace temperature. The following 3 to 4 heating steps will not cause much change, because the samples have been exposed to those temperatures already. The intensity of the low-coercivity group decreases most regularly, while the high-coercivity samples decrease relatively more at lower temperatures ( $\leq 250^\circ\text{C}$ ). Susceptibility monitoring after each thermal demagnetisation step of the Tomea Eksi samples shows different behaviour for each lithology (Figure 2c). The single lignitic clay sample has a more or less constant  $\kappa$ ; both the grey and beige marl and clayey marl samples show a peak in susceptibility at 450°C (marl) or 500°C (clayey marl) and the lignitic marl samples strongly increase at 200°C (combustion), but the decrease above 450°C shows that the effect related to the peak observed in the other lithologies is probably present here as well.

### *Megalopolis*

The NRM in Megalopolis often has a small viscous component that is completely removed at 15 mT AF; the remaining characteristic component is fully demagnetised at 150 mT AF. The intensity of this ChRM varies between nearly zero and  $\sim 100$  mA/m, with an average of  $\sim 2.5$  mA/m; clay and silt have generally higher intensities than organic-rich lithologies. The broad range in NRM intensities might indicate different sources or generations of magnetic minerals. In our experiments we distinguished two end-member types of behaviour that are likely related to two magnetic phases; a high-intensity type and a low-intensity type.

**High-intensity type:** Five samples belonged to the high-intensity type (see Table 2 and Figure 3 left panel), that was only found in samples without visible organic material, their lithology often being clay. These samples have an NRM intensity decrease – between AF fields of 15 and 150 mT, the interval in which the characteristic component is removed – of more than 1 mA/m. Their susceptibility is higher than  $150 \cdot 10^{-6}$  SI units, and their maximum unblocking temperature is between 350 and 380°C (Figure 3a). The ARM intensity is relatively low, on average twice as high as the NRM intensity; the SIRM intensity is on average 8600 mA/m, i.e.  $\sim 650$  times as high as the NRM intensity.

Megalopolis		N	k(20°)	k(280°/20°)	NRM (mA/m)	ARM (mA/m)	IRM (mA/m)	NRM/ARM	ARM/IRM (E-3)	NRM/IRM (E-3)	lithology
high- intensity	mean	5	304	81%	11,30	20,83	8,600	0,52	4,10	1,55	clay (4)
	std. dev.		146	20%	8,99	13,56	7,829	0,29	3,73	65,60	
	range		174 - 541	48 - 102%	2,4 - 24	10 - 43	1 - 21E3	0,23 - 0,92	2 - 11	1,2 - 81,3	
mixed	mean	8	135	118%	0,39	2,27	261	0,15	13,20	1,70	clay or silt with org. material (6)
	std. dev.		71	28%	0,33	1,39	269	0,10	6,25	0,89	
	range		45 - 232	95 - 170%	0,014 - 0,906	0,22 - 4,12	13 - 821	0,06 - 0,33	5 - 20	0,6 - 3,0	
low- intensity	mean	15	83	483%	0,08	0,79	96	0,09	24,20	2,03	lignite or organic-rich clay (14)
	std. dev.		53	648%	0,08	0,46	238	0,05	10,70	1,11	
	range		36 - 223	98 - 2264%	0,01 - 0,32	0,26 - 1,97	13 - 947	0,03 - 0,19	2 - 37	0,1 - 4,3	

Table 2: Megalopolis results per intensity-group. See also caption to Table 1. The last column lists the lithology of most samples in each group, the percentage indicates how many samples from this group belong to the mentioned lithologies.

The NRM and ARM intensity decay curves have a convex shape at low fields and change to concave above  $\sim 50$  mT (Figure 3b, NRM not shown). This results in a median destructive field (MDF) of more than 40 mT. The IRM acquisition curve (Figure 3c) shows that the largest part ( $\sim 60\%$ ) of the SIRM is acquired between 60 and 150 mT pulse field; only  $\sim 35\%$  of the SIRM is acquired up to 60 mT. Upon heating (up to  $280^\circ\text{C}$  in a magnetically shielded furnace), the SIRM intensity – induced at room temperature after each thermal demagnetisation step – decreases (Figure 3d), indicating a chemical reaction of magnetic grains to less-magnetic material. This is supported by the fact that  $\kappa$  decreases or is stable between room temperature and  $280^\circ\text{C}$  (Table 2).

Low-intensity type: Fifteen samples belonged to the other, low-intensity end member (see Table 2 and Figure 3 right panel). All these samples contain visible organic material, their lithology is generally lignite or organic-rich clay. The NRM intensity decrease – between AF fields of 15 and 50 mT – is less than  $0,15 \text{ mA}\cdot\text{m}^{-1}$ . The maximum unblocking temperature is distinctly higher than  $380^\circ\text{C}$  and in some samples it can be determined to be near  $500^\circ\text{C}$  (Figure 3e). Determination of the true maximum unblocking temperature is often inhibited because both the intensity and direction of the NRM may change drastically above  $380^\circ\text{C}$ . The magnetic susceptibility is generally below  $150 \cdot 10^{-6}$  SI units. The ARM intensity is relatively high: on average ten times as high as the NRM intensity; the SIRM is on average  $96 \text{ mA}\cdot\text{m}^{-1}$ , i.e. 500 times as high as the NRM intensity (Table 2).

The NRM and ARM decay curves are concave and the MDF is less than 35 mT (Figure 3f). The largest part of the SIRM ( $\sim 65\%$ ) is acquired at low pulse fields, up to 60 mT;  $\sim 25\%$  between 60 and 150 mT and  $\sim 10\%$  at higher pulse fields (Figure 3g). Upon heating (up to  $280^\circ\text{C}$ ), the SIRM (induced at room temperature after each heating step) and magnetic susceptibility increase, generally by much more than 200%, indicating a chemical reaction that produces more magnetic material (Figure 3h and Table 2).



MEGALOPOLIS

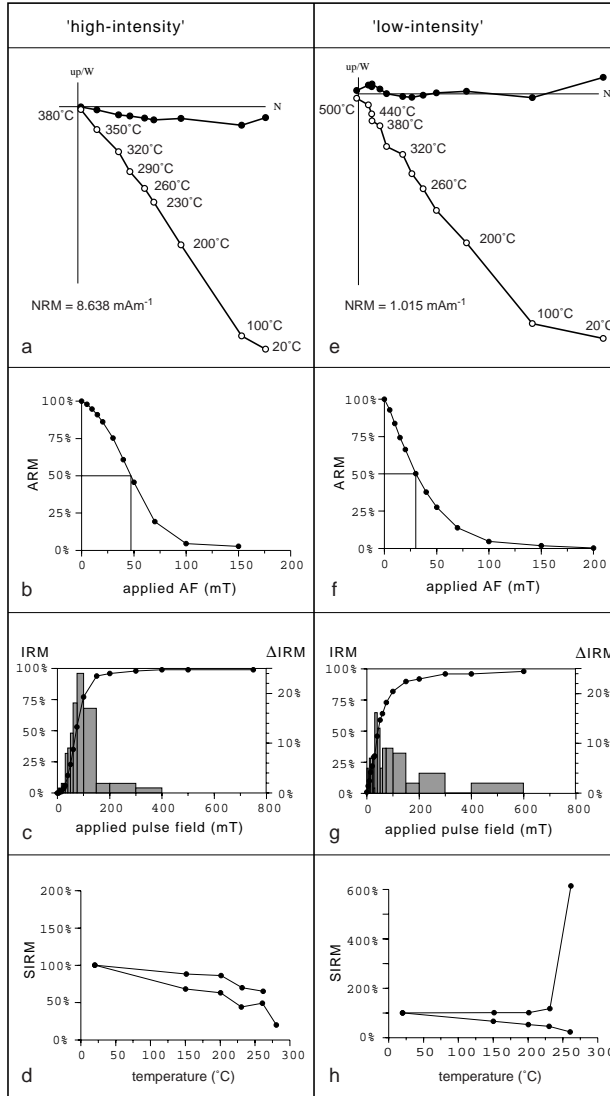


Figure 3: Magnetic behaviour of examples of the two end member types of Megalopolis. Left panel: high-intensity type; right panel: low-intensity type. a&e: demagnetisation diagrams; closed (open) circles denote the projection on the horizontal (vertical) plane; demagnetisation temperature or alternating field intensity for each step is indicated; the intensity of the remanent magnetisation is shown at 230°C or 15 mT. b&f: normalised ARM intensity during AF demagnetisation. c&g: line with dots represents normalised IRM intensity during remanence acquisition in a pulse field (left vertical axis) and histogram shows relative increment in IRM for each field step (right axis). d&h: upper curve: normalised SIRM induced at room temperature after heating, lower curve: normalised IRM decay during thermal demagnetisation.

Eight samples showed mixed behaviour, with characteristics generally intermediate between those of the end members (Table 2). These are usually samples containing visible organic material.

The Curie balance results (Figure 4) show that the concentrated sample from the high-intensity type has a total magnetisation of  $\sim 0.21 \text{ Am}^2\text{kg}^{-1}$  that decreases irreversibly between 200 and  $350^\circ\text{C}$ , indicating a chemical reaction. Between  $420$  and  $600^\circ\text{C}$  there is a magnetisation peak, upon cooling to room temperature, the magnetisation slightly increases again to approximately half its initial value. The low-intensity type samples have a much lower initial total magnetisation ( $0.022\text{--}0.043 \text{ Am}^2\text{kg}^{-1}$ ), that gently decreases upon heating. This decrease is recovered in the successive heating runs until  $300^\circ\text{C}$ . A slight, irrecoverable decrease is seen between  $300$  and  $350^\circ\text{C}$ . One sample had a peak in magnetisation between  $430$  and  $600^\circ\text{C}$ , and the final total magnetisation was slightly higher than the initial value. The total magnetisation of the other sample ended slightly lower than its initial value (not shown).

## Discussion & conclusions

### *Magnetic mineralogy of Ptolemais*

The ARM saturation at low alternating field and IRM saturation at low pulse field combined with the maximum unblocking temperature slightly below  $580^\circ\text{C}$  indicate (fine grained) magnetite as the most important carrier of the remanence for all the studied lithologies except maybe lignite. The lignite consistently has a higher coercivity, but it does reach IRM saturation at  $1500 \text{ mT}$ , suggesting partly-altered ferri-magnetic iron sulphides, and/or maybe partly-oxidised magnetite. Thermal experiments to

## MEGALOPOLIS

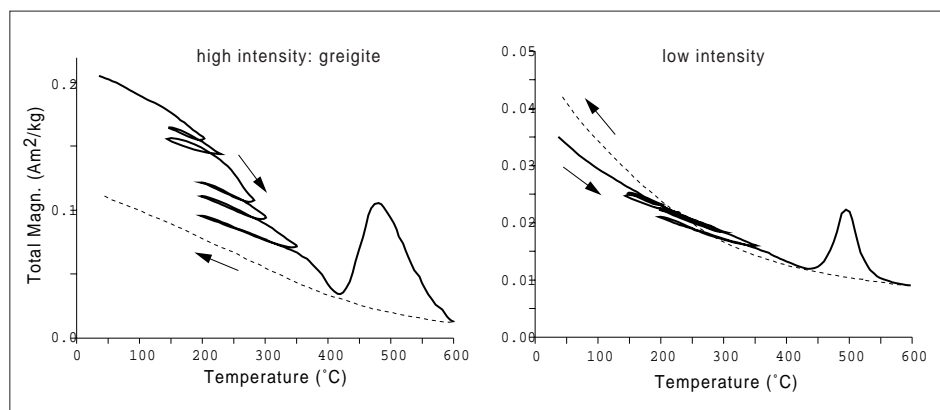


Figure 4: Curie balance results (in air) of magnetically concentrated samples from Megalopolis.

check this mineralogy were not performed on lignite, because of the combustion of the samples at temperatures of 200°C and higher (in air).

The marl samples have a peak in susceptibility at high temperatures (~450°C) caused by the oxidation of iron sulphides. These must be non-magnetic iron sulphides, because they were not detected by any of the remanent magnetic experiments; it is probably pyrite, which is very common in organic-rich environments. The lignitic marl samples do not show the same peak, caused by the combustion of the organic material. However, the decrease in susceptibility above ~450°C suggests that iron sulphides are oxidised in these samples as well. Maximum susceptibility is reached at lower temperatures for the marls and lignitic marls than for the clayey marls, possibly caused by the lower porosity of clay, which hinders the transport of air inside the sample.

The only lithology that can be distinguished based on univariate analysis of the measured magnetic parameters is lignite, with its low NRM, ARM, and IRM values, especially low NRM/ARM and NRM/IRM ratio's and high coercivity. The range of other lithologies are magnetically similar, so no curve with subtle variations that might be indicative of climate changes can be made in Ptolemais.

### *Magnetic mineralogy of Megalopolis*

The maximum unblocking temperature between 350 and 380°C in the high-intensity samples points to an iron sulphide as the main magnetic mineral. The combined high NRM, ARM and IRM intensities and  $\kappa$  values indicate a relatively high concentration of magnetic material with respect to the other end-member type, suggesting an enrichment of magnetic minerals in these samples. The chemical reaction during heating towards less-magnetic material points to greigite as the dominant remanence-bearing mineral (Torii et al., 1996). The convex intensity decay curve and the high gyromagnetic remanent magnetisation point to a single domain grain size (Snowball, 1997a; Snowball, 1997b). Greigite commonly occurs as an authigenic phase in fresh water lakes with a high influx of organic matter (Snowball, 1991; Jeloukowski et al., 1997; Snowball and Torii, 1999). Authigenic means formed during or (shortly) after deposition, for greigite most often as a consequence of bacterial sulphate reduction, although greigite-producing bacteria may occur as well. When greigite is chemically formed, it generally shows stable single-domain type behaviour (Snowball and Torii, 1999), as is the case for our samples. The bacteria that mediate the formation of greigite can live at considerable depth below the sediment-water contact – up to several hundreds of metres in full marine environments, but complete sulphate removal can also occur at depths of less than one metre in near-shore marine environments (Goldhaber and Kaplan, 1982). The moment of remanence acquisition in greigite can therefore not be determined. The magnetic polarity pattern in the Megalopolis section showed a zone of alternating normal and reversed directions around the Matuyama-Brunhes boundary, indicating delayed remanence acquisition (van Vugt et al., 2000). Exclusion of the greigite-bearing samples resulted in a polarity transition interval with less normal-polarity data points, suggesting that they were indeed formed post-depositionally.

## MEGALOPOLIS

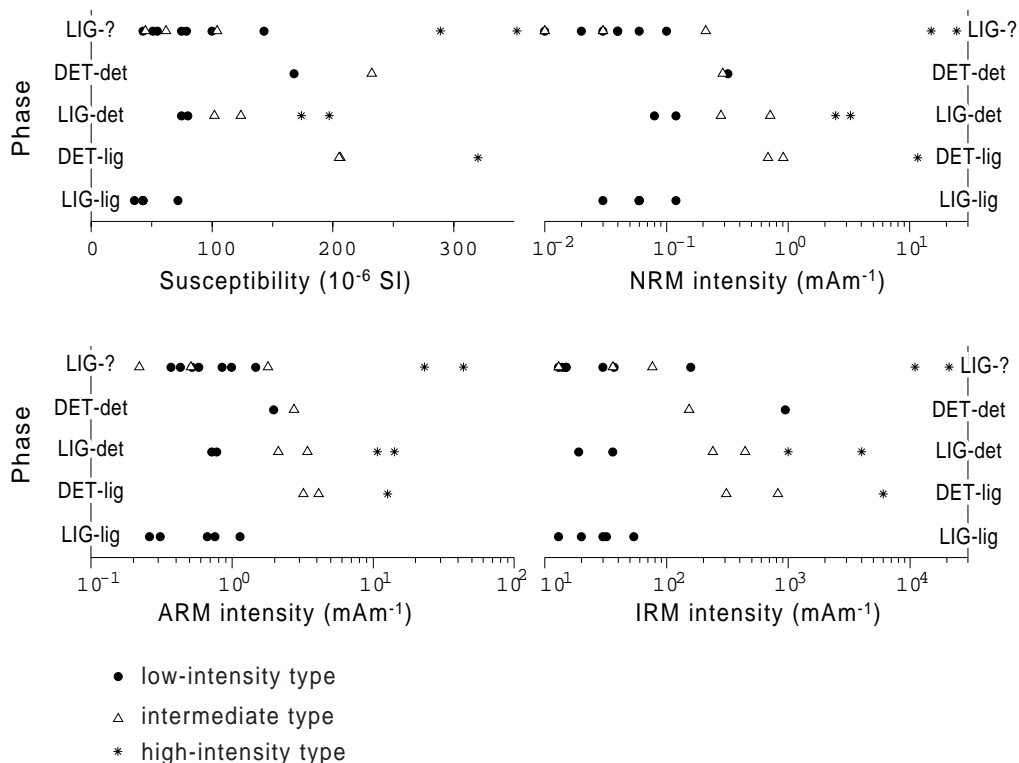


Figure 5: Results from Megalopolis displayed per cyclic phase (see text). DET/LIG (det/lig) indicates the detrital/lignite phase of the LARGE-SCALE (small-scale) cycles. LIG-? indicates samples from a large-scale lignite without subdivision into small-scale cycles. Different symbols indicate the end-member types of magnetic behaviour (see text).

The mineralogy of the other end-member type is uncertain. The IRM is saturated at  $\sim 600$  mT, which is too low for hematite and too high for pure magnetite. The maximum unblocking temperature well above  $380^\circ\text{C}$  still points to an iron oxide, so partially oxidised magnetite is likely to carry the remanence in these type of samples. The peak in one of the Curie balance curves indicates that non-magnetic iron sulphides (pyrite) may be present in these samples. In the intermediate samples, probably some greigite formed, but not enough to dominate the magnetic signature.

The results from Megalopolis are also displayed per cyclic phase (Figure 5), i.e. divided into groups corresponding to the two phases (lignite vs. detrital) of the large-scale cycles and similar for the small-scale cycles. It should be noted that, although a lignite lithology always corresponds to a lignite-phase, the other lithologies can correspond

to different phases, depending on the under- and overlying lithologies. For example, an (organic-rich) clay may represent either a small-scale detrital phase in a large-scale lignite, or a small-scale lignite phase in a large-scale detrital unit. Despite this confusing definition, the pattern of the lithological phases is clear in the field, because a clay – silt cycle in the eastern end of the basin changes gradually via an organic-rich clay – silty-clay cycle to a lignite – clay cycle in the western end. From Figure 5 it can be seen that low values for any of the parameters mainly occur in the large-scale lignite phase, but this phase has not only low values. The only distinct group is the small-scale lignite phase in the large-scale lignite phase (LIG-lig), with consistently low values for all parameters. The other phases cannot be distinguished in a univariate analysis of the measured magnetic parameters.

### *Comparison*

Since the greigite in Megalopolis is related to early diagenesis, we will compare only the low-intensity samples from Megalopolis with the samples from Ptolemais (Tomea Eksi). These samples all probably have magnetite as the main remanence carrier. The intensity of NRM, ARM and IRM is lower in Megalopolis than in Ptolemais (even when the intermediate ‘mixed-behaviour’ type is included in the comparison), and their ratios are comparable, suggesting a lower magnetite concentration in Megalopolis.

The origin of the magnetite in both basins is probably different: since the detrital input in the Ptolemais basin is negligible, the magnetite could only have been blown in as dust or formed in situ. The Megalopolis basin has a high detrital input, it is therefore reasonable to assume the magnetite is of detrital origin. The lower concentration in Megalopolis than in Ptolemais seems thus strange; it might be caused by the type of basement around the Megalopolis basin, which is limestone, metamorphic quartz-rich facies and flysch.

The low-field magnetic susceptibility is somewhat higher in Megalopolis, in accordance with the higher content of detrital components (e.g. clay) and the lower carbonate content.

## **References**

- Dankers, P.H.M. and Zijdeveld, J.D.A., 1981. Alternating field demagnetization of rocks, and the problem of gyromagnetic remanence. *Earth and Planetary Science Letters* 53, 89-92.
- Goldhaber, M.B. and Kaplan, I.R., 1982. Controls and consequences of sulphate reduction rates in recent marine sediments. In: J.A. Kittrich, D.S. Fanning and C.R. Hossner (Eds.), *Acid sulphate weathering*, SSSA, Madison, pp. 234.
- Jelonowski, A., Tucholka, P. and Wiekowski, K., 1997. Magnetic properties of sediments in a Polish lake: evidence of a relation between the rock-magnetic record and environmental changes in Late Pleistocene and Holocene sediments. *Geophysical Journal International* 129, 727-736.

- Maher, B.A. and Thompson, R., 1999. Quaternary climates, environments and magnetism. Cambridge University Press, Cambridge.
- Mulder, C., Sakorafá, V., Burrigato, F. and Visscher, H., submitted. Ecohydrological perspective of phytogenic organic and inorganic components in Greek lignites: a quantitative reinterpretation. *Earth and Planetary Science Letters*.
- Mullender, T.A.T., Velzen, A.J.v. and Dekkers, M.J., 1993. Continuous drift correction and separate identification of ferrimagnetic and paramagnetic contribution in thermomagnetic runs. *Geophys. J. Int.* 114, 663-672.
- Snowball, I.F., 1991. Magnetic hysteresis properties of greigite (Fe<sub>3</sub>S<sub>4</sub>) and a new occurrence in Holocene sediments from Swedish Lapland. *Physics of the Earth and Planetary Interiors* 68, 32-40.
- Snowball, I.F., 1997a. The detection of single-domain greigite using rotational remanent magnetization (RRM) and the effective gyro field (Bg): mineral magnetic and palaeomagnetic applications. *Geophysical Journal International* 130, 704-716.
- Snowball, I.F., 1997b. Gyroremanent magnetization and the magnetic properties of greigite-bearing clays in southern Sweden. *Geophys. J. Int.* 129, 624-636.
- Snowball, I.F. and Torii, M., 1999. Incidence and significance of magnetic iron sulphides in Quaternary sediments and soils. In: B.A. Maher and R. Thompson (Eds.), *Quaternary Climates and Magnetism*. Cambridge University Press, Cambridge.
- Steenbrink, J., Vugt, N.v., Hilgen, F.J., Wijbrans, J.R. and Meulenkamp, J.E., 1999. Cyclostratigraphy and <sup>40</sup>Ar/<sup>39</sup>Ar dating of lower Pliocene lacustrine sequences of the Ptolemais Basin, NW Greece. *Palaeogeography, Palaeoclimatology, Palaeoecology* 152, 283-303.
- Stephenson, A., 1993. Three-axis static alternating field demagnetization of rocks and the identification of natural remanent magnetization, gyroremanent magnetization and anisotropy. *Journal of Geophysical Research* 98, 373-381.
- Torii, M., Fukuma, K., Horng, C.-S. and Lee, T.-Q., 1996. Magnetic discrimination of pyrrhotite- and greigite-bearing sediment samples. *Geophysical Research Letters* 23, 1813-1816.
- van Vugt, N., de Bruijn, H., van Kolfshoten, M., Langereis, C.G. and Okuda, M., 2000. Magneto- and cyclostratigraphy and mammal-fauna's of the Pleistocene lacustrine Megalopolis Basin, Peloponnesos, Greece. *Geologica Ultrajectina* 189, Chapter 3.
- van Vugt, N., Steenbrink, J., Langereis, C.G., Hilgen, F.J. and Meulenkamp, J.E., 1998. Magnetostratigraphy-based astronomical tuning of the early Pliocene lacustrine sediments of Ptolemais (NW Greece) and bed-to-bed correlation with the marine record. *Earth and Planetary Science Letters* 164, 535-551.
- Vinken, R., 1965. Stratigraphie und Tektonik des Beckens von Megalopolis (Peloponnes, Griechenland). *Geologisches Jahrbuch* 83, 97-148.
- von Dobeneck, T. and Schmieder, F., 1998. Using rock magnetic proxy records for orbital tuning and extended time series analyses into the super- and sub-Milankovitch bands. In: G. Fisher and G. Wefer (Eds.), *Use of proxies in paleoceanography: examples from the south Atlantic*. Springer-Verlag, Berlin Heidelberg.



## Epilogue

The time frames constructed in this thesis will place the results of the other components of our multi-disciplinary research project on a firm foundation. Palynological studies from several parts of the Ptolemais section have already enhanced our understanding of interactions between climate and environment, and these will be published later this year in another thesis. Another quantitative palynological study of the Megalopolis succession, in combination with sedimentological research, will start this year and focuses on short-term climate-induced environmental variations. The stratigraphy and basinal evolution of the entire Ptolemais basin, including the late Miocene successions, will be correlated in detail to the marine record, to compare the syn- or diachrony of major lithological changes, in particular in terms of climatic and environmental change. The accurate ages presented in this thesis, have allowed to date fauna localities for the first time. Examples are the hominid from Megalopolis and an ape from Ptolemais.

An additional goal of this component was to understand the acquisition mechanisms of palaeomagnetic signals (environmental magnetism) and appreciate the reliability of this signal as a recorder of geomagnetic variations, especially in cyclic sedimentary records. An environmental-magnetic study of the magnetomineralogy in these basins will benefit from the abundance of environmental constraints based on the other programme components.

In each succession described in this thesis, we have searched for cyclic or rhythmic patterns in the stratigraphy, and tried to match them with climatic cycles, in particular to those cycles already known – and proven to be orbitally forced – from marine Mediterranean successions. We especially selected our sections for their potential (at first sight) to express such cycles, and we are aware of the fact that our techniques may not readily apply to all possible sedimentary environments. However, it is good to realise that we applied our methods in environments that many previously thought were unsuitable for this kind of analysis. Since the aim of the entire multi-disciplinary research programme has been to study a wide range of environments along a gradient from full continental to deep marine, other environments suitable for cyclostratigraphic studies and astronomical tuning will no doubt be discovered, and this will likely continually enhance our understanding of the mechanisms that relate the expression of sedimentary systems to orbital and thus climatic forcing. An additional goal of this component was to understand the acquisition mechanisms of palaeomagnetic signals (environmental magnetism) and appreciate the reliability of this signal as a recorder of geomagnetic variations, especially in cyclic sedimentary records.



# ΤΡΟΧΙΑΚΕΣ ΕΠΙΔΡΑΣΕΙΣ ΤΟΥ Α. ΝΕΟΓΕΝΟΥΣ ΣΕ ΛΙΜΝΑΙΕΣ ΔΕΚΑΝΕΣ ΤΗΣ ΜΕΣΣΟΓΕΙΟΥ

## ΜΑΓΝΗΤΟΣΤΡΩΜΑΤΟΓΡΑΦΙΚΗ ΚΑΙ ΚΥΚΛΟΣΤΡΩΜΑΤΟΓΡΑΦΙΚΗ ΜΕΛΕΤΗ

Οι περιστροφές της Γης γύρο από τον άξονα της και γύρο από τον Ήλιο δεν είναι σταθερές. Περιοδικές μεταβολές προκαλούν στην Γη κλιματικές αλλαγές, όπως οι εποχές των παγετώνων. Οι κλιματικές αυτές αλλαγές αναγνωρίζονται γεωλογικά κυρίως σε ιζήματα που έχουν αποθεθεί στον βυθό της θάλασσας, σε λίμνες ή σε βάλτους. Οι γεωλόγοι με την μελέτη των ιζημάτων αυτών παίρνουν πληροφορίες για το κλίμα πριν από εκατομμύρια χρόνια. Οι πληροφορίες αυτές χρησιμοποιούνται από τους επιστήμονες για καλλίτερη πρόγνωση των κλιματολογικών αλλαγών του μέλλοντος. Επιπλέον, η καθορισμένη περιοδικότητα αυτών των κλιματολογικών αλλαγών προσφέρει την δυνατότητα του ακριβούς καθορισμού της ηλικίας της ιζηματογενούς ακολουθίας.

Οι πιο σημαντικές μεταβολές στην τροχιά της γης γύρο από τον ήλιο είναι η εκκεντρότητα και η μετάπτωση των ισημεριών. Η εκκεντρότητα δείχνει το πόσο επιμήκης είναι η τροχιά, π.χ. εάν είναι κυκλική ή ελλειψοειδής. Η εκκεντρότητα μεταβάλλεται περιοδικά και υπάρχει ένας κύκλος που διαρκεί 100.000 έτη και άλλος ένας που διαρκεί 400.000 έτη. Η μετάπτωση των ισημεριών διαγράφει ένα πλήρη κύκλο κάθε 21000 έτη. Ήδη οι αρχαίοι Έλληνες γνώριζαν τις περιόδους αυτές οι οποίες αργότερα συμπεριλήφθηκαν στο γεωκεντρικό μοντέλο του σύμπαντος από τον Κλαύδιο Πτολεμαίο.

Οι αστρονομικοί αυτοί κύκλοι προκαλούν περιοδικές μεταβολές της ποσότητας ηλιακής θερμότητας που φθάνει στην γη και συνεπώς και στο κλίμα. Παράδειγμα οι παγετώδεις εποχές, είχαν σαν αιτία μεγάλες περιόδους με κρύα καλοκαίρια στο βόρειο ημισφαίριο, όπου τα χιόνια του χειμώνα δεν έλειψαν στα βουνά, δημιουργώντας στρώματα πάγου. Οι γεωλόγοι αναγνωρίζουν τα ίχνη των παγετωδών εποχών σαν χαραγές στα πετρώματα ή σαν μοραίνες. Αλλά και ασθeneίες κλιματικές αλλαγές άφησαν τα ίχνη τους στην γεωλογία, κυρίως στα στρώματα των ιζημάτων. Πολλά ιζήματα που σχηματίστηκαν κατά τα τελευταία 5 εκ. έτη βρίσκονται στην περιοχή της Μεσογείου. Ένα μεγάλο τμήμα των ιζημάτων αυτών αποτέθηκαν στον βυθό της θαλάσσης αλλά σήμερα βρίσκονται στην ξηρά κάνοντας την μελέτη τους εύκολη. Η εμφάνιση σκούρων σε χρώμα στρωμάτων σε αυτά τα ιζήματα συμφωνούν με τις περιοδικές μεταβολές της τροχιάς της γης. Είναι λοιπόν προφανές ότι η σύνθεση των ιζημάτων επηρεάστηκε από το κλίμα, που άλλαξε περιοδικά λόγω των αστρονομικών μεταβολών. Μπορούμε λοιπόν να πούμε ότι η θάλασσα είναι μία φωτογραφική μηχανή και το ιζήμα είναι το φωτογραφικό φιλμ στο οποίο καταγράφονται οι κλιματικές μεταβολές. Παρατηρώντας το φιλμ εικόνα με εικόνα, δηλαδή μελετώντας τα ιζήματα στρώμα με στρώμα, αναπαριστούμε τις κλιματικές μεταβολές των 5 εκ. ετών πριν από σήμερα.

Οι κλιματικές είναι πιο έντονες στην ξηρά από ότι στον βυθό της θάλασσας. Είναι σαν μια φωτογραφική μηχανή έχει ένα φίλτρο στον φακό της που επιτρέπει σε άλλα αντικείμενα να περάσουν και σε άλλα όχι. Μία πλήρης εικόνα δίνεται από φιλμ από διαφορετικές φωτογραφικές μηχανές με διαφορετικά φίλτρα. Έτσι, για μία πλήρη εικόνα του κλίματος, μελετάμε ιζήματα που έχουν σχηματιστεί στην ξηρά, σε λίμνη ή σε βάλτο. Η διατριβή αυτή

έχει σαν αντικείμενο την μελέτη των ιζημάτων από τις λιγνιτικές λεκάνες της Πτολεμαΐδας και της Μεγαλόπολης στην Ελλάδα και της λεκάνης Luproaia στην Ρουμανία καθώς και των ποταμιολιμναίων ιζημάτων της Απολακκίας στην Ρόδο.

Τέσσερα με πέντε εκατομμύρια χρόνια πριν από σήμερα υπήρχε κοντά στην Πτολεμαΐδα μια λίμνη μικρού βάθους η οποία άλλαζε σε βάλο κάθε 20 χιλ. έτη. Επειδή το κλίμα έγινε ξηρό, λόγω των αλλαγών στην μετάπτωση των ισημερινών, η στάθμη του υδροφόρου ορίζοντα έπεσε και αναπτύχθηκαν εκτεταμένοι καλαμιώνες. Το οξυγόνο των υδάτων της λίμνης δεν ήταν αρκετό ώστε να διαλύσει τις τεράστιες ποσότητες του νεκρού φυτικού οργανικού υλικού το οποίο μετετράπη συν τω χρόνω σε λιγνίτη. Δέκα χιλιάδες χρόνια αργότερα το κλίμα έγινε και πάλι υγρό και ο υδροφόρος ορίζων ανέβηκε. Οι καλαμιώνες εξαφανίστηκαν και δημιουργήθηκε μία ανοιχτή λίμνη με συνέπεια την καθίζηση ανθρακικού υλικού. Σήμερα παρατηρείται αυτό στην εναλλαγή των στρωμάτων λιγνίτη και μάργας στα ιζήματα της λεκάνης.

Στην Μεγαλόπολη υπήρχε ένα εκατομμύριο χρόνια πριν από σήμερα μια λίμνη διαφορετικού τύπου, με απότομες κλιτύς στα ανατολικά και ομαλές στα δυτικά. Από τις απότομες κλιτύς, άμμος και άργιλος έπεσαν στη λίμνη και στις ομαλές αναπτύχθηκαν καλαμιώνες. Όταν το κλίμα ήταν ζεστό και υγρό οι καλαμιώνες κατέλαβαν μεγάλο τμήμα της λίμνης και μεγάλη ποσότητα οργανικού υλικού διατηρήθηκε δημιουργώντας τον σημερινό λιγνίτη. Ανά εκατό χιλιάδες χρόνια εξαιτίας της αλλαγής της εκκεντρότητας της τροχιάς της γης τα καλοκαίρια έγιναν ψυχρότερα και ξηρότερα (τις ίδιες εποχές η Β. Ευρώπη καλύπτεται από πάγους), με αποτέλεσμα οι καλαμιώνες να εξαφανιστούν. Το ίζημα τότε χωρίς τα φυτικά εμπόδια εξαπλώθηκε στην λίμνη δημιουργώντας στρώματα άμμου και αργίλου.

Στην ΝΔ. Ρουμανία υπήρχε πριν από 4 εκ. έτη μια λίμνη όμοια με αυτή της Μεγαλόπολης. Οι ίδιες εναλλαγές λιγνίτη και αργίλου εμφανίζονται και εδώ οι οποίες σχετίζονται με τις κλιματικές αλλαγές ανά εκατό χιλιάδες χρόνια που οφείλονται στις μεταβολές της εκκεντρότητας της γης. Δεν υπάρχουν όμως πάγοι στην Ευρώπη πριν από 4 εκ. ετη όπως φαίνεται σε ιζήματα της ίδιας ηλικίας π.χ. Πτολεμαΐς.

Οι τρεις αυτές λιγνιτικές λεκάνες έχουν μεταξύ τους ομοιότητες και διαφορές από τις οποίες υπολογίζουμε ότι οι εναλλαγές των στρωμάτων στο ιζηματογενές πλήρωμα εξαρτώνται από αστρονομικές επιδράσεις και όχι από τον γεωλογικό χρόνο ή τις παγκόσμιες κλιματολογικές συνθήκες. Εναλλαγές ανά 100 χιλ. έτη επικρατούν σε λίμνες τροφοδοτούμενες με άμμο και άργιλο όπου η ποσότητα του φυτικού υλικού έχει κρίσιμο ρόλο. Οι λίμνες με ανθρακικά ιζήματα, όπου η στάθμη των υδάτων τους παίζει σημαντικό ρόλο, υπόκεινται σε εναλλαγές ανά 20 χιλ. έτη.

Στην Ρόδο, η λεκάνη ηλικίας 3-4 εκ. χρόνια πριν από σήμερα, πληρώνεται από αδρομερές ίζημα, όπου και παρατηρούνται κανονικές εναλλαγές των στρωμάτων.

Αυτό οφείλεται στην κανονική αλλαγή της λεκάνης από βαλτώδη λίμνη σε ρηχή ανοιχτή λίμνη σε ποτάμιο δέλτα. Με την βοήθεια του παλαιομαγνητισμού αποδεικνύουμε ότι οι εναλλαγές των στρωμάτων με πάχος 30μ. είναι ισόχρονες με την μετάπτωση των ισημερινών. Αυτό όμως δεν είναι αρκετά σαφές ώστε να συγκριθεί λεπτομερώς με τις τροχιακές κινήσεις της γης.



## Acknowledgements

The care, attention and support of many people have helped me complete this thesis and relieved the lonely feeling it gave me from time to time. The freedom of conducting research is terrific and geological field work is the best way there is to gather data. At other times, I gave myself a hard time; wanting to compose the perfect first draft of a new chapter just resulted in nothing on the screen. Luckily, such a stage never lasted long. I have experienced the last months of completing this thesis as one of the nicest periods, with many people supporting me, (former) colleagues, friends and family alike. Thank you all for being there for me.

There are several people I specifically want to acknowledge. First of all my professor Cor Langereis, for doing a great job. His supervision was friendly, critical and always aimed for my growth and development. I'll remember the pleasant atmosphere during our field trips, scientific discussions and the *Fort-borrels*. Further supervision was provided by Frits Hilgen, Mark Dekkers and Johan Meulenkamp. Frits taught me the ins and outs of observing sedimentary cycles in the field and he was willing to listen to and comment on crazy theories about these cycles. Mark was a walking rock-magnetic encyclopaedia available to me at all times. I sometimes found he was splitting hairs over technical details, but I must admit that his precision improved the manuscript. Johan, as leader of the multi-disciplinary research program, set up the contacts with our Greek and Romanian counterparts, and with his broad exposure to Mediterranean sections he focused this research program on suitable basins.

The co-operation with my team-members Marloes Kloosterboer and Joris Steenbrink has been very important to me. From our first field trip to our last collective paper, we formed a good team. This close co-operation might easily have led to conflicts, but I have never experienced any competition between us. Furthermore, sharing experiences of ups and downs during this research has motivated me to continue at times I might have quitted had I been on my own. Thanks for being wonderful buddies.

An important aspect of this research, and also the most enjoyable one, has been the field work. Innumerable trips to Greece and Romania led friends and family to comment on my supposed travel-agency job, but they never accepted my invitation to join me in the dusty lignite mines. Palaeomagnetic sampling cannot be done alone, and I want to thank everyone who accompanied me in the field. In addition to all the people mentioned so far, these are: Hans de Bruin (taught us barbarians how to have a decent field lunch), Konstantin Doukas (the program's ambassador in Greece), Kostas Theocharopoulos (showed us how to hunt for beaver-teeth), Wout Krijgsman (my drilling teacher and worm-beater), Erik Snel (the indispensable digging champion with an extraordinary memory, who almost managed to split my skull with a flying rock on Rhodes), Charon Duermeijer (good fun in the heat wave, even despite her locking in the car keys), Sorin and Maria Radan from Romania, Rob Satter, Hendrik-Jan Bosch, Davide Duranti and Sander Ernst.

Essential for conducting research is the free exchange of scientific ideas and comments. I have enjoyed the discussions with Joris, Marloes, Wout, Hayfaa Abdul Aziz,

Luc Lourens, Pauline Kruijver, Sorin and Maria, Masaaki Okuda and last but not least: Cor and Frits.

The *Fort Hoofddijk* laboratory, located in the botanical gardens of the university, has been an agreeable place to work in. I have especially appreciated the positive, professional and *gezellige* atmosphere brought forward by my room mates and the support of Tom and Carla Mullender. I thank Henk for helping me with (sometimes hopeless) measurements of many 'black stuff' samples.

I am grateful for the critical and compassionate love of my friends, who never tired of my enthusiastic lessons in geology. They accept me for who I am, yet do not permit me to be any less. Finally, I thank my parents, who have supported me in all my choices and actions through life, without ever making me feel pressured. *Tenslotte bedank ik mijn ouders, die mij op iedere mogelijke manier ondersteund hebben in al mijn keuzen en ondernemingen, zonder me ooit druk op te leggen.*

## **Curriculum Vitae**

Nicole van Vugt werd geboren op 12 december 1970 in Leende. Zij begon haar middelbare schoolopleiding aan het Hertog Jan College te Valkenswaard in 1983, alwaar zij haar Atheneum B diploma behaalde in 1989. Datzelfde jaar begon zij aan de studie geofysica aan de Universiteit Utrecht. Een jaar later startte ze haar studie geologie, die met een doctoraal examen geologie/geofysica afgesloten werd in 1995. Aansluitend werkte ze als onderzoeker in opleiding voor ALW/NWO op het Paleomagnetisch Laboratorium 'Fort Hoofddijk' van de Universiteit Utrecht. Vanaf maart 2000 is ze werkzaam als geoloog bij Shell International Exploration and Production in Rijswijk.